



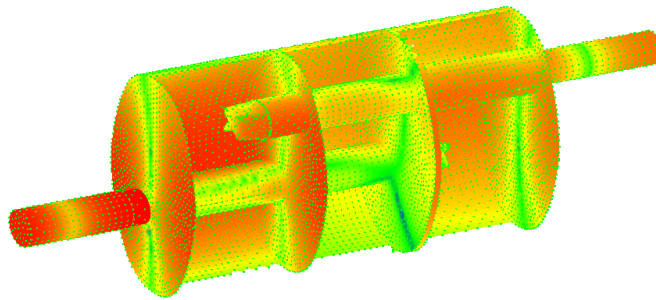
UNIVERSITÀ DEGLI STUDI DI NAPOLI FEDERICO II

DOTTORATO DI RICERCA IN INGEGNERIA DEI SISTEMI MECCANICI

XXIV CICLO

**THE ACOUSTICS OF AUTOMOTIVE MUFFLERS: 1D-3D BEM
ANALYSES, EXPERIMENTAL VALIDATION AND OPTIMIZATION**

Fabio Auriemma



Doctoral Thesis

Naples, Italy 2012

Tutors:

Ch.mo prof. Fabio Bozza (DIME)

Ing. Daniela Siano (CNR, Istituto Motori)

Abstract

A number of numerical and experimental studies, performed in the field of technical flow duct acoustics, are presented in this thesis. The analyses have been implemented on the automotive mufflers, and the fluid-dynamic aspects have been taken into account too.

The noise attenuation characteristics of a three pass perforated muffler with final end resonator have been investigated. Acoustic performances have been quantified by the Transmission Loss (TL) parameter, and different numerical methods have been adopted. Firstly, a non-linear one-dimensional (1D) time domain approach is utilized to predict the TL profile in a low frequency range. Secondly, a linear three dimensional (3D) boundary element method (BEM), in the frequency domain, has been utilized to obtain more accurate results at higher frequencies. The effects on muffler performance of different mean flow velocities and gas temperatures have been investigated too.

Advantages and disadvantages of the above mentioned numerical approaches have been highlighted by analyzing a two-tube cross-flow commercial muffler. Besides the obvious differences due to the non linear/linear and 1D/3D formulations, the 1D method has been successfully used in simulations where a mean flow was present. On the other hand, after importing the results of a previously modal analysis, a complex BEM fluid-structure interaction analysis has been performed. Interesting results about the structure excitation, at certain frequencies, have been carried out. Moreover, the radiated noise has been assessed, once imposed a certain excitation at inlet.

An experimental campaign has been carried out in the acoustic laboratory of Tallinn University of Technologies (TTU), Estonia, aimed to validate the above numerical results. Testes have put in evidence the strong effects, on muffler performances, of the constructive features related to the manufacturing process, such as the coupling of adjacent surfaces and the actual shape of components. Hence, although numerical analyses are usually performed on ideal geometries (perfectly matched and shaped), when the behaviour of a real muffler must be simulated, a more detailed schematization must be used. To this aim, a number of tricks are suggested.

A brand new acoustic optimization procedure, based on a 1D non-linear solver coupled to a genetic algorithm through a number of external routines, has been developed, aimed to maximize the acoustical attenuation or to find the best tradeoff between acoustical and fluid-dynamic performances. The proposed approach constitutes a valid instrument to improve the muffler design process, providing a consistent enhancement of TL and a contemporary reduction of back pressure for the examined case.

Keywords: IC-engine, muffler, silencer, acoustics, exhaust system, flow duct, one-dimensional simulation, non linear simulations, boundary element method, finite element method, fluid-structure analysis, radiated noise, two-port source, two-microphone approach, optimization, genetic algorithm.

Acknowledgements

The numerical simulations and the theoretical studies on acoustics have been mainly carried out in the Facoltà di Ingegneria Meccanica of Università Federico II, Dipartimento di Meccanica ed Energetica, Naples, and in cooperation with CNR, Istituto Motori, Naples. Experimental tests have been performed in the acoustic laboratory of Tallinn University of Technologies, Tallinn, Estonia.

First of all, I would like to acknowledge my tutors, ing. Daniela Siano, who gave me the opportunity to continue the acoustical studies started with my master thesis, and prof. Fabio Bozza, for his technical teachings and his continuous support in the performed works.

I'm very grateful to my supervisor in TTU, Hans Rammal, for transmitting me his optimistic and open minded approach to the work and to the life.

Thanks to the friends and colleagues I've met in the University of Naples: Salvina Giacobbe, Francesco Langella, Gabriele di Blasio, Massimiliano Muccillo, Giuseppe Fioretto, Giovanni Vorraro, Ugo Sorge and Vincenzo de Bellis (this latter also for the interesting conversations on scientific topics).

I'm grateful to Raimo Kabral, for giving a valuable support to the experimental sessions in Tallinn, and to all the TTU team, including prof. Yurj Lavrentiev, for the unforgettable time spent together, not only "inside the university"...

A special thank goes to my friends, Francesco Ugliano and Carmine Auriemma, for their priceless presence.

Everything I am, comes from my family, who is the last but not least deserving all my gratefulness.



Fabio Auriemma, January 2012

This doctoral thesis consists of an introduction, 5 chapters and the final conclusions.

- In the first chapter, a global overview on mufflers is given.
- In the second one, 1D methods for linear and non linear acoustic simulations are summarized.
- In the third one, 3D methods for linear acoustics are described.
- In the fourth one, main experimental techniques for muffler acoustic analyses are explained.
- In the fifth one, a number of results, carried out in the doctoral studies, are presented.

The results included in Chapter 5 widely refers to the following technical papers:

1. D. Siano, F. Auriemma, F. Bozza, A Correlation Study of Computational Techniques of a Three Pass Perforated Tube Muffler Including FEM and 1D Methods, SEEP 2009.
2. D. Siano, F. Auriemma, F. Bozza, Pros and Cons of Using Different Numerical Techniques for Transmission Loss Evaluation of a Small Engine Muffler, SAE Paper 2010-32-0028, Linz, 2010.
3. D. Siano, F. Auriemma, F. Bozza, Svantaggi e Vantaggi Legati all'Utilizzo di Diversi Metodi Numerici per la Caratterizzazione Acustica di un Silenziatore per Applicazioni Automobilistiche, ATI Cagliari, 2010
4. D. Siano, F. Auriemma, F. Bozza, H. Rämmal, Validation of 1D and 3D Analyses for the Prediction of an Automotive Silencer Performance, SAE Technical Paper SAE 2011-24-0217, 2011.
5. F. Auriemma, F. Bozza, Acoustic and Fluid-dynamic Optimization of an Automotive Muffler, *in submission*.

Other publications, related to the performed studies, are:

1. R. Kabral, H. Rämmal, J. Lavrentjev, F. Auriemma, Acoustic Studies on Small Engine Silencer Elements, SAE 2011-32-0514, 2012.
2. D. Siano, Three-Dimensional/One-Dimensional Numerical Correlation Study of a Three-Pass Perforated Tube, Simulation Modelling Practice and Theory 19 (2011) 1143–1153.

The acoustics of automotive mufflers: 1D-3D Boundary Element analyses, experimental validation and optimization

INTRODUCTION	10
FUNDAMENTALS OF MUFFLERS – A GLOBAL OVERVIEW.....	10
NUMERICAL METHODS.....	13
EXPERIMENTAL METHODS.....	17
RESULTS OF DOCTORAL STUDIES.....	18
REFERENCES.....	20
 CHAPTER 1 FUNDAMENTALS OF SILENCERS	 24
1.1 INTRODUCTION.....	22
1.2 SILENCERS CLASSIFICATION	26
1.3 MODELS OF SOURCE, SILENCER AND TERMINATION.....	27
1.3.1 ONE-PORT MODEL OF THE SOURCE.....	27
1.3.2 TWO-PORT MODEL OF THE SILENCER.....	30
1.3.3 SOURCE-SILENCER-TERMINATION MODEL.....	32
1.4 SILENCER PERFORMANCE CRITERIA.....	33
1.5 REACTIVE SILENCERS.....	38
1.5.1 SILENCER EXEMPLIFICATION.....	38
1.5.2 BASIC SILENCER ELEMENTS: STRAIGHT TUBE.....	39
1.5.3 BASIC SILENCER ELEMENTS: CROSS SECTIONAL DISCONTINUITIES.....	40
1.6 ACOUSTIC BEHAVIOUR OF EXPANSION CHAMBERS	42
1.6.1 SIMPLE EXPANSION CHAMBERS.....	42
1.6.2 EXTENDED OUTLET EXPANSION CHAMBERS.....	44
1.6.3 DOUBLE TUNED EXPANSION CHAMBERS.....	45
1.7 ACOUSTIC BEHAVIOUR OF SIDE BRANCH RESONATORS	46
1.7.1 FUNDAMENTALS ON SIDE BRANCH RESONATORS.....	46
1.7.2 QUARTER WAVE AND HELMHOLTZ RESONATORS.....	49
1.7.3 CONCENTRIC HOLE-CAVITY RESONATOR AND PERFORATE TUBES.....	51
1.8 END EFFECTS AT DISCONTINUITIES	53
1.9 DISSIPATIVE SILENCERS	54
1.10 POROUS ABSORBENTS.....	56
1.11 TYPICAL SILENCER CONFIGURATIONS	58

REFERENCES.....	61
 CHAPTER 2 NUMERICAL 1D METHODOLOGIES	62
2.1 INTRODUCTION.....	62
2.2 GOVERNING EQUATIONS.....	64
2.3 LINEARIZED EQUATIONS AND LINEARIZED WAVES.....	66
2.4 METHOD OF CHARACTERISTICS.....	68
2.5 THE COURANT-FRIEDERICHS-LEWY (CFL) STABILITY CRITERION.....	72
2.6 FINITE VOLUME METHODS.....	73
2.6.1 DEFINITION OF FINITE VOLUME SCHEME.....	74
2.6.2 LAX-WENDROFF SPACE-CENTRED SCHEMES.....	75
2.6.3 TWO STEPS LAX-WENDROFF SCHEMES.....	76
2.7 IMPROVEMENT OF THE SECOND ORDER DIFFERENCE SCHEMES.....	78
2.7.2 TVD FLUX LIMITERS.....	78
2.7.3 FLUX CORRECTED TRANSPORT.....	80
2.8 CONSERVATION ELEMENT – SOLUTION ELEMENT.....	81
2.9 BOUNDARY CONDITIONS.....	81
2.10 COMPARISON OF NUMERICAL SCHEMES IN SILENCER ANALYSES.....	82
2.11 MODELLING SIMPLE REACTIVE SILENCERS.....	84
2.12 WHITE NOISE PERTURBATION.....	85
2.13 PERFORATED TUBE SILENCERS.....	86
2.14 QUASI 3D APPROACHES.....	87
2.15 DISSIPATIVE SILENCERS MODELLING.....	88
REFERENCES.....	90
 CHAPTER 3 3D LINEAR NUMERICAL METHODS IN ACOUSTICS	93
3.1 INTRODUCTION.....	93
3.2 ACOUSTIC WAVE EQUATION AND BOUNDARY CONDITIONS.....	94
3.3 FEM: ACOUSTIC MODEL.....	98
3.4 FEM: GENERAL FORMULATION FOR INTERIOR PROBLEMS.....	99
3.4.1 WEAK VARIATIONAL FORMULATION	102
3.5 FEM: TYPES OF ANALYSES.....	103
3.5.1 FREQUENCY RESPONSE ANALYSIS.....	103
3.5.2 NORMAL MODE ANALYSIS.....	104
3.5.3 ACUSTO-STRUCTURAL COUPLING.....	104

3.5.4 TRANSIENT RESPONSE.....	105
3.6 FEM: EXTERNAL PROBLEMS.....	105
3.7 FEM: ACOUSTICS IN PRESENCE OF MEAN FLOWS.....	107
3.8 BEM: GENERAL FORMULATION – DIRECT AND INDIRECT APPROACHES.....	108
3.8.1 DIRECT METHOD.....	108
3.8.2 INDIRECT METHOD.....	110
3.8.3 PROBLEM FORMULATION	111
3.9 BEM: STRUCTURAL COUPLING.....	114
3.10 BEM: THE NON UNIQUENESS PROBLEM.....	116
3.11 BEM: FAST MULTIPOLE FOR LARGE PROBLEMS.....	117
3.12 FURTHER COMPUTATIONAL ASPECTS IN ACOUSTIC 3D SIMULATIONS.....	118
3.12.1 TYPES OF ELEMENTS IN FEM.....	118
3.12.2 NUMERICAL ERRORS: APPROXIMABILITY.....	118
3.12.3 NUMERICAL ERRORS: POLLUTION.....	119
REFERENCES.....	120

CHAPTER 4 EXPERIMENTAL TECHNIQUES122

4.1 TWO-MICROPHONE RANDOM-EXCITATION TECHNIQUE.....	123
4.1.1 PHYSICS OF WAVE DECOMPOSITION	123
4.1.2 SEYBERT AND ROSS TECHNIQUE	126
4.2 TWO PORT MODEL – TWO LOAD/TWO SOURCE TECHNIQUES	131
4.2.1 LINEAR SYSTEMS.....	131
4.2.2 TWO PORT SOURCES.....	133
4.2.3 THE TWO-LOAD CASE.....	137
4.2.4 THE TWO-SOURCE CASE.....	139
4.2.4. INFLUENCE OF ERRORS.....	141
4.2.5 CALCULATION OF THE TRANSFER-MATRIX FROM A GIVEN SCATTERING-MATRIX.....	142
4.3 TEST RIG OF TTU LABORATORY.....	144
APPENDIX.....	147
A.1 CORRELATION.....	147
A.2 ENSEMBLE AVERAGE.....	148
A.3 AUTO-CORRELATION.....	149
A.4 CROSS-CORRELATION.....	151
A.5 DETECTION OF SIGNAL IN NOISE.....	152
A.6 POWER SPECTRAL DENSITY.....	152
A.7 CROSS POWER SPECTRAL DENSITY, CROSS SPECTRUM.....	154

REFERENCES.....	156
CHAPTER 5 RESULTS	157
5.1 1D AND 3D BEM ANALYSIS OF A REACTIVE THREE PASS	
PERFORATED MUFFLER	157
5.1.1 MUFFLER CONFIGURATION.....	158
5.1.2 1D SIMULATIONS.....	158
5.1.2 3D-BEM SIMULATIONS.....	160
5.1.3 RESULTS AND DISCUSSION.....	163
5.1.4 EFFECTS OF THE GAS TEMPERATURE AND FLOW VELOCITY	166
5.1.5 CONCLUSIONS.....	169
5.2 1D AND 3D BEM ANALYSIS OF A COMMERCIAL CROSS FLOW MUFFLER,	
INCLUDING FLUID-STRUCTURE INTERACTIONS AND RADIATED NOISE	170
5.2.1 MUFFLER DESCRIPTION AND CAD MODEL.....	171
5.2.2 1D AND 3D MODELS.....	172
5.2.3 TL RESULTS AND DISCUSSION.....	174
5.2.4 RADIATED SOUND PRESSURE LEVEL.....	185
5.2.5 CONCLUSIONS.....	188
5.3 VALIDATION OF THE 1D AND 3D BEM ANALYSES FOR THE	
PREDICTION OF PERFORMANCES OF A COMMERCIAL CROSS FLOW MUFFLER	191
5.3.1 PECULIARITIES OF THE MUFFLER STUDIED.....	191
5.3.2 NUMERICAL SIMULATIONS.....	194
5.3.2 EXPERIMENTAL DATA.....	195
5.3.3 RESULTS AND DISCUSSION.....	197
5.3.4 FURTHER EXPERIMENTAL STUDIES.....	205
5.3.5 CONCLUSIONS.....	207
5.4 ACOUSTIC AND FLUID-DYNAMIC OPTIMIZATION OF AN AUTOMOTIVE COMMERCIAL	
CROSS FLOW MUFFLER	209
5.4.1 1D TL AND PRESSURE DROP DATA	210
5.4.2 MUFFLER OPERATING CONDITIONS	210
5.4.3 OPTIMIZATION PROCEDURE.....	211
5.4.4 RESULTS.....	215
5.4.5 CONCLUSIONS.....	220
REFERENCES.....	223
CONCLUSIONS AND FUTURE RESEARCH.....	225

Introduction

The studies carried out in these three years doctorate have been driven by the will to understand the principles founding the duct acoustics applied to the silencers for ICE. A gradual approach, based on the use of numerical simulations, to the study of more complicated problems has revealed its effectiveness. In fact, after performing the first analyses, aimed to prove well known results from the literature, the attention has been addressed to less explored areas, e.g. the sound radiation due to the interaction of the muffler structure with the surrounding fluid, the tuning of numerical 1D and 3D models of a commercial muffler through experimental tests, the description of the effects of the manufacturing quality on the acoustic silencer performance, and the development of an optimization procedure.

The target has been, on one hand, a better description of the silencers behavior, including usually neglected aspects. On the other hand, the improving of the muffler design process, by means of suggestions aimed to enhance the numerical simulations, and by means of a tool, represented by the above optimization procedure, focused on the obtaining of the best trade-off between acoustic and fluid-dynamic performances.

FUNDAMENTALS OF MUFFLERS – A GLOBAL OVERVIEW

Mufflers play an important role on the environmental impact associated with the sound emission of internal combustion engines (ICE). They are designed to reduce the exhaust noise originated from the pressure pulses occurring in the periodic charging and discharging processes. A good design of a muffler must also account the requirement of minimizing the back pressure, i.e. the extra static pressure exerted by the muffler on the engine. This second necessity is needed to avoid consistent reductions of the volumetric efficiency, consequent increasing of the brake specific fuel consumption, and decreasing of mechanical power output. Usually these requirements are contradictory so the right trade off must be chosen at design phase [1-3].

Eventually, mufflers are also designed and tuned to give a positive contribution to the vehicle sound quality, which is an important point of emphasis in NVH work: interior sound

quality can be used to differentiate vehicles or brands as well as to give an overall impression of the vehicle quality. This aspect puts an increased emphasis on the importance of understanding exhaust noise and its frequency content [4].

A variety of muffler typologies and models can be found in literature and on the market. They are usually constituted by a certain number of tubes and chambers, divided each other by baffles. Tube and baffles can also present perforated areas, and chambers can include a certain quantity of absorptive material. Fundamentals of mufflers, including a summary of the different typologies, a resume of their performances and guide line about the main geometrical parameters, are given in the Chapter 1 of this work.

Regarding the acoustic analyses, a very powerful and widely used simplification for IC-engine intake or exhaust ducts is to assume small perturbations and perform a linearization of the governing equations, i.e., a set of coupled non-linear equations for conservation of mass, momentum and energy. This simplification allows to neglect the energy equation (linear acoustics). When a homogeneous and isentropic mean flow is present, the final result will be the convective *wave equation* and then 3D effects can also be addressed without too much difficulty.

Another possible simplification is to consider one-dimensional (1D) fields only. This assumption implies that the variables of pressure, density, velocity and temperature are treated as being constant over the cross-section of the duct under consideration. Consequently, the solution of the coupled nonlinear equations will be greatly simplified [2]. If only small perturbations are considered, the wave equation will be reduced to a 1D linear wave problem, which can be efficiently analyzed via so called two-port (or four-pole) methods [6]. On the contrary, when the excitation overwhelms certain limits, the linear assumption does not stand anymore, and a non-linear approach is required to solve the acoustic problem.

Historically, the hypotheses of plane linear waves have been extensively utilized in silencer analyses, allowing to study a variety of configurations, in an *analytical* way. In particular, many studies have been focussed on devices including one or more expansion chambers, which act as low frequency resonators, and a certain number of perforated tubes, often used as high-frequency resonators.

Roughly following a chronological order, aero-acoustic analysis of perforated elements, in the form of a series expansion for the straight through silencer elements, was first presented by Sullivan and Crocker [7]. A *segmentation method* was developed by Sullivan [8-9], lumping the effect of perforations into a number of discrete planes with solid pipes present in between. This was followed up by Jayaraman and Yam [10] who developed a

decoupling method to obtain a closed form analytical solution. In fact in these studies the complete analysis of mufflers including perforate tubes involves the elimination of velocity variables from the basic governing equations to obtain the coupled ordinary differential equations in terms of acoustic pressure variables. Thawani and Jayaraman demonstrated the use of this decoupling method [11] by analyzing straight-through resonators in the absence of flow. Rao and Munjal [12] extended the analysis of Jayaraman and Yam by allowing the Mach numbers in the inner perforated duct and the outer casing to be different. Later, Peat [13] presented another numerical decoupling approach removing the numerical instability problems associated with other methods described thus far.

All of these studies, were limited to concentric tube resonators, plug mufflers, or two-pass mufflers (two perforated ducts plus an expansion chamber). As many of the commercially available mufflers implement *three passes* (three perforated ducts plus an expansion chamber), such configurations have been of more recent interest.

Munjal presented a frequency domain analysis of a three pass muffler via a decoupling method [14], which was also refined to include the extended-tube three-pass perforated element muffler [15]. This decoupling approach was shown by Peat [13] to lead to numerical instability problems, especially near transmission loss peaks. Selamet *et al.*, developed a quasi-one-dimensional theoretical model for the analysis of a three-pass perforated duct muffler based on the transfer matrix method and the numerical decoupling of Peat. The method was then generalized to include the analysis of three-pass mufflers where the ducts extend into the end cavities [16].

Further attempts have been made to analyze similar acoustical elements for different configurations and flow conditions. In a recent development, Munjal [17] analyzed an axisymmetric pod silencer and Kar *et al.* [18] developed an algebraic algorithm for modelling a configuration with any number of interacting tubes or parallel ducts. This latter provided a clarity of thought for completeness, and hence a generality, in a way, to preclude tedious algebraic manipulations.

Since the 1D plane wave regime is suitable only for low frequencies, a *multi dimensional approach* was needed for accurate predictions in wide frequency range of interest. During the past decades several *analytical* studies, discussing the effects of higher order modes on the performance of expansion chamber mufflers, have been published. In [19] Ih *et al.* presented the results in the four-pole form for a circular expansion chamber and a circular reversing chamber. Abom derived the four-pole parameters, with higher order mode effects, for an

expansion chamber muffler with extended inlet and outlet [20], by utilizing the analytical mode matching method [21].

NUMERICAL METHODS

In the Chapters 2 and 3 the main techniques based on 1D and 3D numerical approaches are explained.

As previously shown, giving a look to the duct acoustic literature of last 2-3 decades, a number of fundamental studies, based on one-, two- or three-dimensional approaches can be found. They are basically *analytical* approaches, in which the algebra involved, particularly for asymmetric chambers, has been found to be relatively complex. Moreover, in case of multi-dimensional approaches, analytical solutions to the acoustic problem can be found only for easy cases (rectangular and circular, elliptic and parabolic cylindrical cross-sections).

For these reasons numerical models, based on various approximations, are often necessary, sometimes compulsory.

A variety of modeling procedures have been proposed in by the experts, and are currently applied to predict the propagation of pressure waves in the gas flowing along intake and exhaust systems. Also in these cases, the procedures can be divided into *linear acoustic models* and *non-linear fluid dynamic models*, according to the assumptions they are based on.

As above mentioned, the acoustic linear models are widely used when there are small acoustic excitations, and they include *linear 1D*, *finite element method* (FEM) and *boundary element method* (BEM). These methods are usually based on frequency domain approaches, solving the so called linear *Helmholtz's equation* [5] (derived from linear wave equation) or its 1D form in case of 1D linear codes.

1D linear methods are very fast and require low computational costs. The quality of the predictions is often improved by introducing some length corrections to the 1-D model, in a way that the complex wave reflections at discontinuities (sudden expansion and contractions in duct cross-section) are taken into account [22]. Even though the 1D linear theory is a useful approach to the acoustics of muffler [1] and a variety of excellent results are present in the literature, nowadays the computing research is focused on the development of numerical 1D non-linear tools. These latter, described afterwards, preserve a quite low computational cost and contemporary are able to deal with more complex problems.

Back to the linear theory, the 3D approaches (FEM and BEM) are preferred when the analysis regards the acoustic performance of some components in which non-planar higher modes are excited. 3D effects, in fact, appear when the transverse dimensions of the system are comparable to the wavelength of the excitation, and in proximity of the cross section discontinuities.

The first attempt to study the acoustic behaviour of a muffler by using the finite element method, was made by Ross [23] on a three pass perforated system, but he only demonstrated the results for the case where the middle pipe was just pass through (not perforated).

A major challenge for using FEM for Helmholtz's equation is that a specific resolution requirement for minimal wavelength must be respected for control of the approximation error [24]. Dispersion analysis demonstrates that it is generally more difficult to meet the resolution requirements for higher frequencies [25]. Several finite element methods have been developed to ease resolution requirements which are seemingly an open problem. In practice, finite element simulation requires high computational and memory resources, particularly at higher frequencies and, due to restrictions in computational resources, most of the past published applications of FEM for time-harmonic wave propagation had been limited to two-dimensional domains. This, obviously, has changed in recent years, and more examples of three-dimensional applications for the mufflers performance prediction can be found in the literature [26-27].

Also the boundary element method has been widely utilized for the solution of the Helmholtz's equation in a variety of problems. They include mufflers with perforated tubes and irregular geometries (such as edges or corners), effects of porosity of perforation and flow-resistivity of sound absorbing material [28-30]. Predicted transmission loss curves are generally in good agreement with those from experimental measurements.

The major advantage of the BEM is that only the boundary surface needs to be discretized. This saves considerable modeling effort when compared to domain discretization methods such as the finite element method (FEM). In order to deal with certain classes of acoustic problems where very complicated geometries are involved (for example acoustic mufflers with thin obstacles or projecting surfaces within the cavity volume) in [29] a multidomain BE solution is proposed, in which the cavities of the muffler are divided into several subdomains so that the boundary surface of each subdomain is well defined and the conventional BEM can be applied to each one of them. The BEM equations for different subdomains are coupled to each other by enforcing the continuity conditions of pressure and normal velocity at the interface between two neighboring subdomains.

Owing to the high requirements of development time and computational cost, such investigations focus only on particular components of intake/exhaust system, without providing a description of their interaction with the engine.

As previously mentioned, nowadays the non-linear numerical methods are of great interest: since in engine intake and exhaust systems, the pressure fluctuations are characterized by much larger amplitude than that assumed in the linear approach, these approaches are often mandatory. In fact they furnish quite realistic predictions, taking into account of the distortion of high amplitude waveform, during the propagation in ducts, and the interaction between the engine and the ducts system. Non-linear fluid dynamic models are mainly used to predict the intake and exhaust system performance in terms of pressure, velocity crank angle histories, and are based on lumped parameter (0-D), one-dimensional (1-D) or three-dimensional (3-D) schemes. 0-D schemes are usually adopted coupled with 1-D models, the former one in the investigation of cylinder behavior and of flow across intake and exhaust valves, the latter one to describe the intake/exhaust system [31-34]. Recently, some 1-D models have been proposed to analyze complex geometries, such as mufflers, in which perforations and adsorptive materials are included [35].

More refined 1D based approaches, like the one proposed by Montenegro *et al.* [36] utilize *quasi-3D* elements to model chambers or after-treatment devices, which are specifically designed to account for conservation of momentum in three dimensions, even though the code is otherwise nominally one-dimensional. They are composed by a 0D element at the center of the volume, where the continuity and energy equations are integrated, and a number of volume openings (ports) where the momentum equation is integrated.

The computed results allow the evaluation of the noise radiation from the tailpipe, by assuming that the open end acts as a monopole source (see, for example, reference [33]).

Anyway, also in this case, when transverse dimensions of the analyzed components are not small compared with the perturbation wavelength and there is the necessity of a detailed flow investigation including non linear effects, a 3-D approach must be utilized: in this case a 3D non linear approach [38-39]. However, due to the large computing requirements, the complete engine system cannot be modeled, and the 3-D investigation must be focused only on the analysis of some components, such as junction, fuel injector, intake and exhaust valve regions.

For the prediction of performance of a silencer in a non linear regime, the non linear gas dynamic models in time-space domain are usually preferred [39-40]. In fact, the time space domain method is more useful for understanding the non linear acoustic field and its physics,

since this method is similar to actual experiments. Tam *et al.* [41] computed the reflection of the silt resonator by using a high-order finite-difference-method (FDM) in the time–space domain; his findings agreed well with experimental results. Dickey *et al.* [42] investigated the acoustic behavior of a perforated tube silencer at a high level of sound. Hwang *et al.* [44] calculated the insertion loss (a characteristic parameter) of an exponential pipe silencer for an N-wave of a single frequency. Cho *et al.* [69] predicted nonlinear acoustic propagation in a lined duct for single frequency sinusoidal and saw-tooth waves. These works demonstrate that time–space domain methods are more attractive than traditional frequency-domain approaches for analyzing non linear acoustic performance and understanding the related physics.

However, due to physical and numerical issues [45], it is challenging for engineers, who work in related industrial fields, to apply the time–space domain computational aero-acoustic techniques for the assessment of the acoustic performance of silencers. In fact, acoustic waves are intrinsically unsteady, their amplitudes are several orders smaller than the mean flow and their frequencies are generally very high. Thus, to ensure that the computed solution is uniformly accurate over the entire computational domain, the numerical scheme must be free of numerical dispersion, dissipation and anisotropy [45].

More recently, in order to overcome the limitations of linear acoustic and non-linear fluid dynamic methods, some hybrid approaches, retaining the features of both models, have been developed. In the hybrid methods, the non-linear time-domain analysis is performed to compute the evolution of the thermodynamic condition of the cylinder and associated valve gas flow, while acoustic frequency-domain theory is applied to the intake/exhaust system. Due to the cyclic characteristics of engine operations, the Fourier transformations are used to pass from one domain to the other one. In this way, the information between the simulations carried out in time domain and the frequency domain are inter-changed [46-47].

A recent example of the first group is the work by Shaw *et al.* [48], where fluctuating velocities predicted from 1D gas dynamics simulations were used as input to linear boundary element simulations, but without taking into account the frequency-dependence of the boundary impedance at the coupling section.

An example of how nonlinear effects can be included in a one-port source model was suggested by Rämmäl and Bodén [49]. The method of coupling acoustic 1D nonlinear simulations to 3D nonlinear CFD is provided as a built in function in some commercial software packages but is still not very useful for acoustic optimization due to extremely long computational times.

EXPERIMENTAL METHODS

In the Chapter 4 the main experimental techniques for the description of the acoustical behaviour of a ICE muffler are explained. This chapter also includes a detailed description of the acoustic laboratory of Tallinn University of Technologies (TTU), Tallinn, Estonia, where a period of studies has been spent in order to perform several experiments on mufflers. These latter were aimed on the improving, extension and validation of numerical results described in the Chapter 5.

One of the most utilized parameter to describe the attenuation performance of a muffler is probably the transmission loss (TL), which constitute the difference in the sound power level between the incident wave entering and the transmitted wave exiting the muffler when the muffler termination is anechoic; the

TL is a property of the muffler only. The muffler TL may be calculated from models but is difficult to measure. The TL can be measured by using the decomposition method [50]. This method is based on decomposition theory, which was originally used to measure acoustic properties in ducts (such as the absorption coefficient and surface impedance of absorbing materials). If a two microphone random-excitation technique is used, the sound pressure may be decomposed into its incident and reflected waves. After the wave is decomposed, the sound power of the input wave may be calculated.

The major drawback of the decomposition method is that an anechoic termination is required for measuring TL in order to carry out the sound power of the output wave. In practice, an anechoic termination could be constructed using a long exhaust tube, high absorbing materials, horn shaped pipes or an active sound anechoic termination. However, a “fully” anechoic termination is difficult to build, particularly one that is effective at low frequencies.

An acoustical element, like a muffler, can also be modeled via its so-called four-pole parameters [1]. Assuming plane wave propagation at the inlet and outlet, the four-pole method is a mean to relate the pressure and velocity (particle, volume, or mass) at the inlet to that at the outlet. Using the four-pole parameters, the transmission loss of a muffler can also be readily calculated. Furthermore, if the source impedance is known, the four-pole parameters of the muffler can be used to predict the insertion loss of the muffler system [1].

The experimental determination of the four poles has been investigated by many researchers. The most accepted approach today is the approach developed by Munjal and Doige [51] who proposed a two-source method for measuring the four-pole parameters of an

acoustic element or combination of elements. The method can also be used in the presence of a mean flow.

RESULTS OF DOCTORAL STUDIES

In the Chapter 5, all the results obtained and published in the three years of Ph.D., are shown and commented. In the work presented at the section 5.1 [52], the noise attenuation curve, expressed in terms of transmission loss (TL) versus frequency, of a three pass perforated muffler with end Helmholtz resonator is carried out. Different numerical analyses are employed. At first, a non-linear one-dimensional (1D) time domain approach is used to predict the TL profile in a low frequency range. 1D simulations, in fact, may be only applied under the hypothesis of a planar wave propagation. A linear 3D BEM in the frequency domain, specifically designed for acoustic applications, is utilized too. Obviously, such analysis allows to obtain more accurate results at high frequencies, depending on the mesh size. Different flow velocities and gas temperatures are investigated through the numerical models. The predicted TL profiles are compared and discussed in order to assess the potentiality and limitations of the employed numerical approaches.

The purpose of the works shown in the paragraph 5.2 [53-54] is to put evidence on advantages and disadvantages of the above mentioned 1D and 3D BE approaches in evaluating the acoustic performance of a commercial cross flow muffler, under different conditions. The studied silencer under is composed by three chambers and two perforated tubes. A 1D non linear acoustic approach in time domain and a 3D BEM acoustic linear approach in frequency domain have been utilized also in this work. Many information about this two different way to model the acoustic phenomenon have already been given, but here further practical applications and differences are highlighted. The 1D approach obviously assumes rigid wall hypothesis, while the BEM can take into account the surface vibrations is when a preliminary FEM modal analysis of the structure is realized. The computed structure natural frequencies can be imported in the BEM model in order to carry out the complex fluid-structure interaction. The effects of this last condition on TL calculation have been assessed and discussed. In addition, both flow and temperature effects have been included in the modeling and discussed with the previous analyses. Agreement among these numerical evaluations and related limitations have been put into evidence for different configurations.

In the work described in section 5.3 [55-56], the previous 1D-3D acoustical analysis of a commercial muffler, has been improved and experimentally validated. Features related to the manufacturing process, like the coupling of adjacent surfaces and the actual shape of components, have been noticed to heavily affect the muffler behaviour. Hence, although numerical analyses are usually performed on ideal geometries (perfectly matched and shaped), schematizations utilized for acoustic simulations of real mufflers are being suggested to do not neglect these important aspects. On the other hand, for a given initial muffler design, the manufacturing process is assessed to be a critical aspect also for its remarkable effects on the acoustics. The results have been carried out under different muffler operating conditions related to different mean flow velocities and presence or not of internal insulating material. 1D approach has also been utilized to evaluate the fluid dynamic behaviour of the studied muffler in terms of pressure drop when a mean flow is imposed. Also in this case, the 3D results are obtained in absence of mean flow. Finally, during the experimental tests, the muffler has been treated as an acoustic two-port element.

In the section 5.4 [57], acoustic and fluid-dynamic optimizations of the previously studied commercial muffler have been carried out. To this aim, an external optimizer, based on a genetic algorithm, has been coupled with the 1D solver in two different optimizations: the first one has been addressed on the improving of the muffler TL, in absence of mean flow, and in 100-800Hz frequency range. The second one has been focused on the best trade-off between acoustic and fluid-dynamic muffler performances, in terms of TL and Δp in 100-400Hz frequency range. The 3D BEM approach has not been used in the optimization process since it is much more time consuming, it is suitable and it has been validated only in absence of mean flow. Moreover, the investigated frequency range, which correspond to the range where most critical frequencies occur in typical operating conditions, is widely covered by the 1D approach.

REFERENCES

1. M.L. Munjal, *Acoustics of Ducts and Mufflers*, Wiley-Interscience, New York, 1987.
2. D.E. Winterborne, R.J. Pearson, *Design Techniques for Engine Manifolds*, SAE Int. Publisher, St. Edmunds, UK, 1999.
3. P.O.A.L. Davies, Piston Engine Intake and Exhaust System Design, *Journal of Sound and Vibration* (1996) 190 (4), 677-712.
4. S.H. Kim, J.M. Lee, A practical method for noise reduction in a vehicle passenger compartment, *Trans. of ASME*, January 1998, vol.120.
5. L.L. Beranek, I.L. Ver, *Noise and Vibration Control Engineering: Principles and Applications*. New York: John Wiley and Sons Inc. , 1992.
6. M. Abom, Measurement of the scattering matrix of acoustical two-ports, *Mechanical systems and signal processing* (1991) 5 (2), 89, 104.
7. J.W. Sullivan, M.J. Crocker, Analysis of concentric-tube resonators having un-partitioned cavities, *Journal of Acoustical Society of America*. 64, 207-215 (1978).
8. J.W. Sullivan, A method of modelling perforated tube muffler components – I Theory, *Journal of Acoustical Society of America*. 66, 772–778 (1979).
9. J.W. Sullivan, A method of modelling perforated tube muffler components - II Applications, *Journal of Acoustical Society of America*. 66, 779–788 (1979).
10. K. Jayaraman, K. Yam, Decoupling approach to modelling perforated tube muffler components, *Journal of Acoustical Society of America*. 69, 390–396 (1981).
11. P.T. Thawani, K. Jayaraman, Modelling and applications of straight through resonators, *Journal of Acoustical Society of America*. 73, 1387–1389 (1983).
12. K.N. Rao, M.L. Munjal, A generalized decoupling method for analyzing perforated element mufflers, *Nelson Acoustic Conference*, Wisconsin (1984).
13. K.S. Peat, A numerical decoupling analysis of perforated pipe silencers, *Journal of Sound and Vibrations*. 123, 199–212 (1988).
14. M.L. Munjal, Analysis of a flush-tube three-pass perforated muffler by means of transfer matrices, *International Journal of Sound and Vibration*. 2 (2) (1997) 63–68.
15. M.L. Munjal, Analysis of extended-tube three-pass perforated element muffler by means of transfer matrices, *Proceedings of the Fifth International Congress on Sound and Vibration*, Adelaide, South Australia, 15–18 December 1997, Vol. III, pp. 1701–1714.
16. A. Selamet and V. Easwaran, Three-pass mufflers with uniform perforations, *The Journal of the Acoustical Society of America*, Volume 105, Issue 3, March 1999, pp.1548-1562.
17. M.L. Munjal, Analysis and design of pod silencers, *Journal of Sound and Vibration*. 262 (2003) 497–507.
18. T. Kar, M.L. Munjal, Generalized analysis of a muffler with any number of interacting ducts, *Journal of Sound and Vibration*. 285 (2005) 585–596.
19. J.G. Ih, B.H. Lee, Analysis of higher order mode effects in the circular expansion chamber with mean flow, *Journal of the Acoustical Society of America*. 77, 1377-1388, 1985.

20. M. Abom, Derivation of four-pole parameters including higher order mode effects for expansion chamber mufflers with extended inlet and outlet. *Journal of Sound and Vibration*. 137(3), pp. 403-418.
21. R. Mittra, S.W. Lee, *Analytical Techniques in the Theory of Guided Waves*, Macmillan, NewYork, 1971.
22. A. Onorati A white noise approach for rapid gas dynamic modelling of IC engine silencers, *Proceedings of 3rd International Conference on Computers in Reciprocating Engines and Gas Turbines*, 219-228, 1996.
23. D. F. Ross, A finite element analysis of perforated component acoustic systems, *Journal of Sound and Vibrations*. 79, 133–143 (1981).
24. J. Kim, Y. Kim, J. Maeng, M. Lyu and Y. Ku, Unstructured grid finite volume analysis for acoustic and pulse wave propagation characteristics in exhaust silencer systems, *Numerical Heat transfer, Part A*, 30, 439-457, 1996.
25. O.Z. Mehdizadeh, M. Paraschivoiu, A three-dimensional finite element approach for predicting the transmission loss in mufflers and silencers with no mean flow, *Applied Acoustics*. 66 (2005) 902–918.
26. F. Ihlenburg, I. Babuska, S. Sauter, Reliability of finite element method for the numerical computation of waves. *Adv. Eng. Software* 1997;28:417–24.
27. F.D. Denia, A. Selamat, F.J. Fuenmayora, R. Kirby , Acoustic attenuation performance of perforated dissipative mufflers with empty inlet/outlet extensions, *Journal of Sound and Vibration*. 302 (2007) 1000–1017.
28. T.Tanaka, T. Fujikawa, , T. Abe, H.A. Utsuno, A method for the analytical prediction of insertion loss of a two-dimensional muffler model based on the transfer matrix method derived from the boundary element method. *ASME, Journal of Vibration, Acoustics, Stress and Reliability in Design*. 107 (1985) 86-91.
29. C.Y.R. Cheng, A.F. Seybert, T.W. Wu, A multi-domain boundary element solution for silencer and muffler performance prediction, *Journal of Sound and Vibration* - 19 November 1990.
30. Z.L. Ji Boundary element analysis of a straight-through hybrid silencer, *Journal of Sound and Vibration* 292 (2006) 415–423.
31. R. S. Benson, *The Thermodynamics and Gas Dynamics of Internal Combustion Engines*. Oxford, Clarendon Press, 1982.
32. A. Onorati, Numerical simulation of exhaust flows and tailpipe noise of a small single cylinder Diesel engine, *Society of Automotive Engineers*. Paper No. 951755, 1995.
33. F. Payri, A. J. Torregrosa, M. D. Chust, Application of MacCormack schemes to IC engine exhaust noise prediction, *Journal of Sound and Vibration*. 195, 757-773, 1996.
34. A. D. Jones G. L. Brown Determination of two-stroke engine exhaust noise by the method of characteristics, *Journal of Sound and Vibration*. 82, 305-327, 1982.
35. G. Ferrari, A. Onorati, Modellazione fluidodinamica non-lineare di silenziatori ad elementi perforati e con materiale fonoassorbente, *Proceedings of the 51st ATI Conference*, 937-952, 1996.
36. G. Montenegro, A. Onorati, A.d. Torre, The 3D cell approach for the acoustic modeling of after-treatment devices, *SAE 2011-24-0215*, 2011

37. P.O.A.L. Davies, E.A.A. Yaseen, The reflection of waves of finite amplitude at an open exhaust, *Journal of Sound and Vibration* 122, 594-597, 1988.
38. A. Broatch, X. Margot, A. Gil, F.D. Denia, A CFD approach to the computation of the acoustic response of exhaust mufflers, *Journal of Computational Acoustics*, 13 (2); 301-316, June 2005.
39. A. Broatch, J.R. Serrano, F.J. Arnau, D. Moya, Time domain computation of muffler frequency response: comparison of different numerical schemes, *Journal of Sound and Vibration*, 305:333-347, 2007.
40. A. Onorati, G. Ferrari, Calculation of complex silencer performances by non-linear fluid dynamic simulation models, *Proceedings of the International Conference Inter-Noise '94*, Yokohama, Japan, 1994, pp.1631-1634.
41. C.K.W. Tam, H. Ju, M.G. Jones, W.R. Watson, T.L. Parrott, A computational and experimental study of slit resonators, *Journal of Sound and Vibration*. 284 (2005) 947-984.
42. N.S. Dickey, A. Selamet, J.M. Novak, The effect of high-amplitude sound on the attenuation of perforated tube silencers, *Journal of the Acoustical Society of America*. 180 (3) (2000) 1068-1081.
43. C. Hwang, D.J. Lee, K.S. Chae, Time accurate finite difference method for performance prediction of a silencer with mean flow and non linear incident wave, *Journal of Mechanical Science and Technology*. 21 (1)(2007)1-11.
44. C.H. Cho, D.J. Lee, Time domain simulation of non linear acoustic propagation in a lined duct, 29th AIAA Aero acoustics Conference, 2008, pp. 2008-2830.
45. C.K.W. Tam, Computational aero acoustics: issues and methods, *AIAA Journal* 33 (1995)1788-1796.
46. O. Chiavola, Multi-dimensional CFD-transmission matrix modelling of IC engine intake and exhaust systems, *Journal of Sound and Vibration*. 256 (2) (2002) 835-848.
47. M. Knutsson, Modelling of IC-Engine Intake Noise, doctoral thesis, KTH, Stockholm, Sweden, 2009.
48. C.E. Shaw, D.J. Moenssen, W.C. Montgomery, On the use of BEA with engine simulation as an input to predict air induction inlet noise, *SAE Technical Paper* 2005-01-2350, 2005.
49. H. Rämmäl, H. Bodén, Modified multi-load method for nonlinear source characterization, *Journal of Sound and Vibration*. 299 (2007) 1094-1113.
50. A.F. Seybert, D.F. Ross, Experimental Determination of Acoustic Properties Using a Two microphone Random Excitation Technique, *Journal of Acoustical Society America*. 61, 1362-1370 (1977).
51. M.L. Munjal, A.G. Doige, Theory of a Two Source-location Method for Direct Experimental Evaluation of the Four-pole Parameters of an Aeroacoustic Element, *Journal of Sound and Vibration*. 141(2), 323-333 (1990).
52. D. Siano, F. Auriemma, F. Bozza, A Correlation Study of Computational Techniques of a Three Pass Perforated Tube Muffler Including FEM and 1D Methods, *SEEP* 2009.

53. D. Siano, F. Auriemma, F. Bozza, Pros and Cons of Using Different Numerical Techniques for Transmission Loss Evaluation of a Small Engine Muffler, SAE Paper 2010-32-0028, Linz, 2010.
54. D. Siano, F. Auriemma, F. Bozza, Svantaggi e Vantaggi Legati all'Utilizzo di Diversi Metodi Numerici per la Caratterizzazione Acustica di un Silenziatore per Applicazioni Automobilistiche, ATI Cagliari, 2010
55. D. Siano, F. Auriemma, F. Bozza, H. Rämäl, Validation of 1D and 3D Analyses for the Prediction of an Automotive Silencer Performance, SAE Technical Paper SAE 2011-24-0217, 2011.
56. R. Kabral, H. Rämäl, J. Lavrentjev, F. Auriemma, Acoustic Studies on Small Engine Silencer Elements, SAE Technical Paper SAE 2011-32-0514, 2012
57. F. Auriemma, F. Bozza, Acoustic and Fluid-dynamic Optimization of an Automotive Muffler, *in submission*.

Chapter 1

Fundamentals of silencers

1.1 INTRODUCTION

The intake/exhaust system design process is a demanding task for engineers, since it involves the study of a number of interacting elements (air box, turbocharger, engine, catalytic converter, silencer) whose functioning and operating conditions are mutually influenced. Moreover, the above systems are often deputed to accomplish contradictory functions, in a way that compromise choices must be taken. In particular, the purpose of an exhaust system is to *efficiently* evacuate the exhaust gasses. Obviously, a secondary task of noise reduction is compulsory, as well as a consistent pollutant reduction. The above mentioned word “*efficiently*” means without exerting high pressure losses which can affect the engine performances in terms of fuel consumption and output power. In fact, the air treatment and noise reduction performed by these devices, is always associated with pressure losses, in a way that the best trade-off between minimizing noise emission and maximizing engine output and fuel efficiency must be achieved [1].

The choice of the correct trade-off is usually guided by the requirements of quality vehicle, which can be used to differentiate the brands or the models (cheapness, high comfort, sport attitude) [2]. This optimization process is completely defined by including geometrical constraints, i.e. the available space for setting up the systems. For example, in passenger cars the silencer is often located behind the rear axle, adjacent to the spare tire, which inevitably limits the total volume and imply a specific outer form and layout. Other constraints of the problem are the unit cost, the reliability, the durability and the complexity of the designed system [3].

In the past decades the design procedure was usually based on the empirical experience and background of designers, implying time consuming and expensive “build and test” procedures. Nowadays, the design phase has been strongly improved thanks the aiding of numerical simulation models. They permit the development of integrated design strategies,

where conflicting requirements are simultaneously accounted during the development loop [4].

An integrated design process usually starts from the evaluation of the pressure waves generated by the periodic charging and discharging process occurring in the engine. In fact, aerodynamic processes associated with the cyclic flow through the valves, separation and vortex generation at junction and expansion sections, constitute the source of intake and exhaust noise. These processes involve a transfer of flow energy to wave energy generating noise, which is radiated at open terminations. Consequently the intake and exhaust acoustic emissions can be controlled either by reducing the energy transfer from sources or by silencing the noise propagating in the duct system [1].

Concretely, the spectral characteristics of exhaust pulses are dominated by a sequence of discrete tones related to the engine firing frequency. The fundamental frequency of an n_{cyl} cylinders engine is F_0 :

$$F_0 = n_{cyl} \frac{rpm}{60\epsilon} \quad (1.1)$$

where rpm are the engine revolutions per minute, and ϵ equal to 1 or 2 for a 2 stroke or a 4 stroke engine respectively. For a four stroke 4 cylinder engine, it corresponds to the second engine order frequency, where the k -engine order frequency is defined as

$$F_0 = k \frac{rpm}{60} \quad (1.2)$$

This frequency and its entire multiplies detect the most critical acoustic conditions due to the discharging process. Consider, for example a 4-cylinder, 4-stroke automobile engine driven at 3000 rpm. The fundamental tone in the exhaust noise corresponds to gas scavenging of cylinders, twice per revolution, giving a frequency of 100 Hz. Additionally, a number of overtones are typically obtained as well, i.e. tones at 200 Hz, 300 Hz. Because of high velocity of the gas through valve orifices and the exhaust manifold (at temperature around 900-1200 °C), broad banded sound is also generated, with maximal strength somewhere between a half and a few kHz. The sound generated because of the coupling between the turbulent average flow field and the acoustic field is said to be *self-excited* [3].

Object of this study are the silencers utilized in the exhaust system of internal combustion engines (ICE). In the present chapter they will be described and classified, as well as the main functioning parameters will be introduced. The resonant systems constituting silencers will be presented, as well as the classical transfer-matrix approach for the study of these components. Also the dissipative silencers are described, aimed to attenuate broadband noise with minimum pressure drop. A number of attenuation curves of different typologies of silencers are included in this chapter: the numerical 1D results shown in this chapter are performed with the package software GTPowerTM based on non-linear time-domain approach.

1.2 SILENCERS CLASSIFICATION

The silencers are passive noise control devices, also known as *mufflers* (amer.), whose performance is a function of the geometric and sound-absorbing properties of their component. Other kind of devices for noise control in duct systems are the active noise control silencers, whose cancellation features are controlled by various electromechanical feed-forward and feedback techniques [5]. These latter are not object of the present study.

The operations of noise cancelling performed by the silencers can be regarded as based on two different principles: reflection of sound waves and dissipation of acoustic energy. Silencers based on the first principle are said to be *reactive*, and are used to abate sound consisting of discrete tones, especially in low frequency region. Silencers based on the latter principle are called *resistive*, and are those best suited to addressing high frequency broadband noise. In practice, most silencers are a synthesis of the two types.

Wave reflections happen every time a wave encounters a physical discontinuity, such as a cross section variation (expansion or restriction) and a temperature gradient. Simply reflective components exhibit attenuation minima at each time an acoustically significant length corresponds to an integer multiple of half the acoustic wavelength of the excitation, which is obviously undesired. With stationary piston engines this correspondence can be avoided by designing mufflers including a multiplicity of simple elements (such as chambers or tubes) which have different characteristic lengths. In this way, the attenuation minimum at a certain frequency of one of the constituting muffler element, is compensated by the maximum attenuation exerted by another element. Anyway, the introduction of reactive elements, such

as flow reversal, perforations on tubes and baffles, and fibrous packing, is often needed in order to damp acoustic resonances [1].

1.3 MODELS OF SOURCE, SILENCER AND TERMINATION

1.3.1 ONE-PORT MODEL OF THE SOURCE

Fundamentals of acoustic theory will be given in the chapters 2, 3 and 4, where the wave equation will be introduced and numerically integrated, as well as the travelling waves in ducts will be experimentally measured thorough the use of a proper microphone setup.

What is of interest in this section is that, in the duct system, connecting a muffler to an ICE (*exhaust pipe*) and in the one connecting the muffler to the external environment (*tail pipe*), the assumption of plane wave propagation is realistic. Plane wave propagation means uniformity of the physical properties (pressure, particle velocity, temperature), on the points belonging to the generic cross section, at a time t . This hypothesis stands whenever the transverse dimensions of the duct are a small fraction of the significant wavelengths. Moreover, when the fluctuating pressure amplitude remains a small fraction of the ambient pressure, the waves propagate without change of shape, and one can adopt the acoustic approximation of describing the wave motion by linear acoustic models in the frequency domain [1].

In the chapter 4 will be shown that, a generic spectral component of a plane wave, with wavenumber $k=2\pi f/c$ or ω/c , can always be seen as a sum of a progressive and a regressive plane wave, travelling in the two opposite directions of the duct. Therefore, with plane acoustic waves, at each frequency the spectral component amplitudes of pressure and particle velocity are respectively expressed by

$$\hat{p} = \hat{p}_+ + \hat{p}_- \quad (1.3)$$

and

$$\hat{u} = \hat{u}_+ + \hat{u}_- \frac{\hat{p}_+ - \hat{p}_-}{\rho_0 c} \quad (1.4)$$

where \hat{p}_+ and \hat{p}_- are the amplitudes of the progressive and regressive free plane waves, ρ_0 and c_0 are, respectively, the local ambient density and sound speed.

Acoustic *one-port source* models can be used to calculate the acoustic field generated in duct systems by fluid machines, e.g., pumps, fans, IC-engines. They can also be used for the design of mufflers and silencers, and to gain a better understanding for the sound generating mechanisms in the machines. The source has to behave as a linear time invariant system for the one-port model to be valid. For machines such as IC engines and compressors, which generate high sound levels in the connected pipes, the condition of linearity might be violated. There is therefore a need for experimental methods to check if the conditions of linearity and time invariance are fulfilled [6,7]. If a linear time-invariant model is applicable for the machine it can be described as an acoustic one-port source.

The behaviour in the frequency domain of the one-port (see Fig. 1.1) can be described by:

$$\hat{p}_+ = R_s \hat{p}_- + \hat{p}_+^s \quad (1.5)$$

where R_s is the source reflection coefficient at cross section at $x=0$, and \hat{p}_+^s is the source strength. The source strength can be interpreted as the pressure generated by the source-side when the system is reflection free.

In the literature the source model for one-ports is often expressed in terms of source strength and normalized source impedance Z_s :

$$\hat{p} = \hat{p}_s - Z_0 Z_s \hat{q} \quad (1.6)$$

where \hat{p}_s is the source pressure, \hat{p} and \hat{q} are acoustic pressure and volume velocity respectively ($\hat{q} = S\hat{u}$ where S is the tube cross section area and \hat{u} is the particle velocity), and Z_0 is the characteristic impedance of the fluid ($Z_0 = \rho c / S$, where ρ is the air density and c is the sound velocity). The source impedance Z_s represents the acoustic impedance seen from the reference cross section towards the source.

The Figure 1.2 shows the equivalent acoustic circuit for a linear and time invariant source. In this figure \hat{p} and Z denote the acoustic load data (the load pressure and the load impedance), while \hat{p}_s , \hat{q}_s and Z_s denote the source data respectively. Theoretically the two

representations a) and b) of the source shown in the Figure 1.2 are equivalent, and it is possible to go from one representation to the other by using the relationship $\hat{q}_s = \hat{p}_s / Z_s$.

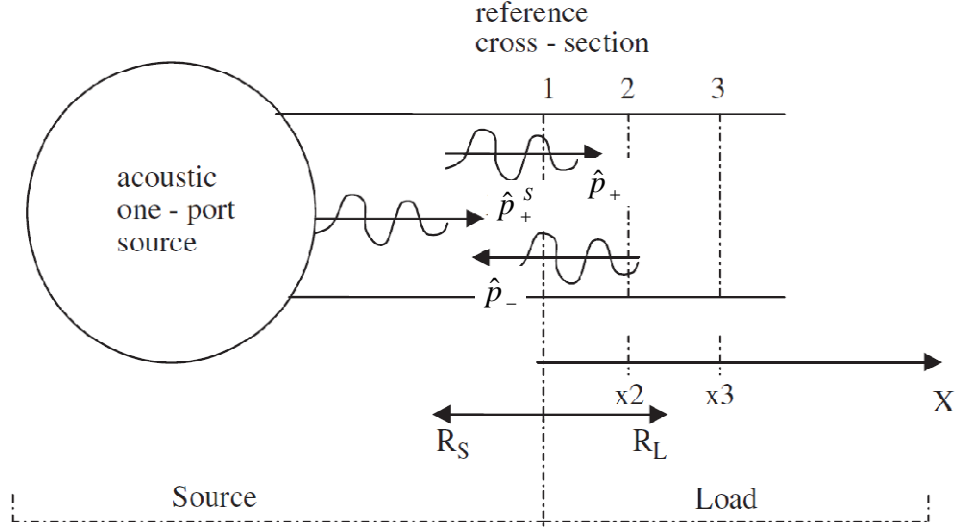


Figure 1.1 – An in-duct source modelled as an acoustic one-port.

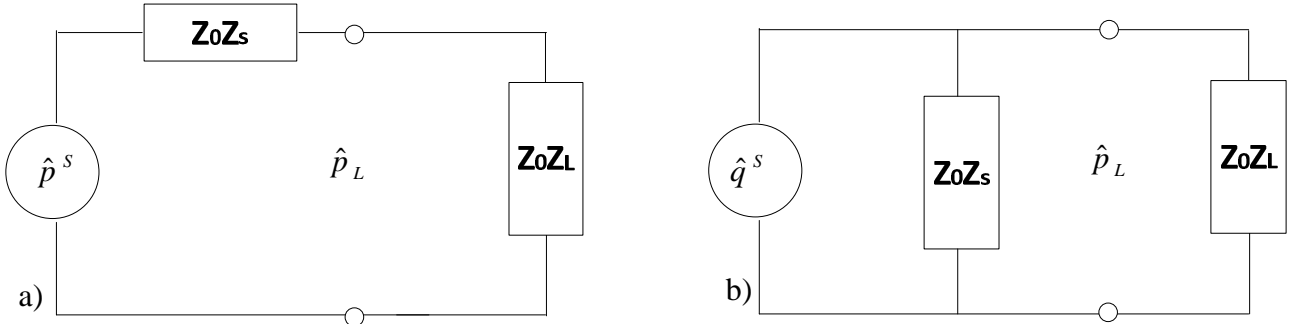


Figure 1.2 – Equivalent acoustic circuits for linear time invariant source. (a) Pressure source, (b) volume velocity source.

The Figure 1.3 illustrates source impedance from a practical standpoint. The sound waves generated by the source propagate along the duct. While a portion of the energy propagates through the attenuating element, some of the energy is reflected by the attenuating element back to the source. The reflected sound waves, though partially absorbed by the source, are also reflected back from the source. The amount of sound energy reflected or absorbed by the source is a function of the source impedance [8].

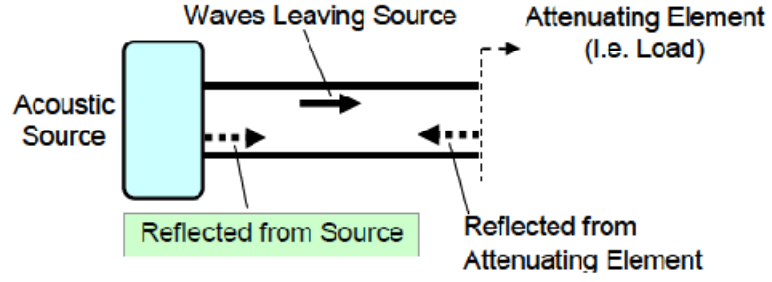


Figure 1.3 – Schematic of a realistic source.

1.3.2 TWO-PORT MODEL OF THE SILENCER

An efficient way to analyze the sound transmission, when linear theory is valid, is acoustical two-port theory (see chapter 4) [9]: the relation between the input and output states of a time-invariant and passive two-port can be written, in the frequency domain, as

$$\mathbf{y} = \mathbf{H}\mathbf{x} \quad (1.7)$$

where \mathbf{x} and \mathbf{y} are the state vectors at the inlet and outlet, \mathbf{H} is a $[2 \times 2]$ matrix which is independent of \mathbf{x} and \mathbf{y} .

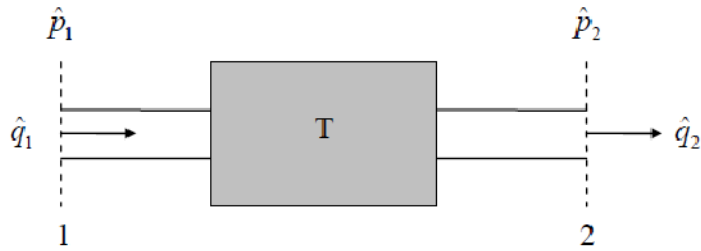


Figure 1.4 – Schematic of a two-port source for transfer matrix determination.

In particular, considering state vector composed by pressure and volume velocities (i.e. the product cross section area S times particle velocity u) with, $\mathbf{x}=[p_a, q_a]^T$ and $\mathbf{y}=[p_b, q_b]^T$, (the subscript a and b indicate the inlet and outlet respectively), after the inversion of \mathbf{H} matrix, one obtains:

$$\mathbf{x} = \mathbf{T}\mathbf{y} \quad (1.8)$$

that is:

$$\begin{bmatrix} \hat{p}_a \\ \hat{q}_a \end{bmatrix} = \begin{bmatrix} T_{11} & T_{12} \\ T_{21} & T_{22} \end{bmatrix} \cdot \begin{bmatrix} \hat{p}_b \\ \hat{q}_b \end{bmatrix} \quad (1.9)$$

The matrix

$$\mathbf{T} = \begin{bmatrix} T_{11} & T_{12} \\ T_{21} & T_{22} \end{bmatrix} \quad (1.10)$$

is called *transfer matrix* and it is widely utilized to describe the behaviour of mufflers and its acoustical parameters. It can be seen, from the equation (1.9), that

$$T_{11} = \left. \frac{\hat{p}_a}{\hat{p}_b} \right|_{\hat{q}_b=0} \quad T_{12} = \left. \frac{\hat{p}_a}{\hat{q}_b} \right|_{\hat{p}_b=0} \quad (1.11)$$

$$T_{21} = \left. \frac{\hat{q}_a}{\hat{q}_b} \right|_{\hat{q}_b=0} \quad T_{22} = \left. \frac{\hat{q}_a}{\hat{p}_b} \right|_{\hat{p}_b=0}$$

In this way it is possible to give a physical interpretation to each of the 4 terms belonging to the T matrix. For example: T_{11} represents the ration of the upstream pressure and downstream pressure for the hypothetical case of the downstream end being rigidly fixed ($Z_L=\infty$); T_{12} is the ration of the upstream pressure to the velocity at the downstream end for the hypothetical case of the downstream end being totally free or unconstrained ($Z_L=0$) [10].

One advantage of using the transfer-matrix formalism is that a cascade-coupled chain of n elements easily can be combined to yield a representation of a complete system. Mathematically this corresponds to a series of matrix multiplications as

$$\mathbf{T} = \mathbf{T}_1 \cdot \mathbf{T}_1 \cdot \dots \cdot \mathbf{T}_n \quad (1.12)$$

Here, it has been assumed that there is continuity of p and q at the element interfaces. This is strictly valid only for interconnections in a straight duct where only entirely plane waves exist. If the element interface has to be located at a sudden expansion, a special coupling two-port matrix has to be introduced to handle the discontinuity [10].

1.3.3 SOURCE-SILENCER-TERMINATION MODEL

Once the acoustic source has been schematized through a one-port model and the silencer through a two-port model, the entire system composed by the noise source, the silencer, and obviously the connecting pipes and the surrounding medium can be analyzed (see Figure 1.5a).

The exhaust pipe connecting the source to the silencer can be seen as a part of the source. In the Figure 1.5b the electrical system analogue to the acoustical one is shown. Also in this model the pressure \hat{p} is used instead of the voltage and the volume velocity \hat{q} instead of current. \hat{p}_s is the source pressure and Z_s is its internal impedance. **T** and **D** are respectively the muffler and the pipe segment transfer matrices. Z_L is the impedance of the termination.

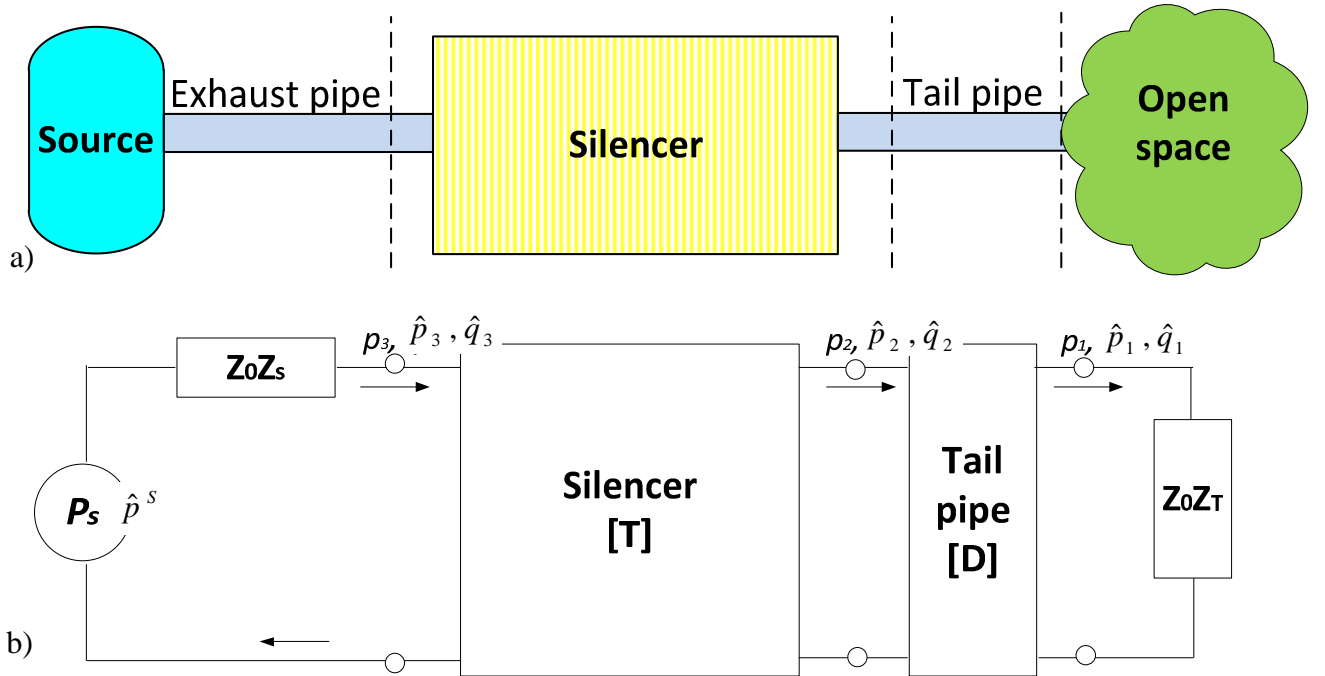


Figure 1.5 – a) Schematic of a source-silencer-termination system; b) Equivalent acoustic circuit.

Let \hat{p}_i and \hat{q}_i , $i = 1, 2, 3$, designate the acoustical pressure and volume velocity at the interfaces of the acoustical components of the source–silencer–load system. These quantities may be obtained by solving the system of equation describing the response of the components shown in Figure 1.5b:

$$\hat{p}_3 = \hat{p}_s - Z_0 Z_s \hat{q}_3 \quad (1.13)$$

$$\begin{bmatrix} \hat{p}_3 \\ \hat{q}_3 \end{bmatrix} = \begin{bmatrix} T_{11} & T_{12} \\ T_{21} & T_{22} \end{bmatrix} \cdot \begin{bmatrix} \hat{p}_2 \\ \hat{q}_2 \end{bmatrix} \quad (1.14)$$

$$\begin{bmatrix} \hat{p}_2 \\ \hat{q}_2 \end{bmatrix} = \begin{bmatrix} D_{11} & D_{12} \\ D_{21} & D_{22} \end{bmatrix} \cdot \begin{bmatrix} \hat{p}_1 \\ \hat{q}_1 \end{bmatrix} \quad (1.15)$$

$$\hat{p}_1 = Z_0 Z_T \hat{q}_1 \quad (1.16)$$

The calculated quantities \hat{p}_i , \hat{q}_i , $i=1,2,3$, can be then utilized for the evaluation of the selected silencer performance criterion.

1.4 SILENCER PERFORMANCE CRITERIA

The performance of an acoustic filter is measured in terms of one of the following parameters [10]:

- Insertion loss (IL)
- Transmission loss (TL)
- Level difference (LD), or noise reduction (NR)

All these parameters are based on sound power difference as a performance indicator. Consequently they do not require any explicit knowledge of the source strength p_s of equation (1.13).

The IL is defined as the difference between the sound pressure levels (L_b and L_a) measured in a certain relative position, with respect the exhaust outlet, before and after the installation of the silencer (see Figure 1.6). In this two configuration, the exhaust pipe l_1 and the tail pipe l_2 can have different lengths.

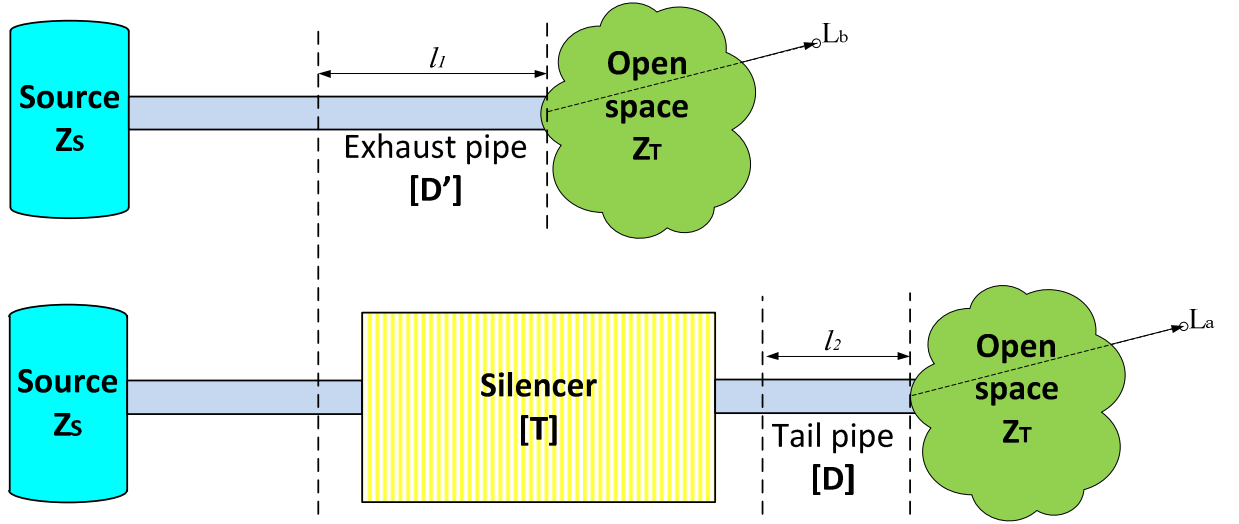


Figure 1.6 – Scheme for insertion loss determination.

Symbolically:

$$IL = L_b - L_a \text{ (dB)} \quad (1.17)$$

or, in terms of acoustic pressure p_b and p_a :

$$IL = 20 \text{Log} \frac{\hat{p}_b}{\hat{p}_a} \text{ (dB)} \quad (1.18)$$

The IL can be expressed in terms of transfer matrix elements:

$$IL = 20 \text{Log} \left| \frac{\bar{T}_{11} Z_T + \bar{T}_{12} + \bar{T}_{21} Z_S Z_T + \bar{T}_{22} Z_S}{D'_{11} Z_T + D'_{12} Z_S Z_T + D'_{22} Z_S} \right| \quad (1.19)$$

where \bar{T}_{ij} is the combined transfer matrix element of the silencer and its tail pipe ($\bar{\mathbf{T}} = \mathbf{T}\mathbf{D}$), and D'_{ij} are the transfer matrix elements of the replaced exhaust pipe. In case of $l_1 = l_2 = 0$, then both \mathbf{D} and \mathbf{D}' are identity matrices and equation (1.19) reduces to:

$$IL = 20 \text{Log} \left| \frac{T_{11} Z_T + T_{12} + T_{21} Z_S Z_T + T_{22} Z_S}{D'_{11} Z_T + D'_{12} Z_S Z_T + D'_{22} Z_S} \right| \quad (1.20)$$

The noise reduction is the difference between the sound pressure levels measure at upstream and downstream the silencer (pressures p_1 and p_2 in Figure 1.7):

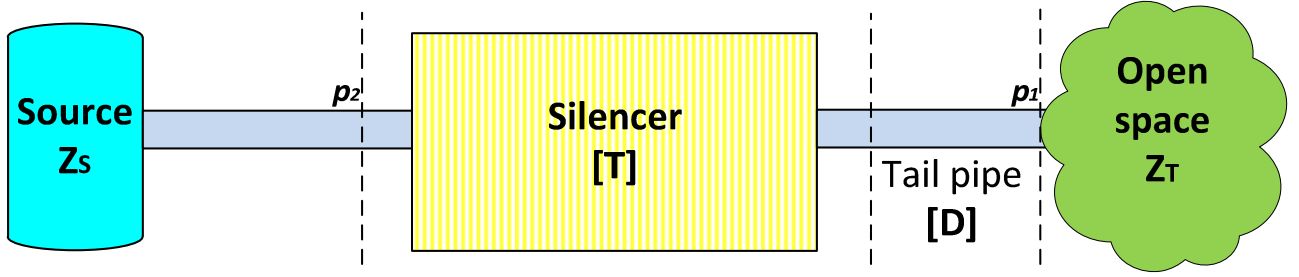


Figure 1.7 – Scheme for noise reduction determination.

Mathematically :

$$NR = L_2 - L_1 = 20\text{Log} \left| \frac{\hat{p}_2}{\hat{p}_1} \right| \text{ (dB)} \quad (1.21)$$

If \mathbf{D} is the transfer matrix of the tail pipe and $\bar{\mathbf{T}}$ is the transfer matrix of the muffler, the NR can be written as:

$$NR = 20\text{Log} \left| \frac{\bar{T}_{11}Z_T + \bar{T}_{12}}{D_{11}Z_T + D_{12}} \right| \text{ (dB)} \quad (1.22)$$

The transmission loss describes the performance of the “proper silencer”, it is independent of the source and presumes an anechoic termination at downstream the silencer. TL is defined as the difference between the acoustical power incident on the silencer (LW_i) and that transmitted downstream into the anechoic termination (LW_t), see Figure 1.8.

Symbolically:

$$TL = LW_i - LW_t \text{ (dB)} \quad (1.23)$$

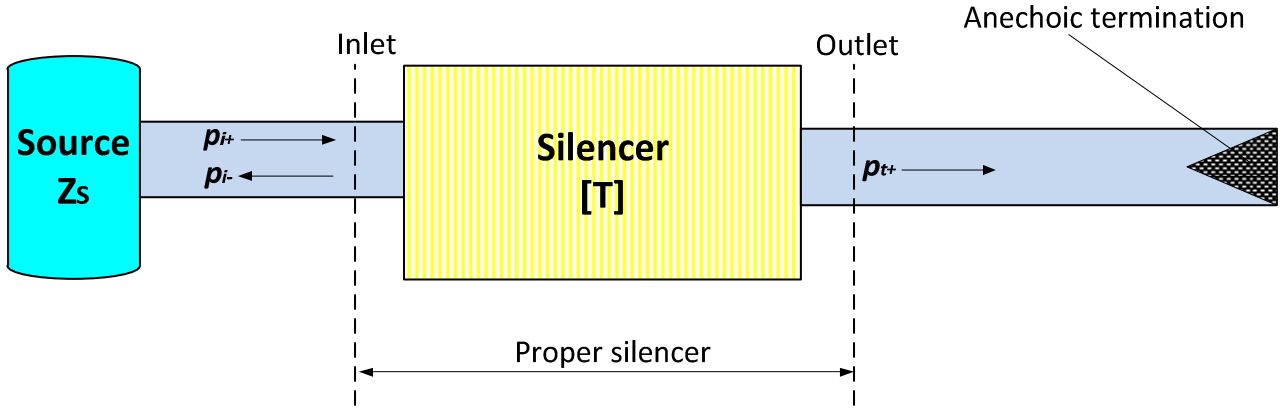


Figure 1.8 – Scheme for transmission loss determination.

As previously mentioned, in the duct the wave can be considered plane and, consequently, the acoustic power W can be expressed as a product of the acoustic pressure, the particle velocity and the duct cross section areas. In particular, in order to evaluate the *incident* and the *transmitted* acoustic power, not the entire acoustic pressure and velocity must be considered, but only the progressive components, at inlet and at outlet. Consequently, according to the wave decomposition theory expressed by equations (1.3) and (1.4), the utilized pressure and velocity contributions will \hat{p}_+^{in} and \hat{u}_+^{in} at inlet, and \hat{p}_+^{out} and \hat{u}_+^{out} at outlet. As a result:

$$\begin{aligned}
 LW_i &= 10\text{Log} \frac{W_i}{W_{ref}} = 10\text{Log} \frac{S_{in} \hat{p}_+^{in} \hat{u}_+^{in}}{10^{-12}} = 10\text{Log} \frac{S_{in} \hat{p}_+^{in} \hat{p}_+^{in} Z_0}{10^{-12}} = 10\text{Log} \frac{S_{in} (\hat{p}_+^{in})^2 Z_0}{10^{-12}} \\
 LW_t &= 10\text{Log} \frac{W_t}{W_{ref}} = 10\text{Log} \frac{S_{out} \hat{p}_+^{out} \hat{u}_+^{out}}{10^{-12}} = 10\text{Log} \frac{S_{out} \hat{p}_+^{out} \hat{p}_+^{out} Z_0}{10^{-12}} = 10\text{Log} \frac{S_{out} (\hat{p}_+^{out})^2 Z_0}{10^{-12}}
 \end{aligned} \tag{1.24}$$

where S_{in} and S_{out} are the cross section areas at inlet and outlet muffler, and $Z_0 = \rho c / S$ is the acoustic impedance of the medium. In conclusion:

$$TL = 20\text{Log} \frac{\hat{p}_+^{in}}{\hat{p}_+^{out}} + 10\text{Log} \frac{S_{in}}{S_{out}} \tag{1.25}$$

Also the TL can be expressed in terms of T_{ij} elements:

$$TL = 20\text{Log} \left(\frac{T_{11} + \frac{T_{12}}{Z_0} + T_{21}Z_0 + T_{22} \frac{S_{out}}{S_{in}}}{2} \right) + 10\text{Log} \frac{S_{in}}{S_{out}} \quad (1.26)$$

In the next section will be clarified the importance of the TL parameter, which will be extensively utilized in the results shown in the Chapter 5. For this reason another consideration must be done regarding TL in presence of mean flow. In this case, in fact, the (1.26) cannot be utilized, since the presence of a mean flow alters the expressions of the pressure and particle velocity [11].

It can be shown that the TL assumes the following expression:

$$TL = 20\text{Log} \left[\frac{1 + M_{in}}{1 + M_{out}} \left(\frac{T_{11} + \frac{T_{12}}{Z_{out}} + T_{21}Z_{in} + T_{22} \frac{Z_{in}}{Z_{out}}}{2} \right) \right] + 10\text{Log} \frac{Z_{out}}{Z_{in}} \quad (1.27)$$

where M_{in} and M_{out} are respectively the Mach number of the flow at inlet and outlet. Moreover, the equation (1.27) also contemplates the possibility to have different impedances at inlet and outlet, $Z_{in} = \rho_{in}c_{in}/S_{in}$ and $Z_{out} = \rho_{out}c_{out}/S_{out}$ respectively.

The various performance parameters have relative advantages and disadvantages: the IL is, for the user, the only criterion for the performance of a given filter, since it truly represents the performance of the acoustic filter. Anyway, it requires prior knowledge or measurement of the internal impedance of the source.

The TL does not involve the source impedance and the radiation impedance, since it represents the difference between incident acoustic energy and transmitted into an anechoic termination. Being made independent of the terminations, the TL finds favour of researcher who are sometimes interested in finding the acoustic transmission behaviour of an element or set of elements in isolation of the terminations. But measurements of the incident wave in a standing wave acoustic might be quite laborious (see chapter 4).

The NR does not require knowledge of source impedance and, like IL, it does not need anechoic termination. It is therefore the easiest to measure and calculate and has come to be used widely for experimental corroboration of the calculated transmission behaviour of a muffler [10].

1.5 REACTIVE SILENCERS

1.5.1 SILENCER EXEMPLIFICATION

As previously mentioned, the acoustic behaviour of a reactive silencer is mainly driven by reflection phenomena which occur inside the component and reflect the acoustic waves back to the source. A wave reflection happens every time a wave encounters a physical and, consequently, an impedance discontinuity. In case of reactive silencers such discontinuities are due to sudden cross area changes (e.g. expansion chambers), wall property changes (e.g. perforations along pipes), and combination of these ones [5].

The reactive silencers are made up by internal elements such as orifices, axial side-branches, flow reversal, duct segments connecting adjacent chambers, etc. The inner geometry of these components can be definitely complex. Anyway, imagining the path of a travelling progressive plane wave inside the muffler, the internal complex shape can be decomposed in a number of elementary elements, mainly straight tubes and expansion chambers (see Figure 1.9). The behaviour of each one of these elements is simpler to describe in terms of transfer matrix. As a result, the transfer matrix of the entire silencer can be easily obtained by utilizing the equation (1.12). For the silencer in Figure 1.9 one can write:

$$\mathbf{T} = \mathbf{T}_1 \cdot \mathbf{T}_1 \cdot \dots \mathbf{T}_g \quad (1.28)$$

A number of basic elements are here briefly analyzed and the corresponding transfer matrices are carried out. The common hypotheses are: plane wave behavior in presence of superimposed mean flow, acoustic linear approach and absence of thermal gradients. Moreover, the acoustical energy dissipation, that may result from friction between the gas and the rigid walls and from turbulence phenomena, is neglected.

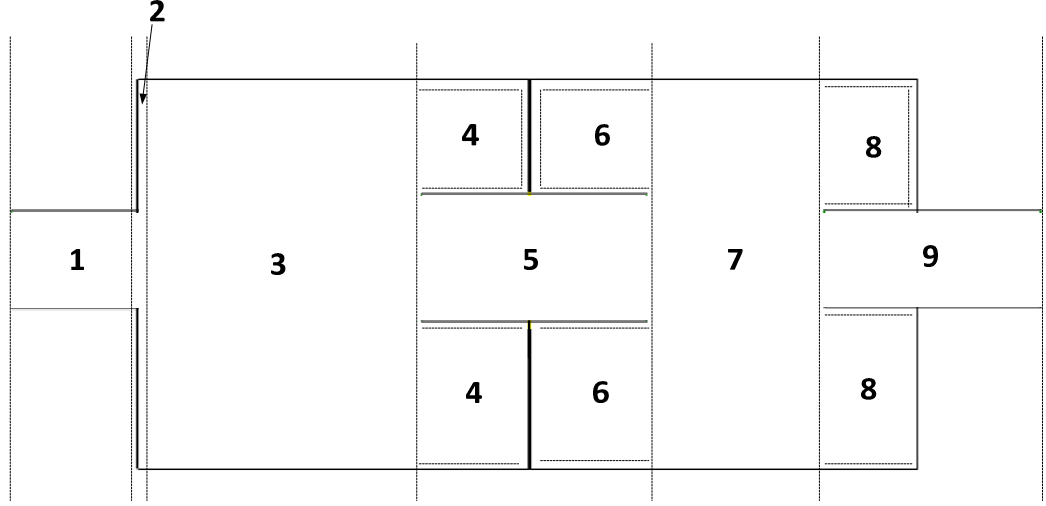


Figure 1.9 – Decomposition of a silencer into basic elements.

1.5.2 BASIC SILENCER ELEMENTS: STRAIGHT TUBE

In the Chapter 4 it will be shown that, when a plane wave travels, with a certain frequency $f=\omega/2\pi$, in a straight duct and in absence of mean flow, the acoustical pressure p and the particle velocity u at a certain point x along the duct are given by:

$$\mathbf{p}(x,t) = \hat{p}_+ e^{i(\omega t - kx)} + \hat{p}_- e^{i(\omega t + kx)} \quad (1.29)$$

$$\mathbf{u}(x,t) = \frac{\hat{p}_+}{\rho_0 c} e^{i(\omega t - kx)} - \frac{\hat{p}_-}{\rho_0 c} e^{i(\omega t + kx)} \quad (1.30)$$

where the bold print means that the variable concerned is complex and $i = \sqrt{-1}$. The subscript + and – respectively represent the progressive and regressive free plane wave constituting the plane wave, and $k=2\pi f/c$ is the wavelength (c is the speed of sound).

When a mean flow velocity V is imposed, the (1.29) and (1.30) must be changed in to:

$$\mathbf{p}(x,t) = \hat{p}_+ e^{i(\omega t - k_+ x)} + \hat{p}_- e^{i(\omega t + k_- x)} \quad (1.31)$$

$$\mathbf{u}(x,t) = \frac{\hat{p}_+}{\rho_0 c} e^{i(\omega t - k_+ x)} - \frac{\hat{p}_-}{\rho_0 c} e^{i(\omega t + k_- x)} \quad (1.32)$$

where $k_+ = k/(1+M)$ and $k_- = k/(1-M)$, being the number of Mach $M=V/c$. Instead of the particle velocity u , the volume velocity $q=Su$ (where S is the cross section area) can be utilized:

$$\mathbf{q}(x,t) = \frac{\hat{p}_+}{\rho_0 Y} \cdot e^{i(\omega t - k_+ x)} - \frac{\hat{p}_-}{\rho_0 Y} \cdot e^{i(\omega t + k_- x)} \quad (1.33)$$

where $Y=c/S$. Equations (1.31) and (1.33) can be evaluated at $x=0$ (beginning of the duct) and $x=l$ (end of the duct) in order to obtain the corresponding fields $\hat{p}_2, \hat{q}_2, \hat{p}_1, \hat{q}_1$, respectively. One can obtain:

$$\begin{bmatrix} \hat{p}_2 \\ \hat{q}_2 \end{bmatrix} = \begin{bmatrix} T_{11} & T_{12} \\ T_{21} & T_{22} \end{bmatrix}_{pipe} \cdot \begin{bmatrix} \hat{p}_1 \\ \hat{q}_1 \end{bmatrix} \quad (1.34)$$

where the transmission matrix \mathbf{T} is given by:

$$\begin{bmatrix} T_{11} & T_{12} \\ T_{21} & T_{22} \end{bmatrix}_{pipe} = e^{-iMl \frac{k_+ k_-}{k}} \begin{bmatrix} \cos \frac{k_+ k_- l}{k} & iY \sin \frac{k_+ k_- l}{k} \\ \frac{i}{Y} \sin \frac{k_+ k_- l}{k} & \cos \frac{k_+ k_- l}{k} \end{bmatrix} \quad (1.35)$$

1.5.3 BASIC SILENCER ELEMENTS: CROSS SECTIONAL DISCONTINUITIES

In the Table 1.I typical cross sectional discontinuities are represented. Terms C_1 and C_2 are utilized to satisfy the following compatibility relation between the cross sectional areas S_1, S_2, S_3 :

$$C_1 S_1 + C_2 S_2 + S_3 = 0 \quad (1.36)$$

For each configuration, the Table 1.I also shows the pressure loss coefficient K related to the partial conversion of mean flow energy and acoustical energy into heat [5].

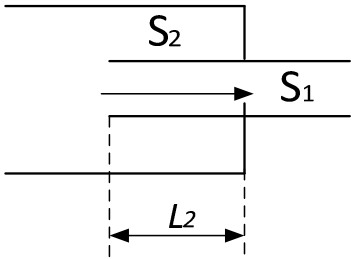
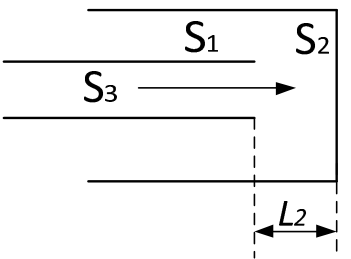
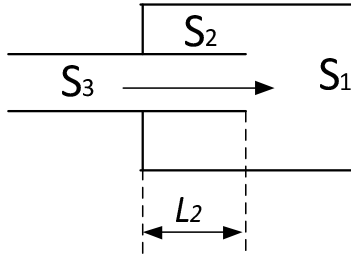
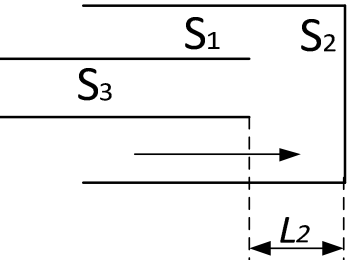
CROSS SECTIONAL DISCONTINUITY	C_1	C_2	K
	-1	-1	$\frac{1 - S_1/S_3}{2}$
	-1	1	$\left(\frac{S_1}{S_3} - 1\right)^2$
	1	-1	$\left(\frac{S_1}{S_3}\right)^2$
	1	-1	0.5

Table 1.I – Transition element parameters

Transfer matrices for cross discontinuities in presence of mean flow assume an exemplified expression when $M \ll 1$ and the terms $1 + M^n$ (with $n \geq 2$) are set to unity, which is a correct assumption in most silencer design. In this case one can obtain:

$$\begin{bmatrix} \hat{p}_2 \\ \hat{q}_2 \end{bmatrix} = \begin{bmatrix} T_{11} & T_{12} \\ T_{21} & T_{22} \end{bmatrix}_{disc} \cdot \begin{bmatrix} \hat{p}_1 \\ \hat{q}_1 \end{bmatrix} \quad (1.37)$$

$$\begin{bmatrix} T_{11} & T_{12} \\ T_{21} & T_{22} \end{bmatrix}_{disc} = \begin{bmatrix} 1 & KM_1 Y_1 \\ \frac{C_2 S_2}{C_1 S_2 Z_2 + S_2 M_3 Y_3} & \frac{C_2 S_2 F_2 - M_1 Y_1 (C_1 S_1 + S_3 K)}{C_2 S_2 Z_2 + S_3 M_3 Y_3} \end{bmatrix} \quad (1.38)$$

where $Z_2 = -i(c/S_2)\cot(kl_2)$, $Y_1 = c/S_1$ and $Y_3 = c/S_3$.

In the case of sudden expansion or sudden contraction $l_2 = 0$. In this case one can obtain:

$$\begin{bmatrix} T_{11} & T_{12} \\ T_{21} & T_{22} \end{bmatrix}_{disc} = \begin{bmatrix} 1 & KM_1 Y_1 \\ 0 & 1 \end{bmatrix} \quad (1.39)$$

Other important silencer elements are represented by the expansion chambers and the side-branch resonators. The second ones include quarter wave, Helmholtz and perforated tube resonators. All of these silencer components will be treated in the following sections [5].

1.6 ACOUSTIC BEHAVIOUR OF EXPANSION CHAMBERS

1.6.1 SIMPLE EXPANSION CHAMBERS

An expansion chamber is the simplest type of silencer, consisting of a cross section expansion, a straight chamber and a cross section contraction .

Obviously its behaviour can be described considering the above formulas related to cross section discontinuities and to the straight tubes. It can be shown that the transmission loss of a generic expansion chamber is equal to:

$$TL = 10 \log \left[1 + \left(\frac{S_1}{2S_2} - \frac{S_2}{2S_1} \right)^2 \sin^2(kl) \right] \quad (1.40)$$

From this expression, maximal attenuation is obtained when:

$$f_{\text{exp}} = \frac{nc}{4l} \quad (1.41)$$

where $n=1,3,5,\dots$. The above expressions means that the attenuation maxima happens when the length of the chamber coincides with an odd multiple of a quarter of wavelength. In fact, the wave reflected at area change at the chamber outlet contains a phase factor $\exp(i\pi)$ when it interferes with the field at inlet, which generate a destructive interference. The maximal attenuation increases with increasing magnitude of the area discontinuity [3].

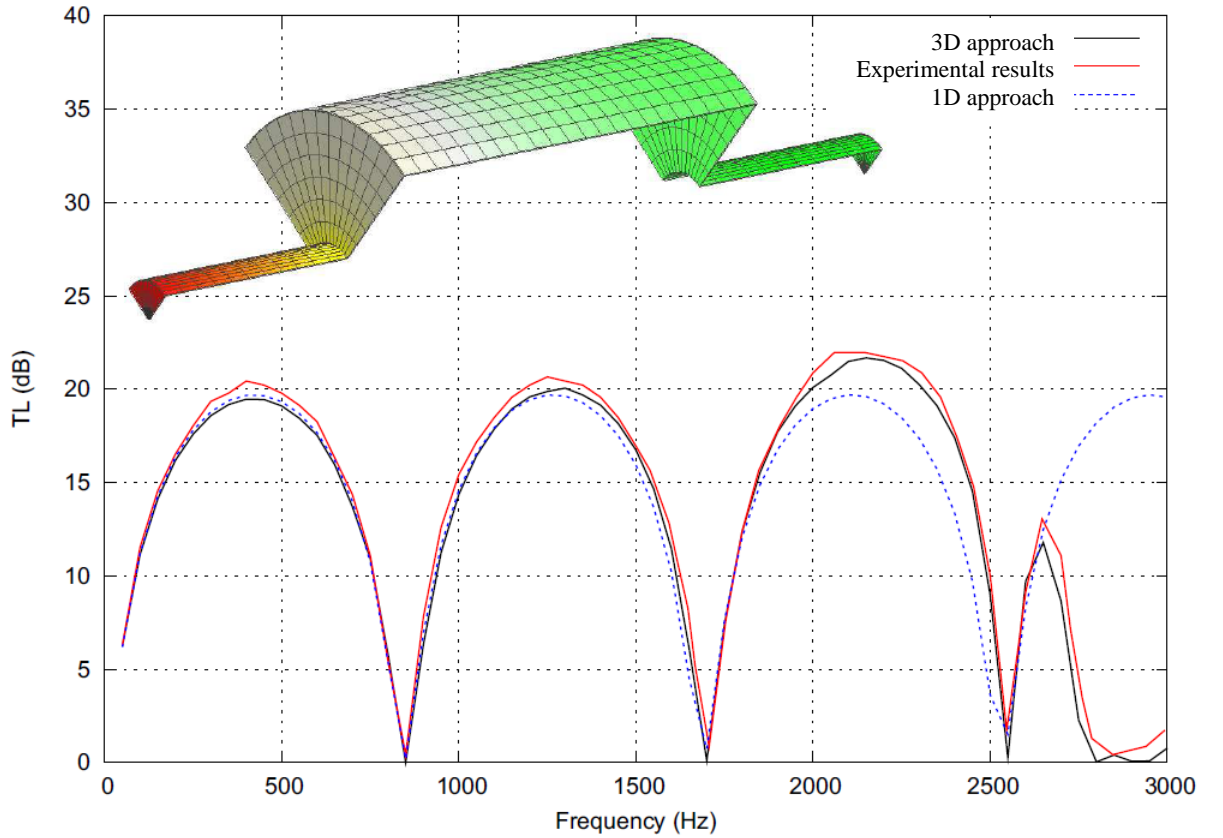


Figure 1.10 – Expansion chamber transmission loss: 1D, 3D numerical and experimental results.

The equation (1.44) and (1.45) are obtained in hypothesis of plane waves. The acoustic problem represented by the wave equation can be resolved utilizing a modal approach [3]. The result is that an infinite number of modes can be detected in a certain duct. The lowest mode is planar, and the cut-on-frequencies of the first higher order mode can be calculated, depending on the shape of the duct. For a circular duct, such as an expansion chamber, this frequency is:

$$f_{cut} = 1.841 \frac{c}{\pi D} \quad (1.42)$$

The Figure 1.10 shows the TL of an expansion chamber with centrally located inlet and outlet, obtained with a planar and a 3D approach. The latter one is able to take into account the higher order modes.

It can be noted that the 1D analysis is nevertheless not valid all the way up to the first “cut-on”. This is because the attenuation of higher modes is so low just beneath cut-on that a significant near field develops at the inlet and outlet. It is also evident a drastic reduction of the TL as more as higher modes propagates. When the inlet and outlet tube are perfectly centred on the axis chamber, a symmetrical problem arises and only radial varying modes are excited. Contrariwise, when the inlet and outlet tubes are eccentrically placed, the circumferentially varying higher modes are well driven, and the lowest cut-on frequency occurs at lower frequencies, clearly influencing the silencer behaviour [3].

1.6.2 EXTENDED OUTLET EXPANSION CHAMBERS

Expansion chambers provided of extended outlet pipe, represents a first successful attempt of improving the acoustic attenuation of a simple expansion chamber. In this case, the length of the extended outlet constitutes another *tuning* parameter, added to the length of the expansion chamber and the ratio S_1/S_2 of cross sections.

The extended outlet and the external chamber surface form a side branch element, in a way that this type of silencer can be decomposed into three basic components, as shown in Figure 1.11. The transfer matrix of the entire silencer can be obtained by multiplying the transfer matrices of the sudden cross section variation, the straight tube and the extended inlet, given by the equations (1.39), (1.34), (1.38) respectively.

It is noticeable that, for certain frequencies, the impedance Z_1 of the extended-outlet element approaches to zero, and the branch element generates a pressure release condition. In this situation the incident wave appears to interact with a closed-end-cavity, and no acoustical power is transmitted downstream. This condition occurs when $\cot(kL_I)=0$, corresponding to $kL_I/\pi=(2n-1)/2$. Consequently, a dominant peak in the source spectrum can be significantly reduced by proper selection of the tube length extended into the chamber.

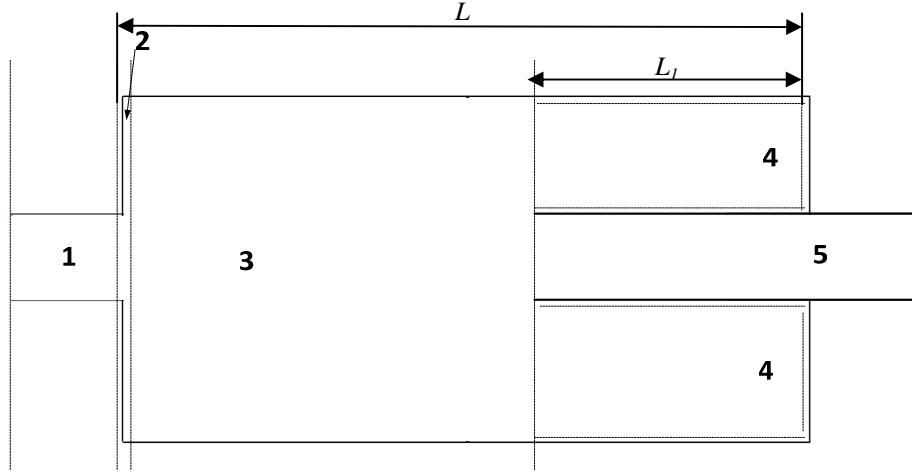


Figure 1.11 – Basic elements of an extended outlet expansion chamber.

1.6.3 DOUBLE TUNED EXPANSION CHAMBERS

A further enhancement of an extended outlet expansion chamber is the extended inlet-extended outlet configuration. In this case the silencer is also called double-tuned expansion chamber, since another *tuning* parameter is added, that is the length L_2 . The additional parameter can be used to enhance the silencer behaviour filling up the attenuation troughs of the extended outlet configuration, in a way to improve the TL over a broader frequency. L_1 and L_2 should be chosen so as to neutralize different sets of troughs [5].

Now the silencer can be decomposed into three basic elements, as shown in Figure 1.12: an extended inlet, a pipe element and an extended outlet, whose TL matrices are expressed by the equations (1.38), (1.34) and again (1.38) respectively. It is easy to show that, in order to better the attenuation performance, the conditions $L_1=L/2$ and $L_2=L/4$ is particularly favourable [5]. In fact the extended inlet element includes a term proportional to $\cot(kL_2)$, which produces stop bands at $kL=2(2n-1)\pi$, filling up the troughs at $kL/\pi=2,6,10\dots$. Similarly, since the extended outlet includes terms proportional to $\cot(kL_1)$, it produces stop bands at $kL=(2n-1)\pi$, filling up the troughs at $kL/\pi=1,3,5\dots$. In conclusion the only troughs will remain at $kL/\pi=4n$, n being an integer. Accordingly this design offer a better solution for broadband performance than any previous configurations

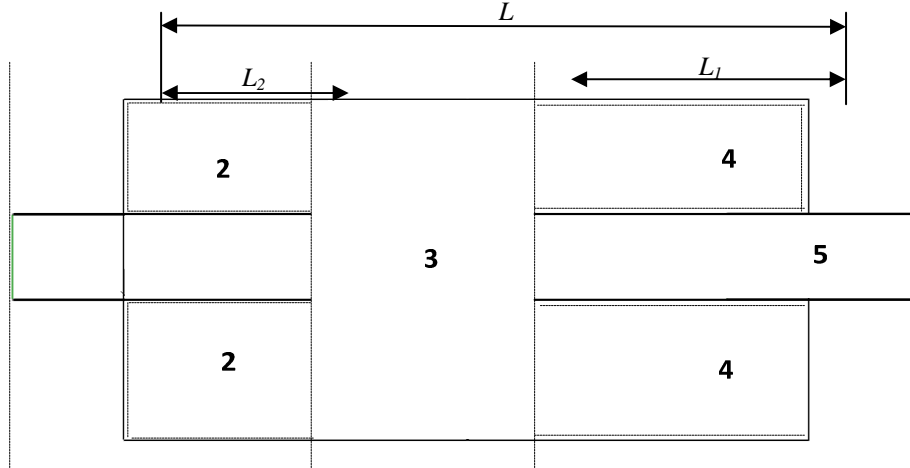


Figure 1.12 – Basic elements of an double tuned extended expansion chamber

1.7 ACOUSTIC BEHAVIOUR OF SIDE BRANCH RESONATORS

1.7.1 FUNDAMENTALS ON SIDE BRANCH RESONATORS

The side branch resonators are reactive element often utilized in silencers. The Table 1.2 shows the most common types and their characteristic dimensions. These elements usually consist of a resonant cavity connected to a pipe through a single hole, or a multiplicity of holes, and a throat whose length can be equal or greater than the wall thickness of the pipe [3], [5].

For the generic side branch, under the hypothesis of plane wave behavior, and assuming that the dimensions of the branch inlet are considerably smaller than the wavelength, i.e. $kr \ll 1$, the following condition exist between the sound field upstream and that downstream of the branch (see Figure1.13):

$$\hat{p}_1^+ + \hat{p}_1^- = \hat{p}_s = \hat{p}_2 \quad (1.43)$$

and

$$\hat{u}_{x,1}^+ + \hat{u}_{x,1}^- = \hat{u}_s S_s / S + \hat{u}_{x,2}^+ \quad (1.44)$$

where the cross sectional area of the duct is the same upstream and downstream of the side branch.

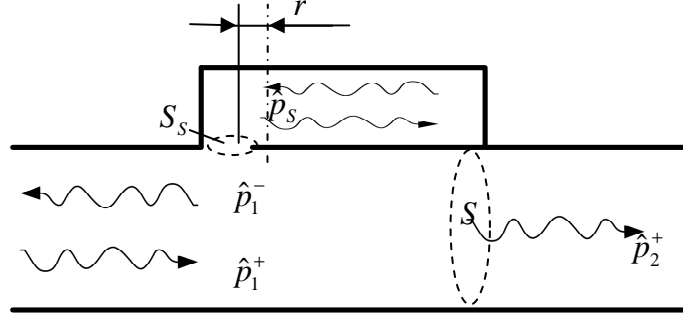


Figure 1.13 – Plane waves in a generic side branch resonator.

The index s is used to refer to quantities pertaining to the side branch.

It is easy to show that:

$$TL = 10 \log \left| 1 + \frac{S_s \rho_0 c}{2S \hat{Z}_s} \right|^2 \quad (1.45)$$

where $\hat{Z}_s = \hat{p}_s / \hat{u}_s$. The (1.42) implies that the maximum TL is obtained when $\hat{Z}_s = 0$, that is $\hat{p} = 0$, which occurs at resonance frequencies [3].

The transfer matrix of a resonator in a stationary medium is given by:

$$\begin{bmatrix} T_{11} & T_{12} \\ T_{21} & T_{22} \end{bmatrix}_r = \begin{bmatrix} 1 & 0 \\ \frac{1}{Z_r} & 1 \end{bmatrix} \quad (1.46)$$

where $Z_r = Z_{th} + Z_{ch} + Z_{th}$. In this sum, Z_{th} is the impedance of the throat connecting the pipe to the cavity, Z_c is the impedance of the cavity. It is possible to show that:

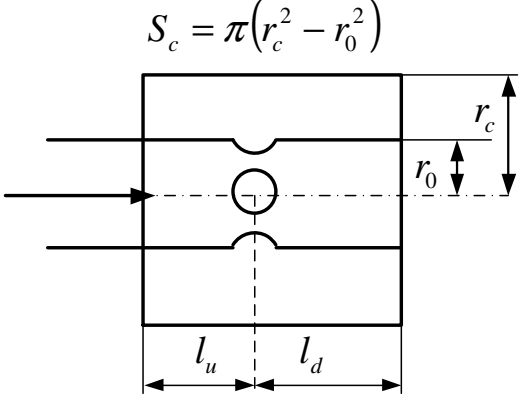
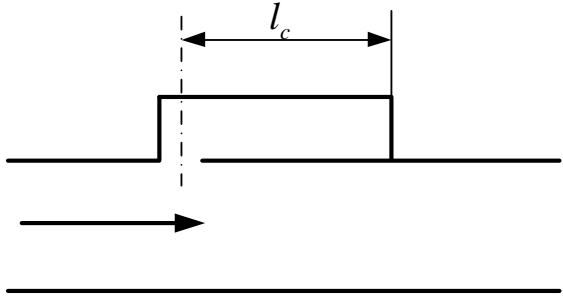
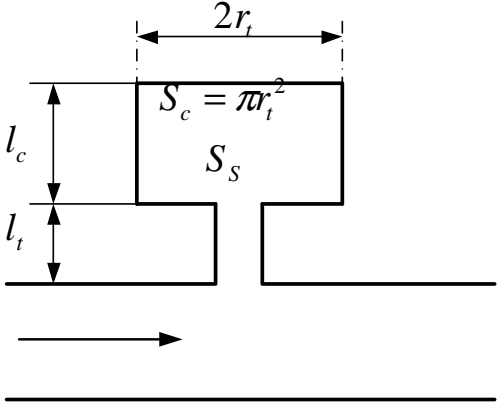
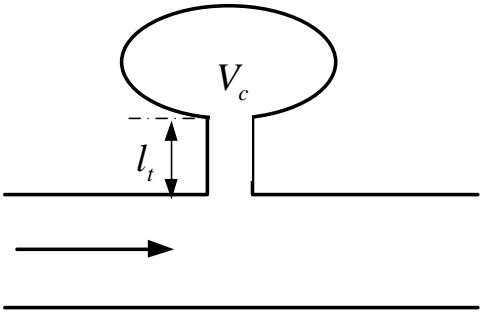
 <p>a) Concentric hole-cavity resonator</p>	 <p>b) Quarter wave resonator</p>
 <p>c) Helmholtz resonator</p>	 <p>d) Helmholtz resonator</p>

Table 1.II – Side branch resonators.

$$Z_c = \begin{cases} Z_{qw} = -i \frac{c}{S_c} \cot kl_c \\ Z_{ch} = -i \frac{c}{S_c} \frac{1}{\tan kl_u + \tan kl_d} \\ Z_{gv} = -i \frac{c}{kV_c} \end{cases} \quad (1.47)$$

where the subscript qw, ch and gv refer to the quarter wave resonator, concentric-hole-cavity, and general-volume cavities. The lengths l_u , l_d , and l_c , the cross section S_c and the volume V_c

are shown in Table 1.II. It can be shown that at low frequencies both Z_{tt} and Z_{cc} are reduced to the expression of Z_{gv} [5].

The impedance of the throat, Z_t , has different expression in case of absence and presence of grazing flow. For $M=0$,

$$Z_t^{M=0} = \frac{1}{n_h} \left(\frac{ck^2}{\pi} + i \frac{ck(l_t + 1.7r_0)}{S_0} \right) \quad (1.48)$$

where l_t is the length of the connecting throat, r_0 the orifice radius, S_0 the area of single orifice, and n_h the total number of perforated holes.

The presence of grazing flow ($M \neq 0$) in the duct has strong effect on the impedance Z_t of the resonator throat. Measurements conducted using single and multi hole throats lead to the empirical expression:

$$Z_t^{M \neq 0} = \frac{c}{\sigma S_0} \left[7.3 \times 10^{-3} (1 + 72M) + j 2.2 \times 10^{-5} (1 + 51l_t)(1 + 408r_0)f \right] \quad (1.49)$$

where the parameters l_t and r_0 are in meters and σ is the porosity (i.e. the ratio between the perforated area and the total area) [5].

1.7.2 QUARTER WAVE AND HELMHOLTZ RESONATORS

The quarter wave resonator and the Helmholtz resonator are two common types of side branch resonators, widely employed to improve the attenuation performance of a silencer at a certain (usually low) frequency. In fact a quarter wave resonator (see Table 1.II) consists of a duct with a constant cross sectional area, terminated by hard wall. The resonance frequency of this element is:

$$f_{qw} = \frac{nc}{4l_c} \quad (1.50)$$

where $n=1,3,5,\dots$ and l_c is the column length.

Another common type of a side branch resonator is the Helmholtz resonator depicted in Table 1.II, which is the acoustic equivalent of the mechanical mass-spring system. It consists of a closed volume that communicates with the duct system through a small duct-neck, with area S_s and length L . The acoustical system, in which pressure and particle velocity vary continuously in the space, can be approximated by a system consisting of parts in which either the pressure or the particle velocity is constant, obtaining a particle system or a *lumped system*. The lumped approximation implies that, for wavelengths much larger than the diameter of the resonator volume, the pressure is uniform throughout, and therefore only a function of time. The reduction of the time and space dependent variables to merely time-dependent ones, implies that the wave propagation within the resonator cannot be taken into account. Obviously this means that the lumped analysis always neglect the effects of higher order modes. An exemplified analysis of this type of resonator, also assumes that the acoustic compression of the gas mass V in the resonator volume $V_c=S_s l_c$ takes place without heat transfer. Under these hypothesis it is easy to show that the eigenfrequency of the Helmholtz resonator is:

$$f_{Hr} = \frac{c}{2\pi} \sqrt{\frac{S_s}{l_t V_c}} \quad (1.51)$$

In the Figure 1-14 the effects of volume V_c and throat radius r_t variations of an Helmholtz resonator are eloquently highlighted: the larger the volume, the higher the resonance frequency and the lower the TL. The larger the neck radius, the higher the resonance frequency and the lower the TL.

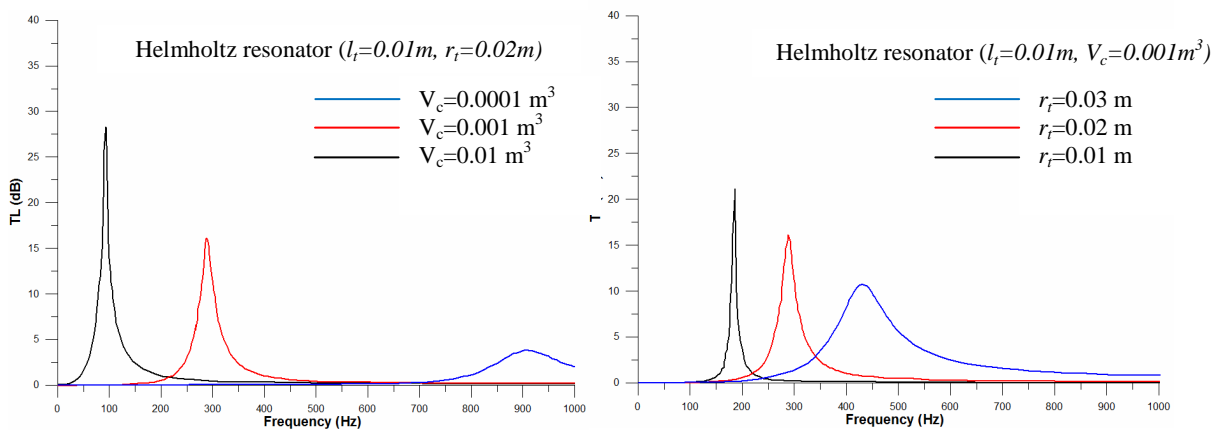


Figure 1.14 – Behaviour of an Helmholtz resonator.

Losses have not been included in the analyses of quarter wave and Helmholtz resonators, but they can be decisive for the effectiveness of the resonator. Such losses as frictions or radiation damping can be included in the preceding models by incorporating a force proportional to velocity of the air column in the resonator neck, that is:

$$\hat{p}_r = -R\hat{u}_s \quad (1.52)$$

In this case the impedance of the resonators will include the term R , and for this reason it can no longer be identically zero. This means that the maximum effectiveness of the resonator is reduced, but with the compensating advantage of a more broad-banded attenuation behaviour [3].

1.7.3 CONCENTRIC HOLE-CAVITY RESONATOR AND PERFORATE TUBES

An example of this typology of resonator is shown in Table 1.II. It consist of an annular tube cavity communicating with the centre tube (propagating tube) through a number of holes on its periphery. Such as extended tube and Helmholtz resonators, the concentric cavity resonators can also be represented by a mass spring system. The impedance is different, as shown by the equations (1.47), and this is mainly due to the fact that the annular cavity is acoustically long (kl_u and kl_d are not $\ll 1$). It is made of two quarter wave resonators in parallel and the neck is equal to the thickness of the communicating holes.

The tuning frequency, in this case, is equal to:

$$f_{ch} = \frac{n_h S_h c}{2\pi S_c (\tan k_o l_u + \tan k_o l_d)} \quad (1.53)$$

Where n_h is the number of holes. Since it appears in the numerator of f_{ch} and in the denominator of the throat impedance Z_t , see equation (1.48), the f_{ch} of n_h holes is n_h times that of a single hole, and the Z_t of n_h holes is $1/n_h$ times that of a single hole. This feature leads to considerable flexibility to the design of concentric hole-cavity resonator [3].

The Figure 1.15 shows the influence the number of holes and the length l_u/l_d ratio : the larger the number of holes, the higher the resonance frequency, and the larger the ratio l_u/l_d , the larger the resonance frequency.

An extension of the concentric hole-cavity resonator is represented by the perforated tube elements: many muffler, in fact, include one or more expansion chambers, which act as low frequency resonators, and a certain number of perforated tubes surrounded by a chamber, which can be tuned as high-frequency resonators. Aero-acoustic analysis of perforated elements in the form of a series expansion for the straight through silencer elements was first presented by Sullivan and Crocker [12]. A segmentation method was then developed by Sullivan [13,14], then followed by the decoupled approach techniques of Jayaraman *et al.* to obtain closed-form solutions.

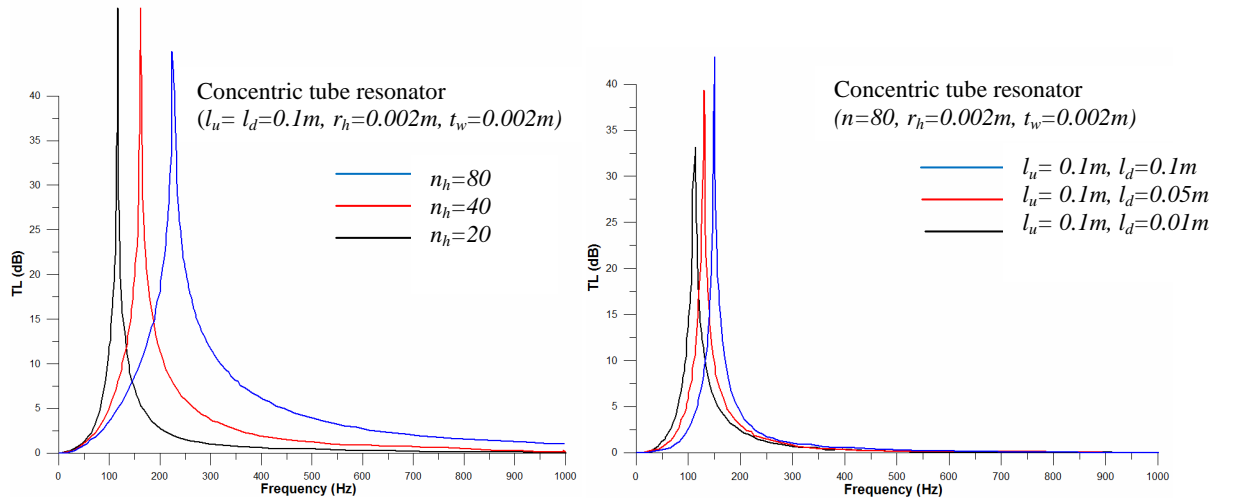


Figure 1.15 – Behaviour of a concentric tube resonator.

In the segmentation approach, the basic element is to be considered is two parallel flow ducts, which are joined together by a perforated section of length l and specific acoustic impedance Z_w (see Figure 1.16). The impedance can vary along the perforate. The main idea of the segmentation approach is to divide the perforated section into a number of segments along the length of the ducts. Each segment consists of two parts. The first part is composed by two parallel hard ducts, where convective plane wave motion is assumed. The second part is a discrete impedance, which can be seen as an open branch representing a parallel coupling of all the holes in the segment.

The parameters characterizing a perforated tube are:

- d_h : diameter of perforated holes

- C : center-to-center distance between consecutive holes
- t_w : wall thickness of perforated tube
- porosity $\sigma = \frac{\pi d_h^2}{4C^2}$ (1.54)

A number of studies, focussed on the acoustic characterization of perforated-tube silencers, prove that the performance of these devices is quite insensitive to the hole diameter d_h and the wall thickness t_w . Contrariwise the above mentioned parameter, and in particular d_h , strongly affect the fluid-dynamic behaviour of the muffler. In fact, in presence of a mean flow, the friction due to the passage of a gas flow thorough the holes increase at the decreasing of d_h , which negatively affect the silencer overall pressure drop.

The presence of a mean flow produces a general increase of TL at increasing of velocity but, obviously, this parameter is not totally under the designer's control.

The behaviour of a silencer composed by an external chamber and one or more interacting straight perforated tubes, also provided of flow deflectors, tends to become similar to that of a simple expansion chamber for sufficiently high values of the porosity, but it is considerably better for low values of this parameter. On the other hand, as previously mentioned, a reduced porosity raises the back pressure, except for the concentric tube resonator (a single perforated tube), where the back pressure is nearly independent of porosity. Consequently the porosity provides another parameter that can be used to trade off between acoustical and mechanical performance [5].

1.8 END EFFECTS AT DISCONTINUITIES

The analyses above exposed, regarding reactive silencer elements, are based on the common hypothesis of plane wave propagation, which cannot take into account of the three-dimensional waves arising at the typical flow discontinuities (sudden cross area variations, open ends, neck of resonators). Generally, an end correction l_c must be added to the length of the duct entering the discontinuity, in order to obtain a proper representation of wave reflection and transmission at boundaries. l_c is usually a function of the geometry and frequency of the propagating waves. The introduction of these corrections is necessary to locate the plane of wave reflection, whose position is shifted by the end correction away from the geometrical discontinuity plane. Different end correction formulae can be found in literature, based on theoretical and experimental investigations [4].

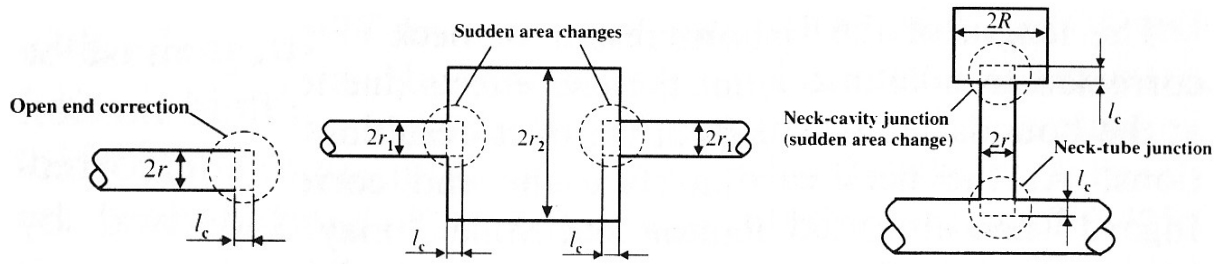


Figure 1.16 – End effects at discontinuities [4].

The importance of the end corrections can be easily shown considering an example of a simple Helmholtz resonator: for a circular duct, when an orifice is placed in a wall that is very large with respect to the sound wavelength, the following approximate expression are obtained:

$$l_c = 0.82 \frac{D}{2} \quad (1.55)$$

For a Helmholtz resonator with a cubic volume with dimensions $0.2 \times 0.2 \times 0.2 \text{ m}^3$, a neck length of 0.01 m and a diameter of 0.10 m , the ratio between the corrected frequency (including end correction length) and the frequency obtained without accounting the end effect is:

$$\frac{f_c}{f} = \sqrt{\frac{L + l_c}{L}} = \sqrt{\frac{0.01 + 0.082 \frac{0.01}{2}}{0.01}} \approx 0.5 \quad (1.56)$$

Which means that the corrected frequency is twice the non-corrected one [3].

1.9 DISSIPATIVE SILENCERS

The acoustic behaviour of most exhaust system elements is essentially reactive but separated flow or flow reversal, perforations, fibrous packing and baffles may all enhance the resistive contribution to their performance [5].

Dissipative silencers are widely utilized devices, which allow good attenuation performances on the broadband, with low backpressure. They are utilized not only in

automotive field, but very frequently also in the intake and exhaust systems of gas turbines, air conditioning and ventilation ducts connected to industrial fans.

In contrast to reactive silencers, which prevent the noise by reflecting the incident sound wave toward the source, dissipative silencers attenuate the sound by converting the acoustic energy of the waves into heat. This conversion is due to the frictions between the oscillating gas particles and the fibrous or porous sound-absorbing material, when the waves propagate into the voids.

In order to accomplish that, the walls of the duct are covered by porous absorbents typically consisting of mineral wool or glass fibres.

Since the damping is mainly obtained from the viscous forces, resistive silencers should be designed to maximize the particle velocities in the porous material. For this reason, it is often good to locate absorbent at a small distance away from the walls, since the normal velocity at the wall is zero.

In industrial application a widely utilized typology of resistive silencer is the so called baffle silencer, since the typically large dimensions of the ducts permit such a silencer.

The global insertion loss of a resistive muffler is a summation of three contributions [5]:

$$IL \approx \Delta L_{ENT} + \Delta L_l + \Delta L_{EX} \quad (1.57)$$

where the flow noise has been neglected, and ΔL_{ENT} , ΔL_l , ΔL_{EX} are, respectively, the entrance loss, the silencer attenuation and the exit loss. The first term is small if the incident sound energy is in the form of a plane wave normally incident on the silencer entrance (for example in straight ducts at low frequencies). For this reason ΔL_{ENT} can be considered as a safety factor in the design of such a silencer. Anyway, when the cross dimensions of the duct are higher than the wavelength, the incident sound field contains a number of higher order modes, and the conversion of the semidiffuse sound field in the entrance duct into a plane wave field in the narrow passages typically results in an entrance loss of 3-6 dB.

The silencer attenuation ΔL_l is proportional to its length and to the lined perimeter of the passage and inversely proportional to the cross area of the passage. It also depends in a complex manner on the geometry of the passage, acoustical characteristics of the porous material, frequency, temperature and flow velocity

At last, exit losses ΔL_{EX} are generated when the silencer is located at the open end of a duct and the typical cross dimensions of the opening are small compared with wavelength. In this case the exit losses are dominated by the end reflection.

Obviously the importance of the entrance and exit losses diminishes as the silencer length increases, since both quantities are independent of the length [5].

It must be noticed that, because of the non-reflecting character of resistive silencers, the coupling effects due to other system elements are not as strong as for reactive silencers. In contrast to the resonator, the performance of resistive silencer is consequently not as sensitive to the silencer's location in the system. This fact, together with its undrammatic frequency dependence, has made the resistive silencer widely used.

1.10 POROUS ABSORBENTS

Porous absorbents utilized in silencers consist usually of thin mineral, metal or glass wool fibres (with a diameter of 2-30 μ m), arranged in layers and with random fibre orientations in planes parallel to the material surface. When the sound propagates, the air is forced to pass thorough the small voids included in the material, which generates frictions converting the acoustic energy into heat. Since the fibres usually conduct the heat better than the air, the consequent heat transfer induces other energy losses. Another phenomenon which occurs is the fluid structure interaction between the vibrating particles and the material fibre which implies kinetic energy losses of the particles. Anyway, this latter process is usually neglect able for porous materials, except at low frequencies (under 300 Hz) [3].

The fibrous materials are usually modelled by assimilating the absorbent bulk to an *equivalent fluid*. With this approach the absorbent material is replaced by a homogeneous fluid with viscous damping. That viscous damping can be incorporated as an extra term into the equation of motion:

$$\rho_0 i \omega \mathbf{u}_x + \frac{\partial \mathbf{p}}{\partial x} + \phi \mathbf{u}_x = 0 \quad (1.58)$$

where the harmonic signal is written in complex form, and ϕ refers to the *flow resistance* [Rayl=Pa s/m²]. The physical meaning of the flow resistance can be easily explained: if a constant differential pressure is imposed across a layer of bulk porous material of open cell structure, a steady flow of gas will be induced through the material. ϕ is the ratio of differential pressure ΔP [Pa] to normal fluid velocity U [m/s] when a transversal steady flow is imposed over a slab of absorbent material:

$$\phi = \frac{1}{U} \frac{p_1 - p_2}{h} \quad (1.59)$$

Here h is the thickness of the slab. It is generally assumed that the gas is air but a flow resistance may be determined for any gas.

The concepts of flow resistivity and impedance are different: the first one relates to a steady flow of air through a porous material when subject to a constant pressure gradient. The second one relates to the resistance offered by a porous absorber to an oscillating pressure gradient. Obviously in air they are equal and represented by a real number. In porous material the impedance is a complex number.

Experimental investigations confirm the correctness of the (1.58) under certain limits, showing that, for a wide range of materials, the differential pressure and the induced normal velocity are linearly related, provided that the normal velocity is small.

Diagrams representing the *flow resistivity* σ (i.e. flow resistance divided by sample thickness) as a function of material bulk density and fibre diameter, can be found in literature [5].

The most common way to use a porous absorbent is to place it in front of a hard wall, for the purpose of reducing the wall reflections. It is possible to determine how to choose the flow resistance and absorbent thickness, in order to obtain the best possible sound absorption. Usually the most utilized model, in case of absorbent material, is the semi-empirical equivalent fluid model developed by Delany and Bazley [16] which is able to directly estimate the characteristic impedance and the *wavenumber*, k , of the material. The wavenumber is a frequently utilized parameter that describes how a wave travels through a medium. It is the angular reciprocal of the wavelength. It represents what angle of rotation (in radians) the wave makes in the space of one meter. In the air it is obviously a real number. Contrariwise, for the sound travelling in a porous absorber, the wavenumber is a complex number.

Delany and Bazley derived the following equations that scale the impedance and wavenumber of air to derive the corresponding values for a porous absorber:

$$\begin{aligned} Z_{abs} &= Z_{air} \left(1 + 0.0571X^{-0.754} - i0.087X^{-0.732} \right) \\ k_{abs} &= k_{air} \left(1 + 0.0978X^{-0.7} - i0.189X^{-0.595} \right) \end{aligned} \quad (1.60)$$

where X is a dimensionless quantity : $X = \frac{\rho_0 f}{\sigma}$ (σ is the flow resistivity).

The real part produced by these equations is known as *resistance* and relates to energy loss. The imaginary part is known as *reactance*, and relates to extra “virtual” mass the absorbers appears to have due to the resistance created by the viscous air/fiber boundary layers.

The Delany and Bazley formulae are accurate within the following boundaries:

- The flow resistivity values used to derive the dimensionless term X must fall within the range $1,000 < \sigma < 50,000$
- The dimensionless term X must be within the range $0.001 < X < 1.0$
- The porosity of the material must be close to 1.

Most porous absorbers utilized in mufflers respect these limits.

It can be shown, that the Delany and Bazley model furnishes that the optimal absorption properties can be obtained when the flow resistance is chosen in a way to satisfy the following equivalence:

$$\frac{\phi h}{\rho c} \approx 2 \quad (1.61)$$

(where h is the absorbent thickness). The vicinity of the optimum is, nevertheless, quite flat, so that any value in the interval 1-3 would be almost good. It can be proved that this means that optimal absorbent can be expected to provide good absorption if its thickness is about a quarter wavelength [3].

Moreover, it can be shown that, at high frequencies, the reflection factor of the porous material approaches zero and the sound wave passes directly into the absorbent, without reflection. Consequently a major fraction of acoustical energy converts into thermal energy as it propagates, and the porous material attenuates much more.

1.11 TYPICAL SILENCER CONFIGURATIONS

In this section, a number of typical silencer configurations is shown and commented (see Figure 1.17). Reactive spectral behaviour is cyclic, exhibiting attenuation minima each time an acoustically significant length corresponds to an integer multiple of half the acoustic wavelength of the excitation. Since several lengths are involved simultaneously, a simple

parametric description of their overall acoustic performance is not normally possible. However, their general ranking in terms of relative attenuation per unit volume and relative pressure loss or back pressure has been established from experience [1].

The packed silencers depicted in Figure 1.17a, has a relative efficiency which is roughly proportional to the packing density, the flow resistance of the pack and the other acoustic properties of the fibrous material. Their attenuation performance tends to rise significantly with increasing frequency, in correspondence with the acoustic properties of the pack, while they normally exhibit low back pressure. Their relative volumetric efficiency can be high, but tends to deteriorate in service due to fouling and disintegration of the pack. They are also relatively heavy and may cause suspension problems or may excite mechanical vibration of the vehicle structure.

The relative acoustic efficiency of the snubber and cross flow silencers shown in Figure 1.17b and c, is closely related to the back pressure or flow losses they generate, which often tend to be high. Their behaviour remains significantly reactive so that high acoustic efficiency is often restricted to specific sections of the frequency spectrum. Cross flow silencers are obviously more compact than the other type, and so can have relatively better low frequency attenuation performance for the same overall dimensions. The acoustic influence of perforated pipes diminishes as the porosity increases while observation suggests it becomes negligible with grazing flow at Mach numbers less than 0.2 when the porosity rises above 15%. On the other hand, low porosity implies high through flow losses, so a formulation of the most effective practical configuration may be difficult. Finally, these silencer types can be significant sources of flow noise, particularly at higher frequencies.

The tri-flow mufflers are popular, relatively compact and have a high relative acoustic efficiency. Their behaviour also tends to be strongly reactive at low frequencies so regions of poor attenuation performance are often improved by adding resonators to the flow reversal chamber, as indicated in the example in depicted in Figure 1.17d. Back pressure losses are directly related to the changes in flow momentum at flow reversal and vary as the square of the engine speed; thus they can lead to undesirable reductions in peak engine performance. Vortex shedding at the flow reversals may also introduce significant flow noise. The observations concerning the acoustic behaviour of perforated pipes also apply to these units.

Expansion chambers which include side branch resonators forming the bottom group in Figure 1.16g generally exhibit the lowest back pressure. The acoustic performance at low frequencies can be enhanced by adding a folded side branch, which acts in a similar manner to the resonator included in the tri-flow muffler example [1].

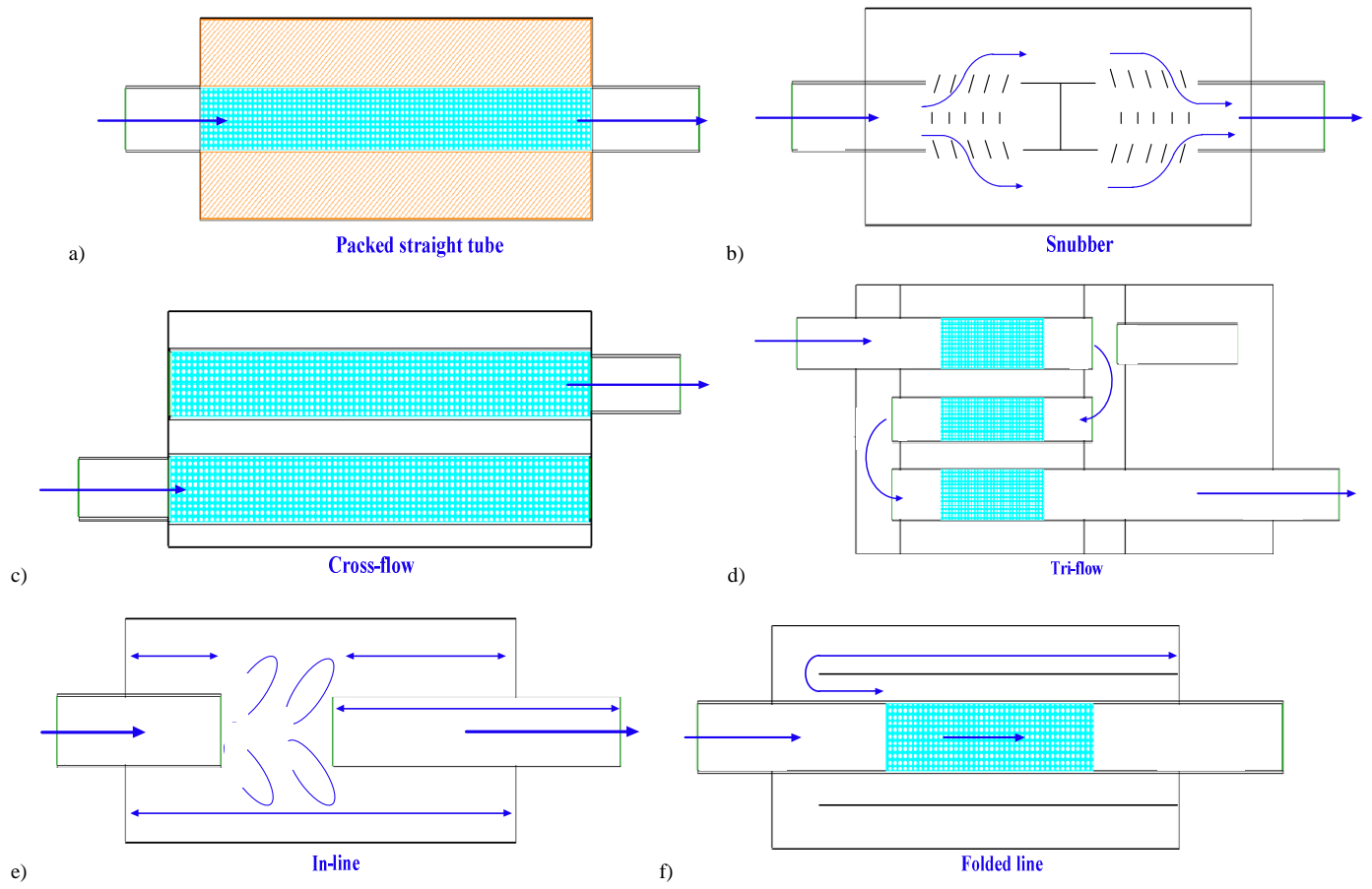


Figure 1.17 – Typical silencer configurations.

REFERENCES

58. P. O. A. L. Davies “Piston Engine Intake and Exhaust System Design”, *Journal of Sound and Vibration* (1996) 190 (4), 677-712.
59. S. H. Kim, J. M. Lee, A practical method for noise reduction in a vehicle passenger compartment, *Trans. of ASME*, January 1998, vol.120.
60. H.P. Wallin, U. Carlsson, M. Abom, H. Boden, *Sound and vibration*, KTH MWL, ISBN 978-91-7415-553-2.
61. D.E. Winterborne, R.J. Pearson: "Design Techniques for Engine Manifolds", Chap.6, SAE Int. Publisher, 1999.
62. L.L. Beranek, I.L.Ver, *Noise and Vibration Control Engineering: Principles and Applications*, John Wiley and Sons Inc., New York, 2006.
63. H. Bodén, F. Albertson, Linearity test for in-duct acoustic one-port sources, *Journal of Sound and Vibration* (2000) 237(1), 45-65.
64. H. Rammal, H. Bodén, Modified multi-load method for nonlinear source characterization, *Journal of Sound and Vibration* 299 (2007) 1094–1113.
65. J. Liu, D.W. Herrin, Measuring acoustic impedance using wave decomposition, *Proceedings of the IMAC-XXVII*, Society for experimental mechanics inc., 2009.
66. M. Abom, Measurement of the scattering matrix of acoustical two-ports, *Mechanical Systems and Signal Processing* (1991) 5(2), 89-104.
67. M.L. Munjal “Acoustics of Ducts and Mufflers”, New York : Wiley-Interscience, 1987.
68. P.O.A.L. Davies, Practical flow duct acoustics, *Journal of Sound and Vibration* (1988) 124(1), 91-115.
69. J-W- Sullivan, M.J. Crocker, Analysis of concentric-tube resonators having un-partitioned cavities, *Journal of Acoustical Society of America*. 64, 207-215 (1978).
70. J.W. Sullivan, A method of modelling perforated tube muffler components – I Theory, *Journal of Acoustical Society of America*. 66, 772–778 (1979).
71. J. W. Sullivan, A method of modelling perforated tube muffler components - II Applications, *Journal of Acoustical Society of America*. 66, 779–788 (1979).
72. K. Jayaraman and K. Yam, Decoupling approach to modelling perforated tube muffler components, *Journal of Acoustical Society of America*. 69, 390–396 (1981).
73. T.J. Cox, P. D’Antonio, *Acoustic absorbers and diffusers: theory, design and application*, Taylor & Francis, London and New York, 2004.

Chapter 2

Numerical 1D methodologies

5.2 INTRODUCTION

The gas dynamics of IC-engines and their components can be essentially described by a set of coupled non-linear equations for conservation of mass, momentum and energy. [1]

A very powerful and often used simplification for IC-engine intake or exhaust ducts is to assume small perturbations and perform a linearization of the governing equations (*linear acoustics*), which allows to neglect the energy equation. When a homogeneous and isentropic mean flow is present, the final result will be the convective *wave equation* and then also the 3D effects can be addressed without too much difficulty [2].

Another possible simplification is to consider one-dimensional (1D) fields only. This assumption implies that the variables of pressure, density, velocity and temperature are treated as being constant over the cross-section of the duct under consideration. From this the solution of the coupled nonlinear equations will be greatly simplified. [3].

A further simplification can be done when only small perturbations are considered in 1D fields: in this case the wave equation will be reduced to a 1D linear wave problem. On the contrary, when the excitation overwhelms certain limits, the linear assumption does not stand anymore, and a non-linear approach is required to solve the acoustic problem [4]. Practical experience demonstrates that, with plane waves and for terrestrial reference conditions, the limit of the amplitude of the pressure fluctuation, for linear acoustic validity, lies somewhere in the range 0.01 to 0.001 bar, the value of the limit falling as the frequency rises. [5]

One-dimensional linear acoustic models are widely adopted for the evaluation of intake and exhaust systems noise performance, due to their simplicity and low computational requirements in the description of complex geometries. The system is considered as a combination of elements, connected in series or in parallel; each one can be efficiently

analyzed via so called two-port methods by means of either a transfer matrix [6] or a scattering matrix [7] .

In order to analyze the acoustic performance of some components in which non-planar higher modes are excited, due to the transverse dimensions that are not much smaller than the wavelength of the excitation and/or to the area discontinuities, some three-dimensional linear studies have been performed by imposing, as excitation source, a single frequency perturbation [8]. Owing to the high requirements of development time and computational cost, such investigations focus only on particular components of intake/exhaust system, without providing a description of their interaction with the engine. [9]

Linear acoustic models are convenient for predicting the behaviour of the muffler proper; the utilized noise prediction tools, based upon linear theory, use a quite simplified representation of the engine as a time-invariant linear source [10]. However, since in engine intake and exhaust systems, the pressure fluctuations are characterized by much larger amplitude than that assumed in the linear approach, non-linear models are required to obtain realistic predictions. In fact these latter approaches are able to account the distortion of high amplitude waveform during the propagation, the corresponding redistribution of the spectral component energies towards higher frequencies, and the interaction between the engine and the ducts system. Moreover, when the position and shape of the duct boundaries vary systematically or cyclically with time, spectral descriptions of wave propagation normally cease to be appropriate. Then any realistic description of the wave action must be formulated in time, even when the wave motion is periodic [11]. This is mainly because of any issues, related with cylinder discharge and back reactions of the exhaust line on the engine, are immediately taken into account.

Non-linear fluid dynamic models are mainly used to predict the intake and exhaust system performance in terms of pressure, velocity crank angle histories, and are based on lumped parameter (0-D), one-dimensional (1-D) or three-dimensional (3-D) schemes. 0-D schemes are usually adopted coupled with 1-D models, the former one in the investigation of cylinder behaviour and of flow across intake and exhaust valves, the latter one to describe the intake/exhaust system [12]. Recently, some 1-D models have been proposed to analyze complex geometries, such as mufflers, in which perforations and adsorptive materials are included [13]. The computed results allow the evaluation of the noise radiation from the tailpipe, by assuming that the open end acts as a monopole source.

The quality of the 1D predictions is usually improved by introducing some length corrections to 1-D modelling, as shown in the Chapter 1. In this way the complex wave

reflection at discontinuities (sudden expansion and contractions in duct cross-section) is taken into account [3].

More refined 1D based approaches, like the one proposed by Montenegro *et al.* [14] utilize *quasi-3D* elements to model chambers or after-treatment devices, which are specifically designed to account for conservation of momentum in three dimensions, even though the code is otherwise nominally one-dimensional. They are composed by a 0D element at the centre of the volume, where the continuity and energy equations are integrated, and a number of volume openings (ports) where also the momentum equation is integrated.

In this chapter, a general overview on the main methodologies utilized to solve non linear one dimensional gas flow equations is presented, including the founding theoretical concepts. Pros and cons related to the usage of different 1D techniques in silencer simulations are highlighted and an introduction to the quasi 3D model is given.

5.3 GOVERNING EQUATIONS

The governing equations describing the one-dimensional flow of a compressible fluid in a pipe with area variation F , wall friction f , heat transfer q , are [3]:

- The continuity equation:

$$\frac{\partial(\rho F)}{\partial t} + \frac{\partial(\rho u F)}{\partial x} = 0 \quad (2.1)$$

- The momentum equation:

$$\frac{\partial(\rho u F)}{\partial t} + \frac{\partial(\rho u^2 + p)F}{\partial x} - p \frac{dF}{dx} + \frac{1}{2} \rho u^2 f \pi D = 0 \quad (2.2)$$

- The energy equation:

$$\frac{\partial(\rho e_0 F)}{\partial t} + \frac{\partial(\rho u h_0 F)}{\partial x} - q \rho F = 0 \quad (2.3)$$

In these equations ρ is the fluid density, u is the flow velocity, p is the pressure, D is the duct diameter, $e_0 = e + u^2/2$ is the stagnation internal energy, e is the internal energy, $h_0 = h + u^2/2$ is the stagnation enthalpy and q is the heat transfer term.

The above equations can be written in symbolic vector form:

$$\frac{\partial \mathbf{W}}{\partial t} + \frac{\partial \mathbf{F}(\mathbf{W})}{\partial x} + \mathbf{C}(\mathbf{W}) = 0 \quad (2.4)$$

where

$$\mathbf{W} = \begin{bmatrix} \rho \\ \rho u \\ \rho e_0 \end{bmatrix}, \quad \mathbf{F}(\mathbf{W}) = \begin{bmatrix} \rho u \\ \rho u^2 + p \\ \rho u h_0 \end{bmatrix}, \quad \mathbf{C}(\mathbf{W}) = \begin{bmatrix} \rho u \\ \rho u^2 \\ \rho u h_0 \end{bmatrix} \frac{1}{F} \frac{dF}{dx} + \begin{bmatrix} 0 \\ \rho G \\ -\rho q \end{bmatrix} \quad (2.5)$$

and

$$G = \frac{1}{2} u |u| f \frac{4}{D} \quad (2.6)$$

is the friction term. In case of no pipe area variation, wall friction and heat transfer, the equations reduce to:

$$\frac{\partial \mathbf{W}}{\partial t} + \frac{\partial \mathbf{F}(\mathbf{W})}{\partial x} = 0 \quad (2.7)$$

which are known as the one-dimensional Euler equations. They constitute a non-homogeneous hyperbolic system.

The form expressed by equation (2.1)-(2.4) is called *conservation form*, since the equations can be obtained directly from the integral conservation equations of mass, momentum and energy applied to a fixed infinitely small control volume [3].

The three above equations contain the four unknowns, ρ , u , p and e . A further relationship is required to close the problem. The properties of the gas must be related by a state equation which, for the gases in engine manifolds and cylinder, can be represented by the ideal gas state equation:

$$\frac{p}{\rho} = RT \quad (2.8)$$

2.3 LINEARIZED EQUATIONS AND LINEARIZED WAVES

In case of *homotropic fluid*¹ and no cross area variations, the continuity equation becomes [3]:

$$\frac{d\rho}{dt} + u \frac{d\rho}{dx} + \rho \frac{\partial u}{\partial x} = 0 \quad (2.9)$$

And the momentum equation becomes:

$$\frac{du}{dt} + u \frac{du}{dx} + \frac{1}{\rho} \frac{\partial p}{\partial x} = 0 \quad (2.10)$$

If perturbations Δp , $\Delta \rho$ and Δu are applied to a static fluid, with undisturbed pressure p_0 , density ρ_0 and velocity u_0 , the local values of these properties can be written as:

$$p = p_0 + \Delta p \quad (2.11)$$

$$\rho = \rho_0 + \Delta \rho \quad (2.12)$$

$$u = u_0 + \Delta u = \Delta u \quad (2.13)$$

Substituting these relationship into equations (2.9) and (2.10) gives the following linearized equations for waves of small magnitude with $\Delta \rho \ll \rho_0$, $\Delta p \ll p_0$, $\Delta u \ll a$:

$$\frac{\partial(\Delta \rho)}{\partial t} + \rho_0 \frac{\partial(\Delta u)}{\partial x} = 0 \quad (2.14)$$

¹A homotropic flow has uniform and constant entropy. It distinguishes itself from an isentropic or particle isentropic flow because, in the latter, the entropy level of each fluid particle does not change with time, but may vary from particle to particle.

$$\rho_0 \frac{\partial(\Delta u)}{\partial t} + \frac{\partial(\Delta p)}{\partial x} = 0 \quad (2.15)$$

For isentropic changes of state $ds=0$ and change in pressure can be related to changes in density by

$$dp = a^2 d\rho \quad (2.16)$$

Where a is the speed of sound. It is, then, easy to obtain the *acoustic wave equation*:

$$\frac{\partial^2(\Delta p)}{\partial t^2} = a_0^2 \frac{\partial^2(\Delta p)}{\partial x^2} \quad (2.17)$$

which can be expressed in terms of the velocity or density:

$$\frac{\partial^2(\Delta u)}{\partial t^2} = a_0^2 \frac{\partial^2(\Delta u)}{\partial x^2} \quad (2.18)$$

$$\frac{\partial^2(\Delta \rho)}{\partial t^2} = a_0^2 \frac{\partial^2(\Delta \rho)}{\partial x^2} \quad (2.19)$$

These equations have simple analytical solutions, represented by a sum of a progressive and regressive term:

$$\Delta p = f(x - a_0 t) + g(x + a_0 t) \quad (2.20)$$

$$\Delta u = \bar{f}(x - a_0 t) + \bar{g}(x + a_0 t) \quad (2.21)$$

$$\Delta p = \tilde{f}(x - a_0 t) + \tilde{g}(x + a_0 t) \quad (2.22)$$

Where the functions at the second terms are arbitrary wave forms [3].

Further discussions regarding the linearized waves for will be done in the Chapter 4, where the progressive and regressive waves components will be utilized in the description of the two-port systems. The main aspect to be highlighted here are that: the pressure at any section is simply the sum of the excess pressure in the individual wave components, which

gives the name *linear waves*. All parts of the waves move with the same propagation speed, given by

$$a_0 = \sqrt{\gamma RT} \quad (2.23)$$

where R is the specific gas constant and T the absolute temperature. Moreover, the waveform does not distort. By retaining their original identity, the waves can be tracked from one end of a pipe to another simply by noting the time delay involved in the propagation.

2.4 METHOD OF CHARACTERISTICS

In most numerical models, the traditional mesh-Method of Characteristics (MOC) has been applied up to the mid 1980's . Despite being first order accurate and not being able to capture shock waves, the method of characteristics is able to retain system nonlinearity, as well as accurately implementing the different boundary conditions, especially duct branching and anechoic termination. For this reason, it is still a valid method for muffler analysis. Moreover, the perforations model implemented by Onorati [15] (see paragraph 2.13) can be implemented with only slight modifications. In [16] a non-linear simulation of single pass perforated tube silencers, based on the method of characteristics, has been proficiently performed.

The equations (2.1)-(2.3) can be rearranged into another form, called *method of characteristic form* which gives the possibility to transform the partial equations, with respect to space and time, of the system (2.4) into ordinary differential equations in time. In fact, once considered the line in the space-time plane defined by [3]:

$$\frac{dx}{dt} = u \pm a \quad (2.24)$$

the mass and momentum equations will give the following expression:

$$\frac{dp}{dt} \pm \rho a \frac{du}{dt} + \Delta_1 + \Delta_2 \pm \Delta_3 = 0 \quad (2.25)$$

which represents the *first compatibility relationship*. Similarly, once defined the line in time-space plane defined as

$$\frac{dx}{dt} = u \quad (2.26)$$

the energy equation will give the following expression:

$$\frac{dp}{dt} - a^2 \frac{dp}{dt} + \Delta_1 = 0 \quad (2.27)$$

which represents the *second compatibility relationship*. The Δ_1 , Δ_2 , Δ_3 , terms represent respectively, the heat transfer, the change of cross sectional area along the pipe and the pipe wall friction:

$$\Delta_1 = -(\gamma - 1)\rho(q - uG) \quad (2.28)$$

$$\Delta_2 = \frac{\rho u a^2}{F} \frac{dF}{dx} \quad (2.29)$$

$$\Delta_3 = \rho a G \quad (2.30)$$

The (2.25) relates the pressure and velocity of the gas along the characteristic lines defined by the equation (2.24), and the (2.27) relates the pressure and density of the gas along the characteristic line defined by the (2.26). The characteristic speeds given by equations (2.24) and (2.26) represent the speed of propagation of signals, or disturbances, through the fluid medium. In the case of equation (2.24), the disturbance is propagated at the local speed of sound relative to the fluid, $u \pm a$. This disturbance is often called *wave characteristic*, or *Mach wave*, and causes changes in the fluid pressure, density, temperature and velocity. The equation (2.26) represents a disturbance propagating with the local fluid velocity, u , which transports, by advection, the bulk gas temperature (energy) level and composition, and is called *path line characteristic* [3].

The compatibility equation (2.25), in case of finite amplitude wave, travelling in the positive x-direction in absence of pipe wall friction, heat transfer and area variation (*homotropic flow*) reduces to:

$$dp \pm \rho a du = 0 \quad (2.31)$$

This equation relates the changes of pressure and velocity along the path of the wave as the wave form changes on propagation. The corresponding characteristic equation is given by the (2.24). If the fluid is a perfect gas and only isentropic changes of state are considered, then from the compatibility equation, one obtains:

$$\frac{2}{\gamma-1} da \pm du = 0 \quad (2.32)$$

where the upper signs relates to wave travelling from left to right in the duct, called λ *characteristics*, and the lower signs relates to waves going from right to left, called β *characteristics*. In this case the number of variables in the compatibility equation has been reduced from four to two, and the changes in pressure are represented by changes in speed of sound a . The equation (2.32) relates the change of speed of sound a to the velocity u along the paths of the waves given by equation (2.23), which treat waves travelling in both directions [3]. For an homotropic flow it can be shown that the parameter defined as:

$$\lambda = a + \frac{\gamma-1}{2} u \quad (2.33)$$

is constant along a rightward propagating wave, so that:

$$\lambda_1 = \lambda_2 \quad (2.34)$$

Similarly, for a leftward propagating wave, the parameter defined as

$$\beta = a - \frac{\gamma-1}{2} u \quad (2.35)$$

is constant, giving:

$$\beta_1 = \beta_2 \quad (2.36)$$

The equations (2.41) and (2.43) constrain the relationship between a and u to be constant along the path wave. The parameters λ and β are often referred as *Riemann invariants* in homentropic flow or *Riemann variables*.

In order to appreciate the physical meaning of these results, the Figure 2.1 can be helpful: it shows a distance-time plane and a $\Delta t \times 2\Delta x$ interval [3].

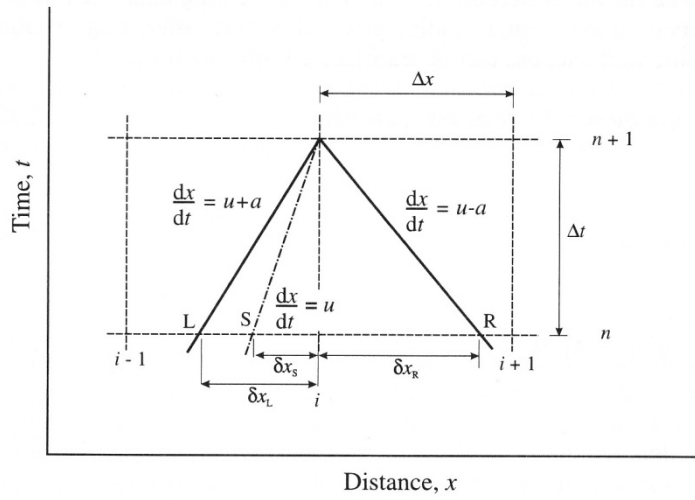


Figure 2.1 – Characteristic lines in the x - t diagram [3].

The rightward propagating wave, travelling at the speed $u+a$, sets off from the point L at time level n , and arrives at point i at time level $n+1$. Similarly, the leftward travelling wave originates from the point R at time level n and arrives at point i at time level $n+1$. If the gas velocity, u , is not zero then L and R are not at the same distance from the mesh point i . The (2.41) and (2.42) then give:

$$\lambda_i^{n+1} = \lambda_L^n \quad (2.37)$$

$$\beta_i^{n+1} = \beta_R^n \quad (2.38)$$

Equations (2.46) and (2.47) are simultaneous equations which define the values of the two quantities a and u at mesh point $[i\Delta x]$ and the new time level $[(n+1)\Delta t]$ in terms of their values at the points L and R. These two equations can be used at every point in a pipe which

is surrounded by two other points. At boundaries, the values of the gas properties in the pipe are available on only one side of the mesh point under consideration, and a modified procedure must be adopted. The values at points L and R are usually obtained by linear interpolation of the values at $[(i-1)\Delta x, n\Delta t]$, $[i\Delta x, n\Delta t]$ and $[(i+1)\Delta x, n\Delta t]$, therefore producing first-order special accuracy.

In case of *non homentropic* flow, also the variations in the entropy must be taken into account, which involves the solution of the energy equation along the path line characteristics (above defined). Consequently, in the generic case of non homentropic flow and cross sectional area variations, the first characteristic equations (2.25) must be considered along the wave characteristics (2.24), and the second characteristic equation (2.27) along the path line (2.26). As a result, the Reimann variables are modified into:

$$\lambda_i^{n+1} = \lambda_L^n + d\lambda_L \quad (2.39)$$

$$\beta_i^{n+1} = \beta_R^n + d\beta_R \quad (2.40)$$

where

$$d\lambda = \frac{\gamma-1}{2} \frac{T}{a} ds - \frac{\gamma-1}{2\rho a} [\Delta_1 + \Delta_2 + \Delta_3] dt = 0 \quad (2.41)$$

$$d\beta = \frac{\gamma-1}{2} \frac{T}{a} ds - \frac{\gamma-1}{2\rho a} [\Delta_1 + \Delta_2 - \Delta_3] dt = 0 \quad (2.42)$$

The change in entropy along the wave characteristics is obtained by using information available from the path line characteristic, starting from the point S of Figure 2.1 [3].

2.5 THE COURANT-FRIEDERICHS-LEWY (CFL) STABILITY CRITERION

The mesh size, Δx , utilized for the spatial discretization of the ducts is chosen on the basis of a compromise between accuracy and computational speed. In many cases the upper limit for the mesh length is the length of the smallest pipe element in the system [3].

On the other hand, the value of the time step, Δt , is subject to the constraints defined by the stability considerations coming from the so called *CFL criterion*. According to this, the waves cannot travel more than one mesh length in one calculation time increment, i.e.:

$$\Delta t = \nu \frac{\Delta x}{c_{\max}^n} \quad (2.43)$$

where

$$0 < \nu \leq 1 \quad (2.44)$$

and c_{\max}^n represents the largest wave speed present in the entire solution domain at time level n . The parameter ν is called CFL number, and the time marching procedure will be most efficient when the value of this parameter is close to 1.

2.6 FINITE VOLUME METHODS

The Method of Characteristics is based on the governing equations in non-conservation form, that is the (2.17) and (2.18). These equations are not able to conserve properties well (for example the mass flow), and for this reason they are not capable of dealing with discontinuities, e.g. shock waves. As previously mentioned the MOC is still utilized in muffler simulations, but it is widely used also in the resolution of boundary conditions, owing to the comprehensive and well-documented work existing on the treatment of every kind of flow boundary [17], [18].

Anyway, in order to take into account the presence of the shock waves, in last decades the new generation of 1-D fluid dynamic models has adopted *finite volume symmetric* or *upwind shock-capturing* numerical methods in order to solve the hyperbolic problem of conservation equations. The origin of these two important families of schemes, is represented by the numerical technique developed in the form of first-order methods by Courant et al. [19] and Lax [20]. On one hand, symmetric schemes apply a discretization which is independent from inviscid flow characteristics. On the other hand, upwind schemes apply directional space discretizations according to the physical behaviour of inviscid flows.

The second-order symmetric scheme proposed by Lax & Wendroff [21] is one of the most representative symmetric schemes and a description of this method will be given in the following section. [17]

A subgroup of upwind schemes is based on *Godunov's method* [22] to solve, over each mesh interval, the local 1-D Euler equations for discontinuous neighbouring states. The second subgroup of upwind schemes is the *flux vector splitting methods*, proposed by Steger and Warming [17],[23], [24].

2.6.1 DEFINITION OF FINITE VOLUME SCHEME

The integral form of the governing equations can be written as [3]:

$$\iint_{x,y} \left(\frac{\partial \mathbf{W}}{\partial t} + \frac{\partial \mathbf{F}(\mathbf{W})}{\partial x} + \mathbf{C} \right) dx dt = 0 \quad (2.45)$$

which gives:

$$(\mathbf{W}_i^{n+1} - \mathbf{W}_i^n) \Delta x + (\mathbf{F}_{i+1/2}^n - \mathbf{F}_{i-1/2}^n) \Delta t + \mathbf{C}_i^n \Delta x \Delta t = 0 \quad (2.46)$$

where \mathbf{W} and \mathbf{F} respectively represent the average of dependent variables for the cell shown in Figure 2.2 and the average flux across the boundary of this cell:

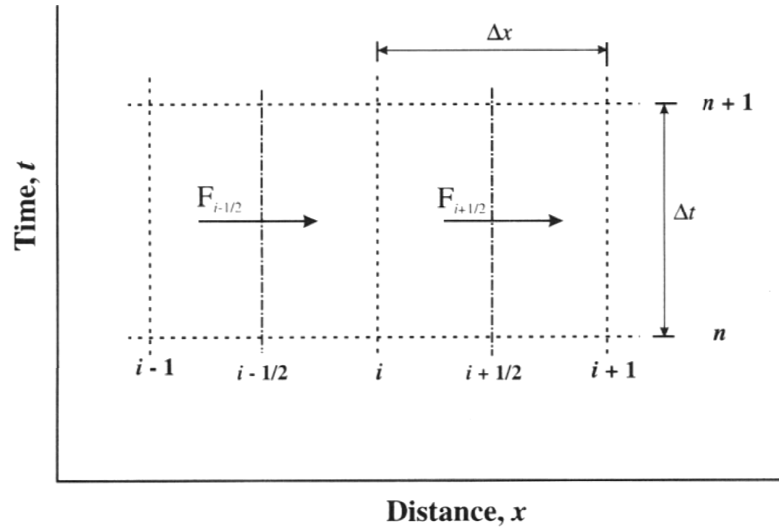


Figure 2.2 – Computational cell for conservation equations [3].

In other words:

$$\mathbf{W}_i = \frac{1}{\Delta x} \int_{x_{i-1/2}}^{x_{i+1/2}} \mathbf{W} dx \quad (2.47)$$

$$\mathbf{F}_{i\pm 1/2} = \frac{1}{\Delta t} \int_{t_n}^{t_{n+1}} \mathbf{F} dx \quad (2.48)$$

In absence of the source term \mathbf{C} , the (2.46) gives:

$$\mathbf{W}_i^{n+1} = \mathbf{W}_i^n - \frac{\Delta t}{\Delta x} (\mathbf{F}_{i+1/2}^n - \mathbf{F}_{i-1/2}^n) \quad (2.49)$$

The left-hand side of the (2.49) represents the solution at the time level $n+1$ and the first term on the right-hand side represents the solution at time level n . Summing the equation with respect to the spatial index i in the (2.49), one obtains:

$$\Delta x \sum_{i_{\min}}^{i_{\max}} \mathbf{W}_i^{n+1} = \Delta x \sum_{i_{\min}}^{i_{\max}} \mathbf{W}_i^n + \Delta t (\mathbf{F}_{i_{\min}-1/2}^n - \mathbf{F}_{i_{\min}+1/2}^n) \quad (2.50)$$

If there are no cross area variations, the fluxes are null. The (2.50) guarantees the conservation of the integral property of the governing equations, ensuring for example the conservation of mass.. The finite difference methods based on the equations (2.46)-(2.48) are called *conservative finite volume schemes*.

2.6.2 LAX-WENDROFF SPACE-CENTRED SCHEMES

The Lax-Wendroff method [21] is based on the Taylor series for the state vector [3]:

$$\mathbf{W}^{n+1} = \mathbf{W}^n + \frac{\partial \mathbf{W}}{\partial t} \Delta t + \frac{\partial^2 \mathbf{W}}{\partial t^2} \frac{(\Delta t)^2}{2!} + \dots \quad (2.51)$$

In case of source term \mathbf{C} set to zero, it can be shown that, by utilizing the (2.51), the (2.4) becomes:

$$\mathbf{W}^{n+1} = \mathbf{W}^n - \frac{\partial \mathbf{F}}{\partial x} \Delta t + \frac{\partial}{\partial x} \left(\mathbf{A} \frac{\partial \mathbf{F}}{\partial x} \right) \frac{(\Delta t)^2}{2!} + O(\Delta t)^3 \quad (2.52)$$

where \mathbf{A} is a 3 by 3 Jacobian matrix defined as:

$$\mathbf{A}^{lm} = \frac{\partial F_l}{\partial W_m} \quad (2.53)$$

The spatial differences can be approximated by central differences, $\left. \frac{\partial \mathbf{F}}{\partial x} \right|_i = \frac{\mathbf{F}_{i+1} - \mathbf{F}_{i-1}}{2\Delta x} + O(\Delta x)^2$, and the series is truncated at second-order terms, giving:

$$\mathbf{W}_i^{n+1} = \mathbf{W}_i^n - \frac{\Delta t}{2\Delta x} [\mathbf{F}_{i+1}^n - \mathbf{F}_{i-1}^n] + \frac{(\Delta t)^2}{2(\Delta x)^2} [\mathbf{A}_{i+1/2}^n (\mathbf{F}_{i+1}^n - \mathbf{F}_i^n) - \mathbf{A}_{i-1/2}^n (\mathbf{F}_i^n - \mathbf{F}_{i-1}^n)] \quad (2.54)$$

The combination of centred temporal and spatial discretization results in second-order accuracy in both time and space on a three point computational stencil. The scheme can be graphically represented as in Figure 2.2, and it is the unique second-order central explicit scheme for the linear equation on three point support [3].

2.6.3 TWO STEPS LAX-WENDROFF SCHEMES

The main disadvantage of this method is the Jacobian matrix evaluation. To prevent the calculation from this difficulty, Richtmyer and Morton [24] suggested a two-step variant of the Lax & Wendroff method, leading to a whole family of variants when applied to non-linear systems [3].

This method retain the second order accuracy. The first step, utilized to solve the equations, is based on space-centred differences about the point $(i\Delta x, n\Delta t)$, while the second step is a mid-point leapfrog calculation, with the time difference centred on the point $[i\Delta x, (n+1)\Delta t]$. The values of \mathbf{W} can be then written as:

$$\mathbf{W}_i^{n+1} = \frac{1}{2} (\mathbf{W}_{i+1}^n + \mathbf{W}_{i-1}^n) - \frac{\Delta t}{2\Delta x} (\mathbf{F}_{i+1}^n - \mathbf{F}_{i-1}^n) \quad (\text{first step}) \quad (2.55)$$

and

$$\mathbf{W}_i^{n+2} = \mathbf{W}_i^n - \frac{\Delta t}{\Delta x} (\mathbf{F}_{i+1}^{n+1} - \mathbf{F}_{i-1}^{n+1}) \quad (\text{second step}) \quad (2.56)$$

where the values of \mathbf{F} in the second step are obtained using the values of \mathbf{W} from the first step. This approach is called Richtmyer method, and it can be applied over half-mesh intervals, by using space differences centred about the points $[(i+1/2)\Delta x, n\Delta t]$ and $[(i-1/2)\Delta x, n\Delta t]$, while the time differences are centred about the point $[i\Delta x, (n+1/2)\Delta t]$. In this way the following equations can be written:

$$\mathbf{W}_{i+1/2}^{n+1/2} = \frac{1}{2} (\mathbf{W}_{i+1}^n + \mathbf{W}_i^n) - \frac{\Delta t}{2\Delta x} (\mathbf{F}_{i+1}^n - \mathbf{F}_i^n) \quad (2.57)$$

$$\mathbf{W}_{i-1/2}^{n+1/2} = \frac{1}{2} (\mathbf{W}_i^n + \mathbf{W}_{i-1}^n) - \frac{\Delta t}{2\Delta x} (\mathbf{F}_i^n - \mathbf{F}_{i-1}^n) \quad (2.58)$$

$$\mathbf{W}_i^{n+1} = \mathbf{W}_i^n - \frac{\Delta t}{\Delta x} (\mathbf{F}_{i+1/2}^{n+1/2} - \mathbf{F}_{i-1/2}^{n+1/2}) \quad (2.59)$$

When the source term \mathbf{C} is not neglect able, the full system of equations is represented by the equation (2.4) and it can be discretized, in accordance with the two step Lax-Wendroff method, in this way:

$$\mathbf{W}_{i+1/2}^{n+1/2} = \frac{1}{2} (\mathbf{W}_{i+1}^n + \mathbf{W}_i^n) - \frac{\Delta t}{2\Delta x} (\mathbf{F}_{i+1}^n - \mathbf{F}_i^n) - \frac{\Delta t}{4} (\mathbf{C}_{i+1}^n + \mathbf{C}_i^n) \quad (2.60)$$

and

$$\mathbf{W}_i^{n+1} = \mathbf{W}_i^n - \frac{\Delta t}{\Delta x} (\mathbf{F}_{i+1/2}^{n+1/2} - \mathbf{F}_{i-1/2}^{n+1/2}) - \frac{\Delta t}{2} (\mathbf{C}_{i+1/2}^{n+1/2} + \mathbf{C}_{i-1/2}^{n+1/2}) \quad (2.61)$$

Two-step variant of the Lax & Wendroff method leads to a whole family of variants when applied to non-linear systems, represented by the MacCormack method [25].

2.7 IMPROVEMENT OF THE SECOND ORDER DIFFERENCE SCHEMES

The Lax-Wendroff and the two step Lax-Wendroff methods are classical shock capturing schemes which can be proficiently used in engine simulations when used in conjunction with appropriate *flux limiting* techniques. The need of such a conjunction is due to the fact that finite difference schemes, with greater than first-order accuracy and constant coefficients, produce local instabilities in the presence of shock waves and contact surfaces as a consequence of Godunov's theorem [22]. These oscillations are nonphysical and are known as *Gibb's phenomenon* [22].

This difficulty is intrinsic in all linear second-order difference schemes, that is second order accuracy schemes with constant coefficients, such as that defined by the equations (2.57)-(2.59).

2.7.2 TVD FLUX LIMITERS

The issue of the non-physical overshoots produced by simple second-order schemes can be sorted out by using non-linear difference schemes, where the coefficients of the schemes depend on the value of the solution itself at each mesh point [3]. The goal is to use a higher order approach, but increasing locally the amount of numerical dissipation in the region where a discontinuity is revealed. For a generic linear advection equation, such as

$$\frac{\partial w}{\partial t} + a \frac{\partial w}{\partial x} = 0 \quad (2.62)$$

the one step Lax-Wendroff scheme can be written in the form:

$$w_i^{n+1} = \underbrace{w_i^n - v w_{i-1/2}^n}_{\text{first order scheme}} - \underbrace{\frac{1}{2} v(1-v) \Delta_- \left(\Delta w_{i+1/2}^n \right)}_{\text{additional term}} \quad (2.63)$$

second order scheme

where

$$v = a \frac{\Delta t}{\Delta x} \quad (2.64)$$

$$\Delta_- (\Delta w_{i+1/2}^n) = (w_{i+1}^n + w_i^n) - (w_i^n - w_{i-1}^n)$$

As shown, the equation (2.63) represents a second order scheme, and it is composed by two terms: a first order scheme, and an additional term. Since the first one is first order accurate, and therefore diffusive and not susceptible to give spurious oscillations at discontinuities, the additional term will represent the anti-diffusive flux which will give rise to instabilities in solution.

In order to circumvent the problem of spurious oscillations and contemporarily retain the second order accuracy, a solution is given limiting selectively the order of accuracy, or better the magnitude of the anti-diffusive flux, in the regions with steep gradients, and applying the full anti-diffusive term in the other regions.

In order to do that, a gradient monitor is required, which must be able to locally change the coefficients of the scheme. From this point of view, the resulting scheme will be non-linear. In fact the (2.64) will be transformed into:

$$w_i^{n+1} = w_i^n - v w_{i-1/2}^n - \frac{1}{2} v(1-v) \Delta_- \left(\Delta_i w_{i+1/2}^n \right) \quad (2.65)$$

where ϕ is a form of limiter function, called *flux limiter*. This latter must be a function of the solution, meaning that, if the data adjacent to w_i is smooth, then ϕ_i should be close to 1 in order to maintain the second-order accuracy. Contrariwise, in the proximity of a discontinuity, ϕ_i should be close to 0 in order to reduce the accuracy of the scheme to first order and to introduce a sufficient dissipation to reduce oscillations of the solution [3].

The smoothness of the data can be measures in many ways. One widely accepted possibility was proposed by van Leer and consist of a function of the ratio of consecutive gradients of the solution, which change sign at points of extreme (maxima and minima):

$$\phi_i = \phi(r_i) \quad (2.66)$$

where

$$r_i = \frac{\Delta w_{i-1/2}^n}{\Delta w_{i+1/2}^n} \quad (2.67)$$

The most common used criterion for the function ϕ is based on *the total variation diminishing* (TVD) concept. The total variation of the solution at time $n\Delta t$ is defined by:

$$TV(w^n) = \sum_i |w_{i+1}^n - w_i^n| \quad (2.68)$$

When a spurious oscillation is generated a new extreme is introduced in the solution or a maximum point increases or a minimum point decreases. In this case the total variation increases. If the total variation of the solution does not increase from one time step to another one, then

$$TV(w^{n+1}) \leq TV(w^n) \quad (2.69)$$

and the data is said to be total variation diminishing. In this case no spurious oscillations are generated at discontinuities.

As a consequence of this concept, a post-processing routine which converts the results obtained with the Lax-Wendroff scheme into TVD form has been developed by Davies [26], [3].

2.7.3 FLUX CORRECTED TRANSPORT

These techniques were developed by Boris and Book [27] in order to avoid non-physical overshoots produced by simple second-order schemes. As Niessner and Bulaty described later [28] these techniques consist of three different steps.

The first step, named transport, obtains the preliminary solution at the next time step by means of a simple second-order accuracy scheme like Lax-Wandroff. Next, at the diffusion step, these results are post-processed applying an artificial smoothing operation to eliminate the gas property discontinuities. The last step, named anti-diffusion recovers the second-order accuracy, where diffusion is not needed, to eliminate non-physical overshoots, and the original solution is smooth.

Applying these techniques directly to vector \mathbf{W} would lead, if source terms are present, to a violation in the conservation laws. For this reason, conservative parameters such as mass

flow rate, stagnation enthalpy and stagnation pressure, given in equation. (2.62), should be used in the smoothing process instead of the components of vector \mathbf{W} :

$$\dot{m} = \rho u S, \quad h_0 = \frac{\gamma R T}{\gamma - 1} + \frac{u^2}{2}, \quad p_0 = p \left[1 + \frac{\gamma - 1}{2} \frac{u^2}{\gamma R T} \right]^{\gamma/(\gamma - 1)} \quad (2.70)$$

Under homentropic flow with constant section, it is not necessary to change the vector \mathbf{W} to conservative parameters and this technique is applied directly to the solution vector.

2.8 CONSERVATION ELEMENT – SOLUTION ELEMENT

This scheme was proposed by Chang and To [29] for the homentropic problem and later adapted by Briz and Giannattasio [30] in order to allow consideration of source terms. In this case, the numerical overshoot, typical in simple second-order schemes, is removed by replacing the simple averaging formula, initially used, with a weighted averaging formula. The space–time plane is divided into rhombic non-overlapping regions, referred to as *solution elements* (SEs), centred at a mesh point, in which the solution is approximated by first-order Taylor series as:

$$w_m(x, t, j, n) = (\sigma_m)_j^n + (\alpha_m)_j^n (x - x_j) + (\beta_m)_j^n (t - t_n), \quad m = 1, 2, 3. \quad (2.71)$$

Additionally, the space–time plane is also divided into rectangular regions that fill the space–time domain without overlap, called *conservation elements* (CEs), in which the conservation laws are satisfied. In order to advance a half-time step, the coefficients of all Taylor series of the next SEs must be calculated.

2.9 BOUNDARY CONDITIONS

An important aspect of the calculation is represented by the boundary conditions: every pipe has two ends associated with it, and hence has two boundaries. There are various types of boundary and these must be simulated in a satisfactory manner.

Winterbone [3] indicates that the best solution is to try to use the same boundary conditions as for the method of characteristics by means of the generation, from the results of

the finite-differences calculation, of auxiliary characteristic lines at the boundaries. This solution has the advantage that physical insight into the flow at the boundaries is preserved. The reason is that the only way to get to the end of the pipe, in a logical manner, is to go along a wave. A full derivation of boundary characteristics is given in [1] where typical boundaries for which methods exist are given: open ends, closed ends, inflow boundaries, valve boundaries, junctions (both with and without pressure losses), pulse converter, orifices or valves in pipes, throttle bodies, turbines, compressors, intercoolers, and anechoic terminations for acoustical purposes. These all have one feature in common: they are all treated as if the flow is quasi-steady, which means that the characteristics of the boundary is not a function of the frequency of the incident waveform. Such an assumption is more appropriate to a simple boundary, such as a closed end, then one with relatively large volume, such as a turbine.

2.10 COMPARISON OF NUMERICAL SCHEMES IN SILENCER ANALYSES

In the work [31], Broatch *et al.* compared the performance of different schemes, used to solve one-dimensional gas flow equations, when applied to the computation of the frequency response of exhaust mufflers. Simple geometries with well-known acoustic behaviour, and sufficiently representative of attenuation mechanisms present in real mufflers, were chosen, such as the expansion chamber and the Herschel-Quincke tube in Figure 2.3.

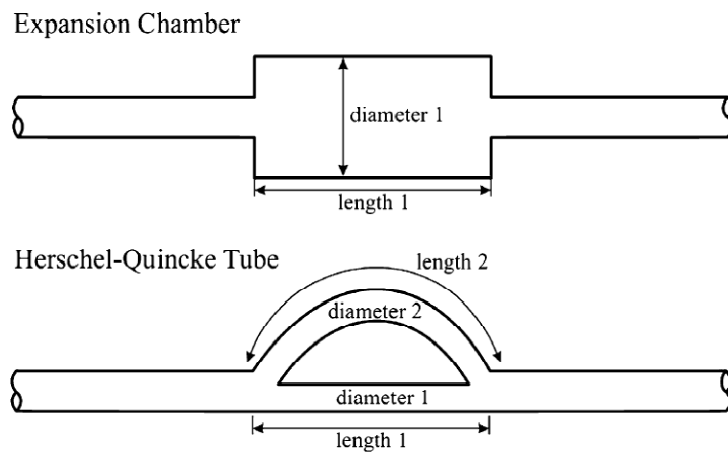


Figure 2.3 – Utilized silencers for the numerical tests carried out in [31].

The numerical schemes tested were:

- two centred schemes (two-step Lax–Wendroff and MacCormack predictor–corrector;

- four high-resolution schemes: the FCT method (based on the Lax–Wendroff scheme), two TVD schemes (one using Sweby’s flux limiting techniques and the other using Harten’s correction techniques) and
- the innovative space–time conservation element and solution element scheme.

With this choice a representative set of currently used numerical schemes is available that should provide a rather complete picture of the problem.

The study was focused on the quality of the results obtained, taking into account the sensitivity to the mesh spacing used and the computational cost. Also the theoretical computational cost, required to achieve a certain accuracy, has been analysed. In this sense, it has been shown that good results may be obtained from any method if the mesh spacing is sufficiently small.

However, when considering global engine simulations, aiming at exhaust noise prediction, such small meshes may imply an excessive computation time. This represents a serious penalty for high resolution schemes, which are considerably slower than simple centred schemes. In addition, these differences in computational time are higher if a certain accuracy is required, since high-resolution schemes need more *points per wavelength* (PPW).

In the Figure 2.4 a comparison of computational times is depicted, once an arbitrary time unit, the time required to simulate the entire engine-plus-muffler system with the conservation element–solution element method, has been chosen. In this picture the following abbreviations are utilized:

- CE–SE: conservation element–solution element
- FCT: flow corrected transport
- LW: two-step Lax–Wendroff
- TVDC: total variation diminishing with flux correction
- TVDL: total variation diminishing with flux limitation

The sensitivity of the different methods to the mesh spacing was then investigated, with the main conclusion that both the two-step Lax–Wendroff method and the CE–SE method do not exhibit an important influence of the mesh spacing, and thus relatively high values may be used without any loss of information.

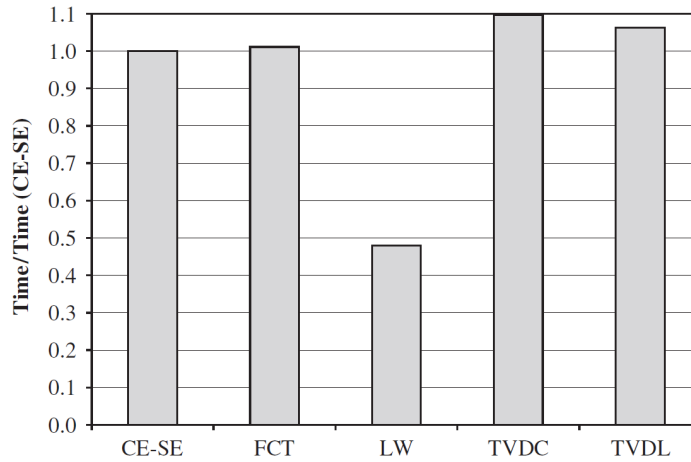


Figure 2.4 – Comparison of computation time for different schemes and equal mesh spacing [31].

In that work, also the theoretical computational effort, required by the different methodologies, has been compared. This effort has been obtained by multiplying the CPU steps times the PPW required to achieve a certain accuracy in reproducing the resonance frequency of a Herschel-Quincke tube. Considering a phase error lower than 0.2%, the points per wavelength needed to reach that accuracy are obtained from the results with different mesh sizes. Also in this case, the Lax–Wendroff scheme presents the lowest computational effort and CE–SE is the fact that the Lax–Wendroff method (and, in general, simple schemes) is considerably faster suggests that it is a better option.

The other high-resolution schemes (FCT and TVD) exhibit a considerable influence of the mesh spacing on the frequency results. Therefore, they should not be considered as a valid option for exhaust noise prediction with global engine simulations. On the contrary, the CE–SE method is comparably robust when sharp discontinuities are present in the flow and, being less sensitive to mesh spacing, it provides a better compromise between the useful frequency range and the computation time required [31].

2.11 MODELLING SIMPLE REACTIVE SILENCERS

Reactive silencers have been introduced in the Chapter 1. Simple reactive silencers include expansion chambers, quarter wave and Helmholtz resonators.

The gas dynamic modelling of these components is relatively simple, and can be based on the existing boundary conditions developed in [3]. The sudden area change of the expansion chamber can be treated by the sudden enlargement-contraction model devised by Benson [32],

as can the abrupt area change of the Helmholtz resonator and the interface between the neck and the volume. [3]

The cavity of the Helmholtz resonator has to be represented by an equivalent cylindrical duct with the appropriate volume and geometrical length to avoid the limitations of a lumped parameter approach and to enable all the resonant frequencies of the system to be captured. The closed end boundary condition [3] is used for end wall of both the cavity and the column resonator. The “T” junction, arising in both of the resonators at the interface with the tube can be satisfactorily described by the constant pressure model of Benson [32]. The proper end correction must be used at each geometrical discontinuity to take into account the side effects (see Chapter 1).

Since the mean flow in the side resonators is zero, the pressure losses in the junction are not significant, but taking them into account may provide a more accurate prediction of the resonator attenuation [3].

2.12 White noise perturbation

When the attenuation curve of a silencer must be carried out, two different numerical non linear strategies can be followed. The first one, in the frequency domain, uses an upstream excitation characterized by an harmonic pressure perturbation. This procedure must be repeated many times, imposing every time a different harmonic law, in order to obtain the transfer function of the silencer over the frequency band. An advantage of this approach is the high precision, but the main disadvantage is represented by the high time computational requirements. For this reason it becomes unattractive when complex silencers must be analyzed [3].

An alternative approach is based on a different upstream excitation source, represented by a *white noise*, in which the pressure signal has a spectral content which is uniformly distributed over the frequency band, so that it is possible to evaluate the gas dynamic response of the muffle to all the concurrent excitation frequencies at once. When a steady pattern of standing waves has been reached, the pressure and velocity oscillations in the system are characterized by a significant amplitude of the spectral components for each frequency of the white noise introduced in the silencer. Fourier analysis of the signals enables the transfer function, that is the attenuation curve, to be predicted. This white noise approach is very rapid

compared to using acoustic excitation by means of large set of single harmonic pressure oscillations.

The numerical generation of a white noise periodic pressure signal may be carried out as the sum of N sinusoidal pressure oscillations with a fixed amplitude, Δp , and frequency multiple of the fundamental frequency f :

$$p(t) = p_0 + \sum_{n=1}^N \Delta p \sin(2\pi n f t + \varphi_n) \quad (2.72)$$

where p_0 is a constant value which represents the mean ambient pressure upstream of the duct-system, It is essential to make a suitable choice of the phase φ_n . The generation of N random numbers k_n in the range 0-1, via a dedicated numerical routine, enables a random phase, $\varphi_n = 2\pi k_n$, to be determined for each sinusoidal component of the sum. This choice yields a pressure signal $p(t)$ with a random character, which falls in the band of prescribed pressure values [3].

2.13 PERFORATED TUBE SILENCERS

Perforated ducts are quite common elements in silencers and many different numerical approaches have been developed in order to obtain an accurate model. Selamet *et al.* [33] proposed a non-linear time domain approach to describe the perforate sections, based on the approach of Sullivan [34] for the treatment of the flow through the holes. The appropriate momentum equation in the radial direction at the perforate boundary has been considered, obtaining a branch point model of the system which involves a sequence of three way branches to account for the coupling of the perforated tube and the cavity.

Onorati proposed a different approach [35]: a boundary condition of equal total enthalpy (constant pressure) was imposed to branches of several ducts in order to represent the flows in every single hole. Let's consider a perforated tube of diameter d , length l , characterized by m groups of n holes distributed on a circle, each group separated from the adjacent by a distance p . In this case the silencer is schematized by mean of m contiguous axial elements, representing the tube, connected to other m contiguous axial elements, schematizing the surrounding camera, by mean of $m+1$ groups of n short ducts, schematizing the holes [3]. The

diameter and the length of these short ducts are equal to the tube thickness and hole diameter. The axial elements have a length equal to the hole spacing p and an equivalent diameter which is function of the tube and chamber diameters.

2.14 QUASI 3D APPROACHES

Montenegro *et al.* recently proposed a quasi 3D approach, named *3Dcell*, for modelling silencers and catalytic converters [36]. A similar approach is implemented in a variety of software packages, such as GTPowerTM [37] utilized in this thesis (see Chapter 5).

The *3Dcell* approach consists in reproducing a 3D geometry as a network of 0D elements, such as volumes, to which characteristic length in the space are assigned [36]. As shown in Figure 2.5, the 3Dcell framework is defined by means of two fundamental elements, namely *cell* and *connector*. The cell element is defined by its volume and by a list of connectors linked to it. The connector element stores information about the connectivity between neighbouring cells, and geometrical parameters such as the distance from the adjacent cell centres, the flow area and the direction, with respect to an absolute orientation system, given by the normal to the surface it represents. The 3Dcell method is based on the formulation of the conservation equations of mass, momentum and energy for unsteady flows in which the gas viscosity, both in the intake and exhaust system, has been neglected. Since its value is very low, this approximation is acceptable and allows to considerably simplify the solution procedure. This system of equations is then closed by the perfect gas equation of state.

The 3Dcell model is based on a pseudo-staggered grid approach, meaning that intensive properties such as pressure, temperature, density, internal energy and other derived quantities are defined over the cell element, while velocity and momentum are defined on the connectors [36].

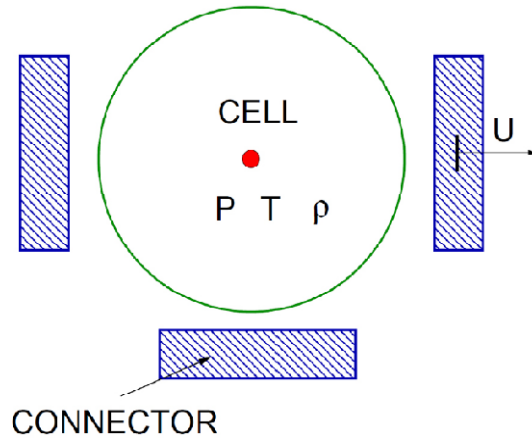


Figure 2.5 – Quasi 3D element: cell and connectors [36].

The continuity and energy conservation equations are solved with respect to the cell element, taking into account the net flux of the conserved variables through all the connectors linked to the cell. According to this type of discretization, the continuity equation can be integrated over the volume and over the time.

To allow the construction of the connector momentum equation, the velocity has been defined also in the centroid of the cell element. The cell velocity is oriented in the space and consequently has three components. Hence, when the solution of the connector momentum is addressed, the projection of the velocity along the connector normal direction is considered. This reduces a 3D problem to a 1D problem arbitrarily oriented in space [36].

2.15 DISSIPATIVE SILENCERS MODELLING

Dissipative silencers are widely utilized devices, as explained in the Chapter 1. They are able to provide good attenuation performances over the broad band, especially if dissipative and reflective behaviour are combined together.

In order to model the dissipative action of these silencers, a typical approach consists of introducing high distributed and concentrated pressure losses in some regions of the system, rendered via acoustically equivalent schemes [3]. First, a very high friction coefficient ($f=0.1$ compared with the typical $f=0.004-0.005$) can be adopted for all the ducts adjoining the sound absorptive material. Second, adiabatic pressure losses can be introduced in the middle of all the ducts representing the cavity, by means of the adiabatic pressure loss boundary conditions described in [3], with a value of the resistance coefficient K equal to 50. Both the losses enable the dissipation of the incident acoustic energy to be accounted for as heat in the

absorption lining. Obviously the sound absorptive features of the silencer, which depend on the lining thickness and properties, may be simulated approximately by a suitable combination of distributed and concentrated losses [3].

REFERENCES

74. D.E. Winterbone, R.J. Pearson, Theory of engine manifold design, Wave action methods for IC engines, Professional engineering publishing, London, 2000
75. C. Hirsch, Numerical Computation of internal and external flows – Computational methods for inviscid and viscous flows, John Wiley & sons, Baffins Lane, Chichester, England, 1990.
76. D.E. Winterbone, R.J. Pearson, Design Techniques for Engine Manifolds – Wave action methods for IC Engines, Professional engineering publishing, London, 1999.
77. M. Knutsson, Modelling of IC-Engine Intake Noise, doctoral thesis, KTH, Stockholm, Sweden, 2009.
78. P. O. A. L. Davies, Practical flow duct acoustics. 1988 Journal of Sound and Vibration 124, 91-115.
79. M.L. Munjal, Acoustics of Ducts and Mufflers, New York, Wiley-Interscience, 1987.
80. M. Abom, Measurement of the scattering matrix of acoustical two-ports, Mechanical systems and signal processing (1991) 5 (2), 89, 104.
81. J. Kim, Y. Kim, J. Maeng, M. Lyu, Y. Ku, Unstructured grid finite volume analysis for acoustic and pulse wave propagation characteristics in exhaust silencer systems, Numerical heat transfer, Part A, 30, 439-457, 1996.
82. O. Chiavola, Multi-dimensional CFD-transmission matrix modelling of IC engine intake and exhaust systems, Journal of Sound and Vibration 256 (2) (2002) 835–848.
83. A. D. Jones, Modelling the exhaust noise radiated from reciprocating internal combustion engines -A literature review, Noise Control Engineering Journal 23(1), pp. 12-31, 1984.
84. P. O. A. L. Davies, M.F. Harrison, Predictive acoustic modelling applied to the control of intake/exhaust noise of internal combustion engines, Journal of Sound and Vibration 202(2), 249-274, 1997.
85. F. Bozza, A. Gimelli, R. Piazzesi, F. Fortunato, V. Pianese, and D. Siano. The prediction of the performance and gasdynamic noise emitted by a medium-size spark-ignition engine by means of 1d and 3d analyses. SAE Int. Congress & Exp., 2007-01-0380, 2007.
86. G. Ferrari, A. Onorati, Modellazione Fluidodinamica non-lineare di silenziatori ad elementi perforati e con materiale fonoassorbente, Proceedings of the 51st ATI Conference, 937-952, 1996.
87. G. Montenegro, A. Onorati, A.d. Torre, The 3D cell approach for the acoustic modeling of after-treatment devices, SAE 2011-24-0215, 2011.
88. A. Onorati, Non-linear fluid dynamic modeling of reactive silencers involving extended inlet/outlet and perforated ducts, Noise Control Engineering Journal 45 (1997) 35–51.
89. A.I. Abd El-Rahman, A.S. Sabry, A. Mobarak, Non-linear simulation of single pass perforated tube silencers based on the method of characteristics, Journal of Sound and Vibration 278 (2004) 63–81.
90. J.R Serrano, F.J. Arnau, P. Piqueras, A. Onorati, G. Montenegro, 1D gas dynamic modeling of mass conservation in engine duct systems with thermal contact discontinuities, Mathematical and Computer Modelling 49 (2009) 1078–1088

91. R.S. Benson, *The Thermodynamics and Gas Dynamics of Internal-Combustion Engines*, vol. 1, Clarendon Press Oxford, 1982.
92. R. Courant, E. Isaacson, M. Rees, On the solution of nonlinear hyperbolic differential equations by finite differences, *Communications on Pure and Applied Mathematics* 5.
93. P.D. Lax, Weak solutions of non linear hyperbolic equations and their numerical computation, *Communications on Pure and Applied Mathematics* 7 (1954) 159–193.
94. P.D. Lax, B. Wendroff, Systems of conservation laws, *Communications on Pure and Applied Mathematics* 17 (1964) 381–398.
95. S.K. Godunov, A difference scheme for numerical computation of discontinuous solutions of hydrodynamics equations, *Mathematics of the USSR, Sbornik* 47 (1959) 271–306. english translation in US Joint Publication Research Service, JPRS 7226, 1969.
96. J.L. Steger, R.F. Warming, Flux vector splitting of the inviscid gas dynamic equations with application to finite-difference methods, *Journal of Computational Physics* 40 (1981) 236–293
97. R.D. Richtmyer, K.W. Morton, *Difference methods for initial value problems*, Interscience, New York.
98. R.W. MacCormack, The effect of viscosity in hypervelocity impact cratering, *AIAA Paper* (1969-354).
99. S.F. Davies, A simplified TVD finite difference scheme via artificial viscosity, *SIAM Journal on scientific computing*, 8, 1-18.
100. J.P. Boris, D.L. Book, Flux-corrected transport I. SHASTA: a fluid transport algorithm that works, *Journal of Computational Physics* 11 (1973) 39–69.
101. H. Niessner, T. Bulaty, A family of flux-correction methods to avoid overshoot occurring with solutions of unsteady flow problems, *Proceedings of the GAMM Conference of Numerical Methods of Fluid Mechanics*, Paris, France, 2003, pp. 241–250.
102. S.C. Chang, W.M. To, A new numerical framework for solving conservation laws—The method of space–time conservation element and solution element, *NASA TM* 104495, 1991.
103. G. Briz, P. Giannattasio, Applicazione dello schema numerico conservation element—solution element al calcolo del flusso instazionario nei condotti dei motori a C.I, *Proceedings of the 48th ATI National Congress*, Taormina, Italy, 1993, pp. 233–247.
104. A. Broatch, J.R. Serrano, F.J. Arnau, D. Moya, Time-domain computation of muffler frequency response: Comparison of different numerical schemes, *Journal of Sound and Vibration* 305 (2007) 333–347.
105. Benson, *The thermodynamics and gas dynamics of internal combustion engines*, Volume I, Carendon press, Oxford.
106. A. Selamet, N.S. Dickey, J.M. Novak, A time domain-based computational approach for perforated tube silencers, *Proceeding of Noise Congress '93: Noise control in aero-acoustics*, pp-291-296, 1993.
107. J.W. Sullivan, A method for modelling perforated tube muffler components. I. Theory. II. Applications, *Journal of Acoustical Society of America*, 66, 772-788.

108. A. Onorati, Non-linear fluid dynamic modeling of reactive silencers involving extended inlet/outlet and perforated ducts, *Noise Control Engineering Journal*, 45, 35-51, 1997.
109. G. Montenegro, A. Onorati, A.d. Torre, The 3D cell approach for the acoustic modeling of after-treatment devices, *SAE 2011-24-0215*, 2011.
110. Gamma Technologies, *GT-ISE User's Manual Version 6.1*, the GT-SUITE Interactive Simulation Environment, 2004.

Chapter 3

3D linear numerical methods in acoustics

3.1 INTRODUCTION

When the sound excitation is limited to small amplitude perturbations, the most accurate approach to the acoustic problem is represented by the three-dimensional (3D) linear methods. In the specific case of silencers, a 3D description of the acoustic field is mandatory when the frequencies of interest exceed the plane wave region. In this case, the one dimensional (1D) frequency-domain acoustics, as well as the 1D time-domain finite wave theory, fail. The 3D approach is needed especially when the muffler internal shape is complicate, for example when flow reversing chambers are included in the silencer. Finite Element Method (FEM) and Boundary Element Method (BEM) are 3D numerical techniques which have been successfully utilized for more than 30 years. Both methodologies were initially developed, in the late '60s, for structural analyses, and the first commercial software focussed on acoustical problems, D.E. SysnoiseTM (1988), included and FEM and BEM acoustics [1]-[2].

These methods approximate the solution of the acoustical problem in a piecewise form. The difference is that the FEM solves the unknown quantities in the acoustical domain (air), which needs to be entirely discretized, whereas the BEM solves it on the boundary of the domain itself. These latter is the only part to be discretized, and the solution within the domain is then carried out by utilizing the solution on the boundary.

A positive aspect of the BEM is that it requires fewer degrees of freedom than the FEM, due to the type of discretization. On the other hand, the BE formulations typically give rise to fully populated matrices, which means that the storage requirements and computational time will tend to grow according to the square of the problem size. Contrariwise, the FE matrices are typically banded (elements are only locally connected) and the storage requirements for the system matrices typically grow quite linearly with the problem size [3].

The BEM is often preferred in case of homogeneous and uncoupled problems, especially in large domains. In these cases it is definitely faster than the FEM, certainly when a fast multipole procedure is implemented [4]. It is widely utilized in predictions of transmission

loss of complicated exhaust components, in the simulations of the sound radiated from engines and compressors, and in studies on passenger compartment noise. Also a number of results shown in this thesis (see Chapter 5) have been carried out by utilizing this methodology [4].

The strength of FE models lies in their general robustness, their ability to treat inhomogeneous media and to take advantage of the sparse nature of structural discrete models in coupled acoustical-structural computations. A coupled acoustical-structural investigation on a commercial silencer will be presented in this thesis (see Chapter 5), where the FEM has been utilized to perform a modal analysis [1] and the BEM to carry out the acoustic simulation.

In this chapter the essential features of the two methodologies will be presented, and a number of typical FEM-BEM applications are reviewed.

3.2 ACOUSTIC WAVE EQUATION AND BOUNDARY CONDITIONS

As previously mentioned, since the acoustic pressure, density, and particle velocity fluctuations associated with sound waves in air are usually relatively small, the equations governing mass and momentum conservation in a fluid continuum can be considerably simplified, in order to relate these acoustical variables to one another. The general conservation equations can be then linearized, and the terms proportional to the product of the acoustical variables can be discarded from the equations.

In these hypotheses the equation of mass conservation in a homogeneous three-dimensional medium at rest reduces to [1]:

$$\frac{\partial \rho}{\partial t} + \rho_0 \nabla \cdot \mathbf{u} = 0 \quad (3.1)$$

where $\rho(\mathbf{x})$ is the local density, $\rho_0(\mathbf{x})$ is the average density of the medium, and $\mathbf{u}(\mathbf{x})$ is the particle velocity vector.

Similarly, for an inviscid medium, the linearized equations of momentum conservation in these three coordinate directions is:

$$\rho_0 \frac{\partial \mathbf{u}}{\partial t} + \nabla p = 0 \quad (3.2)$$

where $p(\mathbf{x})$ is the local pressure value. Using the relation

$$p = c_0^2 \rho \quad (3.3)$$

which relates the local pressure, $p(\mathbf{x})$, and the local density, $\rho(\mathbf{x})$, through the speed of sound in air, c_0 , in case of small (isoentropic) fluctuations, one obtains:

$$\nabla^2 p - \frac{1}{c_0^2} \frac{\partial^2 p}{\partial t^2} = 0 \quad (3.4)$$

which is the equation governing the behaviour of acoustic pressure fluctuations in three dimensions. In the case of time harmonic disturbances of pulsation ω ,

$$p(\mathbf{x}, t) = \hat{p}(\mathbf{x}, t) e^{i\omega t} \quad (3.5)$$

the equation (3.4) transforms into the *Helmholtz's equation*:

$$\nabla^2 \hat{p} + k^2 \hat{p} = 0 \quad (3.6)$$

where $k = \omega/c_0$ is the angular wave number.

In this chapter, time-domain quantities are denoted by lower-case variables p , \mathbf{u} , . . . and corresponding frequency-domain quantities by an upper symbol on the lower case variables \hat{p} , $\hat{\mathbf{u}}$, . . .

When the considered fluid is inhomogeneous ($\rho_0 c_0$ is not constant) and there is a distributed acoustic source $w(\mathbf{x}, t)$ (i.e. a monopole, dipole, etc.), the (3.6) assumes the most generic form:

$$\rho_0 \nabla \left(\frac{1}{\rho_0} \nabla \hat{p} \right) + k^2 \hat{p} = \hat{w} \quad (3.6b)$$

On a generic boundary surface a fluid particle velocity $\hat{\mathbf{u}}_f$ and a surface velocity $\hat{\mathbf{u}}_s$ can be defined. In fact, if a lining material is present on the surface, $\hat{\mathbf{u}}_f$ and $\hat{\mathbf{u}}_s$ can be different due to the internal damping of the absorber. A relative velocity $\hat{\mathbf{u}}_r$ is then defined as:

$$\hat{\mathbf{u}}_r = \hat{\mathbf{u}}_f - \hat{\mathbf{u}}_s \quad (3.7)$$

On the same boundary surface, the wall impedance is defined as the complex ratio

$$Z(\omega) = \frac{\hat{p}(\omega)}{\hat{u}_{r,n}(\omega)} \quad (3.8)$$

where $\hat{u}_{r,n} = \hat{\mathbf{u}}_r \cdot \mathbf{n}$ is the normal component of the relative velocity (\mathbf{n} is the outward normal). $\hat{u}_{r,n}$ is obviously also equal to the difference of the normal component of the fluid particle velocity, $u_{f,n} = \hat{\mathbf{u}}_f \cdot \mathbf{n}$, and the normal component of the surface particle velocity, $u_{s,n} = \hat{\mathbf{u}}_s \cdot \mathbf{n}$ at the same point:

$$\hat{u}_{r,n} = \hat{u}_{f,n} - \hat{u}_{s,n} \quad (3.9)$$

Moreover, the normal fluid particle velocity is related to the normal derivative of the sound pressure p by means of the following relation in frequency domain:

$$\hat{u}_{f,n} = \frac{1}{i\omega\rho_0} \nabla \hat{p} \cdot \mathbf{n} \quad (3.10)$$

Any solution of the wave equation has to comply with the acoustical properties of the boundary. All the boundary conditions are usually (in FEM and BEM), expressed as a *condition on the pressure normal derivative* itself.

The most common boundary conditions include the Neumann, the Dirichlet, the Robin and the prescribed normal displacement boundary conditions [5]. All of them are here reviewed together with the important Sommerfeld radiation condition:

THE VELOCITY TANGENCY (NEUMANN BC): this BC is useful to impose a known velocity on a structural surface with no lining material, which means $\hat{u}_{r,n} = 0$, that is $\hat{u}_{f,n} = \hat{u}_{s,n}$. It consists of the following relationship:

$$\nabla \hat{p} \cdot \mathbf{n} = -\rho_0 i \omega \hat{u}_{s,n} \quad (3.11)$$

RIGID IMPERVIOUS BOUNDARY (DIRICHLET BC): the normal component of the velocity is imposed to be null on the considered boundary:

$$\nabla \hat{p} \cdot \mathbf{n} = 0 \quad (3.12)$$

LOCALLY REACTING BOUNDARY (ROBIN BC – IN FREQUENCY DOMAIN): by combining the (3.8), (3.9) and (3.10), the above condition implies that:

$$\nabla \hat{p} \cdot \mathbf{n} = -i\rho\omega(\hat{u}_{s,n} - \hat{u}_{r,n}) \quad (3.13)$$

that is:

$$\nabla \hat{p} \cdot \mathbf{n} = -i\rho_0\omega(\hat{u}_{s,n} - \hat{p}A) \quad (3.14)$$

where $A(\omega) = \rho_0 c_0 / Z(\omega)$ is the dimensionless admittance. A rigid impervious boundary can be seen as a particular case of this condition, where a zero admittance is imposed.

LOCALLY REACTING BOUNDARY (ROBIN BC – IN TIME DOMAIN): the same condition of above, is more difficult to define in time domain. An inverse Fourier transform can be applied leading to the following convolutional integral (see Appendix of Chapter 4):

$$p(t) = \int_{-\infty}^{+\infty} z(t) u_n(t - \tau) d\tau \quad (3.15)$$

Where $z(t)$ is the inverse Fourier transform of $Z(\omega)$. This form of boundary condition is not easy to implement, since it requires the time history of u_n . Also $z(t)$ can be difficult to obtain, starting from the impedance models empirically defined in the frequency domain. A time-

domain expression of the (3.15) has been proposed by Van den Nieuwenhof and Coyette, see [1], which gives stable and accurate solutions.

PRESCRIBED NORMAL DISPLACEMENT: normal displacements are imposed on a boundary surface by imposing a local normal acceleration, i.e.,

$$\nabla p \cdot \mathbf{n} = \rho_0 \ddot{s} \quad \text{or} \quad \nabla \hat{p} \cdot \mathbf{n} = -i\omega^2 \rho_0 \hat{s} \quad (3.16)$$

where $s(\mathbf{x}, t) = \hat{s}(\mathbf{x})e^{i\omega t}$ is the normal displacement into the acoustic domain [1].

SOMMERFELD RADIATION CONDITION: it is the simplest non reflecting condition in acoustics and it describes the field produced by an elementary point source (monopole) at a distance R from the source itself. The non reflecting conditions are specific BCs that are applied in order to ensure that, at given boundary surface, the acoustic flow leaves the field without that any portion of the energy is transmitted back in the field itself. The Sommerfeld condition applies for field produced by simple monopolar sources when the distance R from the source is great. It is represented by the following expression:

$$\frac{\partial \hat{p}}{\partial r} + ik\hat{p} = O(R^{-\alpha}) \quad (3.17)$$

Where $\alpha=1/2$ or $\alpha=1$ in case of 2D or 3D respectively. The Sommerfeld condition can be approximated on a distant but finite cylinder (2D) or sphere (3D) by specifying a ρc impedance [1].

3.3 FEM: ACOUSTIC MODEL

As previously mentioned, the FEM is based on a complete discretization (*mesh*) of the entire investigated acoustic domain, as shown in Figure 3.1. To this aim, a finite number of small, but finite and non overlapping sub-regions, called *elements*, are created and connected to each other through a certain number of punctual parts, called *nodes*. These latter are placed on the vertices, edges, surfaces of the elements or at interior points, defining the topology of the single element. Moreover, they represent the points of information exchange between

adjacent elements. Although the unknown nodal pressures constitute the degrees of freedom of the discrete model, the solution is obtained not only at each node p_j , but in the whole domain. In fact a polynomial interpolation of the nodal pressures is carried out, whose nature depends on the typology of the utilized elements and on the number of nodes per each side element. The polynomial interpolation is then related to the notion of *shape function*, which is a founding concept of the FEM, and which will be shown afterwards.

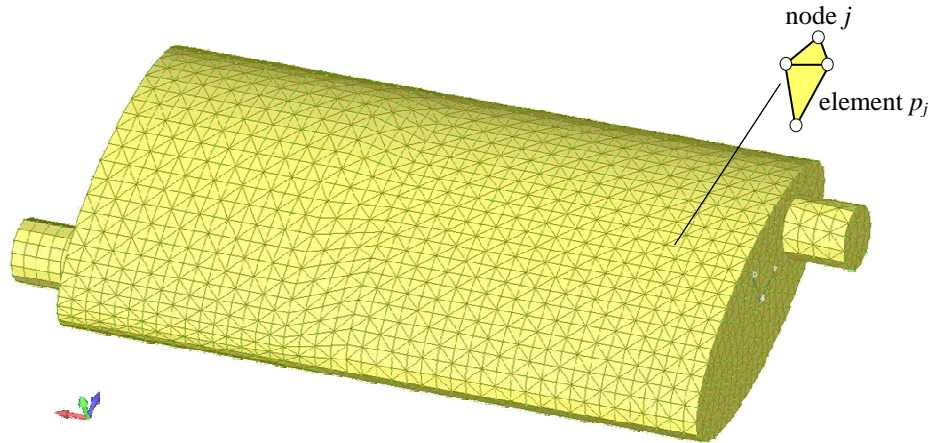


Figure 3.1 – Meshed domain of an automotive silencer.

The quality of the approximate FE solution depends on the mesh characteristics, including the size element and the node spacing. In particular, for acoustical problems, a key aspect for the obtainment of a sufficiently refined mesh is represented by the number of *nodes per wavelength* in the investigated frequency range.

A definitely positive aspect of the FEM is the possibility to use *un-structured* meshes, that is irregular meshes where the element size can vary *almost* arbitrarily. This aspect is an advantage point of FE compared to low-dispersion finite difference schemes, in which the grid points must be aligned in rows and plans. As a consequence the pre-processing software packages must deal with a *less difficult* problem, and the meshing procedure itself is simplified.

3.4 FEM: GENERAL FORMULATION FOR INTERIOR PROBLEMS

Consider the acoustical problem of a cylindrical expansion chamber with a certain excitation at inlet, a lining lateral surface and closed outlet (see Figure 3.2). Let Ω the acoustic domain bounded by a surface Γ . This surface can be divided in: Γ_{st} , which is the inlet

(*structural*) boundary on where a certain displacement, s , is imposed; Γ_h , composed by the rigid (*hard*) surfaces, including the outlet; and Γ_Z , the locally reacting surfaces (Z impedance). The domain Ω is properly discretized, and in Figure 3.2 a little part of the entire mesh, in proximity of the outlet, has been depicted.

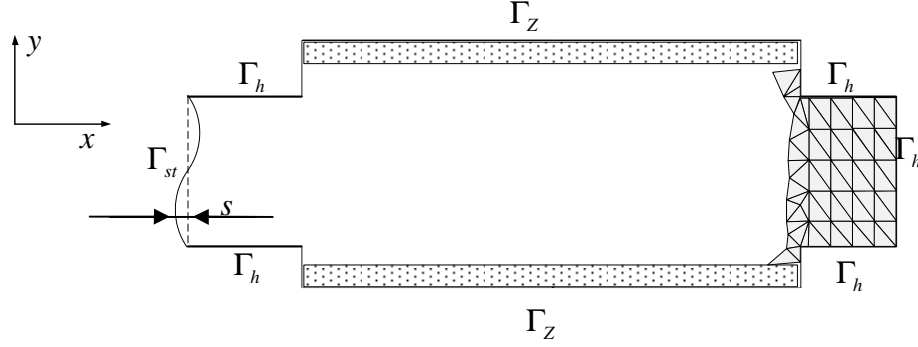


Figure 3.2 – The FE model: geometry, mesh, and boundary conditions.

The acoustic pressure $p(\mathbf{x}, t)$ is approximated by a trial function $p'(\mathbf{x}, t)$ of the form:

$$p'(\mathbf{x}, t) = \sum_{j=1}^n p_j(t) N_j(\mathbf{x}) \quad (3.18)$$

which, in frequency domain, becomes:

$$\hat{p}'(\mathbf{x}, \omega) = \sum_{j=1}^n \hat{p}_j(\omega) N_j(\mathbf{x}) \quad (3.19)$$

p_j and \hat{p}_j represent the nodal values of pressure and pressure amplitude at node j , n is the total number of nodes. The generic function $N_j(\mathbf{x})$ is called *shape function* and it is equal to 1 at node j and 0 at all other nodes (see Figure 3.3). These functions interpolate the nodal quantities all over the domain, although they are defined locally within the single element, as polynomial in physical or spatial coordinates. For this reason the trial solution, expressed by the (3.18) and (3.19), is a summation of these functions weighted by the nodal values of pressure (see Figure 3.4). The shape functions depend on the type of elements and number of nodes: for a simple triangular element with nodes on the corners, they are formed from the basis $\{1, x, y\}$ and in each triangles they have the form $a_1 + a_2x + a_3y$ where a_1, a_2, a_3 , are proper constant values chosen in a way that the shape functions take the correct values on the

nodes. This means that the number of polynomial terms in the basis set must be the same as the number of nodes in the element topology (three in the considered case).

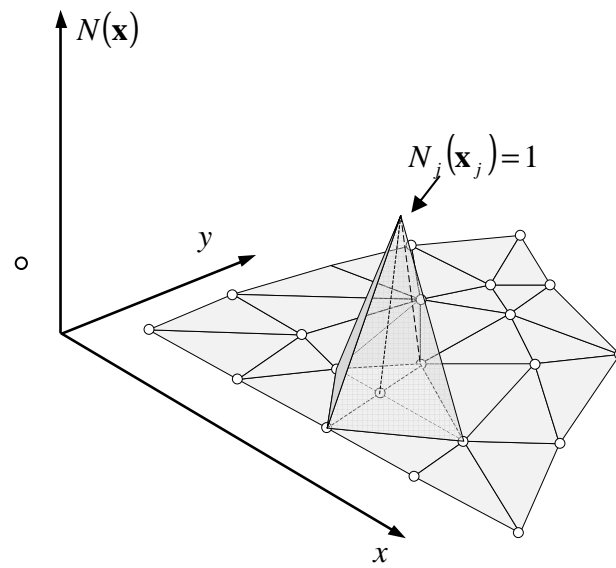


Figure 3.3 – The FE model: global shape function $N_j(x_j)$.

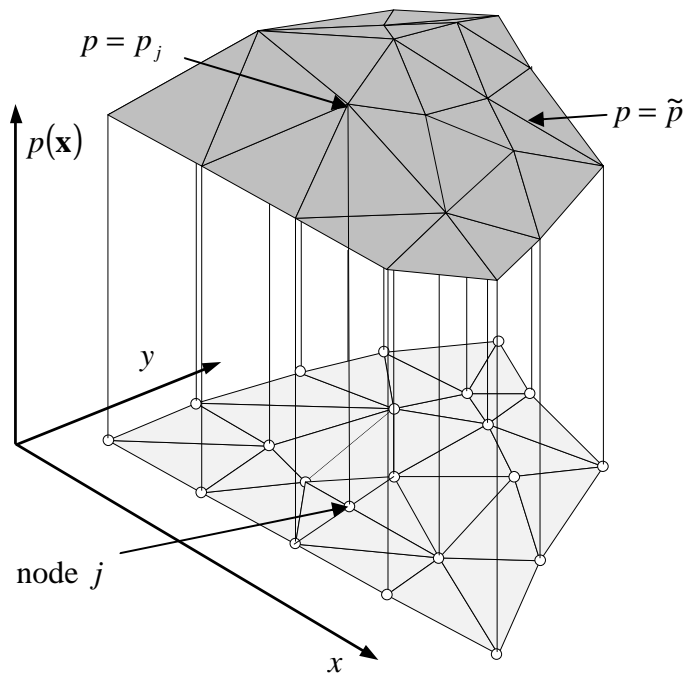


Figure 3.4 – The FE model: trial solution.

3.4.1 WEAK VARIATIONAL FORMULATION

Weak formulations are an important tool for the analysis of mathematical equations, which permit the transfer of concepts of linear algebra to solve problems in other fields, such as partial differential equations [6]. In a weak formulation, an equation is no longer required to hold absolutely and it has, instead, has weak solutions only with respect to certain “test vectors” or “test functions”.

Let $\chi(\mathbf{x})$ a continuous and differentiable test function. By multiplying the (3.6b) by the $\chi(\mathbf{x})$ and integrating over Ω , one can write:

$$\int_{\Omega} \chi(\mathbf{x}) \left[\rho_0 \nabla \left(\frac{1}{\rho_0} \nabla \hat{p} \right) + k^2 \hat{p} - \hat{w} \right] d\Omega = 0 \quad (3.20)$$

Applying the divergence theorem and imposing that the normal derivatives of pressure on the boundaries Γ_h , Γ_{st} , Γ_Z respectively satisfy the conditions (3.11), (3.12), (3.16), it is possible to obtain:

$$\int_{\Omega} \frac{1}{\rho_0} \left[\nabla \chi \cdot \nabla p' - \frac{\omega^2}{c_0} \chi p' \right] d\Omega + i\omega \int_{\Gamma_2} \frac{A(\omega)}{\rho_0 c_0} \chi p' d\Gamma + \int_{\Gamma_2} \omega^2 \chi s_n d\Gamma + \int_{\Omega} \frac{1}{\rho_0} \chi \hat{w} d\Omega = 0 \quad (3.21)$$

It is also possible to notice that, if the admittance A is equal to zero, the integral over Γ_Z reduces to zero, so that if, on a certain boundary surface, there is no specified condition, it naturally acts as a hard surface, *by default*.

When the trial function of (3.18) is substituted in the (3.21), a linear equation is obtained, in the n unknowns p_j . By using a set of n test functions χ_j (with $j=1, \dots, n$), n linear equations in n unknowns are generated. The best choice for the χ_j is represented by the shape functions N_j (with $j=1, \dots, n$) previously defined: by setting $\chi_j(\mathbf{x}) = N_j(\mathbf{x})$, with $j=1, \dots, n$, one obtains the following symmetric system of linear equations:

$$[\mathbf{K} + i\omega\mathbf{C} - \omega^2\mathbf{M}]\{\hat{\mathbf{p}}\} = \{\hat{\mathbf{f}}_{st}\} + \{\hat{\mathbf{f}}_w\} \quad (3.22)$$

where \mathbf{M} , \mathbf{K} and \mathbf{C} are the acoustic mass, stiffness and damping matrices, $\hat{\mathbf{f}}_{st}$ and $\hat{\mathbf{f}}_w$ are the forcing terms due to the structural excitation (at inlet, in case of figure 3.2) and to the acoustic sources. They can be expressed as:

$$\begin{aligned} M_{jk} &= \int_{\Omega} \frac{N_j N_k}{\rho_0 c_0^2} d\Omega, & K_{jk} &= \int_{\Omega} \frac{\nabla N_j \cdot \nabla N_k}{\rho_0} d\Omega, \\ c_{jk} &= \int_{\Gamma_z} \frac{A(\omega)}{\rho_0 c_0} N_j N_k d\Gamma, \\ \{f_{st}\}_j &= \int_{\Gamma_s} \omega^2 N_j s_n d\Gamma, & \{f_w\}_j &= \int_{\Omega} \frac{1}{\rho_0} N_j w d\Gamma, \end{aligned} \quad (3.23)$$

The above integrals are evaluated for each element and then assembled, through a proper procedure [7], in to the global matrices \mathbf{M} , \mathbf{K} , \mathbf{C} and the forcing vectors \mathbf{f}_{st} and \mathbf{f}_w . Numerical integration is generally used within each element.

3.5 FEM: TYPES OF ANALYSES

3.5.1 FREQUENCY RESPONSE ANALYSIS

This kind of problem is represented by the equation (3.22) and solved as above explained. FE methodologies are obviously able to deal with problems with inhomogeneous domains, since it is possible to enforce the value of the normal particle velocity at any discontinuity of material properties in the discretized domain. In this way it is possible to model inhomogeneous fluids by assigning different fluid properties (c_0 and ρ_0) at each homogeneous constituting part.

Consequently, it is also possible to model components provided of absorbing material, e.g. silencers, just imposing a proper complex speed of sound and density in the domain occupied by this material.

In particular, rigid porous material can be modeled, by utilizing semi-empirical formulations where the required complex speed of sound and density are obtained as a function of the frequency, density and type of material (Delany and Bazely approach, see Appendix of Chapter 1) [8].

Finally, by adding an additional FE equation to model the displacement of the elastic frames, also elastic porous bulk materials can be treated [8].

3.5.2 NORMAL MODE ANALYSIS

This kind of problem is described by the equation (3.22), when the forcing terms are null and there is no absorption present. In this case the (damped) acoustic modes of the fluid are described by the equation:

$$[\mathbf{K} + i\omega\mathbf{C} - \omega^2\mathbf{M}]\{\hat{\mathbf{p}}\} = 0 \quad (3.24)$$

The obtained eigenmodes are useful to analyze the behaviour of the system, but also to resolve the frequency response problem represented by the entire (3.22).

3.5.3 ACUSTO-STRUCTURAL COUPLING

Up to now, structural velocities at boundaries have always been considered fixed, known and not influenced by the acoustic field. In several situation this hypothesis is not adequate. Consider, for example, a metallic box, with thin surfaces and in which a strong acoustic source is inserted. In this case the generated acoustic field can enforce some structural vibrations, and these ones can themselves generate an acoustic field inside the box. The problem, therefore, is truly coupled and it can be solved with a coupled approach [8].

Fluid-structure interactions can be modeled by means of a FE analysis. In this case the equation (3.22), involving the fluid, must be combined with another, but similar equation, involving the structural displacement on the boundaries Γ_{st} . Consequently it is possible to model the effects of the acoustic pressure on the nodal structural motions and the other way round. The expression of the trial solution of the structural problem is similar to the one described by the equation (3.19), with the exception that the degrees of freedoms are not the nodal pressure values, but the nodal displacements s_j ($j=1, \dots, n_{st}$).

The resulting system is:

$$\left[\begin{bmatrix} \mathbf{K} & \mathbf{0} \\ -\mathbf{A}^T & \mathbf{K}_{st} \end{bmatrix} + i\omega \begin{bmatrix} \mathbf{C} & \mathbf{0} \\ \mathbf{0} & \mathbf{C}_{st} \end{bmatrix} - \omega^2 \begin{bmatrix} \mathbf{M} & -\rho\mathbf{A} \\ \mathbf{0} & \mathbf{M}_{st} \end{bmatrix} \right] \begin{bmatrix} \hat{\mathbf{p}} \\ \hat{\mathbf{s}} \end{bmatrix} = \begin{bmatrix} \mathbf{f}_w \\ \mathbf{f}_{ext} \end{bmatrix} \quad (3.25)$$

where \mathbf{K}_{st} , \mathbf{C}_{st} , and \mathbf{M}_{st} are stiffness, damping, and mass matrices for the structure, and \mathbf{A} is a coupling matrix that contains integral products of the acoustical and structural shape functions over Γ_{st} . The vector \mathbf{f}_{ext} contains external nodal forces and moments applied to the structure. The mass and stiffness matrices, now, are no more symmetric. If this involves a great computational effort, the equation (3.25) can be previously symmetrized.

3.5.4 TRANSIENT RESPONSE

Once assumed that the damping matrix is frequency independent, an inverse Fourier Transform can be applied to the (3.22), yielding to an equation which can be integrated in time by using a numerical time-stepping scheme, such as the Newmark- β scheme [10], [1]. When the damping matrix is frequency dependent the problem in time-domain formulation is much more complicated, and usually a suitable transient impedance boundary condition must be incorporated in to the discrete problem [11].

3.6 FEM: EXTERNAL PROBLEMS

Unbounded problems with FEM approach have not been dealt in this thesis, and only a general overview on them will be given in this section. When an unbounded problem must be resolved by utilizing a FEM methodologies, two main difficulties must be tackled:

- The construction of an artificial outer boundary to the FE domain, transparent to any outgoing waves.
- The reconstruction of a far field solution which lies beyond the computational domain.

These two issues are not present in case of BE approach. Regarding the FE, many methods have been used to terminate the computational domain of exterior models. They can be divided in *nonlocal* and *local* approaches. The first ones include a mode matching in which the FE domain is matched to a BE model at the truncation boundary. Local methods, usually

preferred for larger problems, include infinite element schemes (IE) and perfectly matched layers (PML) [11], [16].

The IE approach is based on the use of a single layer of infinite elements of variable order, which is matched onto a conventional finite element mesh. The infinite element is based on a infinite geometry mapping, extending the element to infinity, and special shape functions [14].

In order to accommodate different shapes of radiating bodies efficiently, different types of coordinate system are available. Usually the best performance is achieved when radiating body is circumscribed by its closest-fitting coordinate surface. Ideally the base surface of the infinite elements should be smooth, without sharp angles or small radii. The implementation of the infinite wave envelope elements in ellipsoidal coordinates meets this aim, providing a close-fitting surface for a wide range of radiating models.

The development of the shape functions used within the infinite wave envelope elements stems from the observation that, e.g. in spherical coordinates (a particularization of the ellipsoidal coordinates), a three dimensional radiation function $p(r)$, for the exterior region outside a sphere $|r-r_0|$, can be written in the form of an infinite series:

$$p(r) = \frac{e^{+ikr}}{r} \sum_{n=0}^{\infty} \frac{f_n(\theta, \phi, k)}{r^n} \quad (3.26)$$

where (θ, ϕ, k) are spherical coordinates relative to the origin. The functions $f_n(\theta, \phi, k)$ represent the radiation functions corresponding to acoustic multi-poles of increasing order. It is observed that, in order to model the acoustic pressure field in an unbounded domain using a single layer of variable-order infinite wave envelope elements, sufficient degrees of freedom in the radial (infinite) direction are needed to model the amplitude decay of the outgoing propagating waves. This can be achieved by specifying an appropriate order for the infinite wave envelope element, as this directly defines the number of terms in the $(1/r)$ expansion. In addition, satisfactory angular discretization is required to model the angular radiation patterns. [15]

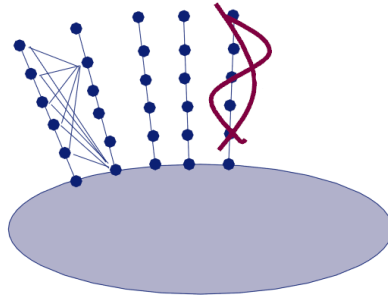


Figure 3.5 – Infinite element schematization. [15]

When IE are utilized, all the degrees of freedom of an element are coupled to all the degrees of freedom of each neighboring elements, as can be seen in Figure 3.5, resulting in large bandwidth of the matrix, especially when high order polynomials are utilized. Moreover, as mentioned, not all kind of radiating geometries can be modeled. This issues have been recently overwhelmed by utilizing the perfectly matched layer approaches, which involve a buffer domain around the computational domain where the outgoing sounds waves are damped, without reflections [16].

3.7 FEM: ACOUSTICS IN PRESENCE OF MEAN FLOW

When a mean flow is present, the propagation of the acoustic waves is influenced by convection. When the mean flow inside the acoustic domain is *irrotational*² the acoustic problem can be formulated in terms of acoustic velocity potential and a convected form of Hemholtz equation can be easily solved [1].

When the mean flow is rotational, the acoustical disturbance is coupled to vortical, and entropy waves and the linearized Euler equations must be integrated. In this case the preferred methods are based on structured, higher-order, finite difference schemes [17], but also FE time-domain schemes based on the discontinuous Galerkin method have been proved to be effective. Anyway, many uncertainties remain about the treatment of shear instabilities and time-domain impedance boundary conditions in rotational flows [18].

² velocity vector field is conservative, i.e. neglect able turbulence and boundary layer.

3.8 BEM: GENERAL FORMULATION – DIRECT AND INDIRECT APPROACHES

The Boundary Element Method is a numerical implementation of the Helmholtz analysis method discussed in the previous section extensively utilized in this thesis (see Chapter 5). This method, as its name implies, only involves discretizing the boundary of an enclosed space or the boundary of a noise radiating structure. The method can be used to analyze acoustic problems such as the noise inside an enclosed volume, the noise radiated from a vibrating structure, and the acoustic field generated by the scattering of noise by objects in a free-field. There are two different boundary element methods that can be used to evaluate an acoustic field generated by a defined forcing function: the direct method and the indirect method [19]. Both will be discussed in this section.

3.8.1 DIRECT METHOD

For *direct* or *collocation approach*, the acoustic problem is defined within a volume Ω bordered by an enclosed surface Γ , and the primary variables are the sound pressure and normal velocity on the side of the boundary that is in contact with the fluid. These variables are related by the (3.10). As known, the propagation of acoustic waves of constant frequency in homogeneous media is described by the (3.6). By using the Green's second theorem, it can be formulated as an integral equation over the closed surface Γ , see Figure 3.6. In fact, the acoustic pressure, at point \mathbf{x} within Ω is given by [20]:

$$\hat{p}(\omega, \mathbf{x}) = -\frac{1}{C(\mathbf{x})} \int_{\Gamma} \left[\hat{p}(\omega, \mathbf{x}_0) \frac{\partial G(\omega, \mathbf{x}, \mathbf{x}_0)}{\partial n} - G(\omega, \mathbf{x}, \mathbf{x}_0) \frac{\partial \hat{p}(\omega, \mathbf{x}_0)}{\partial n} \right] d\Gamma \quad (3.27)$$

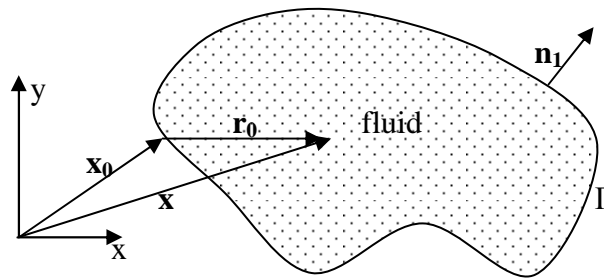


Figure 3.6 – Schematic of direct BEM.

where the acoustic pressure varies with location \mathbf{x} in the field, \mathbf{x}_0 is the location of a point on the surface, \mathbf{n} is a unit outward normal of the surface Γ , and $G(\omega, \mathbf{x}, \mathbf{x}_0) = \frac{e^{-ikr}}{4\pi r}$ is the fundamental solution of the Helmholtz equation, called Green's function ($r = |\mathbf{x} - \mathbf{x}_0|$). $C(\mathbf{x})$ is a constant depending on the location of the point \mathbf{x} . $C(\mathbf{x}) = 1$ when the point \mathbf{x} is within the acoustic domain and $C(\mathbf{x}_0) = 1/2$ when the point \mathbf{x} is on the surface (i.e. $\mathbf{x} = \mathbf{x}_0$). From a mathematical point of view $C(\mathbf{x}) = 0$ when \mathbf{x} not within the acoustic domain or surface Γ , but this condition is rarely used.

It can be noticed that the Green's function represent substantially a monopolar source of unitary intensity placed in the point \mathbf{x}_0 , that satisfy the Helmholtz equation. Similarly the derivative of the Green's function is equivalent to a bipolar source of unitary intensity. As a physical interpretation of the equation (3.27) one can say that the pressure, at a generic point \mathbf{x} (*observer*), can be seen as the effect of distribution on Γ of monopolar sources, whose intensity is equal to the pressure normal derivative, and a distribution of bipolar sources, whose intensity is equal to the pressure itself.

The classic formulation given in Equation (3.27), termed the Helmholtz Integral Equation, is the starting point for the direct BEM analysis. [21]. If the enclosing surface vibrates punctually with a velocity $\mathbf{u}(\omega, \mathbf{x}_0)$, according to the (3.11), equation (3.27) becomes:

$$\hat{p}(\omega, \mathbf{x}) = -\frac{1}{C(\mathbf{x})} \int_{\Gamma} \left[\hat{p}(\omega, \mathbf{x}_0) \frac{\partial G(\omega, \mathbf{x}, \mathbf{x}_0)}{\partial n} + i\rho_0 \omega \hat{u}(\omega, \mathbf{x}_0)_{s,n} G(\omega, \mathbf{x}, \mathbf{x}_0) \right] d\Gamma \quad (3.28)$$

When using the direct BEM, there is a distinction between an interior and exterior problem, as shown in Figure 3.6. This distinction is related to the definitions of $C(\mathbf{x})$ and it is related to the formulation of the direct BEM, which always requires that the normal vector on Γ points away from the acoustic domain. Hence for an interior acoustic problem, the normal vector of the surface must point outwards, away from the acoustic volume. For the analysis of an exterior acoustic field, the normal vectors point away from the acoustic domain, that is, inwards towards the enclosed surface.

If both interior and exterior acoustic domains are of interest, then the indirect BEM must be used which is described in the following section. For this problem two surfaces are used: the surface that is in contact with the interior acoustic domain has surface normal vectors pointing outwards towards the exterior acoustic domain, and the surface that is in contact with the exterior acoustic domain has surface normal vectors that point inwards towards the interior acoustic domain. [21]

3.8.2 INDIRECT METHOD

When an indirect BEM approach is utilized, both sides of the boundary are considered simultaneously: as shown in Figure 3.7 , the boundary consists of the inside (Γ_1) and outside surfaces (Γ_2), and both are analyzed at the same time.

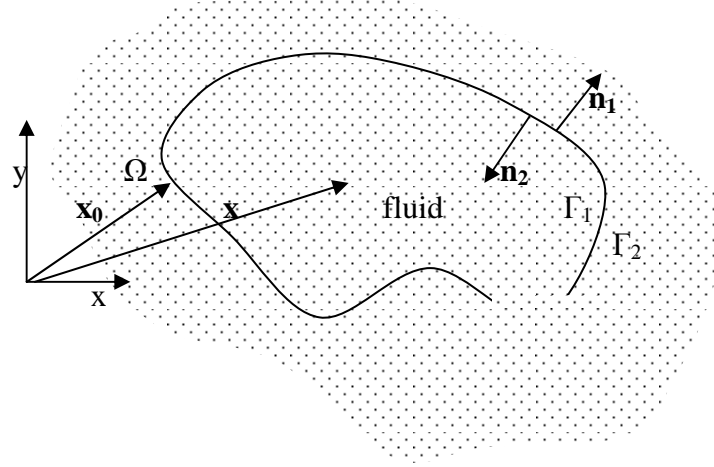


Figure 3.6 – Schematic of indirect BEM.

The indirect method can be used to calculate both interior and exterior acoustic fields as a result of a vibrating surface or acoustic sources, and can include openings that connect an enclosed region to a free field region, or where free edges occur on a surface such as a stiffening rib attached perpendicular to a panel. The matrices resulting from this indirect method are fully populated and symmetric, which can result in faster solution times compared to solving un symmetric matrices such as those associated with the direct method. [20]

In short, boundary integral equations like Eq. (3.28) can be written on both sides of the boundary and then summed resulting in an indirect boundary integral formulation that can be expressed as:

$$\frac{\partial \hat{p}(\omega, \mathbf{x})}{\partial x_i} = -i\rho\omega \hat{u}(\omega, \mathbf{x}_0)_{x_i} = \int_{\Gamma} \left[\delta \hat{p}(\omega, \mathbf{x}_0) \frac{\partial G(\omega, \mathbf{x}, \mathbf{x}_0)}{\partial x_i} - \delta \hat{p}(\omega, \mathbf{x}_0) \frac{\partial G(\omega, \mathbf{x}, \mathbf{x}_0)}{\partial x_i \partial n} \right] d\Gamma \quad (3.29)$$

The left hand side of the expression is the gradient of the pressure at any point \mathbf{x} in the acoustic domain in the direction x_i ; $u_{x,i}$ is the component of acoustic particle velocity in the direction x_i ; the right-hand side is an integral expression over the boundary surface. The term

$$\delta\hat{p}(\mathbf{x}_0) = \hat{p}(\mathbf{x}_0)_{\Gamma_1} - \hat{p}(\mathbf{x}_0)_{\Gamma_2} \quad (3.30)$$

is the difference in pressure across the surface of the boundary element model and is called *pressure jump* or *double layer potential*, [20]. On the other hand, the term

$$\delta d\hat{p}(\mathbf{x}_0) = \frac{\partial\hat{p}(\mathbf{x}_0)_{\Gamma_1}}{\partial n} - \frac{\partial\hat{p}(\mathbf{x}_0)_{\Gamma_2}}{\partial n} \quad (3.31)$$

is called *single layer potential*, [20], and it is the difference in gradient of the pressure normal to the surface of the boundary element model at points \mathbf{x}_{Γ_1} and \mathbf{x}_{Γ_2} on opposite sides of the boundary surface [1].

3.8.3 PROBLEM FORMULATION

Consider now the direct approach, but for the indirect approach the same considerations apply. As already said, the equation (3.27) permit to compute the pressure at any point inside the volume, once that pressure \hat{p} and normal pressure derivative $\partial\hat{p}/\partial n$ are known on the surface Γ . But \hat{p} and $\partial\hat{p}/\partial n$ are actually unknowns. The problem can be seen from another point of view: \hat{p} and $\partial\hat{p}/\partial n$ on Γ can be expressed as:

$$\hat{p}(\mathbf{x}_0) = \lim_{\mathbf{x} \rightarrow \mathbf{x}_0} \hat{p}(\mathbf{x}) \quad (3.32)$$

$$\frac{\partial\hat{p}(\mathbf{x}_0)}{\partial n} = \lim_{\mathbf{x} \rightarrow \mathbf{x}_0} \frac{\partial\hat{p}(\mathbf{x})}{\partial n} \quad (3.33)$$

In this way the $\hat{p}(\mathbf{x})$ at the right hand of the equation (3.27) can be seen, when \mathbf{x} approaches to \mathbf{x}_0 , as a value of \hat{p} on the boundary Γ , and the equation (3.27) becomes a relation between the pressure \hat{p} at one point on the surface Γ with the values of \hat{p} and $\partial\hat{p}/\partial n$ assumed by all the N nodes of the discretized Γ . In other words:

$$\begin{aligned}
 \hat{p}_1 &= f_1(\hat{p}_1, \hat{p}_2, \dots, \hat{p}_N) + g_1\left(\frac{\partial \hat{p}_1}{\partial n}, \frac{\partial \hat{p}_2}{\partial n}, \dots, \frac{\partial \hat{p}_N}{\partial n}\right) \\
 \hat{p}_2 &= f_2(\hat{p}_1, \hat{p}_2, \dots, \hat{p}_N) + g_2\left(\frac{\partial \hat{p}_1}{\partial n}, \frac{\partial \hat{p}_2}{\partial n}, \dots, \frac{\partial \hat{p}_N}{\partial n}\right) \\
 \hat{p}_N &= f_N(\hat{p}_1, \hat{p}_2, \dots, \hat{p}_N) + g_N\left(\frac{\partial \hat{p}_1}{\partial n}, \frac{\partial \hat{p}_2}{\partial n}, \dots, \frac{\partial \hat{p}_N}{\partial n}\right)
 \end{aligned} \tag{3.34}$$

which is a system on N equation in $2N$ unknowns ($f_1, f_2, \dots, f_N, g_1, g_2, \dots, g_N$). By considering equation (3.27) and relation (3.34) it can be noticed that all the functions in (3.34) are linear in \hat{p} and $\partial \hat{p} / \partial n$, [21].

Moreover, the boundary conditions on Γ can be expressed in function of $\partial \hat{p} / \partial n$, as seen in section 3.1. Consequently N boundary conditions (one per each point on Γ) will be inserted directly in the equation (3.27) by eliminating the unknown associated to $\partial \hat{p} / \partial n$. In case of velocity BCs, the (3.27) reduces to equation (3.28). In conclusions there are N equations and N unknowns.

One can show that, when \mathbf{x} approaches to \mathbf{x}_0 , and after a certain number of manipulations, the (3.27) becomes:

$$\begin{aligned}
 4\pi C(\mathbf{x})\hat{p}(\omega, \mathbf{x}) &= \\
 &= -\int_{\Gamma} [K_1(\omega, \mathbf{x}, \mathbf{x}_0)\hat{p}(\omega, \mathbf{x}) + K_3(\omega, \mathbf{x}, \mathbf{x}_0)\hat{p}(\omega, \mathbf{x})]d\Gamma + \int_{\Gamma} K_2(\omega, \mathbf{x}, \mathbf{x}_0)\frac{\partial \hat{p}(\omega, \mathbf{x})}{\partial n}d\Gamma
 \end{aligned} \tag{3.35}$$

where

$$K_1 = \frac{\cos(\theta)}{r^2} e^{-ikr}, \quad K_2 = -\frac{e^{-ikr}}{r}, \quad K_3 = \frac{\cos(\theta)}{r} ike^{-ikr} \tag{3.36}$$

Here θ is the angle between \mathbf{n} and \mathbf{r} . K_1, K_2, K_3 are called *Kernel functions*.

If the discretization of Γ is composed by P panels (i.e. elements), each one of the above integrals reduces to a summation of P integrals executed over the respective panels:

$$4\pi C(\mathbf{x})\hat{p}(\omega, \mathbf{x}) = -\sum_{j=1}^P \left\{ \int_{\Gamma_j} [K_1(\omega, \mathbf{x}, \mathbf{x}_0)\hat{p}(\omega, \mathbf{x}) + K_3(\omega, \mathbf{x}, \mathbf{x}_0)\hat{p}(\omega, \mathbf{x})] d\Gamma_j \right\} + \sum_{j=1}^P \left\{ \int_{\Gamma_j} K_2(\omega, \mathbf{x}, \mathbf{x}_0) \frac{\partial \hat{p}(\omega, \mathbf{x})}{\partial n} d\Gamma_j \right\} \quad (3.37)$$

In order to evaluate the integral over the Γ_j surface, the value of \hat{p} , $\partial \hat{p} / \partial n$, K_1 , K_2 and K_3 are needed over it. To this aim the typical shape functions utilized in FEM can be adopted. In case of a quadrangular element, where a local coordinate system is defined (ξ, η) , it implies :

$$\hat{p}(\omega, \xi, \eta) = \sum_{i=1}^4 \hat{p}_i(\omega) N_i(\xi, \eta) \quad (3.38)$$

$$\frac{\partial \hat{p}(\omega, \xi, \eta)}{\partial n} = \sum_{i=1}^4 \left(\frac{\partial \hat{p}(\omega)}{\partial n} \right)_i N_i(\xi, \eta) \quad (3.39)$$

$$K_1(\omega, \xi, \eta) = \frac{\mathbf{r}(\xi, \eta) \cdot \mathbf{n}(\xi, \eta)}{r(\xi, \eta)^2} e^{-ikr(\xi, \eta)} \quad (3.40)$$

$$K_2(\omega, \xi, \eta) = \frac{e^{-ikr(\xi, \eta)}}{r(\xi, \eta)} \quad (3.41)$$

$$K_3(\omega, \xi, \eta) = \frac{\mathbf{r}(\xi, \eta) \cdot \mathbf{n}(\xi, \eta)}{r(\xi, \eta)^2} ike^{-ikr(\xi, \eta)} \quad (3.42)$$

Considering that, over the generic panel j , the local coordinates (ξ, η) vary in the interval $[-1, 1]$ by $[-1, 1]$, the (3.37) in the i^{th} nodes give the following value of the pressure:

$$2\pi \hat{p}(\omega, \mathbf{x}_i) = -\sum_{j=1}^P \int_{-1}^1 \int_{-1}^1 [K_1(\omega, \xi, \eta) + K_3(\omega, \xi, \eta)] J(\xi, \eta) \sum_{k=1}^4 [N_{jk}(\xi, \eta) \hat{p}_{jk}] d\xi d\eta + \sum_{j=1}^P \int_{-1}^1 \int_{-1}^1 K_2(\omega, \xi, \eta) J(\xi, \eta) \sum_{k=1}^4 \left[N_{jk}(\xi, \eta) \frac{\partial \hat{p}_{jk}}{\partial n_{jk}} \right] d\xi d\eta \quad (3.43)$$

Where 4 is the number of nodes on the j^{th} panel, but can be also another number (e.g. 3, 6,...) depending on the panel typology. N_{jk} is the shape function of the node k of the panel j , and the

function $J(\xi, \eta)$ is the Jacobian that relates the transformation of the surface element $d\Gamma$ to the surface element $d\xi d\eta$. It is easy to show that, after few transformations, one can obtain the following expression in form of matrices:

$$2\pi\{\hat{\mathbf{p}}(\omega)\} = [\mathbf{K}^1(\omega)] \cdot \{\hat{\mathbf{p}}(\omega)\} + [\mathbf{K}^2(\omega)] \cdot \left\{ \frac{\partial \hat{\mathbf{p}}(\omega)}{\partial \mathbf{n}} \right\} \quad (3.44)$$

Where

$$K_{ij}^1(\omega, \xi, \eta) = \sum_{k=1}^4 \left\{ \int_{-1}^1 \int_{-1}^1 [K_1(\omega, \xi, \eta) + K_3(\omega, \xi, \eta)] J(\xi, \eta) N_{kj}(\xi, \eta) d\xi d\eta \right\} \quad (3.45)$$

$$K_{ij}^2(\omega, \xi, \eta) = \sum_{k=1}^4 \left\{ \int_{-1}^1 \int_{-1}^1 [K_2(\omega, \xi, \eta)] J(\xi, \eta) N_{kj}(\xi, \eta) d\xi d\eta \right\} \quad (3.46)$$

3.9 BEM: STRUCTURAL COUPLING

In section 3.5.3 the fluid-structural problem has been handled by utilizing an approach based exclusively on FEM. In acoustic problems when the BE approach is preferred and a fluid-structure study must be carried out, the BE simulation can be efficiently coupled to a modal FE analysis giving a FE/BE coupled approach.

In this case, a *modal method* can be utilized, and the problem, represented by equation (3.24), is decomposed in two parts. The FEM is deputed to solve the normal mode analysis, expressed by:

$$[\mathbf{K}_s + i\omega\mathbf{C}_s - \omega^2\mathbf{M}_s] \{\hat{\mathbf{s}}\} = 0 \quad (3.47)$$

where \mathbf{M}_s , \mathbf{K}_s and \mathbf{C}_s are the mass, stiffness and damping matrices of the structure. The result of this analysis is represented by a number m of mode shapes constituting a shape matrix \mathbf{L} : $[\mathbf{L}] = [\{\mathbf{l}_1\}, \{\mathbf{l}_2\}, \dots, \{\mathbf{l}_m\}]$ whose generic column, \mathbf{l}_i , represents the i^{th} modal shape column, [22].

After that, the BEM is deputed to solve the coupled problem. To this aim one can consider that the frequency response of the structure is expressed by the following equation of motion:

$$[\mathbf{K}_s + i\omega\mathbf{C}_s - \omega^2\mathbf{M}_s]\{\hat{\mathbf{s}}\} = \{\hat{\mathbf{f}}_s\} \quad (3.48)$$

where $\hat{\mathbf{s}}$ is the nodal displacements vector, and $\hat{\mathbf{f}}_s$ is the generalized external forces vector. Moreover, it is known that the modal analysis relies on the assumption

$$\hat{\mathbf{s}} = \mathbf{L}\hat{\mathbf{q}} \quad (3.49)$$

where $\hat{\mathbf{q}}$ is called vector of modal amplitudes, and it is unknown. By substituting this expression of $\hat{\mathbf{s}}$ in (3.48) and pre-multiplying by \mathbf{L}^T one obtains:

$$[\mathbf{K}_m + i\omega\mathbf{C}_{st} - \omega^2\mathbf{M}_m]\{\hat{\mathbf{q}}\} = \{\hat{\mathbf{f}}_m\} \quad (3.50)$$

Where $[\mathbf{M}_m] = [\mathbf{L}]^T[\mathbf{M}_s][\mathbf{L}]$, $[\mathbf{K}_m] = [\mathbf{L}]^T[\mathbf{K}_s][\mathbf{L}]$, $[\mathbf{C}_m] = [\mathbf{L}]^T[\mathbf{C}_s][\mathbf{L}]$ and $\{\hat{\mathbf{f}}_m\} = [\mathbf{L}]^T\{\hat{\mathbf{f}}_s\}$ are respectively the modal mass matrix, the modal stiffness matrix (both diagonal) and the modal forces vector [22]³.

In order to solve the system, an expression for the generalized mode force $\hat{\mathbf{f}}_m$ is required. It is composed by a contribution due to the effect of point structural forces (given by the component of the structural point force in the direction of the mode shape) and a contribution due to the acoustic pressure (given by the component of the pressure forces \mathbf{f}_p in the direction of the mode shape). Consequently it can be expressed as:

$$\{\hat{\mathbf{f}}_m\} = \{\hat{\mathbf{f}}_s \cdot \mathbf{L} - \hat{\mathbf{f}}_p \cdot \mathbf{L}\} \quad (3.51)$$

³ $[\mathbf{M}_m]$ is a m by m diagonal matrix, whose generic element is the modal mass of the i^{th} mode, $m_i = \frac{1}{A_i\omega_i}$,

where A_i is a scaling constant for the i^{th} mode and ω_i is the damped natural frequency of the i^{th} mode.

$[\mathbf{K}_m]$ is a m by m diagonal matrix, whose generic element is the modal stiffness of the i^{th} mode,

$k_i = \frac{\sigma_i^2 + \omega_i^2}{A_i\omega_i}$ where σ_i is the damping coefficient of the i^{th} mode.

$[\mathbf{C}_m]$ is a m by m diagonal matrix, whose generic element is the modal damping of the i^{th} mode, $c_i = \frac{2\sigma_i}{A_i\omega_i}$

Anyway this equation is not sufficient to fully describe the structural coupling. In fact, with the equations (3.51) only the effect of the acoustic field on the structure is described, missing the inverse effect. Therefore, in order to complete the analysis, the displacement of the structural nodes due to the acoustic pressure must be taken into account: for a mode with a complex amplitude $\hat{\mathbf{q}}$, the surface displacement is given by the (3.49), $\hat{\mathbf{s}}_q = \mathbf{L}\hat{\mathbf{q}}$, and then the related surface velocity will be:

$$\hat{\mathbf{u}}_q = -i\omega\mathbf{L}\hat{\mathbf{q}} \quad (3.52)$$

This velocity surface has therefore to be taken into account in the definition of the boundary conditions for Helmholtz equation. Considering the case in which the surface where the mode is defined has also an acoustic impedance, the velocity BC, expressed by equation (3.14), becomes:

$$\nabla\hat{p} \cdot \mathbf{n} = -i\rho_0\omega(\hat{u}_{s,n} - \hat{p}A - \hat{u}_{q,n}) \quad (3.53)$$

where $\hat{u}_{q,n}$ is the component of $\hat{\mathbf{u}}_q$ along the normal \mathbf{n} .

As a result, for an analysis with n nodes and m computed modes, the acoustic system, expressed by the n equations in n unknowns contained in (3.44), can be then combined with the m BCs contained in equation (3.53), since the (3.44) contains the pressure derivatives at the second term. Moreover, the m equations in m unknowns expressed by (3.50) can be combined with the m boundary conditions contained in equation (3.51), since the (3.50) contains the forces \mathbf{f}_m . The coupled problem, is then *completely defined*.

3.10 BEM: THE NON UNIQUENESS PROBLEM

With the direct BEM, the exterior boundary integral equation does not have a unique solution at certain frequencies. These frequencies correspond to the resonance frequencies of the air space interior to the boundary (with Dirichlet boundary conditions). Though the direct BEM results will be accurate at most frequencies, the sound pressure results will be incorrect at these characteristic frequencies.

The most common approach to overcome the non-uniqueness difficulty is to use the *combined Helmholtz integral equation formulation*, or CHIEF, method,[23]. A few overdetermination or CHIEF points are placed inside the boundary, and CHIEF equations are written that force the sound pressure to be equal to zero at each of these points. Several CHIEF points should be identified inside the boundary because a CHIEF point that falls on or near the interior nodal surface of a particular eigenfrequency will not provide a strong constraint, since the pressure on that interior nodal surface is also zero for the interior problem. As the frequency increases, the problem is compounded by the fact that the eigenfrequencies and the nodal surfaces become more closely spaced. Therefore, analysts normally add CHIEF points liberally if higher frequencies are considered. Although the CHIEF method is very effective at low and intermediate frequencies, a more theoretically robust way to overcome the non-uniqueness difficulty is the Burton and Miller method, [24]

Similarly, for an indirect BEM analysis, there is a nonexistence difficulty associated with exterior radiation problems. Since there is no distinction between the interior and exterior analysis, the primary variables of the indirect BEM solution capture information on both sides of the boundary. At the resonance frequencies for the interior, the solution for points on the exterior is contaminated by large differences in pressure between the exterior and interior surfaces of the boundary. The nonexistence difficulty can be solved by adding absorptive planes inside or by specifying an impedance boundary condition on the interior surface of the boundary, [25]. In the end, exterior radiation problems should be approached carefully, even though excellent acoustical predictions can be made using the BEM, provided appropriate precautions are taken.

3.12 BEM: FAST MULTIPOLE FOR LARGE PROBLEMS

Fast multipole BEM is utilized in acoustic problems related to structures with very large dimensions (i.g. airplanes, cars, etc.). It has not been utilized in this thesis, and just general notes are given here, remanding to [26] for more information. This method, pioneered by Rokhlin and Greengard in the mid of 1980's, is employed to dramatically accelerate the solution of a BEM system of equations $\mathbf{Ax}=\mathbf{b}$, in which matrix \mathbf{A} is in general dense and non-symmetrical. The main idea of the fast multipole BEM is to employ iterative solvers (such as GMRES) to solve the BEM system of equations and employ the FMM to accelerate the matrix-vector multiplication (\mathbf{Ax}) in each iteration step, without ever forming the matrix \mathbf{A}

explicitly. In the fast multipole BEM, the node-to-node interactions in the conventional BEM are replaced by cell-to-cell interactions using a hierarchical tree structure of cells containing groups of elements. This is possible by introducing the multipole and local expansions of the kernels and employing certain translations.

3.11 FURTHER COMPUTATIONAL ASPECTS IN 3D ACOUSTIC SIMULATIONS

3.11.1 TYPES OF ELEMENTS IN FEM

A complete description of the elements utilized in FEM and related shape functions can be found in [12]. In general, the most utilized elements are triangular or quadrangular elements for 2D simulations, tetrahedral and hexahedral elements for 3D analyses. These elements have usually two or three nodes per side, i.e. two nodes on the extreme points and, in case, the third node at the mid edge. The polynomial shape functions are obtained in terms of mapped coordinates or Cartesian coordinates on a basis set, whose rank is equal to the number of nodes per element.

Moreover, the trial solution within each element varies linearly with the other variables for elements with two nodes per edge, and quadratically for those with 3 nodes per edge. Consequently the polynomial order of these elements is $p=1$ and $p=2$ respectively. In practice, elements with a polynomial order greater than 2 are rarely utilized, even though they have the positive aspect to radically reduce the pollution error in acoustics [12].

3.11.2 NUMERICAL ERRORS: APPROXIMABILITY

The approximability is an *amplitude* error, i.e. an error obtained when a physically continuous time harmonic disturbance is represented by mean of a continuous polynomial approximation based on a domain discretization. This error is proportional to $(hk)^p$, where h is the node spacing, k is the wavenumber and p is the polynomial order of the shape functions. The approximability error decreases as $(\lambda/h)^p$ where λ is the wavelength and λ/h can be then interpreted as number of nodes per wavelength. The higher polynomial order, the faster reduction of error. It can be proved that the absolute lower limit is $\lambda/h=2$, which correspond to a sawtooth pattern description of the disturbance. Obviously it is always needed a better

representation of the phenomenon. To this aim a widely recognized thumb rule is to have 10 nodes per wavelength. These rule gives satisfactory results at lower frequencies but it must be prudently utilized at high frequencies because of pollution errors which might occur [1].

3.11.3 NUMERICAL ERRORS: POLLUTION

The pollution error is proportional to $L(hk)^p$ where L is a characteristic length of the investigated acoustic domain, and h , k and p have been above introduced. In other words, this error becomes evident when the wavelength of the disturbance is small compared to the dimensions of the computational domain. This error is associated to the numerical dispersion problem, since small differences in phase between the simulated and the calculated solution may not give any significant error over a single wavelength, but accumulate over many wavelengths giving a large global error. Consequently, the pollution error can be considered a *phase* error. Its effects are complicated by the element orientations with respect to the wave propagation in multi-D problems.

The global error constituted by approximability and pollution error can be reduced by refining the mesh and reducing the h , for a certain value of p (h refinement), or by increasing the value of p keeping unaltered the h (p refinement), or acting on both parameters. The most common practice in acoustic applications consists of a h refinement, even though the use of second-order elements instead of the first-order elements is widely recognized to be a valid option [13].

REFERENCES

1. M.J. Crocker, Handbook of noise and vibration control, John Wiley & Sons, Inc., Hoboken, New Jersey, 2007.
2. M.L. Munjal “Acoustics of Ducts and Mufflers”, New York : Wiley-Interscience, 1987.
3. I. Harari, T.J.R. Hughes, Cost Comparison of Boundary Element and Finite Element Methods for Problems of Time Harmonic Acoustics, Computer methods in applied mechanics and engineering, Vol. 97, 1992, pp. 77–102.
4. L. Greengard, J. Huang, V. Rokhlin, S. Wandzura, Accelerating fast multipole methods for the Helmholtz equation at low frequencies, IEEE Computing in science and engineering, Vol. 5, 1998, pp. 32–47.
5. S. Marburg, B. Nolte, Computational acoustics of noise propagation in fluids – Finite and Boundary Element Methods, Springer-Verlag GmbH, 2008.
6. P.D. Lax, A.N. Milgram, Parabolic equations, contributions to the theory of partial differential equations. Annals of Mathematics Studies, no. 33. Princeton University Press. pp. 167–190. MR0067317 (1954).
7. M. Petyt, Introduction to Finite Element Vibration Analysis, Cambridge University Press, Cambridge, England, 1998.
8. J.F. Allard, A. Atalla, Propagation of sound in porous media, John Wilwy and sons publication, 2009.
9. J.F. Sigrist, S. Garreau, Dynamic analysis of fluid–structure interaction problems with modal methods using pressure-based fluid finite elements, Finite Elements in Analysis and Design 43 (2007) 287 – 300.
10. G. Seriani, A Parallel Spectral Element Method for Acoustic Wave Modeling, J. Comput. Acoust., Vol. 5, No. 1, 1997, pp. 53–69.
11. B. Van den Nieuwenhof, J.P. Coyette, Treatment of frequency dependent admittance boundary conditions in transient acoustic finite/infinite element models, J. Acoust. Soc. Am., Vol. 110, 2001, pp. 1743–1751.
12. O. C. Zienkiewicz and R. L. Taylor, The Finite Element Method, 5th ed., Vol. 1, McGraw-Hill, London, 1990.
13. A. Deraemaeker, I. Babuska, P. Bouillard, Dispersion and pollution of the FEM solution for the Helmholtz equation in one, two and three dimensions, Int. J. Numer. Meth. Eng., Vol. 46, 1999, pp. 471–499.
14. K. Gerdes, A summary of infinite formulations for exterior Helmholtz problems, Computer Methods in Applied Mechanics and Engineering. 164 (1998) 95-105
15. LMS Sysnoise User’s manual.
16. O. Ozgun, M. Kuzuoglu. Near field performance analysis of locally-conformal perfectly matched absorbers via Monte-Carlo simulations. Journal of computational Physics, 227:1225–1245, 2007.
17. C.K.W. Tam, J.C. Webb, Dispersion Preserving Finite Difference Schemes for Computational Acoustics, J. Comput. Phys., Vol. 107, 1993, pp. 262–281.

18. P.R. Rao, P.J. Morris, Application of a Generalised Quadrature Free Discontinuous Galerkin Method in Aeroacoustics, in AIAA paper 2003-3120, 9th AIAA/CEAS Aeroacoustics Conference, 12–14 May, Hilton Head, SC, 2003.
19. S. Kirkup, The boundary element method in acoustics, Integrated Sound Software, 2007.
20. D.A. Bies, C.H. Hansen, Engineering noise control – Theory and practice, 4th edition, Spon Press, 2009.
21. P. d. Francescantonio, STS VNoise Theoretical manual, Scientific Technical Software.
22. A.R. Guido, S.d.Valle, Vibrazioni meccaniche nelle macchine, Liguori, Napoli, 2004.
23. H. A. Schenck, Improved integral formulation for acoustic radiation problem, *J. Acoust. Soc. Am.*, Vol. 44, 1968, pp. 41–58.
24. A.J. Burton, G.F. Miller, The application of integral equation methods to the numerical solutions of some exterior boundary value problems, *Proc. Roy. Soc. London*, Vol. A 323, 1971, pp. 201–210.
25. N. Vlahopoulos, Indirect variational boundary element method in acoustics, form Boundary Element Acoustics, Fundamentals and Computer Codes, T. W. Wu (Ed.), WIT Press, Southampton, UK, 2000.
26. N. Nishimura, Fast multipole accelerated boundary integral equation methods, *Appl. Mech. Rev.*, 55, 299-324 (2002).

Chapter 4

Experimental techniques

Experimental analyses of mufflers constitute an integrant part of this thesis. In fact, a number of tests, focused on the acoustic and fluid dynamic characterization of a commercial silencer, have been included in the last chapter of this work, aimed to improve, extend and validate the numerical results.

All of these tests have been carried out during a study period spent abroad, at Tallinn University of Technology (TUT), in Estonia. At that time, also the theory founding experimental techniques, such as two port models and decomposition method, have been studied. Finally, a two-port method has been utilized in TTU acoustic laboratory in order to describe the behavior of the investigated muffler.

The above mentioned methodologies are based on the common hypotheses of plane wave propagation, in the duct sections where the physical properties are measured. In fact, the active or passive acoustical systems involved in duct acoustics (such as turbo-chargers, fans, mufflers, bends, T-junctions, etc.), are often coupled to a pipe system, which can be generally described as a set of uniform (and quite narrow) straight ducts (1, usually 2, or even more). In these ducts, the hypothesis of plane wave propagation is quite realistic.

The two-microphone random excitation method, also known as the Chung and Blaser method [1], uses cross-spectrum between two pressure signals to find reflection coefficient and impedance of an acoustic termination. A variety of two-microphone methods, earlier developed by Seybert and Ross [2], uses auto-spectral and cross-spectral densities of two pressure signals. One method can be developed from the other, but all of them require the use of an anechoic termination downstream the muffler. In practice, such a termination could be constructed by using a long exhaust tube, high absorbing materials, horn shaped pipes or an active sound anechoic termination. However, a “fully” anechoic termination is difficult to build, particularly one that is effective at low frequencies.

Two-port methods are more recent and efficient techniques, since they do not require anechoic terminations and can provide a complete characterization of various acoustic elements: not only passive elements, such as mufflers, but also passive/active elements such as pumps, fans [4] or, more recently, turbochargers [5]. To and Doige [6, 7] introduced this kind of approach to describe the acoustic behavior of uniform tubes, flare tubes and expansion chambers, but the proposed technique did not give stable results. The most accepted approaches today are mainly two: (I) the method developed by Munjal and Doige [8], based on the so called transfer matrix, aimed to measure the attenuation curve of a single element or combination of elements. (II) The method proposed by Abom [3], and based on the so called scattering matrix, which is able to easily extract all the acoustic parameters of a generic element, by utilizing a “two-source” or a “two-load” approach.

The goal of this chapter is to give an overview on the above mentioned measurement methods. In particular, the two-microphone random excitation technique, based on the Seybert approach, and the two-port methods, based on the Abom approach, are explained. Moreover, the test facilities of TTU acoustic laboratory, for two-port sources characterization, are described too [9-10]. In the Appendix, the basic concepts of “applied signal analysis”, utilized in this chapter, are summarized.

4.1 TWO-MICROPHONE RANDOM-EXCITATION TECHNIQUE

4.1.1 PHYSICS OF WAVE DECOMPOSITION

As mentioned in Chapter 2, in a straight duct oriented along an x direction, where plane waves travel, the linear wave equation applies:

$$\frac{\partial^2 p}{\partial x^2} - \frac{1}{c^2} \frac{\partial^2 p}{\partial t^2} = 0 \quad (4.1)$$

where $p(x,t)$ is the acoustic pressure as function of time and position, and c is the speed of sound. The general solution has the following form:

$$p(x,t) = \phi_+ \left(t - \frac{x}{c} \right) + \phi_- \left(t + \frac{x}{c} \right) \quad (4.2)$$

Where the ϕ_+ , depending on $(t-x/c)$, is a wave function propagating in the positive direction along the x axis, with speed c (named progressive wave), and ϕ_- , depending on $(t+x/c)$, is a wave function propagating in the negative direction of the x axis with speed c (named regressive wave). That assumed solution is known as *d’Alambert’s solution*. Since the wave equation is a linear differential equation, then the sum of any two solutions is also solutions. Moreover, also ϕ_+ and ϕ_- , separately, are solutions of the wave equation.

From Fourier analysis, it is known that every periodic process can be constructed by the summation of harmonic, sinusoidal processes with different frequencies, the set of which is called *Fourier series*. If each individual harmonic process is a solution to the wave equation, then their sum is also a solution. Only harmonic waves, therefore will be treated in the following development. In computations, each individual frequency can be treated independently, and the total sound pressure field can therefore be obtained by summation over all frequency components.

The generic harmonic solution for with frequency f and angular frequency $\omega = 2\pi f$, has the form:

$$p(x,t) = p_+ \cos \omega \left(t - \frac{x}{c} \right) + p_- \cos \omega \left(t + \frac{x}{c} \right) \quad (4.3)$$

where p_+ and p_- are the amplitudes of the progressive and regressive waves and the arguments $\omega(t-x/c) = \omega t - kx$ and $\omega(t+x/c) = \omega t + kx$ are the respective *phases*. $k = \omega/c$ is the *wavenumber*. Equation (4.3) can be then written as:

$$p(x,t) = p_+ \cos(\omega t - kx) + p_- \cos(\omega t + kx) \quad (4.4)$$

Since it is significantly more convenient, from the mathematical perspective, to deal with exponential functions rather than trigonometric ones, the development to follow will make extensive use of the complex notation

$$\mathbf{p}(x,t) = p_+ e^{i(\omega t - kx)} + p_- e^{i(\omega t + kx)} \quad (4.5)$$

in which bold prints means that the variable is complex. The first term on the right hand side refers to propagation in positive x direction. For precision, the real part of (4.5) is needed; i.e.

$$p(x, t) = \text{Re}(p_+ e^{i(\omega t - kx)} + p_- e^{i(\omega t + kx)}) = p_+ \cos(\omega t - kx) + p_- \cos(\omega t + kx) \quad (4.6)$$

The equation of motion (4.7)

$$\rho_0 \frac{\partial u_x}{\partial t} + \frac{\partial p}{\partial x} = 0 \quad (4.7)$$

relates the particle velocity to the sound pressure; rearranged, it gives:

$$u_x = -\frac{1}{\rho_0} \int \frac{\partial p}{\partial x} dt \quad (4.8)$$

Next, substituting (4.8) into (4.7) gives the particle velocity

$$\mathbf{u}_x(x, t) = -\frac{1}{\rho_0} \left(-\frac{ik}{i\omega} p_+ e^{i(\omega t - kx)} + \frac{ik}{i\omega} p_- e^{i(\omega t + kx)} \right) \quad (4.9)$$

Since $k/\omega = 1/c$, the particle velocity can be expressed as:

$$\mathbf{u}_x(x, t) = \frac{p_+}{\rho_0 c} e^{i(\omega t - kx)} - \frac{p_-}{\rho_0 c} e^{i(\omega t + kx)} \quad (4.10)$$

The two terms in this expression refer to wave propagation in the positive and negative x directions, respectively. The ratio of pressure to particle velocity is called *specific impedance*

$Z = \frac{p}{u_x}$ For the plane wave case, $Z_0^+ = \rho_0 c$ and $Z_0^- = -\rho_0 c$ for propagation in the positive

and negative directions, respectively. The quantity $\rho_0 c$ is called *wave impedance* [11].

4.1.2 SEYBERT AND ROSS TECHNIQUE

The Figure 4.1 shows the typical setup utilized for this kind of experiments. There is a rigid tube upstream the muffler, excited by a noise source produced by a loudspeaker. This tube is provided of two microphones at the position x_1 and x_2 from the inlet located at $x=0$. Downstream the muffler there is an anechoic termination and a third microphone. Mean flow is included, let v the velocity of the fluid. The acoustic vibration is assumed to be stationary with time.

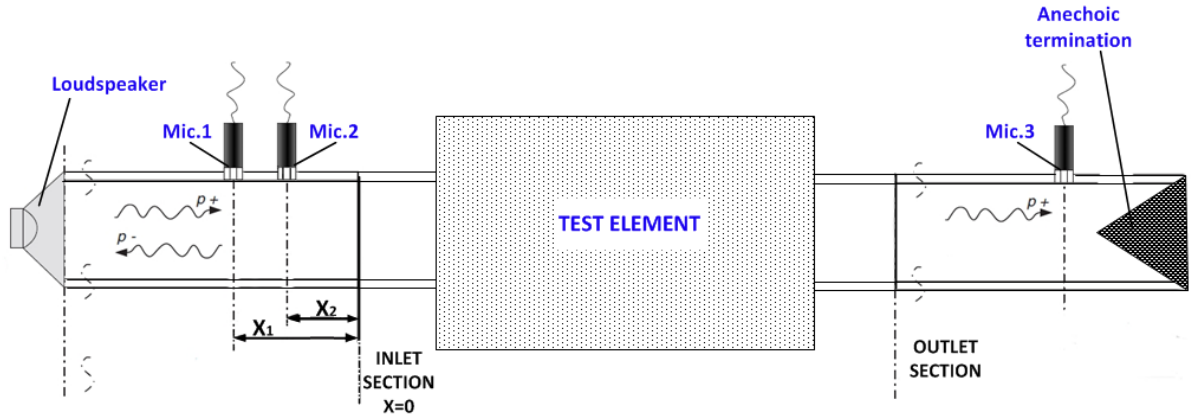


Figure 5.1 – Setup of 2-microphone random-excitation method.

In a narrow bandwidth B_e , centered at frequency f , random motion of loudspeaker membrane can be regarded as harmonic motion of frequency f with a randomly varying amplitude. For plane-wave propagation the incident and reflected waves, according to the equations (4.5) are given by:

$$\phi_+(x,t) = p_+(t) \cdot e^{i(\omega t - kx)} \quad (4.11)$$

$$\phi_-(x,t) = p_-(t) \cdot e^{i(\omega t + kx)} \quad (4.12)$$

where: $\omega = 2\pi f$, $k = \omega/c_0$ is the acoustic wave number, c_0 is the speed of sound, $p_+(t)$ and $p_-(t)$ are stationary random variables. The random amplitudes $p_+(t)$ and $p_-(t)$ are not functions of distance x , since the system is non dispersive. Therefore, the wave shape does not change during propagation. The influence of flow can be included by noting that:

- $c_0 = c + v$ for wave motion with flow,

- $c_0 = c - v$ for wave motion against flow,

where c is the speed of propagation with zero flow. For flow in the $+x$ direction, the incident and reflected wave numbers are given by:

$$\begin{aligned} k_+ &= \frac{\omega}{c + v} = \frac{k}{1 + M} \\ k_- &= \frac{\omega}{c - v} = \frac{k}{1 - M} \end{aligned} \quad (4.13)$$

where $M = v/c$ is the Mach number. Consequently, the incident and reflected waves are

$$\phi_+(x, t) = p_+(t) \cdot e^{i(\omega t - k_+ x)} \quad (4.14)$$

$$\phi_-(x, t) = p_-(t) \cdot e^{i(\omega t + k_- x)} \quad (4.15)$$

The total pressure at two points x_1 and x_2 in the tube is:

$$p(x_1, t) = \phi_+(x_1, t) + \phi_-(x_1, t) = [p_+(t)e^{-ik_+ x_1} + p_-(t)e^{ik_- x_1}]e^{i\omega t} \quad (4.16)$$

$$p(x_2, t) = \phi_+(x_2, t) + \phi_-(x_2, t) = [p_+(t)e^{-ik_+ x_2} + p_-(t)e^{ik_- x_2}]e^{i\omega t} \quad (4.17)$$

The auto- and cross-spectral densities of these two pressures are estimated by [2]:

$$\begin{aligned} S_{11}(f) &= E[\hat{p}_1(f, T)\hat{p}_1^*(f, T)] \\ S_{22}(f) &= E[\hat{p}_2(f, T)\hat{p}_2^*(f, T)] \\ S_{12}(f) &= C_{12}(f) + iQ_{12}(f) = E[\hat{p}_1(f, T)\hat{p}_2^*(f, T)] \end{aligned} \quad (4.18)$$

where: E denotes the ensemble average operator (average over a number of consecutive data records – see Appendix); the asterisk indicates complex conjugate; $S_{11}(f)$ and $S_{22}(f)$ are estimated of the *auto-spectral densities* of the pressure at points 1 and 2; $S_{12}(f)$ is an estimate of the *cross-spectral density* between the pressures at points 1 and 2; $C_{12}(f)$ and $Q_{12}(f)$ are the

real and imaginary components of the cross-spectral density; the quantities $\hat{p}_1(f, T)$ and $\hat{p}_2(f, T)$ are the finite Fourier transforms of the pressure time series at points 1 and 2, respectively. If spectral densities are of interest then the above definitions must be multiplied with an appropriate constant [12].

$\hat{p}_1(f, T)$ and $\hat{p}_2(f, T)$ can be written as:

$$\begin{aligned}\hat{p}_1(f, T) &= \frac{1}{T} \int_0^T p(x_1, t) e^{-i\omega t} dt = \hat{p}_+ e^{-i\omega k_+ x_1} + \hat{p}_- e^{i\omega k_- x_1} \\ \hat{p}_2(f, T) &= \frac{1}{T} \int_0^T p(x_2, t) e^{-i\omega t} dt = \hat{p}_+ e^{-i\omega k_+ x_2} + \hat{p}_- e^{i\omega k_- x_2}\end{aligned}\quad (4.19)$$

where \hat{p}_+ and \hat{p}_- are the finite Fourier transforms of $p_+(x_1, t)$ and $p_-(x_2, t)$ respectively.

By combining the (4.30) with (4.31), the following relationships are developed [2]:

$$\begin{aligned}S_{11}(f) &= S_{\hat{p}_+ \hat{p}_+}(f) + S_{\hat{p}_- \hat{p}_-}(f) + 2[C_{\hat{p}_+ \hat{p}_-}(f) \cos(k_+ + k_-)x_1 + Q_{\hat{p}_+ \hat{p}_-}(f) \sin(k_+ + k_-)x_1] \\ S_{22}(f) &= S_{\hat{p}_+ \hat{p}_+}(f) + S_{\hat{p}_- \hat{p}_-}(f) + 2[C_{\hat{p}_+ \hat{p}_-}(f) \cos(k_+ + k_-)x_2 + Q_{\hat{p}_+ \hat{p}_-}(f) \sin(k_+ + k_-)x_2] \\ C_{12}(f) &= S_{\hat{p}_+ \hat{p}_+}(f) \cos k_+(x_1 - x_2) + S_{\hat{p}_- \hat{p}_-}(f) \cos k_-(x_1 - x_2) + \\ &\quad + C_{\hat{p}_+ \hat{p}_-}(f) [\cos(k_- x_1 + k_+ x_2) + \cos(k_+ x_1 + k_- x_2)] + \\ &\quad + Q_{\hat{p}_+ \hat{p}_-}(f) [\sin(k_- x_1 + k_+ x_2) + \sin(k_+ x_1 + k_- x_2)] \\ Q_{12}(f) &= -S_{\hat{p}_+ \hat{p}_+}(f) \sin k_+(x_1 - x_2) + S_{\hat{p}_- \hat{p}_-}(f) \sin k_-(x_1 - x_2) + \\ &\quad + C_{\hat{p}_+ \hat{p}_-}(f) [-\sin(k_+ x_1 + k_- x_2) + \sin(k_- x_1 + k_+ x_2)] + \\ &\quad + Q_{\hat{p}_+ \hat{p}_-}(f) [\cos(k_+ x_1 + k_- x_2) - \cos(k_- x_1 + k_+ x_2)]\end{aligned}\quad (4.20)$$

where $S_{\hat{p}_+ \hat{p}_+}(f) = E[\hat{p}_+ \hat{p}_+^*]$ and $S_{\hat{p}_- \hat{p}_-}(f) = E[\hat{p}_- \hat{p}_-^*]$ are the auto-spectral densities of the incident and reflected waves, respectively. $C_{\hat{p}_+ \hat{p}_-}(f)$ and $Q_{\hat{p}_+ \hat{p}_-}(f)$ are the real and imaginary components of the cross-spectral density $S_{\hat{p}_+ \hat{p}_-}(f)$ between the incident and the reflected waves: $S_{\hat{p}_+ \hat{p}_-}(f) = C_{\hat{p}_+ \hat{p}_-}(f) + iQ_{\hat{p}_+ \hat{p}_-}(f)$

If the quantities S_{11} , S_{22} , C_{12} , and Q_{12} are estimated from measured time records, the above equations can be solved for the unknowns $S_{\hat{p}_+ \hat{p}_+}(f)$, $S_{\hat{p}_- \hat{p}_-}(f)$, $C_{\hat{p}_+ \hat{p}_-}(f)$, and $Q_{\hat{p}_+ \hat{p}_-}(f)$

For the case with no mean flow equations (4.20) reduce to

$$\begin{aligned}
 S_{11}(f) &= S_{\hat{p}_+ \hat{p}_+}(f) + S_{\hat{p}_- \hat{p}_-}(f) + 2[C_{\hat{p}_+ \hat{p}_-}(f) \cos 2kx_1 + Q_{\hat{p}_+ \hat{p}_-}(f) \sin 2kx_1] \\
 S_{22}(f) &= S_{\hat{p}_+ \hat{p}_+}(f) + S_{\hat{p}_- \hat{p}_-}(f) + 2[C_{\hat{p}_+ \hat{p}_-}(f) \cos 2kx_2 + Q_{\hat{p}_+ \hat{p}_-}(f) \sin 2kx_2] \\
 C_{12}(f) &= [S_{\hat{p}_+ \hat{p}_+}(f) + S_{\hat{p}_- \hat{p}_-}(f)] \cos k(x_1 - x_2) + 2[C_{\hat{p}_+ \hat{p}_-}(f) \cos k(x_1 - x_2) + Q_{\hat{p}_+ \hat{p}_-}(f) \sin k(x_1 + x_2)] \\
 Q_{12}(f) &= [-S_{\hat{p}_+ \hat{p}_+}(f) + S_{\hat{p}_- \hat{p}_-}(f)] \sin k(x_1 - x_2)
 \end{aligned} \tag{4.21}$$

If a third microphone is located downstream of the system under study, the spectral density of the transmitted wave, $S_{p_{out} p_{out}}(f)$ can be measured directly, if an anechoic termination is used:

$$S_{p_{out} p_{out}}(f) = \frac{1}{T} \{ \hat{p}_{out}(f, T) \hat{p}_{out}^*(f, T) \} \tag{4.22}$$

where $\hat{p}_{out}(f, T)$ is the finite Fourier transform of the downstream microphone signal. It can be easily shown that the quantities $S_{\hat{p}_+ \hat{p}_+}(f)$ represent the mean square value of the incident and reflected pressures in a narrow frequency band. As well $S_{p_{out} p_{out}}(f)$ is equal to the mean square value of the progressive wave at outlet:

$$S_{\hat{p}_+ \hat{p}_+}(f) = [r.m.s.(p_+)]^2 = \bar{p}_+ \tag{4.23}$$

$$S_{p_{out} p_{out}}(f) = [r.m.s.(p_+^{out})]^2 = \bar{p}_+^{out} \tag{4.24}$$

The transmission loss (TL) is then given by:

$$\begin{aligned}
 TL &= 10 \log_{10} \left[\frac{W_+^{in}(f)}{W_+^{out}(f)} \right] = 10 \log_{10} \left[\frac{(\bar{p}_+)^2}{\rho_o A_{in}} \cdot \frac{\rho_o A_{out}}{(\bar{p}_+^{out})^2} \right] = 10 \log_{10} \left[\frac{(\bar{p}_+)^2}{(\bar{p}_+^{out})^2} \cdot \frac{A_{out}}{A_{in}} \right] = \\
 &= 10 \log_{10} \left[\frac{S_{AA}(f)}{S_{cc}(f)} \right] + 10 \log_{10} \left[\frac{A_{out}}{A_{in}} \right]
 \end{aligned} \tag{4.25}$$

where A_{in} and A_{out} are the areas of the inlet and outlet section respectively.

A common error is to attempt to apply decomposition method to downstream of the muffler using a pair of microphones if the termination is not anechoic. This will not work as p_+^{out} will change due to the wave reflections caused by the environment and by the silencer itself [2].

The two upstream microphones must be sampled simultaneously for computation of the cross-spectral density $S_{12}(f)$, but the downstream microphone can be sampled independently. Consequently, one of the upstream microphones can be used downstream and only two microphone systems are needed. The location of the upstream microphones is not critical, within certain limitations. The microphones should be located as close to the unknown system as possible (compatibly with the investigated frequency range), so that dissipative losses in the tube are minimized. The microphone spacing should be as small as possible for the same reason. However, each microphone is assumed to measure the sound pressure at a point in the tube, so that for very close microphone spacing the effective spacing ($x_2 - x_1$) is difficult to estimate, particularly for large-diameter microphones. Therefore, the microphone spacing should be much larger than the diameter of the microphones used so that the effective microphone spacing can be assumed to be the distance between the microphone center lines.

Since the sound field varies randomly with time, the estimates of the microphone auto- and cross-spectra also will be random variables. It should be mentioned that the spectral-estimate, eq. (4.18), are inconsistent and some form of smoothing must be done to reduce the random error to an acceptable level. One method of reducing the random error of a spectrum is to divide the total time record T into n segments of equal length T_s , and average individual estimates of the spectrum for each of these segments. Smoothing in this manner reduces the random error to $1/n^{1/2}$ (e.g., for $n = 400$ the random error would be 5%), and the spectral bandwidth is $1/T_s$. One is tempted to make T_s as small as possible so that n is very large for a given length of total time T , thereby reducing the random error to a very small value. However, this leads to a biasing of the spectrum in which spectral peaks are not resolved because the bandwidth is too wide. Consequently, the bandwidth (and therefore T_s) should be determined from a knowledge of the frequency resolution needed for the particular quantity being analyzed [2].

4.2 TWO PORT MODEL – TWO LOAD/TWO SOURCE TECHNIQUES

4.2.1 LINEAR SYSTEMS

For mechanical systems where the interest is in determining the response or output signal, a certain excitation or input signal is applied. The relationship between the input and output signal is, for a *linear time invariant system*, described mathematically by a linear differential equation with constant coefficients. A linear time invariant system has got a number of important properties. The principle of superposition implies that if the input signal $a(t)$ gives the output signal $b(t)$, and the input signal $c(t)$ gives the output signal $d(t)$ the combined input signal $a(t)+c(t)$ gives the output signal $b(t)+d(t)$. The principle of homogeneity implies that if the input signal $a(t)$ is multiplied by a constant k the output signal will be $k_b(t)$. A linear system also preserves frequency which means that the only those frequency components present in the input signal can exist in the output signal.

In general a linear time invariant system does not necessarily have just one input and one output. This type of system is called a single input / single output (SL SO) system. Also multi input / multi output (MI/MO) systems are possible, as well as single input/multi output (SI/MO) systems, and multi input / single output (MI/SO) systems. These are described by a system of coupled linear differential equations with constant coefficients.

Regarding the linear systems in the time domain, if the input to the system is a unit Dirac pulse with the properties

$$X(t) = \delta(t), \quad \delta(t) = 0 \text{ for } t \neq 0, \quad \int_{-\infty}^{+\infty} \delta(t) dt = 1 \quad (4.26)$$

the output from the system $y(t)=h(t)$ is called the impulse response which is the time domain function describing the linear system properties.

An arbitrary input $x(t)$ can be built up from a summation or, considering continuous time functions, from an integral over an infinite number of Dirac functions, located at $t=\tau$, each with the amplitude $x(\tau)$:

$$x(t) = \int_{-\infty}^{+\infty} x(\tau) \delta(t - \tau) d\tau \quad (4.27)$$

This also follows directly from the properties of the Dirac delta function. Each one of the Dirac pulses in (4.26) will give the output $h(t-\tau)$ so the total output will be given by a summation (integration) of these multiplied by the amplitudes $x(\tau)$

$$y(t) = \int_{-\infty}^{+\infty} x(\tau) h(t - \tau) d\tau \quad (4.28)$$

which is called *convolution integral*.

The linear system may thus be characterized by the impulse response $h(t)$ or by the Fourier transform of $h(t)$, which we call the *Frequency Response Function*, FRF, $H(f)$. In fact, in order to study the frequency domain representation of linear time invariant system, one can use the Fourier transform. When it is applied to (4.28) it gives:

$$\begin{aligned} F\{y(t)\} &= F\left\{\int_{-\infty}^{+\infty} x(u) \cdot h(t-u) du\right\} = F\{x(t)\} \cdot F\{h(t)\} \\ \text{or} \\ Y(f) &= X(f) \cdot H(f) \end{aligned} \quad (4.29)$$

$Y(f)$, $H(f)$ and $X(f)$ are the Fourier transforms of $x(t)$, $h(t)$ and $y(t)$. The frequency response function (FRF) $H(f)$ is obtained from (4.29) as

$$H(f) = \frac{Y(f)}{X(f)} \quad (4.30)$$

The FRF is very frequently used in analysis of mechanical and electrical systems. The simplicity of (4.29) for prediction of the output signal and (4.30) for system identification, compared to the time domain expression in (4.28) makes it a powerful tool. The FRF can, according to (4.30), in principle be determined by measuring the input and output signals and calculating their Fourier transforms and dividing the two. Techniques for estimation of FRF:s using sine excitation and transient excitation and using random input signals will be discussed in the Appendix of this chapter.

4.2.2 TWO PORT SOURCES

A *two-port* can be defined as a linear, physical system with an input and an output. The state at the input or output can be completely described by using two state variables, i.e. two independent physical quantities. The relation between the input and output states of a time-invariant and active two-port can, in the frequency domain, be written as [3]:

$$\mathbf{y} = \mathbf{H}\mathbf{x} + \mathbf{y}' \quad (4.31)$$

where \mathbf{x} and \mathbf{y} are the state vectors at the input and output, \mathbf{H} is a $[2 \times 2]$ -matrix which is independent of \mathbf{x} , and \mathbf{y}' is the source strength vector. Every time the active properties of the system are neglected (as usually happen with mufflers), the (4.31) becomes:

$$\mathbf{y} = \mathbf{H}\mathbf{x} \quad (4.32)$$

In extended notation the (4.32) can be written as:

$$\begin{bmatrix} y' & y'' \end{bmatrix} = \begin{bmatrix} H_{11} & H_{12} \\ H_{21} & H_{22} \end{bmatrix} \begin{bmatrix} x' \\ x'' \end{bmatrix} \quad (4.33)$$

In order to experimentally obtain the four unknown constituting the terms of the \mathbf{H} matrix, the two port must be tested utilizing two independent input states, i' and i'' .

Any pair of state variables, i.e. a state vector, belonging to a two-port defines a linear 2D state-space. Let a and b denote two cross-sections in a duct system, the choice of $\mathbf{x}=[p_a, q_a]^T$ and $\mathbf{y}=[p_b, q_b]^T$ as the state vectors, gives the two-port in the so-called *transfer-matrix* form. This form is particularly useful for duct systems where the elements are coupled in cascade, e.g. exhaust systems for automobiles. If, instead, $\mathbf{x}=[p_a, p_b]^T$ and $\mathbf{y}=[q_a, q_b]^T$ are the state vectors, the so-called *mobility-matrix* form is obtained. This form is useful for elements which are coupled in parallel. Another choice of state variables is to use the travelling wave amplitudes p_+ and p_- at two different duct cross-sections. This gives the two-port in the so-called *scattering-matrix* form. This latter can be very efficient for the analysis of complex ducts systems with many branches. The concept of scattering matrix can probably be regarded as the most basic description of a wave interaction problem. In view of this it seems to be a

good idea that a measurement method for characterization of acoustical two-ports, should be based on the scattering-matrix description. Of course, when one form of the two-port is known, all other forms can be obtained from linear transformations. From this point of view the choice of description is not so important [3].

The scattering-matrix S of an acoustical two-port can be defined by

$$\begin{bmatrix} p_{a^-} \\ p_{b^+} \end{bmatrix} = \begin{bmatrix} S_{11} & S_{12} \\ S_{21} & S_{22} \end{bmatrix} \begin{bmatrix} p_{a^+} \\ p_{b^-} \end{bmatrix} \quad (4.34)$$

where a and b are two different duct cross-sections and the positive directions are defined. Equation (4.33) is valid when the fluid to duct wall coupling in region I and III (see Fig. 5.2) is negligible or can be represented by a locally reacting wall. As discussed in the introduction if one matrix description of a two-port is known all other descriptions can be obtained by linear transformations [3].

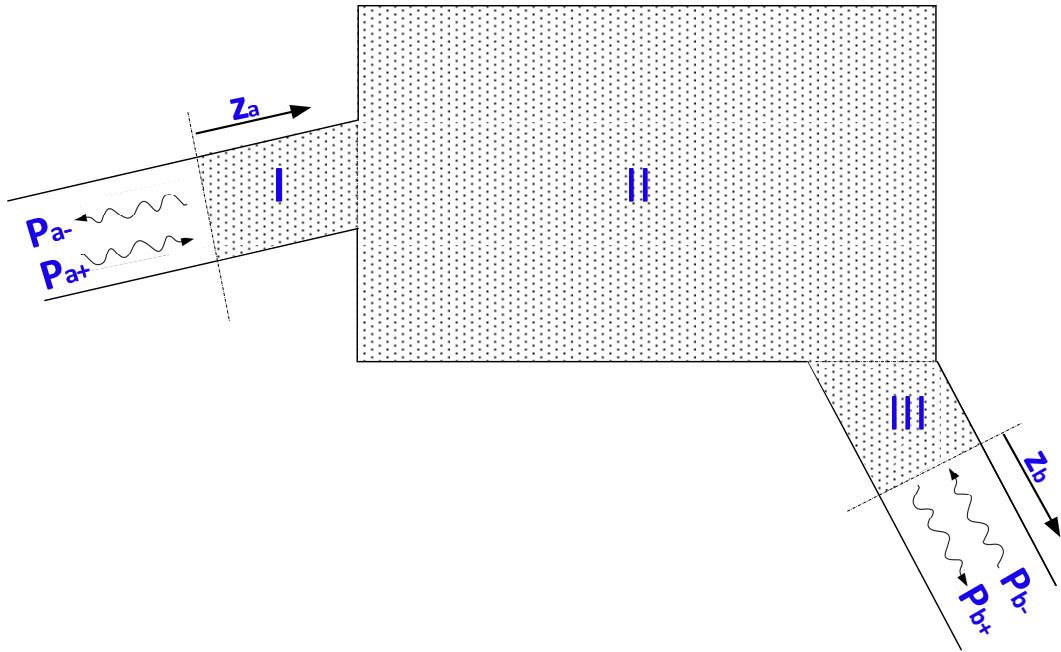


Figure 5.2 – Definition of an acoustical two-port. Uniform straight ducts: I, III; linear time-invariant and passive acoustical system: II

In many duct acoustic applications the so-called transfer-matrix description is of interest. The transformation from the scattering-matrix to the transfer-matrix of an acoustical two-port is therefore described afterwards.

The starting point to explain the measurement procedure for the determination of the scattering matrix is the assumption that a perfect reference signal is available. This reference signal is by definition linearly related to the acoustic signal in the duct and completely uncorrelated with any disturbing noise in the system. With flow present in the duct the disturbing noise is normally dominated by flow noise, i.e., turbulent pressure fluctuations. To determine the scattering-matrix, the two-port must be tested using two different input states. If the input and output state vectors for these test cases are measured, the following matrix equation is obtained.

$$\begin{bmatrix} p'_{a-} & p''_{a-} \\ p'_{b+} & p''_{b+} \end{bmatrix} = \begin{bmatrix} S_{11} & S_{12} \\ S_{21} & S_{22} \end{bmatrix} \begin{bmatrix} p'_{a+} & p''_{a+} \\ p'_{b-} & p''_{b-} \end{bmatrix} \quad (4.35)$$

When the two input states $[p'_{a+}, p'_{b-}]^T$ and $[p''_{a+}, p''_{b-}]^T$ are linearly independent, S can be solved from equation (4.35). This latter can be regarded as the basis for the measurement procedure. In order to reduce the influence of disturbing noise when the state vectors are measured, the reference signal can be used, forming the transfer function between the reference signal and each state vector component. When the transfer function approach is used, to suppress disturbing noise, equation (4.35) can be rewritten as:

$$\mathbf{H}_y = \mathbf{S} \mathbf{H}_x \quad (4.36)$$

where

$$\mathbf{H}_x = \begin{bmatrix} H'_{ra+} & H''_{ra+} \\ H'_{rb-} & H''_{rb-} \end{bmatrix}, \quad \mathbf{H}_y = \begin{bmatrix} H'_{ra-} & H''_{ra-} \\ H'_{rb+} & H''_{rb+} \end{bmatrix} \quad (4.37)$$

Here the symbol \mathbf{H}_{rx} is used to denote a transfer function from a reference signal (r) to a state vector component (x). When the inverse of the matrix \mathbf{H}_x exists the scattering-matrix is given by

$$\mathbf{S} = \mathbf{H}_y \mathbf{H}_x^{-1} \quad (4.38)$$

When equation (4.50) is evaluated, the following results are obtained for the elements of S :

$$\begin{aligned}
 S_{11} &= (H'_{ra-} H''_{rb-} - H''_{ra-} H'_{rb-}) / \det(\mathbf{H}_x) \\
 S_{12} &= (H''_{ra-} H'_{ra+} - H'_{ra-} H''_{ra+}) / \det(\mathbf{H}_x) \\
 S_{21} &= (H'_{rb+} H''_{rb-} - H''_{rb+} H'_{rb-}) / \det(\mathbf{H}_x) \\
 S_{22} &= (H''_{rb+} H'_{ra+} - H'_{rb+} H''_{ra+}) / \det(\mathbf{H}_x)
 \end{aligned} \tag{4.39}$$

where $\det(\mathbf{H}_x) = (H'_{ra+} + H''_{rb-} - H''_{ra+} H'_{rb-})$. To use (4.51), in practice, the transfer functions must be measured from measurable field quantities in the ducts.

In many duct acoustic applications the field quantity which is easiest to measure is the fluctuating pressure. In the plane wave region of a uniform straight duct the travelling wave amplitudes p_+ and p_- , can be obtained from pressure measurements at two duct cross-sections. The theory for this plane wave decomposition has been previously explained, and the following relationships can be obtained for the case of a hard-walled duct with a uniform mean flow:

$$\begin{aligned}
 p_+ &= F [p_1 \cdot e^{ik_-s} - p_2] \\
 p_- &= F [-p_1 \cdot e^{-ik_+s} + p_2]
 \end{aligned} \tag{4.40}$$

where

$$F = [e^{ik_-s} - e^{-ik_+s}]^{-1} \tag{4.41}$$

and p_1, p_2 are acoustic pressures at two different duct cross-sections, see Fig. 3. The complex wavenumbers k_+ and k_- have been defined in (4.13).

With flow present in the duct we can only measure the total fluctuating pressure, i.e., the sum of both the acoustic and turbulent pressure fluctuations. To suppress the influence from turbulent pressure fluctuations one can, as discussed above, use a reference signal. Regarding the choice of reference signal two cases will be treated in detail below. These cases will be referred to as the two-load and the two-source case.

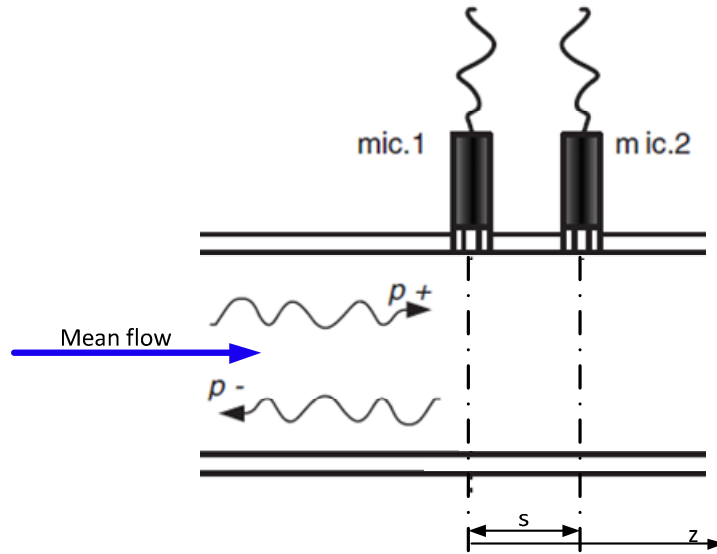


Figure 5.3 – Measurement configuration for plane wave decomposition.

4.2.3 THE TWO-LOAD CASE

Here the two different states of the two-port are obtained by using a fixed acoustic source and two different acoustic loads, see Figure 5.4.

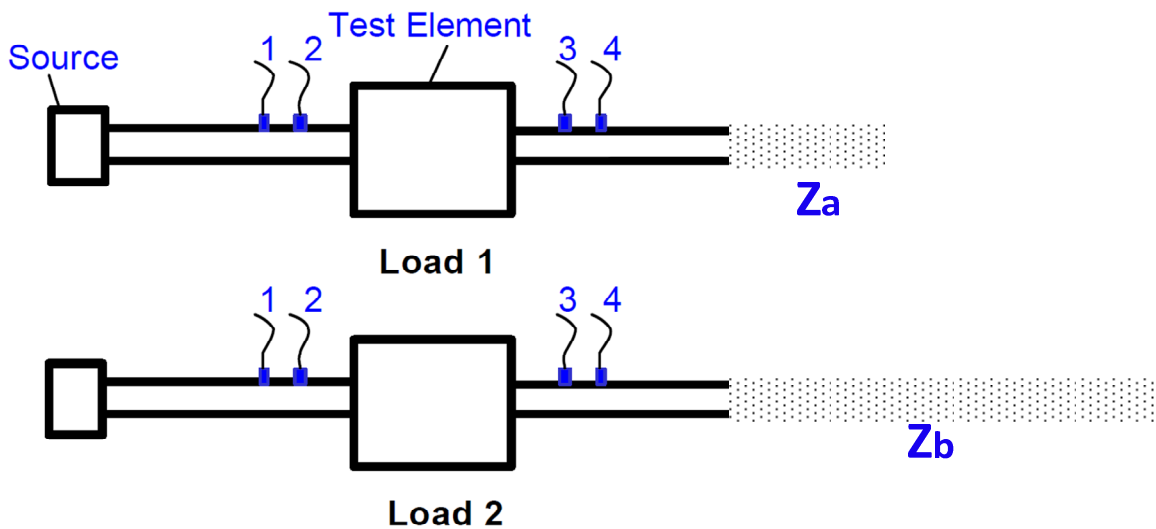


Figure 5.4 – Setup of two-load method.

A possible choice for the reference signal is the incident wave amplitude on the source-side of the unknown two-port. Assume that the source-side corresponds to duct I in Fig. 5.2, then p_{a+} is the reference signal. This choice of reference signal is good if the acoustic pressure

fluctuations in duct I are much stronger than the turbulent pressure fluctuations. For low speed flows ($M < 0.1$) there is no problem to generate a broad-band acoustic signal which fulfils this condition. For higher Mach numbers other choices of reference signal are necessary. If the acoustic source is a loudspeaker the electric signal to the loudspeaker can be used as reference signal. This type of approach is normally referred to as source-correlation. For very difficult measurement conditions source-correlation using a pure harmonic signal should be used. With p_{a+} as reference equation (4.39), which gives the scattering-matrix elements, can be written

$$\begin{aligned} S_{11} &= (H'_{a^+a^-} H''_{a^+b^-} - H''_{a^+a^-} H'_{a^+b^-}) / \det(\mathbf{H}_x) \\ S_{12} &= (H''_{a^+a^-} - H'_{a^+a^-}) / \det(\mathbf{H}_x) \\ S_{21} &= (H'_{a^+b^+} H''_{a^+b^-} - H''_{a^+b^+} H'_{a^+b^-}) / \det(\mathbf{H}_x) \\ S_{22} &= (H''_{a^+b^+} - H'_{a^+b^+}) / \det(\mathbf{H}_x) \end{aligned} \quad (4.42)$$

where $\det(\mathbf{H}_x) = (H''_{a+b-} - H'_{a+b-})$. To obtain equation (4.42) it must be recognized that $H'_{a+a+} = H''_{a+a+} = 1$. The most common way to estimate a transfer function is to use measured cross- and auto-spectra. This type of estimate can be used for all stationary signal types. In our case the reference signal is assumed to be noise free, the best choice of estimate for the transfer function is then given by

$$H_{xy} = \frac{G_{xy}}{G_{xx}} \quad (4.43)$$

where the cross- and auto-spectrum G_{xy} and G_{xx} are estimated with digital Fourier analyzers by use of the Discrete Fourier Transform (DFT) [3]. From this point of view we can simply define, for two stationary signals x and y , the cross- and auto-spectrum as $G_{xy} = E[XY^*]$ and $G_{xx} = E[XX^*]$. Here $E[]$ denotes average over a number of consecutive data records (ensemble average) and X , Y should be interpreted as DFTs of x , y . These DFTs must be calculated from simultaneously sampled values. Of course if spectral densities are of interest then the above definitions must be multiplied with an appropriate constant [12].

By using equation (4.40) the wave amplitudes p_+ and p_- in a duct can be expressed in terms of the acoustic pressure at two points:

$$\begin{aligned}
 p_{a^+} &= F_a [p_1 \cdot e^{ik_a s_a} - p_2] \\
 p_{a^-} &= F_a [-p_1 \cdot e^{-ik_a s_a} + p_2] \\
 p_{b^+} &= F_b [p_3 \cdot e^{ik_b s_b} - p_4] \\
 p_{b^-} &= F_b [-p_3 \cdot e^{-ik_b s_b} + p_4]
 \end{aligned} \tag{4.44}$$

where

$$F_a = [e^{ik_a s_a} - e^{-ik_a s_a}]^{-1} \tag{4.45}$$

$$F_b = [e^{ik_b s_b} - e^{-ik_b s_b}]^{-1} \tag{4.46}$$

The acoustic pressures p_1, p_2 are associated with duct I and p_3, p_4 with duct III, see Fig. 5.2.

It can also be noted that p_1 is the pressure at a and p_3 at b in Fig. 5.2. From equation (4.45) and (4.46) and the definition of cross- and auto-spectrum given above, the following results can be derived:

$$\begin{aligned}
 G_{a^+ a^-} &= E[P_{a^+}^* P_{a^-}] = |F_a|^2 [-G_{11} \cdot e^{-ik_a s_a - ik_a s_a} + G_{12} \cdot e^{-ik_a s_a} + G_{21} \cdot e^{-ik_a s_a} - G_{22}] \\
 G_{a^+ b^-} &= E[P_{a^+}^* P_{b^-}] = F_a^* F_b [-G_{13} \cdot e^{-ik_a s_a - ik_b s_b} + G_{14} \cdot e^{-ik_a s_a} + G_{23} \cdot e^{-ik_b s_b} - G_{24}] \\
 G_{a^+ b^+} &= E[P_{a^+}^* P_{b^+}] = F_a^* F_b [G_{13} \cdot e^{-ik_a s_a + ik_b s_b} - G_{14} \cdot e^{-ik_a s_a} - G_{23} \cdot e^{ik_b s_b} - G_{24}] \\
 G_{a^- a^+} &= E[P_{a^-}^* P_{a^+}] = |F_a|^2 [G_{11} - G_{12} \cdot e^{-ik_a s_a} + G_{21} \cdot e^{ik_a s_a} + G_{22}]
 \end{aligned} \tag{4.47}$$

where $G_{mn} = E[P_m^* P_n]$, $m = 1, 2$ and $n = 1, 2, 3, 4$. By using equations (4.43) and (4.47) we can express the transfer functions in equation (4.43) in terms of measurable quantities [3].

4.2.4 THE TWO-SOURCE CASE

Here the two different states of the two-port are obtained by changing the source location, with the rest of the system kept unchanged, see Figure 5.5.

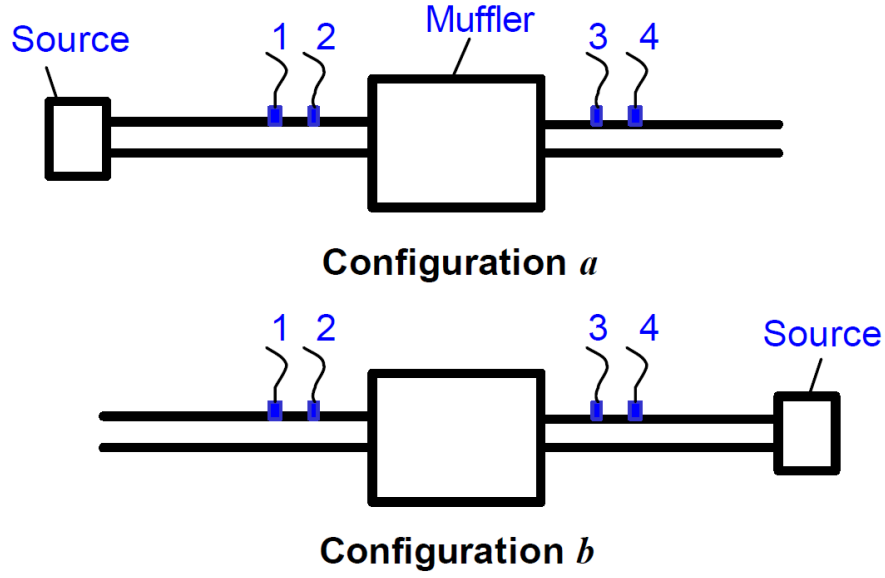


Figure 5.5 – Setup of two-source method.

Just as in section 4.2.3, also here the incident wave amplitude on the source-side is chosen as reference signal. Assume that the source-side for the first test state is duct I and for the second is duct III, see Fig. 5.2. Then p'_{a+} and p''_{b-} are the reference signals. Keeping this in mind equation (4.39) gives:

$$\begin{aligned}
 S_{11} &= (H'_{a^+a^-} - H''_{b^-a^-} H'_{a^+b^-}) / \det(\mathbf{H}_x) \\
 S_{12} &= (H''_{b^-a^-} - H'_{a^+a^-} H'_{b^-a^+}) / \det(\mathbf{H}_x) \\
 S_{21} &= (H'_{a^+b^+} - H''_{b^-b^+} H'_{a^+b^-}) / \det(\mathbf{H}_x) \\
 S_{22} &= (H''_{b^-b^+} - H'_{a^+b^+} H'_{b^-a^+}) / \det(\mathbf{H}_x)
 \end{aligned} \tag{4.48}$$

where $\det(\mathbf{H}_x) = (1 - H''_{b^-a^+} + H'_{a+b-})$. Equation (4-60) contains six different transfer functions, three of these H_{a+a-} , H_{a+b-} and H_{a+b+} can be found in section 4.2.3, see equations (4.43) and (4.47). The remaining three are

$$\begin{aligned}
 H_{b^-a^-} &= \frac{G_{b^-a^-}}{G_{b^-b^-}} \\
 H_{b^-a^+} &= \frac{G_{b^-a^+}}{G_{b^-b^-}} \\
 H_{b^-b^-} &= \frac{G_{b^-b^+}}{G_{b^-b^-}}
 \end{aligned} \tag{4.49}$$

By using the same approach as in section 4.2.3, the auto-spectrum and the cross-spectra in equation (4.49) can be expressed in measurable quantities:

$$\begin{aligned}
 G_{b^-a^-} &= E[P_{b^-}^* P_{a^-}] = F_a F_b^* [G_{31} \cdot e^{-ik_{a^+} s_a + ik_{b^+} s_b} - G_{32} \cdot e^{ik_{b^+} s_b} - G_{41} \cdot e^{-ik_{a^+} s_a} + G_{42}] \\
 G_{b^-a^+} &= E[P_{b^-}^* P_{a^+}] = F_a F_b^* [-G_{31} \cdot e^{ik_{a^-} s_a + ik_{b^+} s_b} + G_{32} \cdot e^{ik_{b^+} s_b} + G_{41} \cdot e^{ik_{a^-} s_a} - G_{42}] \\
 G_{b^+b^+} &= E[P_{b^+}^* P_{b^+}] = |F_b|^2 [-G_{33} \cdot e^{ik_{b^+} s_b + ik_{b^-} s_b} + G_{34} \cdot e^{ik_{b^+} s_b} + G_{43} \cdot e^{ik_{b^-} s_b} - G_{44}] \\
 G_{b^+b^-} &= E[P_{b^+}^* P_{b^-}] = |F_b|^2 [G_{33} - G_{34} \cdot e^{ik_{b^+} s_b} - G_{43} \cdot e^{-ik_{b^+} s_b} + G_{44}]
 \end{aligned} \tag{4.50}$$

where $G_{mn} = E[P_m^* P_n]$, $m=3,4$ and $n=1,2,3,4$. [3]

4.2.4. INFLUENCE OF ERRORS

The resulting errors in a scattering-matrix, obtained by using the procedure above, depend on three things: (I) the errors in the measured input data; (II) the error sensitivity of the plane wave decomposition, equation (8); (III) the error sensitivity of the matrix equation for \mathbf{S} , equation (4.35).

Point (I) and (II) have been discussed by Bodén and Abom [13, 14]. A main conclusion is that, to obtain good measurement results, the plane wave decomposition must be restricted to the frequency range

$$0.1\pi(1 - M^2) < ks < 0.8\pi(1 - M^2) \tag{4.51}$$

Regarding point (III) it will mainly depend on the inversion of the matrix \mathbf{X} . When this matrix is singular; or almost singular, large errors can be expected. To avoid this the two test states for the two-port must be significantly different. Doige and Munjal, in [15], proved that this is much easier to achieve for the two source case than for the two-load case.

Finally, it can be noted that to use this measurement procedure a number of transfer functions must be estimated. To estimate these transfer functions equation (4.43) should be used. For signals of stationary random type the cross- and auto-spectrum in this equation must be obtained from simultaneously measured data. Otherwise large random errors can occur. This means that for random data a four-channel Fourier analyzer is needed to obtain good

estimates of the transfer functions in equations (4.42) and (4.48). For periodic data, e.g., pseudo-random, this type of problem does not exist. Then good estimates of these transfer functions can be obtained by using a two-channel analyzer.

4.2.5 CALCULATION OF THE TRANSFER-MATRIX FROM A GIVEN SCATTERING-MATRIX

The scattering-matrix of an acoustical two-port is defined in equation (4.34). The transfer matrix \mathbf{T} of the same two-port can be defined as

$$\begin{bmatrix} p_a \\ q_b \end{bmatrix} = \begin{bmatrix} T_{11} & T_{12} \\ T_{21} & T_{22} \end{bmatrix} \begin{bmatrix} p_b \\ p_a \end{bmatrix} \quad (4.52)$$

where a and b are two different duct cross-sections and the positive directions are defined as in Fig. 5.2. The key to find the required relationship is a study of state vector transformations. First, we express the state vectors $[p_a, q_a]^T$ and $[p_b, q_b]^T$ in terms of wave amplitudes at a and b:

$$\begin{bmatrix} p_a \\ q_a \end{bmatrix} = B_a \begin{bmatrix} p_a^+ \\ p_a^- \end{bmatrix}, \quad \begin{bmatrix} p_b \\ q_b \end{bmatrix} = B_b \begin{bmatrix} p_b^+ \\ p_b^- \end{bmatrix} \quad (4.53)$$

where

$$B_a = \begin{bmatrix} 1 & 1 \\ Y_a & -Y_a \end{bmatrix}, \quad B_b = \begin{bmatrix} 1 & 1 \\ Y_b & -Y_b \end{bmatrix} \quad \text{and} \quad Y_a = \frac{A_a}{\rho_a c_a}, \quad Y_b = \frac{A_b}{\rho_b c_b},$$

Then, by using equation (4.34), one can express $[p_{a+}, p_{a-}]^T$ and $[p_{b+}, p_{b-}]^T$ in terms of $[p_{a+}, p_{b+}]^T$

$$\begin{bmatrix} p_{a^+} \\ p_{a^-} \end{bmatrix} = C_a \begin{bmatrix} p_{a^+} \\ p_{b^-} \end{bmatrix}, \quad \begin{bmatrix} p_{b^+} \\ p_{b^-} \end{bmatrix} = C_b \begin{bmatrix} p_{a^+} \\ p_{b^-} \end{bmatrix}, \quad (4.54)$$

where

$$C_a = \begin{bmatrix} 1 & 0 \\ S_{11} & S_{12} \end{bmatrix}, \quad C_b = \begin{bmatrix} S_{21} & S_{22} \\ 0 & 1 \end{bmatrix}, \quad (4.55)$$

From equations (4.53) and (4.54) we obtain

$$\begin{bmatrix} p_a \\ p_a \end{bmatrix} = B_a C_a \begin{bmatrix} p_{a^+} \\ p_{b^-} \end{bmatrix}, \quad \begin{bmatrix} p_b \\ q_b \end{bmatrix} = B_b C_b \begin{bmatrix} p_{a^+} \\ p_{b^-} \end{bmatrix}, \quad (4.56)$$

From equations (4.56) one can derive the required relationship

$$T = B_a (C_a C_b^{-1}) B_b^{-1} \quad (4.57)$$

which leads to:

$$\begin{aligned} T_{11} &= \left[S_{12} + \frac{(1 + S_{11})(1 - S_{22})}{S_{21}} \right] \cdot \frac{1}{2} \\ T_{12} &= \left[-\frac{S_{12}}{Y_b} + \frac{(1 + S_{11})(1 + S_{22})}{Y_b S_{21}} \right] \cdot \frac{1}{2} \\ T_{21} &= \left[-Y_a S_{12} + \frac{Y_a (1 - S_{11})(1 - S_{22})}{S_{21}} \right] \cdot \frac{1}{2} \\ T_{22} &= \left[\frac{Y_a S_{12}}{Y_b} + \frac{Y_a (1 - S_{11})(1 + S_{22})}{Y_b S_{21}} \right] \cdot \frac{1}{2} \end{aligned} \quad (4.58)$$

4.3 TEST RIG OF TTU LABORATORY

A number of experimental analyses have been included in the last chapter of this thesis. As mentioned, all of these tests have been carried in acoustic laboratory of Tallinn University of Technology (TUT). This is provided of a dedicated experimental facility which was built in order to determine the sound transmission data of the silencers in high flow velocity and high temperature conditions. The classical two-microphone approach is used to obtain complex pressure amplitudes of the traveling acoustic waves at the inlet and outlet cross-sections of the silencer. A photo and a sketch of the installation used to carry out the experimental work are shown in Figs. 5.6 and 5.7.

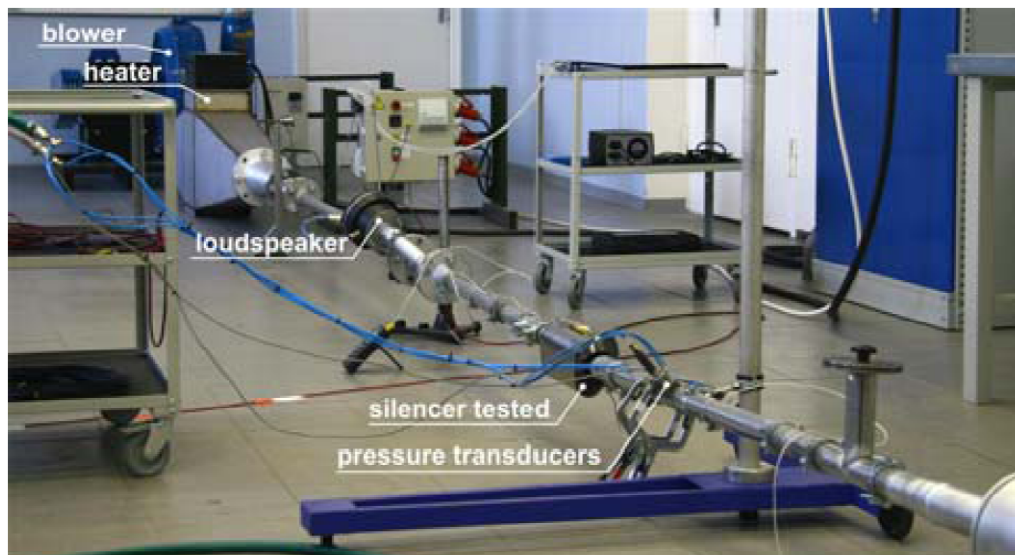


Figure 5.6 – Photo of TTU facilities for acoustic measurements on two port sources [10].

The acoustic measurements have been performed in a test section made of steel pipe with inner diameter of 42mm. The wall thickness of the pipe is 1.5mm.

As the acoustical test section equipped with dynamic pressure and temperature sensors is mounted more than 50 pipe diameters downstream of the stagnation chamber, a fully developed turbulent mean flow is expected during the experiments.

A pressure transducer separation $s=70\text{mm}$ has been chosen. It has been proved that, in order to avoid a large sensitivity to errors in the input data, the two microphone method should be restricted to the frequency range $0.1\pi (1 - M^2) < ks < 0.8\pi (1 - M^2)$, where k is

wave number and M is Mach number. Accordingly, the frequency region covered during the measurements ranged from 245Hz...1.9kHz (for room temperature air at 20°C) to 305Hz...2.4kHz (heated air at 180°C).

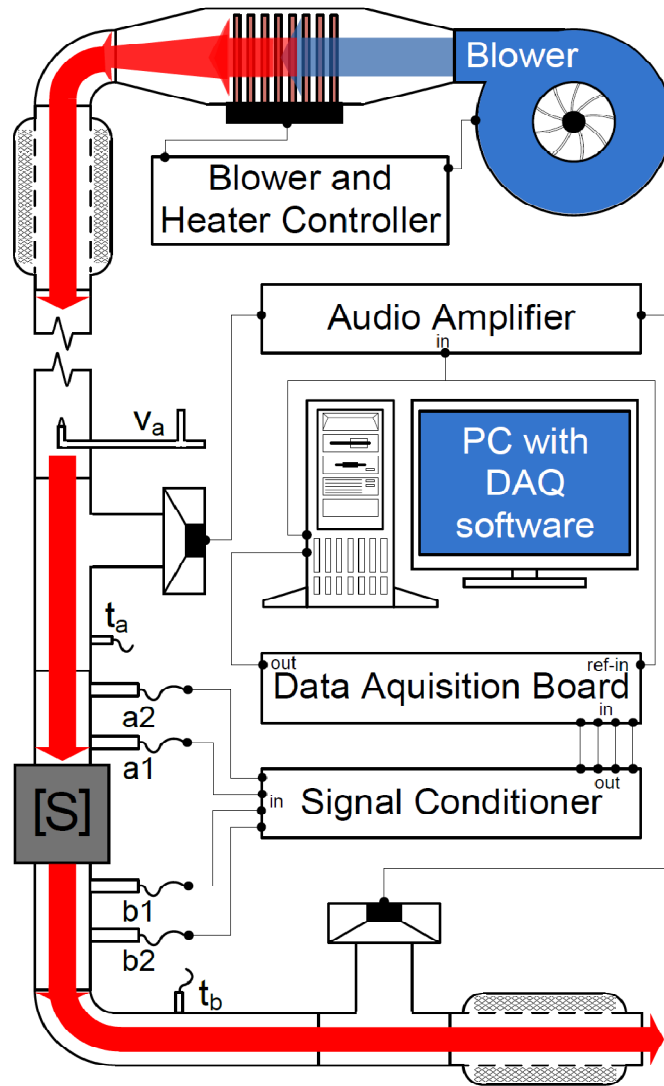


Figure 5.7 – Sketch of the system for acoustic analyses in TTU laboratory [9].

Two piezo-resistive pressure transducers (Kistler 4045A), equipped with water-cooling mounts, are used in the test pipe to simultaneously record the acoustic pressure signals. The transducers are located at the opposite pipe walls in order to suppress uncorrelated flow disturbances around the wall surfaces. Two transducers are installed at the inlet section and two at the outlet section respectively. The pressure signals are conditioned and amplified by piezo-resistive amplifiers (Kistler 4603).

A random acoustic excitation is provided by professional series electro-dynamic driver (DAS ND-8) placed into a side-branch upstream and downstream of the test section. The driver is equipped with a titanium diaphragm which is an appropriate choice for measurements in high temperature conditions. The electro-dynamic driver is driven by a software-based signal generator through a power amplifier (Velleman VPA2100MN).

In order to enhance the acoustic excitation level from the drivers the power has been concentrated only at the frequency range of interest by using numerical filtration technique in LabView. The signal acquisition has been performed by a four-channel dynamic signal analyzer (National Instruments NI PCI-4474). The analyzer is controlled by a purpose built PC based virtual instrument (LabView).

The flow velocity is determined by a portable anemometer (Delta Ohm) using a Pitot tube mounted to the inlet of the measurement section. In order to achieve desired flow velocities in the test section a two-stage high pressure blower (Kongsilde 300TRV, 0.3Pa) is implemented.

An electric heater (22.5kW) is incorporated into the stagnation chamber, with a volume of 0.15m³. Both sides of the acoustic test section are terminated with additional silencers in order to minimize the standing waves in the pipeline and thus to improve the quality of the results. The temperature values at the inlet and outlet of the measurement sections have been obtained by using a dual K-type thermometer (TES-1312).

The measured temperature readings has been used to determine the density and the speed of sound values in the inlet and outlet pipes as important parameters to calculate the transmission loss data. The test-rig is capable to deliver flow velocities in excess of 100 m/s while maintaining a temperature approximately 200 °C..

To be precise it must be highlighted that, in the experiments performed in TTU laboratory, the reduction of flow noise in microphone signals is achieved by using transfer functions taken between the microphone signals and the loudspeaker driving signal, e (reference signal). This is referred to as source-correlation, and it has been preferred to the one shown in the section 4.2.3, where the incident wave amplitude on the source-side of the unknown two-port, p_{a+} is considered as the reference signal. The source-correlation, in fact, is preferred whenever the flow velocities can determine high flow noise disturbances. Since the TTU facilities are equipped to perform tests with high mean flow velocities, the auto-source correlation is appropriate.

APPENDIX

A.1 CORRELATION

When the signal studied is random, a measured time record will give incomplete information to fully analyze the signal. To fully understand the data and the physical phenomenon causing it one must consider all possible realizations of the signal, which could have occurred, see Figure A.1.

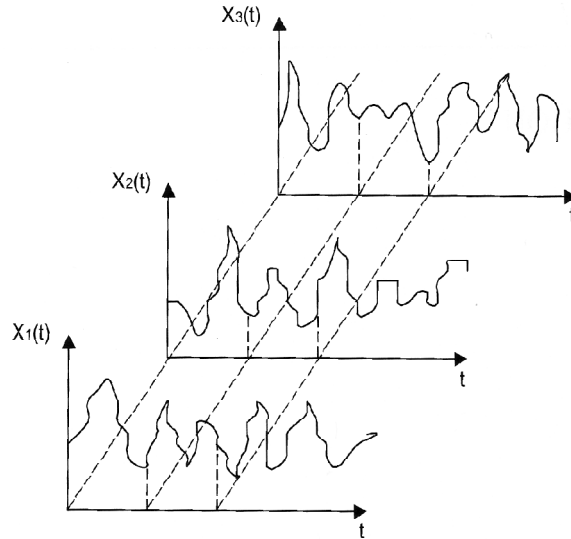


Figure A.1 – Ensemble of time histories for a random process [11].

The collection of time histories $x_i(t)$ defines the ensemble for the random process describing the physical phenomenon. The average properties of the process can be calculated at a given time by averaging over the ensemble. The mean value at a time t is given by,

$$\mu_x(t_1) = \lim_{N \rightarrow \infty} \frac{1}{N} \sum_{i=0}^{N-1} x_i(t_1) \quad (\text{A.1})$$

Similarly the higher order statistical moments can be calculated. For stationary signals all statistical moments are independent of time. For most stationary data the ensemble average calculated according to (A.1) is equal to the time average computed from one

time record,

$$\mu = \lim_{T \rightarrow \infty} \frac{1}{T} \int_0^T x(t) dt \quad (\text{A.2})$$

The same applies for the higher order statistical moments. This type of data is called *ergodic*.

A.2 ENSEMBLE AVERAGE

If the probability density function $p(x)$ for a stochastic variable x is known the different statistical moments can be calculated using the expected value or *ensemble average*, or E-operator:

$$\mu_n = E[x^n] = \int_{-\infty}^{\infty} x^n \cdot p(x) dx, \quad n = 0, 1, 2, \dots \quad (\text{A.3})$$

The first order moment gives,

$$\mu_1 = E[x] = \int_{-\infty}^{\infty} x \cdot p(x) dx = \mu \quad (\text{A.4})$$

which is the mean value of $x(t)$. The second order moment gives,

$$\mu_2 = E[x^2] = \int_{-\infty}^{\infty} x^2 \cdot p(x) dx = \Psi^2 \quad (\text{A.5})$$

which is the mean square value of $x(t)$.

For higher order moments it is often useful to calculate moments about the mean. The second order about the mean is given by

$$\mu_2^c = E[(x - \mu)^2] = \int_{-\infty}^{\infty} (x - \mu)^2 \cdot p(x) dx = \sigma^2 \quad (\text{A.6})$$

which is the variance of $x(t)$. The root mean square of σ^2 is the standard deviation. For stationary, ergodic signals the different statistical moments can be calculated from single time histories.

A.3 AUTO-CORRELATION

The auto-correlation function is defined as,

$$R_{xx}(\tau) = \lim_{T \rightarrow \infty} \frac{1}{T} \int_{T/2}^{T/2} x(t)x(t+\tau)dt \quad (\text{A.7})$$

It is as a measure of how well future values can be predicted using past observations. The definitions in (A.7) is actually only valid for so-called power signals that is signals with infinite energy content. For an energy signal with finite energy content the auto-correlation definition according to (A.7) would give a result equal to zero. Instead the following definition is used for energy signals,

$$R_{xx}(\tau) = \int_{-\infty}^{+\infty} x(t)x(t+\tau)dt \quad (\text{A.8})$$

If the signal is a discrete time series we instead get the following definitions of the auto-correlation function, for a power signal,

$$R_{xx}(k) = \lim_{N \rightarrow \infty} \frac{1}{2N+1} \sum_{i=-N}^N x(i)x(i+k) \quad (\text{A.9})$$

and for a energy signal,

$$R_{xx}(k) = \sum_{i=-N}^N x(i)x(i+k) \quad (\text{A.10})$$

The auto-correlation for a sine wave is a cosine wave with the same period as the original sine wave and with amplitude equal to the mean square value of the sine wave. The auto-correlation for a cosine wave is also a cosine wave with the same period as the original cosine wave and with amplitude equal to the mean square value of the cosine wave. For a general periodic signal with the Fourier series,

$$x(t) = C_0 + \sum_{i=1}^{\infty} C_i \sin(i\omega_0 t - \phi_i) \quad (\text{A.11})$$

the auto-correlation function is

$$R(\tau) = C_0^2 + \sum_{i=1}^{\infty} \frac{C_i^2}{2} \cos(i\omega_0 \tau) \quad (\text{A.12})$$

The auto-correlation function is always an even function in τ and therefore symmetrical around $\tau = 0$. The maximum possible value for the auto correlation is $R_{xx}(0)$,

$$R_{xx}(0) \geq |R_{xx}(\tau)|_{\tau \neq 0} \quad (\text{A.13})$$

where equality can occur only for periodic signals. Auto-correlation is a measure of how similar a signal is to a time delayed copy of itself. It is therefore natural that for zero time delay the signal is completely identical and therefore correlated with its copy. For periodic signals the situation will be the same after a time delay corresponding to one period. For a power signal inserting $\tau=0$ into (A.8) gives

$$R_{xx}(0) = \lim_{T \rightarrow \infty} \frac{1}{T} \int_{-T/2}^{T/2} x^2(t) dt \quad (\text{A.14})$$

which is the mean square value of the signal.

The auto-correlation function for an ideal white noise signal is a Dirac pulse at $\tau=0$ and zero at all other time delays. The interpretation of this is that in a white noise signal the data at any given time is completely independent (uncorrelated) to the data at previous times. The signal therefore only exhibits some similarity (correlation) for zero time delay where it is an identical copy of itself.

For a signal of band limited white noise we get an auto-correlation function which is “smoother” than a Dirac pulse.

If a signal consist of a combination of two independent (un-correlated) signals such as a sine wave plus random noise, the auto-correlation will be a combination of the auto-correlations of the two original signals.

A.4 CROSS-CORRELATION

The cross-correlation function between two time records $x(t)$ and $y(t)$ for power signals, is

$$R_{xy}(\tau) = \lim_{T \rightarrow \infty} \frac{1}{T} \int_{-T/2}^{T/2} x(t)y(t+\tau)dt \quad (\text{A.15})$$

for signals with infinite time duration and consequently infinite energy.

The cross-correlation function reveals the similarity of two signals as a function of the time delay between them. It can for instance be used to analyze propagation problems like convection with fluid flow or sound propagation. For energy signals with finite energy content the cross-correlation definition according to (A.15) would give a result equal to zero. Instead the following definition is used for energy signals,

$$R_{xy}(\tau) = \int_{-T/2}^{T/2} x(t)y(t+\tau)dt \quad (\text{A.16})$$

If the signals are discrete time series we instead get the following definitions of the cross-correlation function, for a power signal,

$$R_{xy}(k) = \lim_{N \rightarrow \infty} \frac{1}{2N+1} \sum_{i=-N}^N x(i)y(i+k) \quad (\text{A.17})$$

and for energy signal,

$$R_{xy}(k) = \sum_{i=-N}^N x(i)y(i+k) \quad (\text{A.18})$$

The cross-correlation function is not in general an even function in τ . The maximum possible value for the cross-correlation can occur at any τ . The cross-correlation function contains information about the relative phase between the signals.

Since cross-correlation provides a measure of the similarity of two signals for different relative time delays, it will only produce a non-zero result if the two signals are

related in some way. They could for instance be generated by the same source but have propagated different distances or be sine or cosine waves of the same frequency. Sine or cosine waves of different frequency are orthogonal or un-correlated and would give zero correlation. Other examples of signals, which would give zero correlation, are a sine wave and a random noise, and two random noise signals of different origin.

A.5 DETECTION OF SIGNAL IN NOISE

An important application of correlation techniques is detection of signals in noise. The basic idea is that the correlation function of a periodic signal is also periodic while the correlation for a random signal decays at large time delays. By evaluating the correlation for large time delays the result of the periodic signal can be separated from random noise.

A major use also of cross-correlation is the detection of signals buried in noise. Typical applications include radar, sonar, ultrasound imaging, and other reflective ranging techniques. The wave shape of the signal is generally known and the problem is to detect the presence and location of the return echo even though it is not visible inside the noise envelope.

A.6 POWER SPECTRAL DENSITY

The Power Spectral Density (PSD) is used to describe the distribution of power over frequency for random signals it is defined as the Fourier transform $S(f)$ of the autocorrelation function.

$$S(f) = \int_{-\infty}^{+\infty} R(\tau) \cdot e^{-2i\pi f\tau} d\tau \quad (\text{A.19})$$

In general, the Fourier transform is a complex-valued function of frequency. In this case, however, $R(\tau)$ is an even function of τ and then the Fourier transform will be real. Furthermore, it may be shown that the Power Spectral Density, PSD, is positive (or zero) for all frequencies. It is also an even function of frequency.

The PSD gives us information about the distribution of the signal power as a function of frequency. The unit of the PSD from equation (A.19) is unit of measured quantity/Hz. Let's consider the relation between $R(\tau)$ and $S(f)$ for the simple case of a Single-Degree-of-Freedom (SDOF) mechanical system excited with a random force. The response of the SDOF is measured as displacement. If this system has a certain resonance frequency covered by the random excitation, the response of the system is concentrated around this frequency and the PSD will have a peak there. The autocorrelation value for time delay zero equals the r.m.s. value squared. The “typical frequency” of the displacement signal can also be seen clearly in the autocorrelation function. The PSD then peaks around the resonance frequency, showing a concentration of signal power around that frequency.

The inverse of Fourier transform can be used to calculate the autocorrelation function from the PSD:

$$R(\tau) = \int_{-\infty}^{+\infty} S(f) \cdot e^{+2i\pi f\tau} df \quad (\text{A.20})$$

Setting $\tau=0$ in equation (A.20), it gives

$$R(0) = \int_{-\infty}^{+\infty} S(f) df = (r.m.s.)^2 \quad (\text{A.21})$$

That is: the integral of the PSD equals the r.m.s. value squared. This is an alternative definition of the Power Spectral Density.

The integral in (A.33) is taken over both positive and negative frequencies. It is quite common to show the PSD for positive frequencies only (remember that it looks the same for negative frequencies). We talk about double-sided or single-sided PSD. Call the single-sided PSD $G(f)$, the correspondence is obtained to:

$$\begin{aligned} (r.m.s.)^2 &= \int_{-\infty}^{+\infty} G(f) df \\ G(f) &= 2S(f) \end{aligned} \quad (\text{A.22})$$

It is good practice to be very clear about single-sided or double-sided PSD when presenting a result. Considering limits in the integral (A.22) as a frequency interval f_1 to f_2 :

$$(r.m.s.)^2 = \int_{f_1}^{f_2} G(f) df \quad (A.23)$$

where now the r.m.s. is referred to the signal in the frequency band from f_1 to f_2 . This is the physical meaning of the PSD, it tell how the r.m.s. value squared is distributed in frequency. As the r.m.s. value squared is the mean square, a better name for PSD would be Mean Square Spectral Density, as the mean square seldom has the direct physical interpretation of power.

A.7 CROSS POWER SPECTRAL DENSITY, CROSS SPECTRUM

The Cross Power Spectral Density (or Cross Spectrum for short) is the Fourier transform S_{yx} of the cross correlation function between two signals $x(t)$ and $y(t)$

$$S_{yx}(f) = \int_{-\infty}^{+\infty} R_{yx}(\tau) \cdot e^{-2i\pi f\tau} d\tau \quad (A.24)$$

The cross spectrum tells where, in frequency, the two signals “have something in common”. The cross spectrum is a complex function of frequency in contrast to the PSD, is real. It means that the cross spectrum also contains information about the phase between the two signals. The PSD is an even function of frequency, while the following is valid for the cross spectrum

$$S_{yx}(-f) = S_{yx}^*(f) = S_{xy}(f) \quad (A.25)$$

where the * means complex conjugation. It is also important to notice that if we change the between x and y in the correlation function, the corresponding cross spectrum will be complex conjugated. Just as for the PSD, it is common to use only positive frequencies:

$$\begin{aligned} G_{yx}(f) &= 2S_{yx}(f) \quad f > 0 \\ G_{yx}(0) &= S_{yx}(0) \end{aligned} \quad (A.26)$$

To distinguish between Power Spectral Density and Cross Spectral Density functions it is common to use the notation G_x (or G_{xx}) and G_y (or G_{yy}) for the PSD of $x(t)$ and $y(t)$ respectively.

REFERENCES

- [1] J.Y. Chung, D.A. Blaser, Transfer function method of measuring in-duct acoustic properties, *Journal of Acoustic Society of America*, Vol. 68, No.3, Sept.1980.
- [2] A.F. Seybert, D.F. Ross, Experimental determination of acoustic properties using a two-microphone random-excitation technique, *Journal of Acoustic Society of America*, Vol. 61, No.5, Sept.1977.
- [3] M. Abom, Measurement of the scattering matrix of acoustical two-ports, *Mechanical Systems and Signal Processing* (1991) 5(2), 89-104.
- [4] J. Lavrentiev, M. Abom, H. Bodén, A measurement method for determining the data source of acoustic two-port sources, *Journal of Sound and Vibration* (1995), 183(3), 517-531.
- [5] H. Rammal, M. Abom, Acoustic of turbochargers, SAE International, SAE paper 2007-01-2205 (2007).
- [6] C.W.S. To, A.G. Doige, A Transient Testing Technique for The Determination of Matrix Parameters of Acoustic Systems, 1: Theory and Principles, *Journal of Sound and Vibration*, 62, 207-222 (1979).
- [7] C.W.S. To, A.G. Doige, A Transient Testing Technique for the Determination of Matrix Parameters of Acoustic Systems, 2: Experimental Procedures and Results,” *Journal of Sound and Vibration*, 62, 223- 233 (1979).
- [8] Munjal, M.L. and Doige A.G., “Theory of a Two Source-location Method for Direct Experimental Evaluation of the Four-pole Parameters of an Aeroacoustic Element,” *Journal of Sound and Vibration*, 141(2), 323-333 (1990).
- [9] R. Kabral, H. Rämmal, J. Lavrentjev, F. Auriemma, Acoustic Studies on Small Engine Silencer Elements, SAE 2011-32-0514, 2012.
- [10] J. Lavrentiev, H. Rammal, On experimental techniques to determine acoustic performance of small exhaust silencers, SAE International, SAE paper 2009-32-0015 (2009).
- [11] H.P. Wallin, U. Carlsson, M. Abom, H. Boden, Sound and vibration, KTH MWL, ISBN 978-91-7415-553-2.
- [12] J. S. Bendat, A.G. Piersol, Random Data – Analysis and Measurement Procedures, 2nd Edition. New York: Wiley-Interscience, 1986.
- [12] H. Bodén, M. Abom, Influence of errors on the two-microphone method for measuring acoustic properties in ducts, *Journal of the Acoustical Society of America* 79, 541-549, 1986.
- [13] H. Bodén, M. Abom, Error analysis of two-microphone measurements in ducts with flow, *Journal of the Acoustical Society of America* 83, 2429-2438, 1988.
- [14] A.G. Doige, M.L. MUNJAL, H.S. ALVES, An improved experimental method for determining transfer matrices or pipeline elements with flow, *Proceedings of Noise-Con* 88, 481-485, 1988.
- [15] H. Boden, K. Ahlin, U. Carlsson, Applied signal analysis 2010, KTH.

Chapter 5

Results

5.1 1D AND 3D BEM ANALYSIS OF A REACTIVE THREE PASS PERFORATED TUBE MUFFLER

The content of this paragraph widely refers to the paper:

D.Siano, F.Auriemma, F.Bozza, A correlation study of computational techniques of a three pass perforated tube muffler including FEM and 1D methods, SEEP 2009.

In this work, the noise attenuation characteristics of a typical perforated muffler for automotive applications are investigated. Acoustic performances are quantified by the Transmission Loss (TL) parameter, which only depends on the geometrical characteristics of the device.

Different numerical analyses are employed. At first, a non-linear one-dimensional (1D) time domain approach is used to predict the TL profile in a low frequency range. 1D simulations, in fact, may be only applied under the hypothesis of a planar wave propagation.

A linear 3D BEM in the frequency domain, specifically designed for acoustic applications, is utilized too. Obviously, such analysis allows to obtain more accurate results at high frequency, depending on the mesh size.

Different flow velocities and gas temperatures are investigated in both 1D and 3D models. The predicted TL profiles are compared and discussed in order to assess the potentiality and limitations of the employed numerical approaches.

5.1.1 MUFFLER CONFIGURATION

The geometrical data of the studied muffler are reported in Figure 5.1.1. The porosity of perforates is 0.45, the hole diameter is 3.0 mm, and the wall thickness is 1 mm.

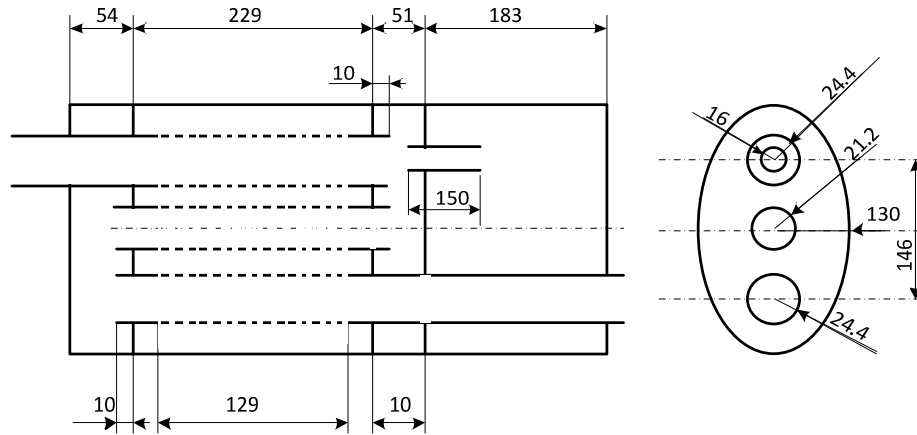


Figure 5.1.1 – Geometrical data of the investigated three-pass perforated tube muffler.

5.1.2 1D SIMULATIONS

The 1D analysis of the muffler has been performed with the commercial software GT-PowerTM. It is a widely employed tool for the analyses of internal combustion engines and it solves the 1D non-linear flow equations in each component constituting the whole engine (air box, intake, exhaust system, muffler, etc.). This software is also provided of a preprocessor tool, named GT-MufflerTM, very useful to describe the complex muffler geometry [1]. In this environment the outer shape of the model can be imported from a CAD file or built in a dedicated drawing area. Moreover, a set of tubes, ducts, baffles, shells, straight pipes, curved pipes and perforated pipes are available to set up the muffler model. In Figure 5.1.2, a 3D rendered model, obtained using the GT-MufflerTM, is depicted [2].

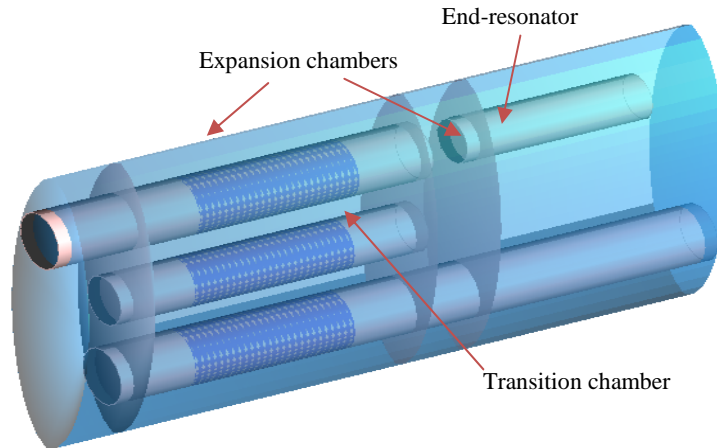


Figure 5.1.2 – Three dimensional muffler model obtained with GT-MufflerTM rendering.

The result of the pre-processing procedure is represented by an ASCII file (file.dat) including the schematization of the geometry. This latter is constituted by 1D elements for pipes modeling, but also by zero-dimensional (0D) and quasi three dimensional (quasi 3D) elements to respectively schematize the orifices and the chambers inside the muffler.

“Pipe” objects model flow through tubes, with either constant or tapered diameter, according the above mentioned 1D equations.

“Orifice” elements are used to join together different physical components. These connections are planes at which the only momentum equation is solved to compute the mass flow and velocity. An orifice can be used to specify a flow restriction by setting the orifice diameter to be smaller than the diameter of the two mating components.

“Quasi 3D” elements are specifically designed to account for conservation of momentum in three dimensions, even though the code is otherwise nominally one-dimensional. They are composed by a 0D element at the center of the volume, where the continuity and energy equations are integrated, and a number of volume openings (ports) where the momentum equation is integrated. [2]

In the specific case of a muffler, the chambers are schematized by sets of quasi-3D elements whose ports are oriented along the three spatial directions. In this way the radial interactions between the perforated tubes and the chambers are accounted.

Straight tubes are obviously schematized by 1D elements. Perforated tubes are represented by a set of quasi 3D elements connected each other along the direction of the tube and linked, through a proper number of orifices, to the quasi 3D elements constituting the chambers.

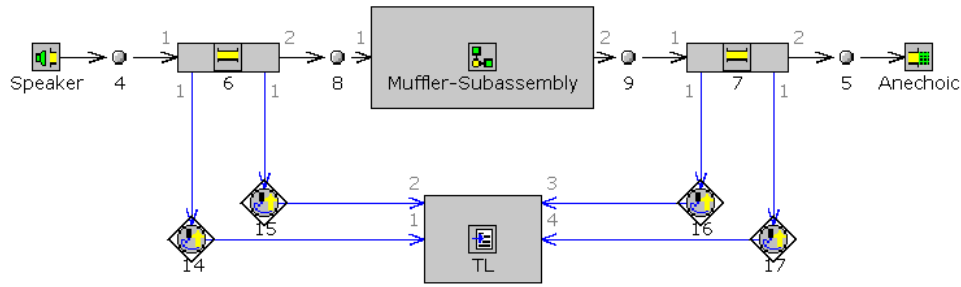


Figure 5.1.3 – Two-microphone random-excitation technique implemented for TL analysis in 1D simulations.

The two-microphone random-excitation technique proposed by Seybert and Ross [3] is used to calculate the transmission loss of the muffler. To this aim the muffler sub-assembly, a single object linked to the complex muffler schematization, is coupled to other components (see Figure 5.1.3). Two short additional pipes are connected to the component. Two pressure sensors are located in the above pipes to measure the incident and reflected pressure wave components upstream and downstream the silencer. A loudspeaker element generates a white noise signal in a certain frequency range and, finally, an anechoic termination is employed to avoid wave reflections from the outer environment. An appropriate tool computes the TL basing on the measured pressures. The final numerical results are then stored in a file and post-processed in a dedicated environment (GT-PostTM).

5.1.2 3D-BEM SIMULATIONS

An alternative methodology for the numerical evaluation of the TL parameter has been utilized in this work. It is based on a linear 3D-BEM, implemented by using the commercial software STS VNoiseTM [4]. The latter constitute a powerful tool for more accurate performance prediction, since it is able to account the wave higher order mode effects. Obviously it requires more computational and memory resources than the 1D approach. Only a surface mesh is required in BEM, which has been constructed utilizing the commercial software FEMAP 9.0TM. The mesh is shown in Figure 5.1.4, and the model consists of 16393 nodes and 14289 shell elements.

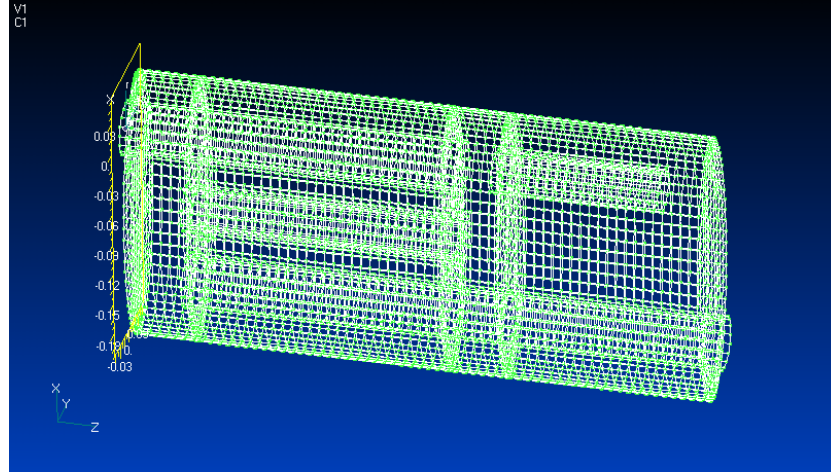


Figure 5.1.4 – Meshed muffler model.

TL has already been defined in the Chapter 1. Briefly, it is the difference between the sound power entering the system and the transmitted sound power, which is related to the ratio between the amplitude pressure (in dB) of the right travelling wave at the inlet (p_1^+) and the amplitude pressure (in dB) of the right travelling wave at the outlet (p_2^+), supposing to have plane waves at inlet and outlet sections [5].

The procedure utilized by BEM solver for the TL characterization is based on the two-port source model, i.e. on the evaluation of the four pole parameters that characterize the component (here named A,B,C,D). The BEM analysis executes two sets of calculations, the first with a zero velocity at the outlet section, the second one with a zero pressure signal in the same section. The inlet velocity is set equal to the unity in both the cases. The four parameters (complex numbers depending on the frequency) can then be computed as:

$$A = \frac{p_1}{p_2} \quad \text{and} \quad C = \frac{v_1}{p_2} \quad \text{from calculation set 1} \quad (5.1.1)$$

$$B = \frac{p_1}{v_2} \quad \text{and} \quad D = \frac{v_1}{v_2} \quad \text{from calculation set 2} \quad (5.1.2)$$

where p_1 , p_2 , v_1 and v_2 are respectively the pressure at inlet and outlet, and the velocity at same locations.

Using equations (5.1.1) and (5.1.2) and the above definitions of four poles it is possible to obtain an expression for the TL, which states:

$$TL = 20 \log \left(\frac{\left| A + \frac{B}{\rho c} + C \rho c + D \right|}{2} \right) \quad (5.1.3)$$

A critical issue for an accurate TL evaluation is represented by the correct application of the boundary conditions (BCs) with particular attention to the region where a possible change of boundary conditions can be seen. As mentioned before, in the inlet section, a constant velocity must be applied while in the other nodes of the duct a zero velocity boundary condition is imposed. For this reason, a correct usage of the software suggests to split the node P (Figure 5.1.5) in two nodes P₁ and P₂, having the same geometrical coordinates but one of them is connected to the panel of the inlet section and the other one is connected to the panel of the duct.

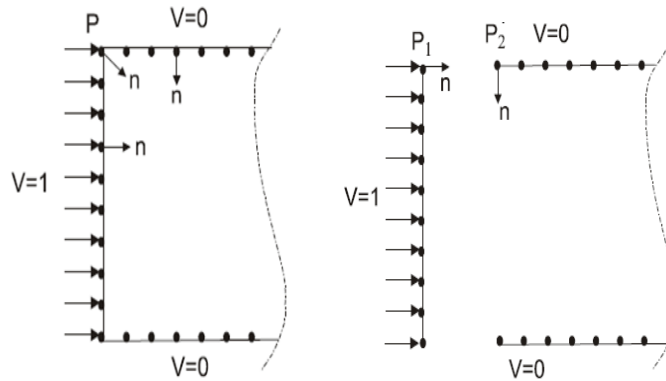


Figure 5.1.5 – Generic Boundary Condition application.

In this case, the system under investigation has been divided in different groups where different BC have been then applied as visible from Figure 5.1.6.

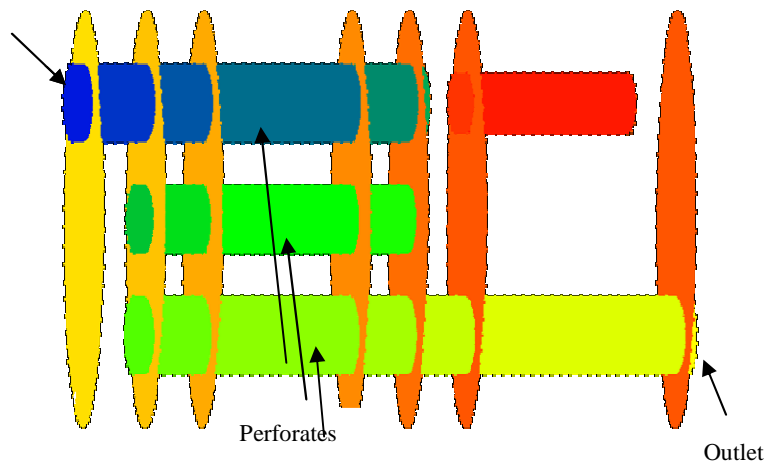


Figure 5.1.6 – Boundary conditions application.

The different colors reported in the Figure 5.1.6 represent disconnected regions where different types of boundary conditions have been applied in terms of porosity, particle velocity and pressure.

Porosity has been imposed utilizing the classical Sullivan and Crocker approach [6], which stands in absence of mean flow and absorbing material in contact with holes. For this reason, as more deeply explained in section 5.2, the BEM analyses have been performed only in absence of mean flow.

In this work the TL has been computed in the frequency range 10-1600 Hz, with a step of 10 Hz. For the chosen mesh size, a maximum frequency of 4000 Hz could be analyzed, still preserving a good accuracy of the results. Moreover, this considered cut-off frequency of 1600 Hz is much higher than the maximum working frequency of the tested system, since the harmonic components of the engine excitation lie below 1000 Hz.

5.1.3 RESULTS AND DISCUSSION

In this paragraph results obtained by using these two different numerical approaches are presented and compared.

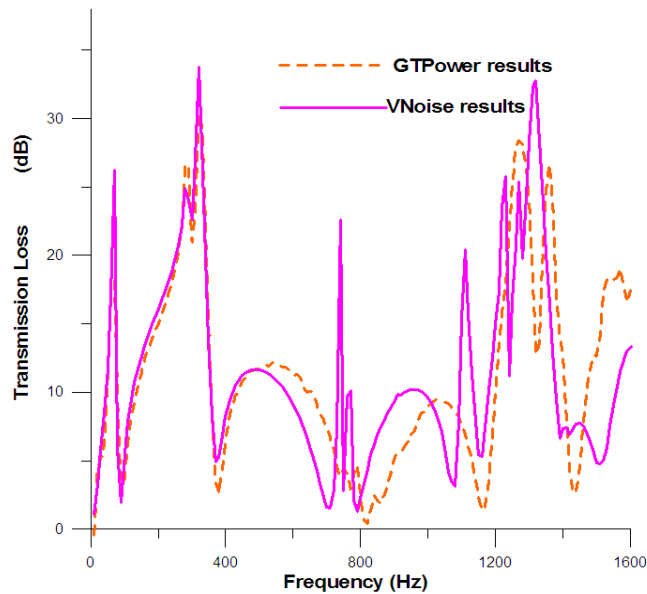


Figure 5.1.7 – Transmission loss comparison of the muffler.

The Figure 5.1.7 shows the TL (dB) versus frequency (Hz) diagrams, and it is noticeable that the two utilized methods give results which almost perfectly agree up to 500 Hz. In

particular, this is confirmed by a further analysis reported in the Figure 5.1.8 and limited to 10-500 Hz frequency range, with a restricted frequency step of 2 Hz. While the 1D analysis is completed within few minutes, this kind of 3D detailed numerical simulation requires a computational time of about 1 day (depending on computer performances). The transmission loss profile reveals two peaks in the low frequency range. In particular, it is possible to associate the peak at 70 Hz to the resonant frequency of the Helmholtz end-resonator included in the muffler [7]. Its geometrical data and the related resonant frequency at ambient temperature, are reported in the Table 5.2.I. The presence of a peak around 70 Hz is highlighted.

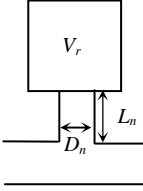
Helmholtz Resonator data:		
D_n	38mm	$f_0 = \frac{c}{2\pi} \sqrt{\frac{k_n}{V_r}} = 66\text{Hz}$
L_n	150mm	
V_r	4.24 l	$k_n = \frac{\pi D_n^2 / 4}{L_n + \pi D_n / 4} = 6.33\text{m}$
		

Table 5.1.I – Geometrical data of the end-resonator and related resonant frequency at ambient temperature.

The presence of a smoother trend at the frequencies 500Hz and 950Hz is mainly due to the expansion in the left end and central chambers (see Figure 5.1.2). The differences between one and three dimensional methods, visible from 500 Hz, depend on the acoustic wave direction, since the sound propagation in the chambers is no more planar, and starts to be radial. In fact, beyond the first higher mode frequency, (about 500 Hz for the investigated geometry), the acoustic wave presents a multi-dimensional shape, and a greater disagreement appears between the two utilized dimensional approaches.

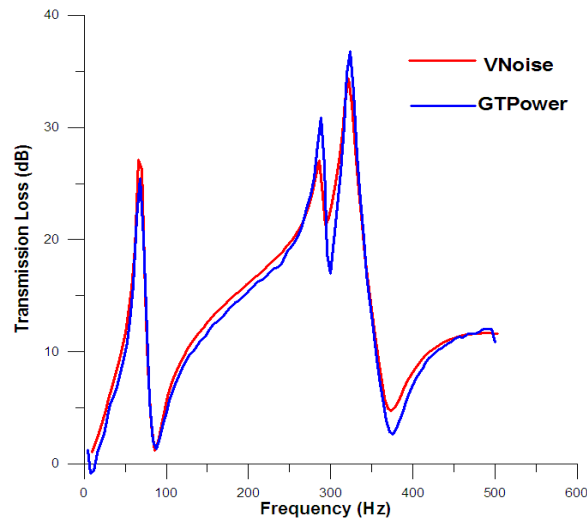


Figure 5.1.8 – Transmission Loss comparison of the muffler (frequency range 10-500 Hz).

The previous considerations are confirmed by the results presented in the Figures 5.1.9 and 5.1.10, where a number of contour plot of the pressure distribution, post-processed from VNOISE calculation, are displayed at different frequencies. The acoustic waves presents a mainly axial propagation at low frequencies. The sound pressure distribution within the muffler is quite totally constant in each muffler cross section. The above behavior can be well reproduced by the one dimensional model, which hence is able to give accurate results up to the above frequency.

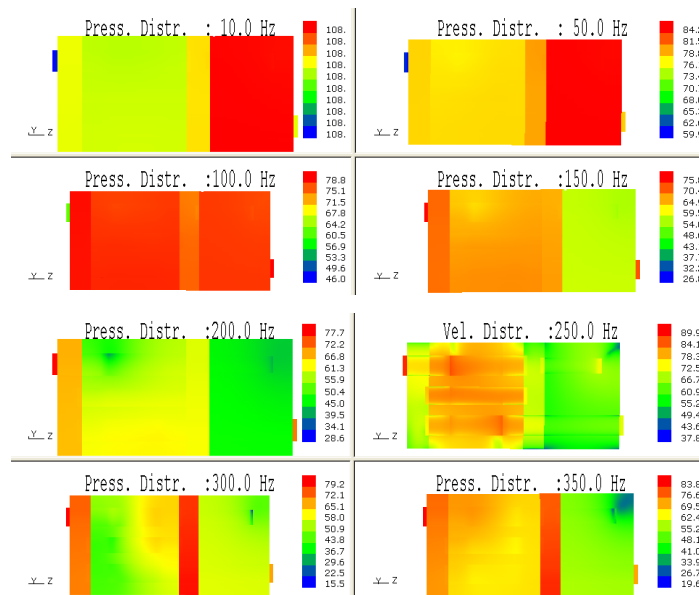


Figure 5.1.9 – Plane pressure distribution at low frequencies.

At higher frequencies, instead, the situation appears to be quite different (see Figure 5.1.10). The pressure level distribution is no more planar and the 1D model is no more able to correctly reproduce the wave propagation phenomena. This is the main reason of the 1D model inaccuracy at high frequencies.

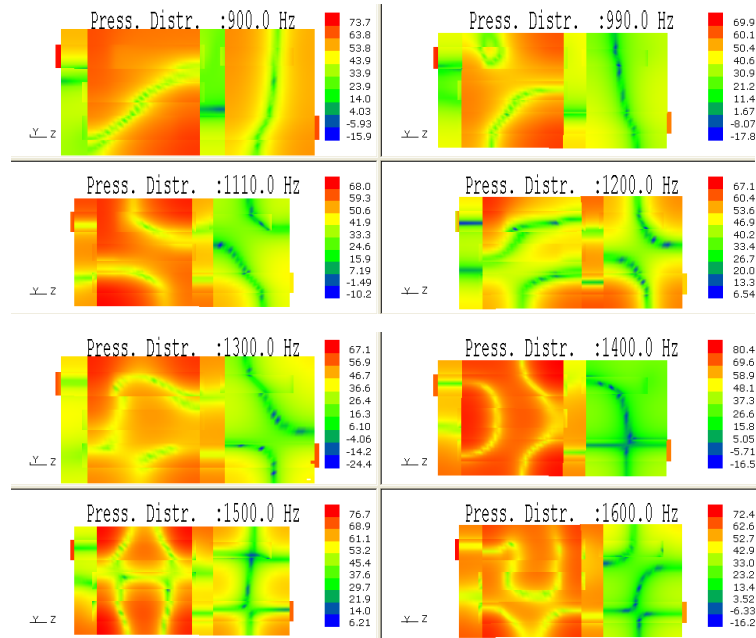


Figure 5.1.10 – Plane pressure distribution at high frequencies.

5.1.4 EFFECTS OF THE GAS TEMPERATURE AND FLOW VELOCITY

In this paragraph the effects exerted by the gas flow velocity and temperature on the transmission loss are investigated. The main results obtained at the temperature of 700°K employing one dimensional and BEM analysis, are depicted in the Figure 5.1.11.

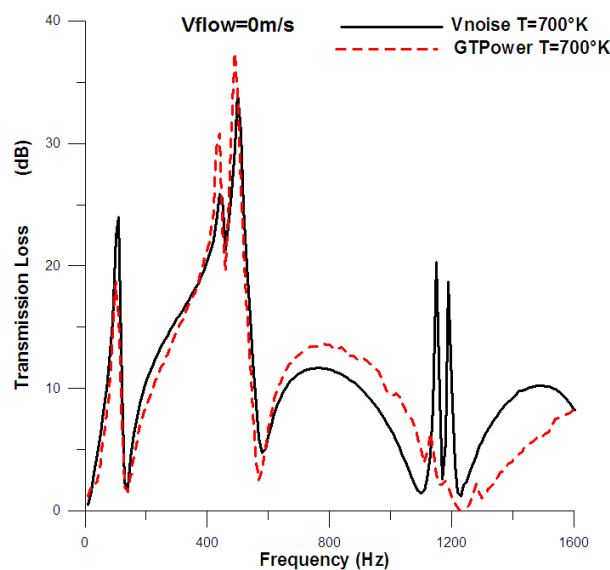


Figure 5.1.11 – Transmission Loss at 700 K.

First of all, it must be pointed out that, in order to implement the TL evaluation at higher temperature in the VNOISE software, the values of sound velocity, c , and air density, ρ , have been changed. The temperature is in fact not directly fixed in VNOISE, who, besides, is able to manage c and ρ . For this reason, in order to consider the effects of the temperature, the following relations have been used:

$$c = \sqrt{kRT} \quad (5.1.4)$$

$$\rho = \frac{P}{RT} \quad (5.1.5)$$

where

$$k = c_p/c_v \quad (5.1.6)$$

where c_p and c_v are the specific heats at constant pressure and volume (for the air at 20°C, $k=1.4$), R is the gas constant (for the air at 20°C, $R= 287 \text{ J/Kg K}$) and T is the absolute gas temperature.

The increasing of the temperature affects the sound speed and shifts the above peak at about 100 Hz, as expected. The same occurs for the other resonant frequencies and explains the extended 1D-3D agreement up to about 700 Hz in Figure 5.1.11.

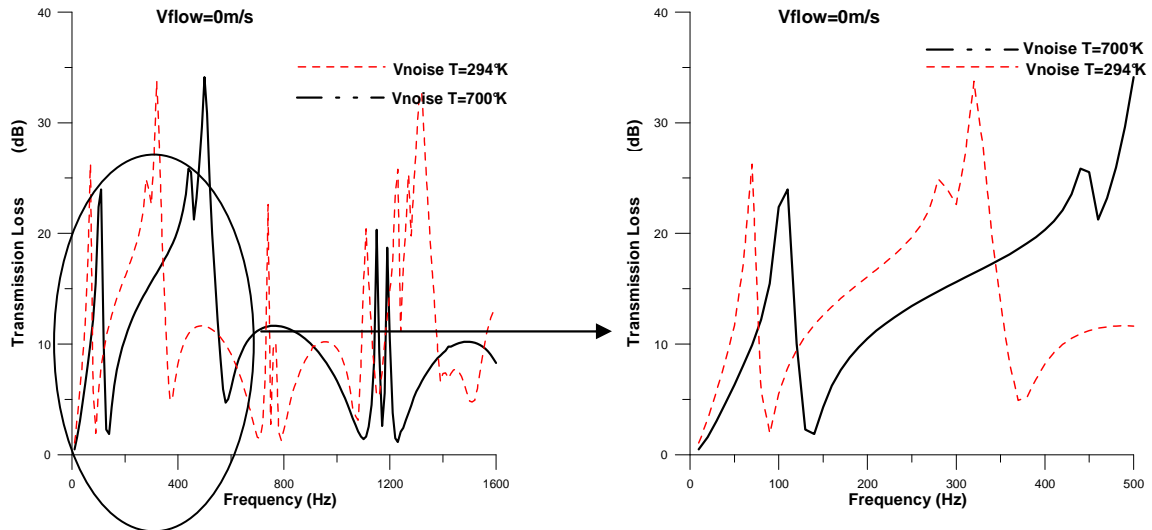


Figure 5.1.12 – TL factor comparison between high and low temperature (BEM calculation).

Looking at the Figure 5.1.12, it can be noticed that an increasing of temperature determines a shift of the TL profile towards higher frequencies. In fact the first TL peak, at about 70 Hz, is now found at about 100 Hz.

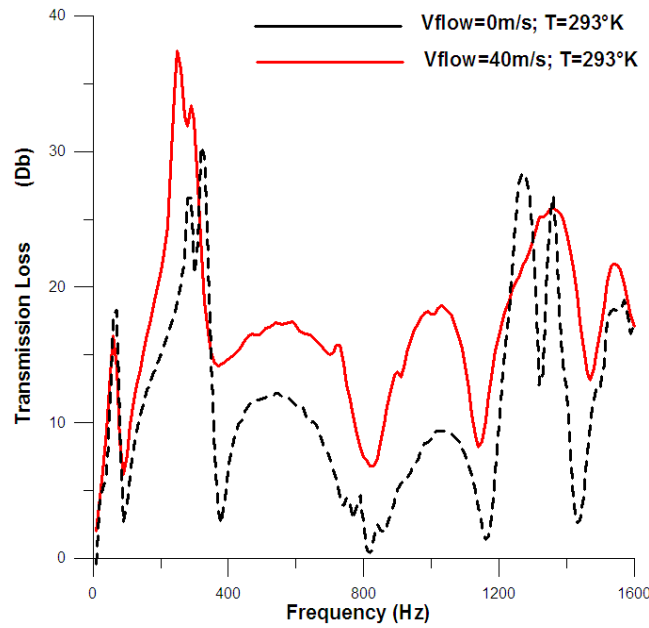


Figure 5.1.13 – GT-Power analysis of transmission loss at different temperatures and flow velocities.

The 1D approach is finally utilized to also perform a TL calculation under the presence of a positive mean flow velocity at the inlet. The presence of a positive mean flow velocity surely affects the wave propagation speed inside the component determining a different fluid-dynamical interaction with the internal structure of the muffler.

The 1D approach, directly solving the wave propagation equation, is able to account for the above mentioned effect. Secondary effects, related, as an example, to the presence of internal sound-generating vortices, may be only considered with more complex Computational Fluid Dynamic (3D-CFD) analyses [8].

The presence of a relevant flow velocity of 40 m/s (Figure 5.1.13, dashed profile), determines the increasing of the transmission loss in all the investigated frequency range. In particular, the first TL peak is improved of about 7dB and occurs at a slight lower frequency. The combined effects of increased temperature and mean flow velocities can be appreciated in the same Figure 5.1.14 (dash-dot profile). The overall behavior in this last case of course comes from the superimposition of the previously discussed variations (high frequency shift and higher attenuation levels).

5.1.5 CONCLUSIONS

In this study two different numerical approaches, one-dimensional and three-dimensional, are employed in order to predict the acoustic behavior of a three-pass perforated tube muffler with an end resonator. In particular, the transmission loss in the frequency domain is estimated with both methods, under the hypothesis of a perfectly rigid wall structure.

Besides, the effects of the temperature and gas flow velocity on the transmission loss are investigated.

The 1D and 3D methods appear to well agree up to about 400 Hz at ambient temperature and confirm the results reported in [9]. Beyond this frequency the acoustic wave indeed presents a multidimensional shape, and a greater disagreement appears between the two approaches. Obviously, in this case the 3D model is expected to better reproduce the experimental TL trend.

The above agreement is extended to higher frequencies (about 700 Hz) for a typical exhaust gas temperature of 700 K. The temperature increase influences the sound speed and shifts the TL profile versus higher frequencies. The presence of a mean flow within in the 1D muffler model was found to produce an improved overall attenuation, too.

The presented results indicate the possibility to carry out very fast 1D analysis in a low frequency range, also depending on the operating conditions of the muffler, when coupled to the real engine. If the device is to be optimized for the high frequency range, the time-consuming 3D approach is to be applied.

Next studies will concern the inclusion of the absorptive material in numerical models, and the implementation of the modal participation, in order to take into account the fluid–structure interactions. This of course is not allowed in the 1D approach.

5.2 1D AND 3D BEM ANALYSIS OF A COMMERCIAL CROSS FLOW MUFFLER, INCLUDING FLUID-STRUCTURE INTERACTIONS AND RADIATED NOISE

The content of this paragraph widely refers to the papers:

D.Siano, F.Auriemma, F.Bozza, “Pros and Cons of Using Different Numerical Techniques for Transmission Loss Evaluation of a Small Engine Muffler”, SAE Paper 2010-32-0028, Linz, 2010.

D. Siano, F. Auriemma, F. Bozza, “Svantaggi e Vantaggi Legati all’Utilizzo di Diversi Metodi Numerici per la Caratterizzazione Acustica di un Silenziatore per Applicazioni Automobilistiche”, ATI Cagliari, 2010.

The purpose of these works is to put evidence on advantages and disadvantages of different numerical approaches in evaluating the acoustic performance in terms of attenuation versus frequency (Transmission Loss) of a commercial cross flow muffler, under different conditions. The studied silencer under is composed by three chambers and two perforated tubes.

A 1D non linear acoustic approach in time domain and a 3D BEM acoustic linear approach in frequency domain have been utilized also in this work. Many information about this two different way to model the acoustic phenomenon have already been given, but here further practical applications and differences are highlighted.

The 1D approach obviously assumes rigid wall hypothesis, while the BEM can take into account the surface vibrations is when a preliminary FEM modal analysis of the structure is realized. The computed structure natural frequencies can be imported in the BEM model in order to carry out the complex fluid-structure interaction. The effects of this last condition on TL calculation have been assessed and discussed. In addition, both flow and temperature effects have been included in the modeling and discussed with the previous analyses. Agreement among these numerical evaluations and related limitations have been put into evidence for different configurations.

5.2.1 MUFFLER DESCRIPTION AND CAD MODEL

The system under investigation is a two perforated tube muffler (see Figure 5.2.1) with two expansion chambers and a transition chamber. It equips small engine cars with 0.9-1 liter displacement.



Figure 5.2.1 – The studied commercial muffler.

Each expansion chamber includes a blister containing 50 g of glass wool. The two blisters burn when the muffler reaches a sufficiently high temperature, leaving the wool depositing on the lower walls. In the present work, however, the presence of the insulating material has been neglected.

The muffler is entirely made of aluminized carbon steel P04. The two tubes lie in different horizontal planes and, for this reason, the structure is not symmetrical. Each geometrical length of the muffler has been accurately measured (Figure 5.2.2a) and a CAD model has been obtained, (see Figure 5.2.2b).

In particular, muffler length is about 310 mm plus the length of external portions of the two tubes (100 mm). Axial cross section is not perfectly elliptical with the maximum and minimum length of 216 mm and 133 mm respectively. The two expansion chambers have a length of 110 mm, while the transition chamber of 90 mm. The two tubes have inner diameter of 35mm. External walls thickness is 1.2 mm and tubes and inner diaphragms thickness is 1.5 mm. Diaphragms are only welded to the tubes, with 2 or 3 spot welds, and are free to vibrate with respect to the external walls. Each tube is provided of an ending restriction, highlighted in Figure 2b. Each tube has two perforated portions provided with a variable number of 3 mm diameter holes (from 52 to 77 holes per portion).

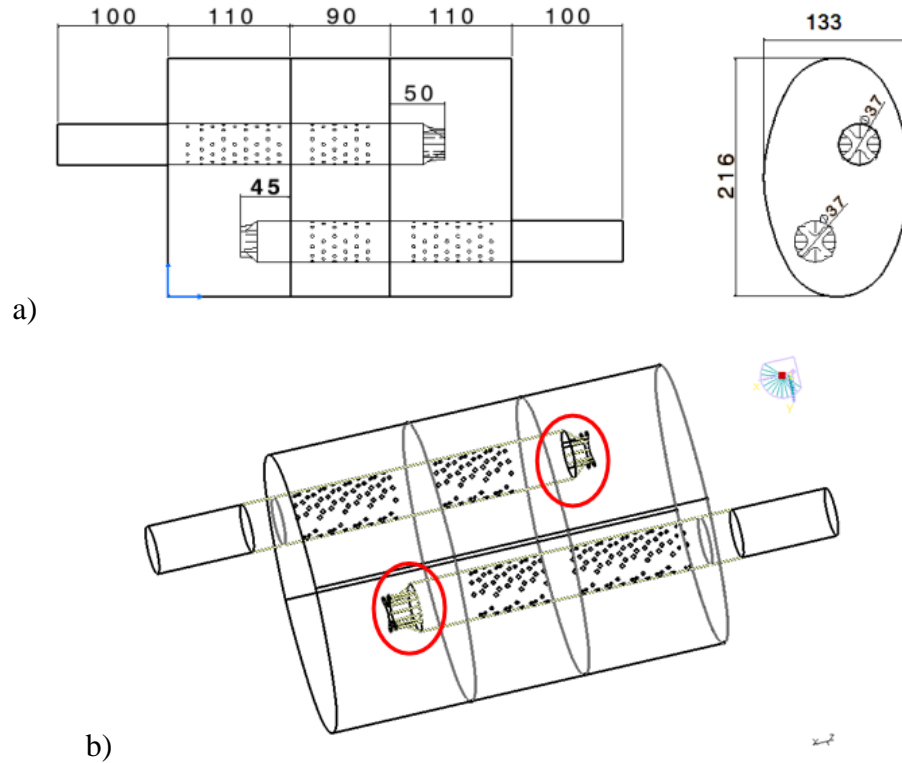


Figure 5.2.2 – a) Nominal dimensions of the system; b) CAD model of the muffler.

5.2.2 1D AND 3D MODELS

The 1D and 3D BEM analyses of the previously described muffler have been performed with the commercial software packages GT-PowerTM and VNOISETM [2], [4]. These latter, and the integrated equations, have been already widely described in the paragraph 5.1 [10]. Here, in Figure 5.2.3, a 3D rendered model, obtained using the GTMufflerTM tool, is depicted.

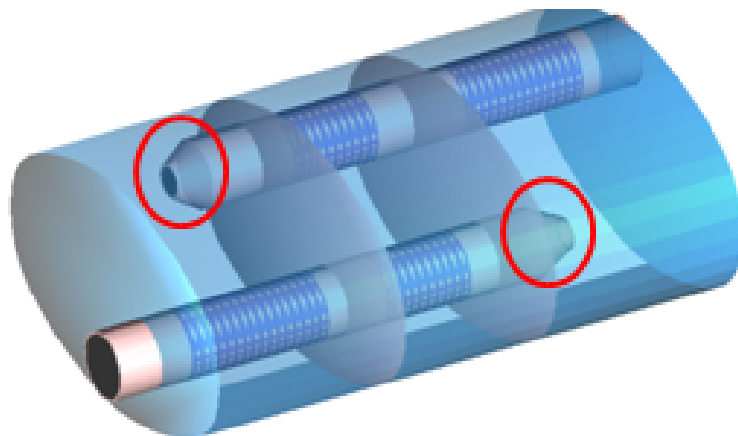


Figure 5.2.3 – 3D rendered model of the muffler derived from GTMufflerTM tool.

As previously mentioned, the major advantage related to the use of BEM is that only boundary surfaces must be discretized. Since the geometry under investigation is relatively complicated and includes several thin obstacles within the cavity volume (i.e. baffles), a multi domain approach has been found to be suitable. In this case, the mesh surface, shown in Figure 5.2.4, consists of 17091 nodes and 32800 shell elements. It has been obtained by meshing the CAD surfaces with the commercial software FEMAP 9.0TM. Thus, the muffler cavity has been divided into a number of sub-domains, subdivided imaginary surfaces. Hence, the conventional BEM is applied to each sub-domain.

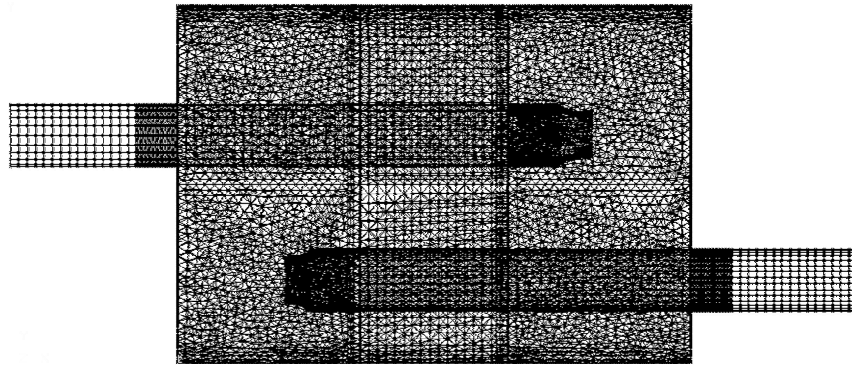


Figure 5.2.5 – Surface mesh model.

The BEM equations for different sub-domains are coupled to each other by enforcing the continuity conditions of pressure and normal velocity at the interface between two neighbouring sub-domains (physical continuity BCs). In this case the word ‘interface’ indicates an imaginary surface where the acoustic pressure and normal velocity are imposed to be continuous, or where conditions of porosity are imposed. Furthermore, velocity BCs are applied on the other internal and external surfaces [11]. Figure 5.2.6a shows the groups with velocity BCs, while in Figure 5.2.6b the groups with interface BCs are depicted.

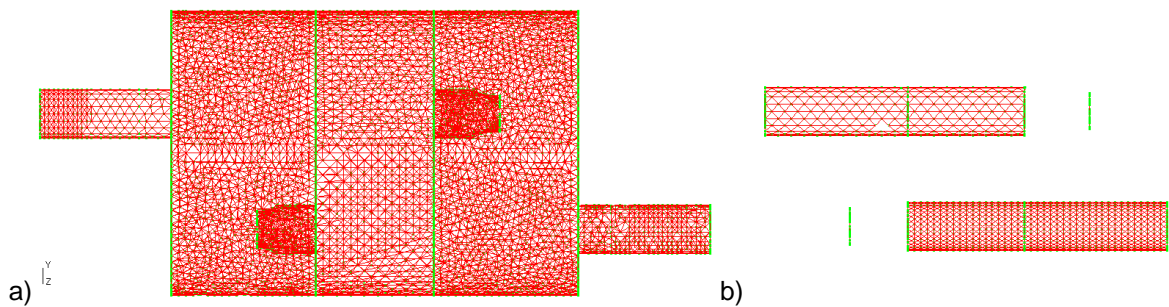


Figure 5.2.6 – a) Groups with Velocity BCs; b) – Groups with Interfaces BCs.

The 3D acoustic analysis requires the specification of the acoustic impedance of perforations. To this aim, the following semi-empirical expression developed by Sullivan and Crocker [6] has been employed:

$$\zeta_p = \frac{[0.006 + jk(t + 0.75d_h)]}{\varphi} \quad (5.2.1)$$

where t is the perforated tube wall thickness, d_h is the holes diameter, and φ the porosity of the perforation. Through the (6), the holes are not geometrically modeled, and each perforated surface can be described as a simple surface. On the other side, the main disadvantage is that it's based on a semi-empirical relation which, in some situations, could not ensure an accurate simulation of the physical phenomenon.

As known, eq. (6) is only valid at zero mean flow and with no contact of adsorbent material with the holes. However, since 3D analyses have been performed in absence of mean flow, the application of eq. (5.2.1) can be accepted.

5.2.3 TL RESULTS AND DISCUSSION

HYPOTHESIS OF RIGID WALLS, 294K TEMPERATURE, ZERO MEAN FLOW

The first analysis has been led under the hypothesis of infinitely rigid structure of the silencer, containing air at rest at 294K.

The real geometry of the muffler presents a complex restriction, accurately described in the mesh model and in BEM analysis. Of course this is not possible in the 1D analysis. For this reason two different simulations have been considered. In the first one (Figure 5.2.3) the restriction is substituted by a small convergent pipe, while in the second one (Figure 5.2.7) a simple orifice ending tube has been considered.

In Figure 5.2.8 a comparison of TL curves obtained with 1D and 3D models is carried out. In particular for the 1D analysis two TL profiles are shown, arising from the previously described ending tubes schematizations.

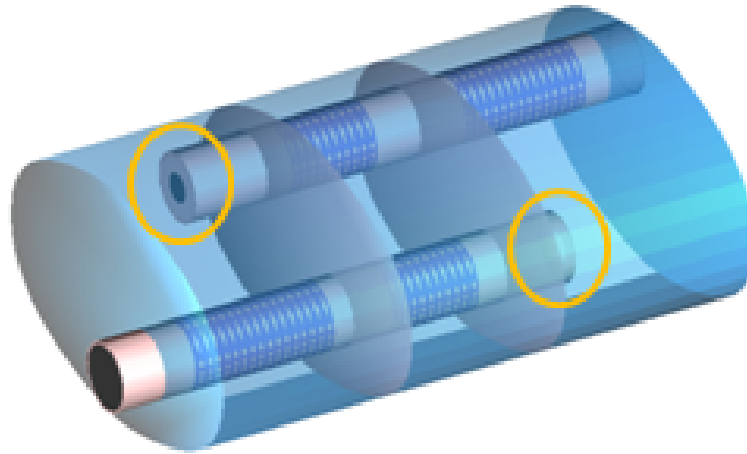


Figure 5.2.7 – Orifice tube ending geometry.

First of all, a good agreement between the three profiles is found up to 450 Hz. From 450 to 800 Hz, and above 1100 Hz, 1D results considerably differ from the BEM ones. Looking at the two 1D sets of calculations, it can be clearly noticed that the orifice ending tube better reproduces the TL peak at 1100 Hz. This behavior can be explained considering the presence of energy loss in the orifice, which is the main cause of TL increasing. This loss is indeed absent in the convergent tube, where an isentropic expansion and kinetic energy production occurs.

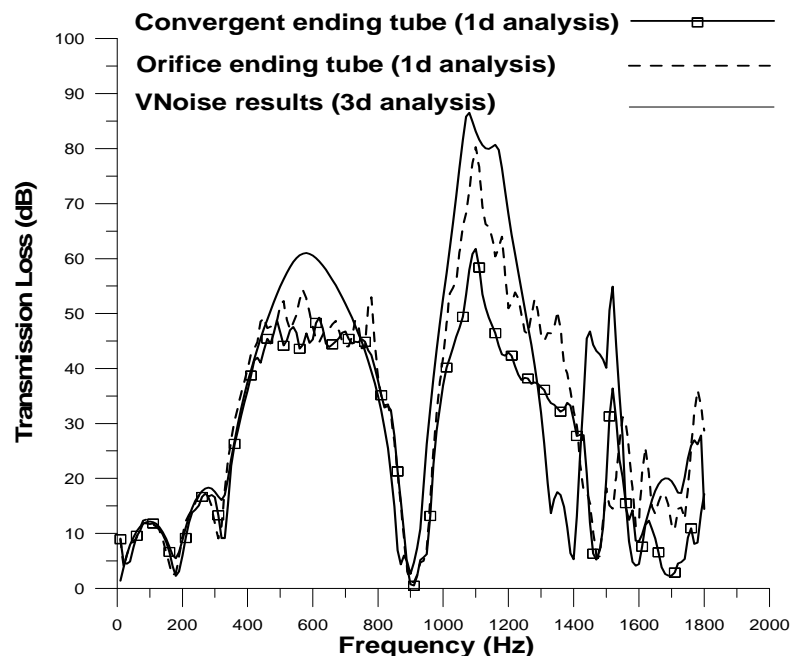


Figure 5.2.8 – 1D-3D TL comparison ($T=294K$).

In terms of computing time, while the 1D analysis is completed within few minutes, the BEM one requires a computational time of about 1 day on a common PC. Of course, computing time is strictly dependent on computer performances.

The 1D – 3D disagreement is mainly due to a non planar wave propagation occurring at high frequencies [12]. This phenomenon, in the simple case of an expansion chamber, is described in detail in the Appendix.

The presence of a non planar wave propagation is confirmed by the results presented in Figure 5.2.9, where a number of contour plots, post-processed from VNOISE calculations, are displayed at different frequencies. The figure reports the amplitude (in dB) of the pressure on the muffler surfaces imposing, at inlet section, an unit value of dp/dn .

At 400Hz, waves propagation appears to be mainly axial and pressure distribution is quite constant in each muffler cross section. The above behavior can be well reproduced by the one dimensional analysis.

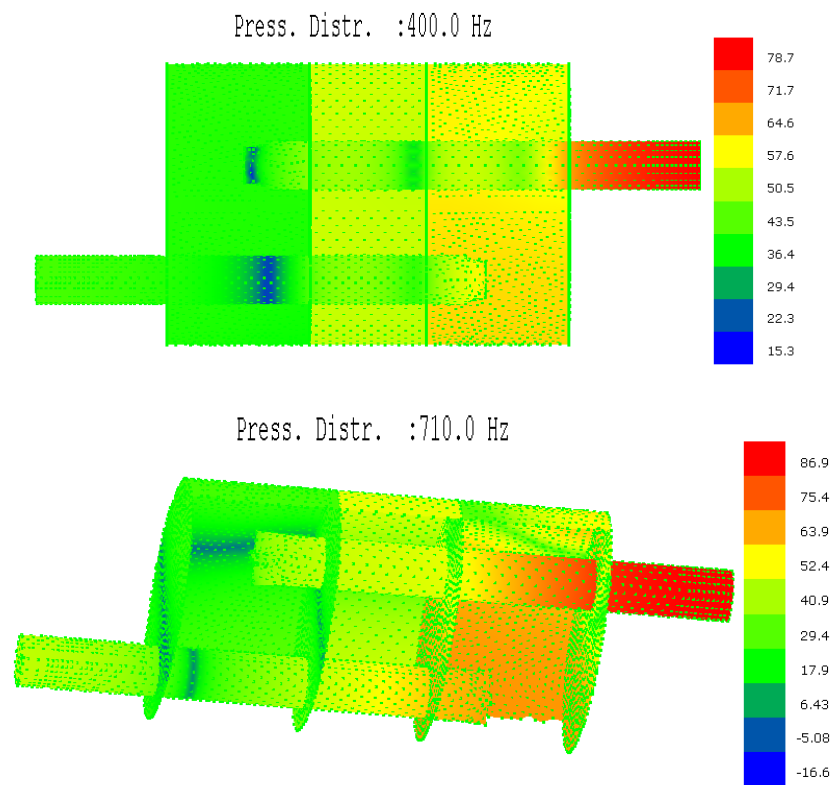


Figure 5.2.9 – Pressure amplitude in muffler chamber at 400, and 710 Hz by imposing unit value of dp/dn at inlet.

At medium frequency (710 Hz) pressure gradients appear in the radial direction, too, and the sound propagation in the two expansion chambers begins to be no more exclusively

planar. At higher frequencies acoustic waves present a complex multi-dimensional shape, and a greater disagreement appears between the two employed dimensional approaches.

HYPOTHESIS OF RIGID WALLS, 950K TEMPERATURE, ZERO MEAN FLOW

In this section, the effects exerted by the gas temperature on the transmission loss factor have been investigated. In particular, air at 950K is now considered in both 1D and BEM analyses. The related results, under the hypotheses of rigid walls and zero mean flow, are displayed in Figure 5.2.10.

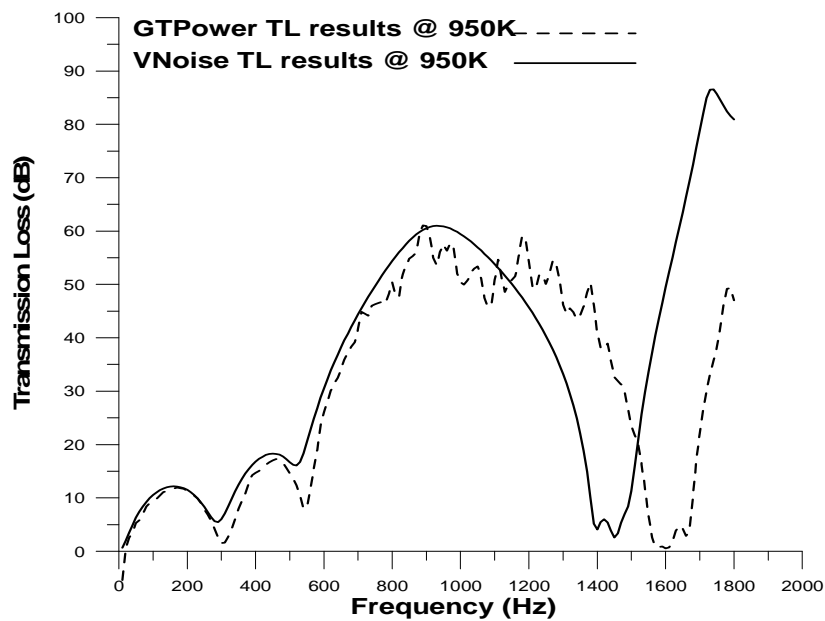


Figure 5.2. 10 – 1D and 3D TL comparison at 950K.

The figure shows a very good agreement between the two approaches up to a greater frequency (about 700 Hz), while a satisfactory matching is still observable up to 900Hz. In Figure 5.2.11 the TL factor comparison at high and low temperatures, both computed with VnoiseTM code, is indeed reported.

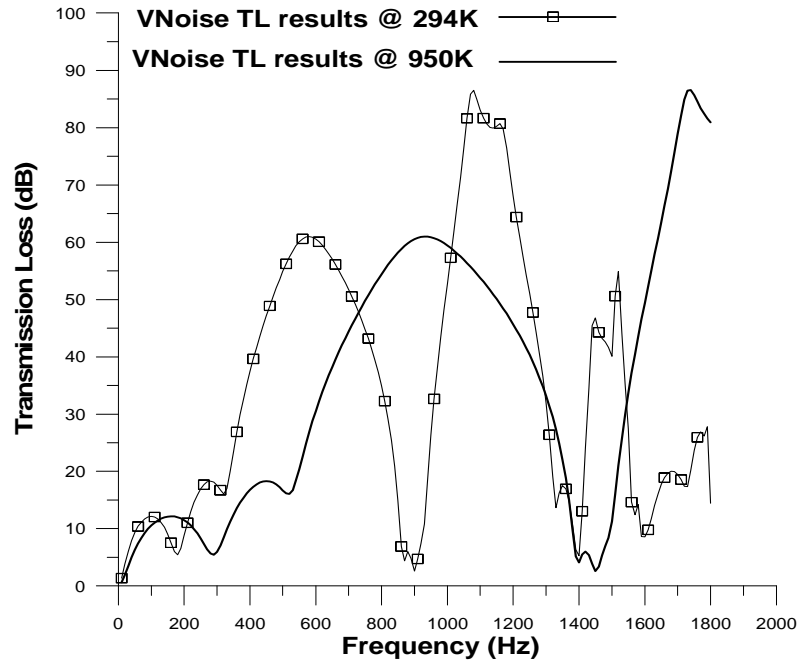


Figure 5.2.11 – BEM TL results at 294 and 950K.

It can be noted that the higher temperature determines a shift of the TL profile towards higher frequencies. In fact, the first TL peak, at about 97 Hz, is now found at about 160 Hz; the second is translated from 274 to 448 Hz and the third from 580 to 938 Hz.

As known, temperature affects the air density δ and the sound velocity, which changes from $c_l=344$ to $c_h=600$ at 294K and 950K respectively, according to the relation:

$$c = \sqrt{kRT} \quad (5.2.2)$$

where $k = c_p/c_v$ is the ratio between the specific heats at constant pressure and volume respectively, R is the gas constant, and T is the absolute gas temperature.

The ratio c_h/c_l defines a sort of abscissa stretching factor, relating the high and low temperature profiles. In this case, in fact, the ratio:

$$\frac{c_h}{c_l} = \frac{600}{344} \approx 1.7 \quad (5.2.3)$$

approximately equals the ratio between the above mentioned shifting peaks. In the following, it will be shown that this simple rule can't be totally applied in the case of flexible structure.

HYPOTHESIS OF FLEXIBILITY, 294K TEMPERATURE, ZERO MEAN FLOW

When an elastic structure, especially a thin-walled assembly, is surrounded or contains a fluid, structure vibrations are induced by the fluid. Similarly, if a fluid is contained within a vibrating thin-walled structure, such as the air within a muffler, there may be significant coupling between the structural vibration and the sound field. The whole system must be hence analyzed as a coupled structural acoustic problem [13].

In a coupled, physically heterogeneous system, mechanical components interact dynamically. The interaction is multi-way, in the sense that the response has to be obtained simultaneously solving the coupled equations which describe the system behavior [14].

For fluid-structure interaction problems, analytical solutions are available for very few simple geometries. For an arbitrarily shaped structure, a numerical solution technique must be used.

In typical situations, to perform a coupled acoustic-structural analysis, two different models should be treated: one for the acoustic analysis, and the other one for the structural FEM analysis. Obviously 1-D analysis cannot account for these issues.

In the examined case, a normal modal analysis of the mesh model shown in Figure 5.2.5, has been performed with the FEM solver MSC Nastran 2005TM. Results are post-processed with FEMAP 9.0TM. The structure has been considered unconstrained.

In the range 0-3000 Hz, 119 modes have been computed. First six modes are rigid body motions due to the absence of constraints. This very high number of modes in a quite narrow frequency range is due to the peculiarity of the geometry: as previously mentioned, the two diaphragms, delimitating the three chambers inside the muffler, are not welded to the external muffler walls. Therefore, these structural components show a high flexibility and this behavior influences the whole computational results. Anyway, modes related to these components don't give an appreciable contribution to the acoustic behavior of the muffler. Only modes involving the walls and the tubes can sensibly influence the TL. Typical "wall modes" are reported in Figure 5.2.12a and 12b at 582Hz and 2723Hz, respectively.

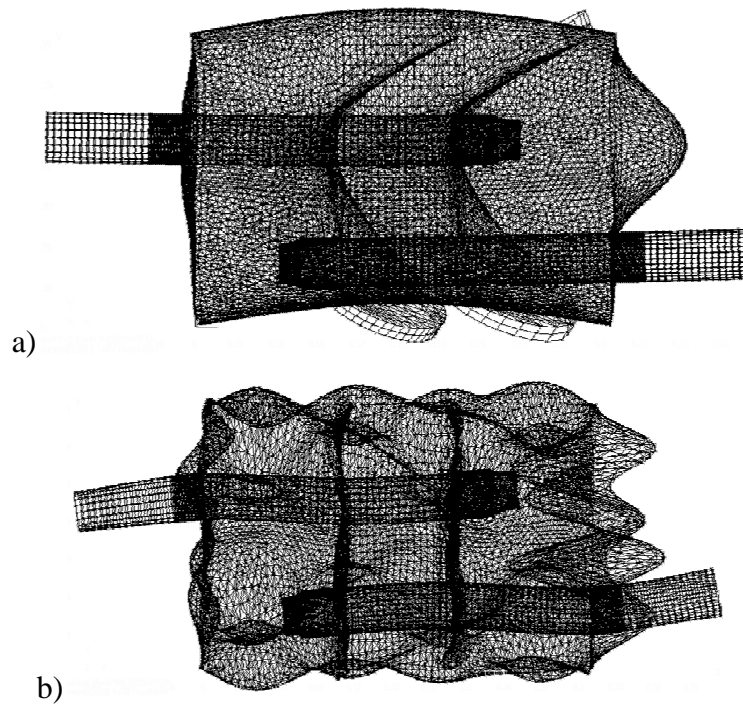


Figure 12 – a) modal shapes at 580 Hz; b) modal shapes at 2723 Hz.

mode	Eigenvalue (Hz)
7	256
...	...
15	565
<u>16</u>	<u>582</u>
17	592
18	605
<u>19</u>	<u>608</u>
<u>20</u>	<u>698</u>
<u>21</u>	<u>762</u>
...	...
<u>27</u>	<u>978</u>
<u>28</u>	<u>1050</u>
29	1059
<u>30</u>	<u>1073</u>
<u>31</u>	<u>1100</u>
32	1148
<u>33</u>	<u>1150</u>
<u>34</u>	<u>1266</u>
35	1271
...	...

Table 5.2.I – Structural modes at 249K (underlined values represent fluid-structure resonances).

Table 5.2.I reports the eigenvalues of the structural modes substantially influencing the acoustic muffler behavior at 294K.

In order to perform a coupled fluid-structure analysis, many commercial BEM codes require the simultaneous presence of both a modal FE model and an acoustic BE model. During the calculations the structural modes are projected on the acoustic mesh. VNoise™,

instead, use a different approach. In fact the structural modes are projected on the acoustic mesh during the import phase, and therefore, once the import of the structural modes is terminated, the user has to deal with a single model (the acoustic one), which will also contain the structural modes.

In Figure 5.2.13, TL results of vibrating muffler structure are compared with the one obtained neglecting the structure flexibility.

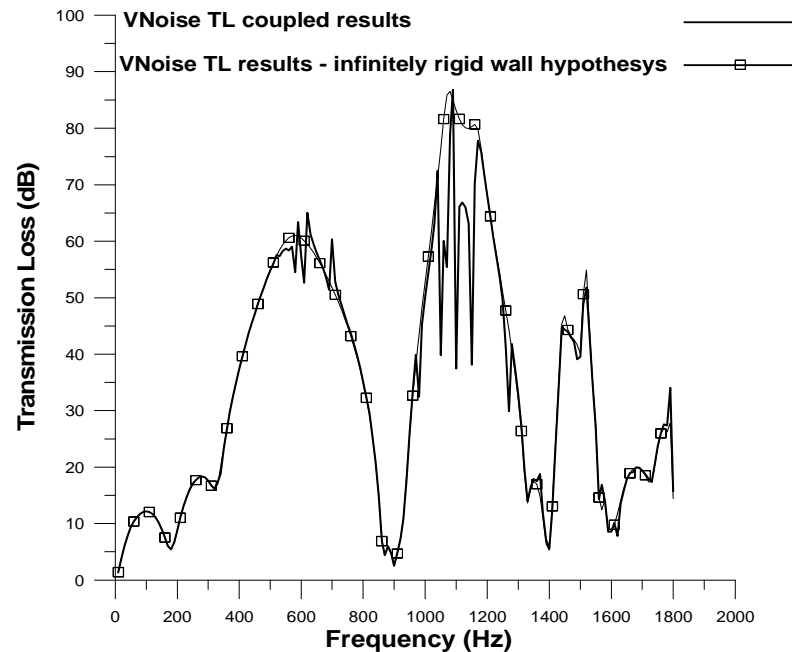


Figure 5.2.13 – TL results from flexible and rigid structure analyses ($T=294K$).

In correspondence of structural and fluid modes, Figure 5.2.13 reveals fluid-structure resonances inducing a TL variation. TL is almost everywhere unchanged, except around few frequencies, underlined in Table 1, that correspond to some of the structural modes. In particular, the structural modes around 1050, 1073 and 1100Hz generate a localized attenuation reduction. Oscillations induced by the other modes are indeed much more reduced.

In this analysis, the effects of the external fluid motion on the structural modes have been neglected, and the modes are only coupled with the internal fluid. Typically this assumption can be considered reasonable, even if, it is possible to extend the analysis to the more realistic case of fully internal-external coupling, where both the internal and the surrounding fluids are coupled with the muffler structure. Since VNoise is based on a Direct BEM solver, the above mentioned problem can be faced with a fully coupled mixed domain approach or with a fully coupled multi domain approach [4].

HYPOTHESIS OF FLEXIBILITY, 950K TEMPERATURE, ZERO MEAN FLOW

The above coupled analysis, was also performed considering high temperature conditions: in particular both the flexible muffler structure and the inner air are considered at 950K.

In order to perform this kind of analysis, a new modal FE computation is required. Temperature, in fact, also affects the modal behavior of the structure, depending on the density (δ_s) and the Young Modulus (M_s) of the constituting material. The above mentioned characteristics vary with the temperature as shown:

$$\delta_s^{294K} = 7850 \text{ Kg/m}^3$$

$$\delta_s^{950K} = 7662 \text{ Kg/m}^3$$

$$M_s^{294K} = 210 \text{ GPa}$$

$$M_s^{950K} = 180 \text{ GPa}$$

Table 5.2.II reports the structural modes at 950K obtained from the high temperature modal FE analysis.

mode	Eigenvalue (Hz)
7	217
...	...
17	506
<u>18</u>	<u>517</u>
19	520
...	...
27	837
<u>28</u>	<u>898</u>
29	906
<u>30</u>	<u>918</u>
<u>31</u>	<u>941</u>
32	982

Table 5.2.II – Structural modes at 950K temperature.

In Figure 5.2.14, coupled analysis results at 950K are plotted and compared with the previously obtained ones. Resonance frequencies of the coupled system are still underlined in Table 5.2.II.

Also in this case the deformability effect is localized around few frequencies where structural and fluid modes are in resonance. Because of the Young Modulus reduction at high temperature, resonance phenomena now occur at a reduced frequency.

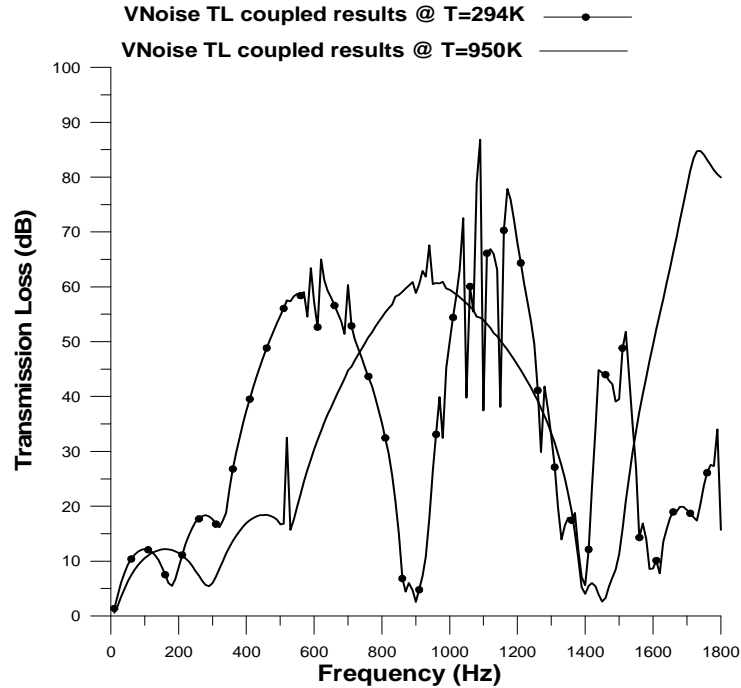


Figure 5.2.14 – Coupled analysis comparison at high and low temperature.

For this reason, the above mentioned simple stretching criterion relating high and low temperature attenuation curves (Figure 5.2.11, eq. 5.2.2), cannot be applied to this case. In fact, while at high temperature the TL profile stretches toward high frequencies, the position of the structure resonances shifts toward lower frequencies. Consequently, when the muffler structural behavior is involved in the analysis, the stretching criterion does not effectively reproduce the TL trend around the resonance frequencies.

HYPOTHESIS OF RIGID WALLS, 294 AND 950K TEMPERATURE, 20m/s MEAN FLOW

Finally, the combined effects due to the presence of a steady mean flow (20 m/s) and high temperature have been investigated.

Unfortunately BEM solver shows its own limitations in this kind of analysis, because this method is based on conditions imposed on surfaces, and many problems occur when a velocity field must be described in a volume. Even if VNoiseTM solver is able to take into

account the presence of an imposed mean flow in each single domain, obviously, it is not able to compute the local values of the velocity field. This problem becomes relevant considering that this field is spatially variable inside the complex internal muffler geometry.

A three dimensional TL analysis in presence of mean flow would hence require a FEM analysis. Moreover, secondary effects, related to the presence of internal sound-generating vortices (flow noise), may be considered with more complex Computational Fluid Dynamic (CFD) analyses. Detailed CFD results can be imported in a BEM solver, like VNoise, in order to also account for unsteady flow induced noise [8].

A simple 1D approach, directly solving the wave propagation equations, is really able to consider the effects of a steady mean flow on the TL. Due to the previously discussed high frequency limitations, the 1D analysis was limited to 900 Hz, as shown in Figure 5.2.15.

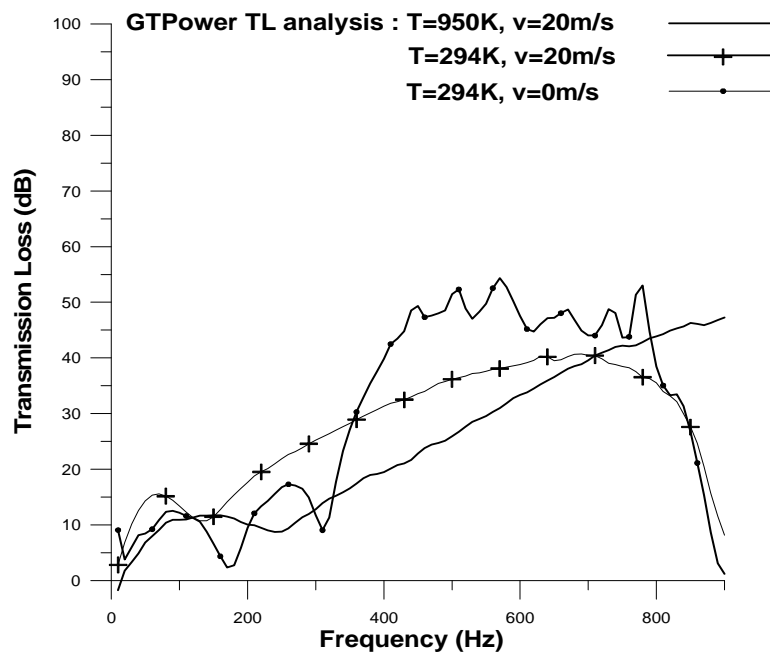


Figure 5.2.15 – GTPowerTM analysis at different temperatures and flow velocities.

The presence of a mean flow determines a generally smoother trend with an increased and reduced attenuation below and upon 350Hz. The combined effects of increased temperature and mean flow presence come from the superimposition of the previously discussed variations (high frequency shift and smoother trend).

5.2.4 RADIATED SOUND PRESSURE LEVEL

A linear Indirect BEM has also been utilized to evaluate the radiated sound pressure level (SPL) in the frequency range 0-1800Hz. It has been calculated at 1 meter distance from the outlet, once a harmonic particle velocity, with 1m/s amplitude, is imposed at inlet.

A 1 meter diameter spherical microphone array has been simulated, whose center is coincident with the muffler center. Performed simulations have been carried out in the hypotheses of absence of reflecting objects surrounding the silencer, and they are focused on the evaluation of different contribution to the overall SPL:

- Contribution due to the acoustic excitation exerted by the outlet.
- Contribution due to the reflections of the rigid external muffler surfaces (shell).
- Contribution due to the shell vibrations and caused by fluid-structure interactions.

To this aim, three different analyses have been carried out, i.e.:

- Acoustic analysis of the simple muffler outlet section (see Figure 5.2.15). In this way only the first one of the above mentioned contribution is evaluated.
- Acoustic analysis of the whole silencer, in the hypotheses of rigid surfaces. In this case, the first two contributions are carried out.
- Complete acoustic analysis of the flexible structure, based on the interaction between the muffler surfaces and the internal/external air. In this simulations, all the above mentioned contributions are taken into account.

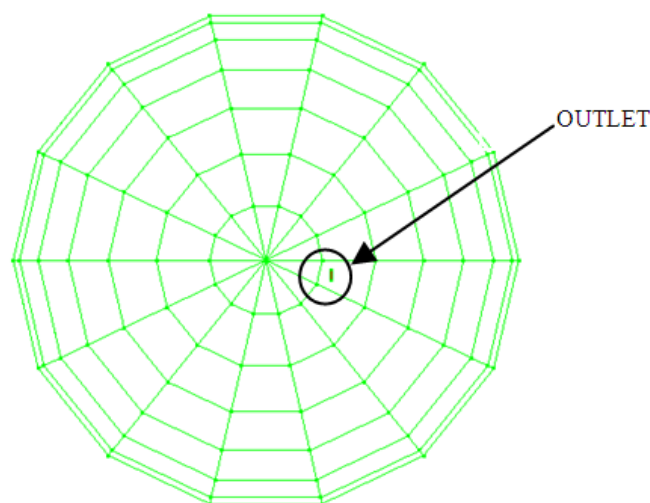


Figure 5.2.15 – BEM model constituted by the outlet and the microphone array.

The analyses 2) and 3) obviously include the presence of the muffler (even though under different hypotheses on the surfaces), which is depicted in the Figure 5.2.16, where two virtual microphone (A and F) are highlighted .

In order to perform the first two analyses, a preliminary studied has been carried out by imposing an “aperture” boundary condition at outlet. The obtained results, in terms of pressure and gradient dp/dn , have been imported on a new model: in case of the analysis 1), this model is made up by the outlet itself, which acts as a source radiating outside the muffler; in case of the analysis 2), all the infinitely rigid panels of the silencer are involved.

In the first case, the pressure distribution on the microphone array is almost uniform, since the outlet is close to the center of the spherical array, and the problem can be traced back to the wave propagation of punctual source.

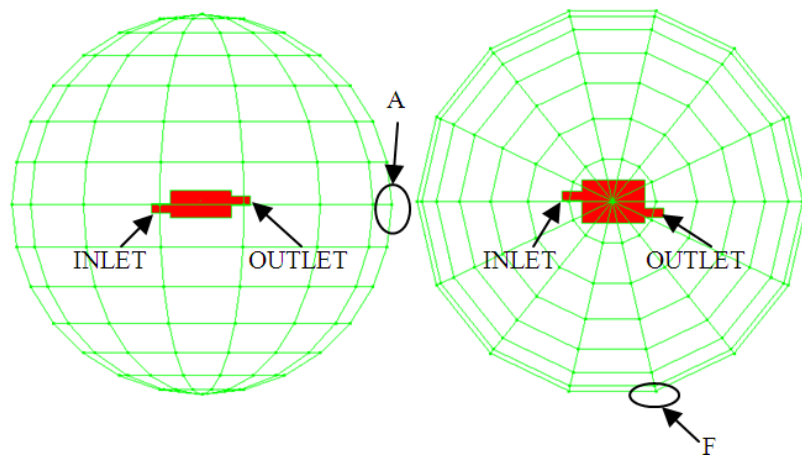


Figure 5.2.16 – BEM model constituted by the muffler and the microphone array (analyses 2 and 3). Two microphone locations are highlighted (A and F).

The results, in terms of sound pressure levels (in dB) calculated at the position A in the investigated frequency range, are plotted in Figure 5.2.17.

As expected, very small reflecting phenomena are present at low frequencies, since they occur when the wavelengths are lower than the characteristic dimensions of the object. This condition, for the considered geometry, is satisfied since 1000-1100 Hz, and in the frequency range 1150-1390 Hz the difference between the calculated SPLs in A in the two analyses is almost 10 dB. In the range 1070-1520 Hz the SPL calculated in A in absence of reflecting phenomena is higher than the one in presence of them. This is due to the disruptive interferences between direct and reflected waves, related to the different paths covered by this two kind of waves, which generate disruptive interferences.

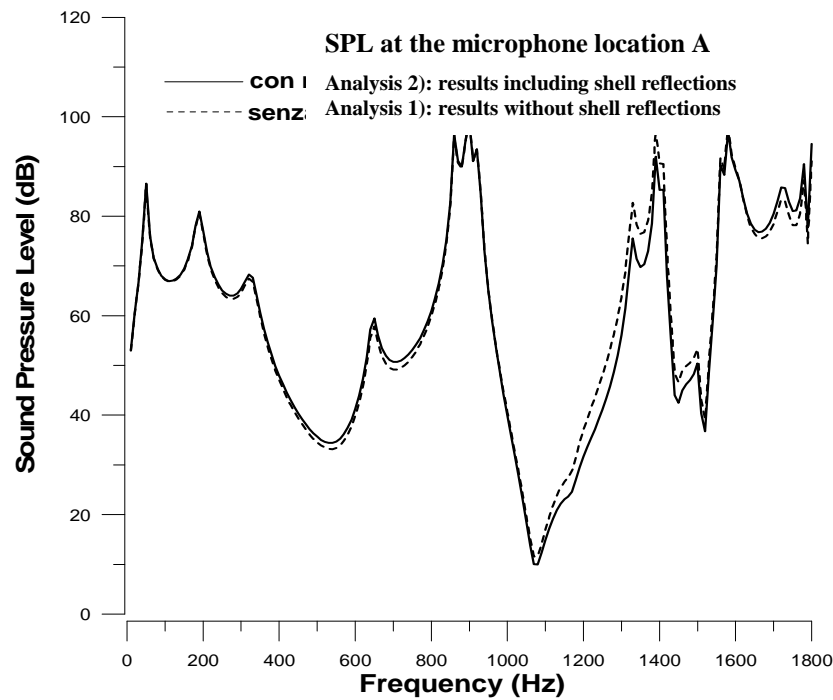


Figure 5.2.17 – Analyses 1) and 2): SPL carried out at the microphone location A.

A fully coupled multi domain approach has been utilized in order to perform the third analysis: this kind of approach is able to take into account the interaction of the structure with both internal and external fluid domain surrounding the muffler. A modal FEM analysis of the unconstrained structure is required to evaluate the eigenvalues and the eigenvectors of the unconstrained structure. An outer air domain has been defined and physically connected to the inner one through a condition of physical continuity at outlet. [4].

A benchmarking between the SPL curves calculated in the microphone position A through the analyses 2) and 3) is shown in Figure 5.2.18. As expected, the levels obtained when the fluid-structure interaction is accounted, are almost always higher than the other ones, since, in this case, the structure itself radiates noise. Around 590Hz, a consistent difference between the calculated SPL in the two analyses is noticeable, and confirmed by the presence of the mode at 582 Hz (see Table 5.2.I) and by the sharp TL trend, at the same frequency, in the Figure 5.2.13 (coupled TL analysis). Similarly at 700, 980, 1050, 1100, 1150, 1340m 1450, 1490 Hz.

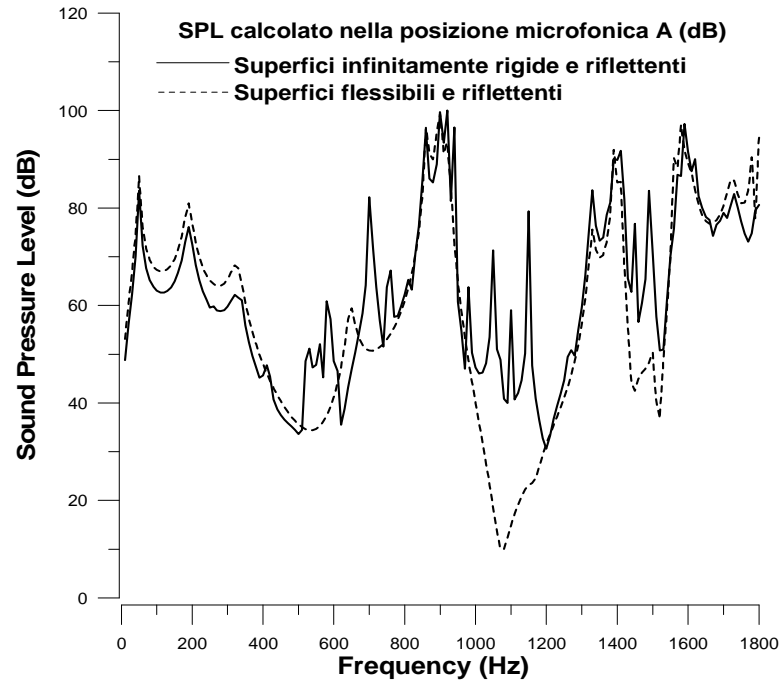


Figure 5.2.18 – SPL calculated in the position A through the analyses 2) and 3).

In the Figure 5.2.19 the SPLs, calculated in the position F and A through the analysis 3), are plotted. In F, the levels calculated in the range 600-1260 Hz are higher than the ones simulated in A. In fact, the microphones A and F are, respectively, in front of the outlet and aside the muffler. For this reason, the first one is more exposed to the noise radiated by the outlet, and the second one to the noise coming from the muffler vibrating surfaces. Obviously in corresponding of the resonance frequencies, the second one is higher than the first one.

5.2.5 CONCLUSIONS

Pros and cons of using 1D acoustic non linear in time domain and 3D acoustic linear BEM in frequency domain for TL evaluation of a two tubes perforated muffler have been analyzed in terms of accuracy, computing time and problem formulation.

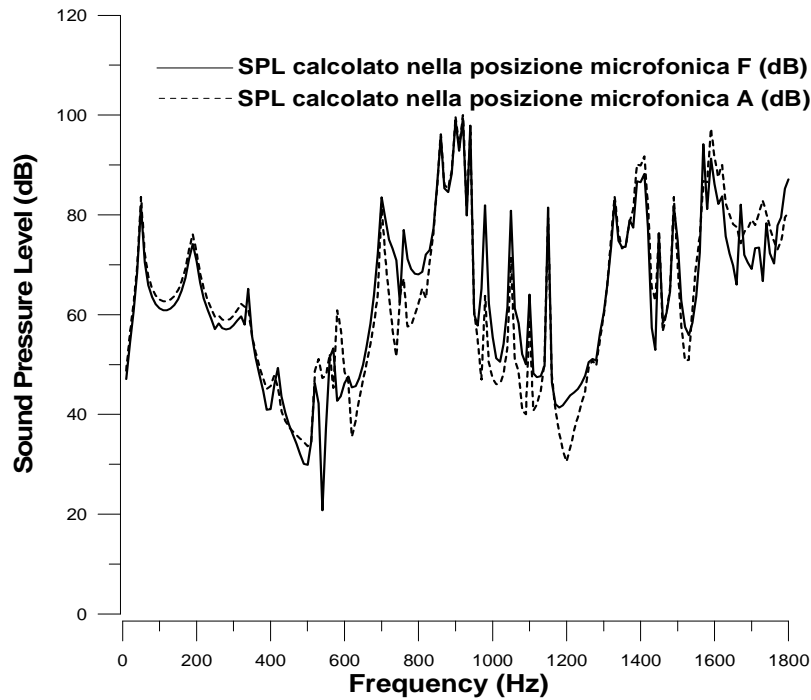


Figure 5.2. 19 – SPLs calculated in the positions A and F through the analysis 3).

Each methodology present its own peculiarities and limitations which vary with the frequency range, and on the assumed physical hypothesis and operating muffler conditions.

In the hypothesis of a infinitely rigid muffler structure, a good agreement between the 1D and BEM computed TL has been found below 450 Hz, when the air temperature is fixed at 294K. As frequency is increased, the 1D results deviate from BEM predictions because of the non planar wave propagation. Due to the very reduced computational effort required, the 1D model is the preferred approach when the low frequencies muffler behavior is under investigation. On the other hand, when a wider frequency range is of interest, a 3D analysis is mandatory.

The TL curve obtained considering 950K air temperature present the same peaks of the previous profile, but stretched toward higher frequencies in accordance with the ratio between the sound velocity at the 950 and 294 K. In this case the matching between the 1D and 3D results is extended up to 900 Hz.

In order to take into account the effect of the muffler structure flexibility, a direct modal FEM analysis has been realized, too. Flexibility effects are localized in proximity of the frequencies where air and structure modes are in resonance. In this case, a different high temperature behavior has been found, depending on different temperature effects on speed of sound and material characteristics.

The effects induced by the presence of a mean flow have been finally investigated with the 1D method. In this latter case, a generally smoother trend has been obtained both at low and medium frequency.

In the last performed investigation, the SPL at 1 meter distance from the center of the muffler, has been evaluated, once a white noise with a certain magnitude is imposed at inlet. Contribution due to the acoustic power radiated at outlet has been separated by the ones due to the wave reflections on the external surfaces (considered infinitely rigid) and to the surface vibrations. Contributions related to the reflections are quite small, and the SPL values rise aside the muffler when air-structure resonance phenomena are taken into account.

The presence Experimental analyses are obviously needed in order to validate the presented results.

5.3 VALIDATION OF THE 1D AND 3D BEM ANALYSES FOR THE PREDICTION OF PERFORMANCES OF A COMMERCIAL CROSS FLOW MUFFLER

The content of this paragraph widely refers to the paper:

D. Siano, F. Auriemma, F. Bozza, H. Rammal, “Validation of 1D and 3D analyses for the prediction of performances of an automotive silencer”, SAE Paper 2011-24-0217.

In this work, the previous 1D-3D acoustical analysis of a commercial muffler, has been improved and experimentally validated. Features related to the manufacturing process, like the coupling of adjacent surfaces and the actual shape of components, have been noticed to heavily affect the muffler behaviour. Hence, although numerical analyses are usually performed on ideal geometries (perfectly matched and shaped), schematizations utilized for acoustic simulations of real mufflers are being suggested to do not neglect these important aspects. On the other hand, for a given initial muffler design, the manufacturing process is assessed to be a critical aspect also for its remarkable effects on the acoustics.

The results have been carried out under different muffler operating conditions related to different mean flow velocities and presence or not of internal insulating material. 1D analyses have been performed by implementing a commercial software, solving the nonlinear flow equations which characterize the wave propagation phenomena. 1D approach has also been utilized to evaluate the fluid dynamic behaviour of the studied muffler in terms of pressure drop when a mean flow is imposed.

3D results are obtained in absence of mean flow by using a commercial software based on Boundary Element approach and solving the three dimensional Helmholtz's equation.

Finally, during the experimental tests, the muffler has been treated as an acoustic two-port element.

5.3.1 PECULIARITIES OF THE MUFFLER STUDIED

The system under investigation is a two perforated tube muffler (see Figure 5.2.1) with two expansion chambers and a transition chamber. An accurate description of the nominal geometry is given in the paragraph 5.2 [15-16] and it is briefly summarized here:

- Total length 303mm.
- Quasi-elliptical cross section with diameters 133mm and 216mm.
- 3 chambers with different lengths (110mm, 90mm, 103mm). The first one and the last one are filled with 150g glass wool.
- 2 perforated tubes, with 37mm diameter, lying in different horizontal planes (not symmetrical structure)
- Material: aluminized carbon steel P04
- Surface thickness: 1.2 mm (external shell) and 1.5 (tubes and baffles)
- Diameter holes: 3mm
- Porosity: 4.5%

As shown in Figure 5.3.1, the absorptive material is included in two blisters which melt up when the muffler reaches a sufficiently high temperature, leaving the wool depositing on the lower walls.

In this work the manufacturing features of the muffler have been deeply studied. In fact, the muffler under observation presents many peculiarities, due to the construction model, which make more difficult the modelling process needed for numerical simulations. In Figure 5.3.2a the geometry of tubes end orifice is shown. Also some welding points between one of the two tubes and one internal baffles can be observed.



Figure 5.3.1 – A photo of the tested muffler. The muffler has been opened to exhibit its internal design.

Since this kind of junction is punctual and not circumferential, same leakages really exist between the two chambers separated by the baffle. In Figure 2b the whole internal muffler configuration can be seen. The two internal baffles are welded only to the tubes, and coupled to the external shell by a punctual strength coupling, which involves other leakages between the chambers separated by this kind of baffles. In figure 2c the technological irregularities of the holes shape due to the punching process are shown.

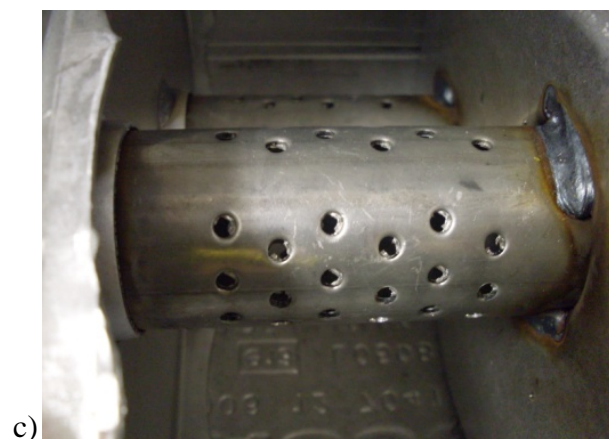


Figure 2 – a (left): tube end orifice; b (center): core muffler; c (right): perforates.

All the above peculiarities have been taken into account in numerical modeling processes in order to obtain good correlation with the experimental data, as shown in results section.

5.3.2 NUMERICAL SIMULATIONS

The utilized 1D and 3D models have been widely presented in the paragraph 5.1 and 5.2. In this sections the previous analyses has been extended in order to include the presence of the absorptive material within the simulations. In case of 1D this implies the choice of a proper friction coefficient for the quasi 3D elements schematizing the chambers. In case of the 3D BEM approach, proper “wool domains” must be defined. In fact, as previously explained, a multi domain approach has been utilized in the BEM approach, and in Figure 5.3.3 the surfaces with interface BC defining the wool domains are depicted.

Also in this case the acoustic analysis requires the specification of the acoustic impedance of perforations, and the Sullivan and Crocker [6] (see Formula 5.2.1) has been utilized. As previously mentioned, this expression is valid in absence of flow, but also the requirement of no contact of absorptive material with the holes must be satisfied. Since 3D analyses have been performed in absence of mean flow, and the wool is not compressed and does not completely fill the first and third chamber (see Figure 5.3.3), the application of the 5.2.1 can be accepted.

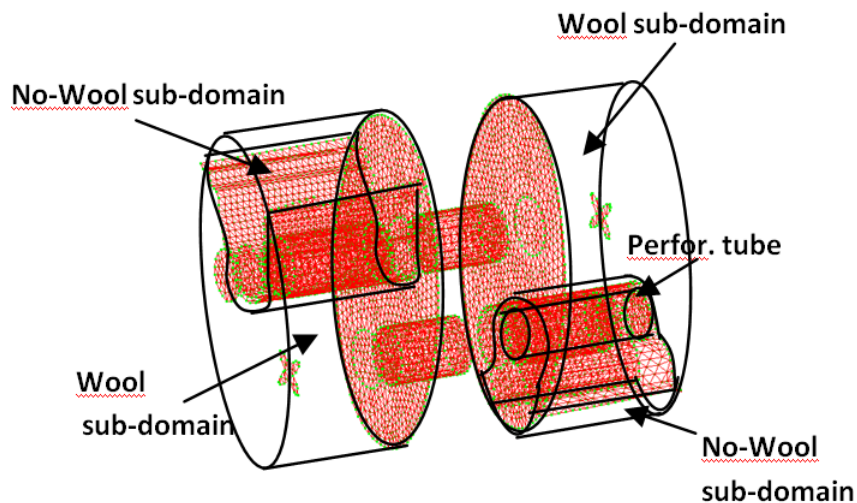


Figure 5.3.3 – Groups with interface BCs defining the wool domains.

In BEM analysis, in addition to the use of multi-domain approach, the absorbing materials can be modelled also through other techniques, like the ‘surface-impedance’. This one is mainly used with thin absorbing surfaces, and requires the knowledge of the material’s impedance. To achieve this, experimental tests on absorbing material samples must be carried out, using an impedance tube. In several situations the ‘surface-impedance’ approach could, in principle, be the preferred solution (for its modelling simplicity), but it can be hardly applied, due to the need of experimentally performed impedance tests.

In this work, the ‘multi-domain’ approach has been preferred. In fact, even though, in this case, the modelling phase is more complex, the evaluation of the proper acoustical parameters could be easily obtained from the flow resistivity data of the considered material. The flow resistivity is mainly related to the packing density of the material and to the fibre diameter [17].

Actually, a third approach is also available in VNoise code: it consists of a double step procedure. Firstly, an impedance tube is virtually simulated with a multi-domain approach, permitting to evaluate the impedance (or, better, the admittance) of the desired material sample. Thereafter, the numerically evaluated admittance is applied to the full model with a surface impedance BC.

5.3.2 EXPERIMENTAL DATA

Numerical results obtained by the previously described 1D and 3D simulations have been validated with experimental data. The experimental work has been carried out in the acoustics laboratory at Tallinn University of Technology, employing a dedicated test facility designed for acoustic characterization of two-port flow duct elements in hot flow conditions. Complete description of test rig and of the utilized experimental technique can be found in the Chapter 4 [18]. Resuming for ease of reading, the silencer has been treated as a two port source in order to describe its acoustic behavior through a transfer matrix (see Figure 5.3.4). A two-source method is employed to set up the two required and independent test states. The classical two-microphone approach has been used to obtain complex pressure amplitudes of the travelling acoustic waves at the inlet and outlet silencer cross-sections. A centrifugal blower and an electrical heater can be utilized to simulate the presence of a hot flow (not considered, however, in this work). Additionally, the pressure drop over the muffler has been

determined for different flow velocities, by using two static pressure sensors positioned across the muffler [18].

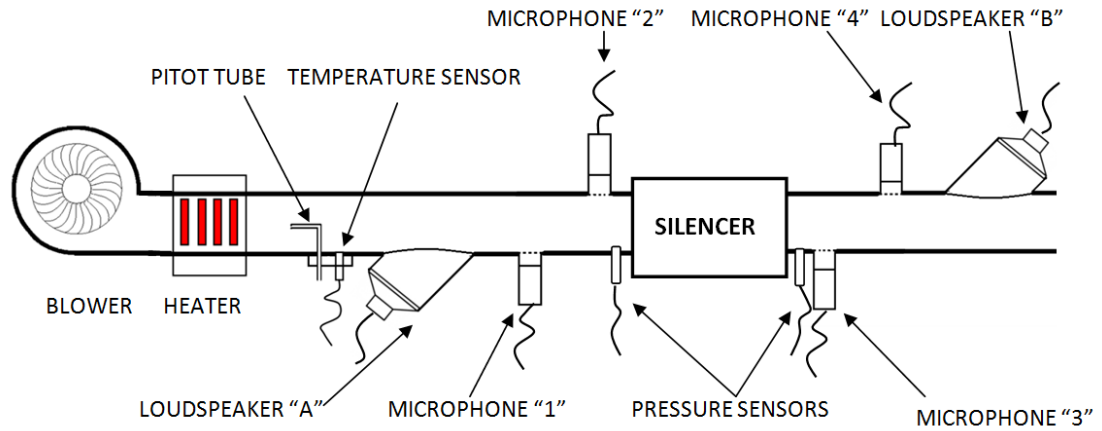


Figure 5.3.4 – A sketch of the test rig utilized for TL evaluation.

The effect of shell vibrations on the propagation of sound has been experimentally taken into account. In fact, the first target of the experimental campaign has been the validation of the numerical results obtained in the hypotheses of rigid surfaces, and the real silencer has been evidently suspected to provide lower attenuation of sound due to vibrating surfaces. This obviously leads to a deviation from the 1D and 3D non-coupled simulation results. In order to avoid unwanted shell noise and uncontrolled TL an additional feature was designed to the rig. A wooden box was set up around the muffler and filled with sand for effective damping of the shell vibrations. A photo of the measurement section with the sand box is presented in Fig. 5.3.5:

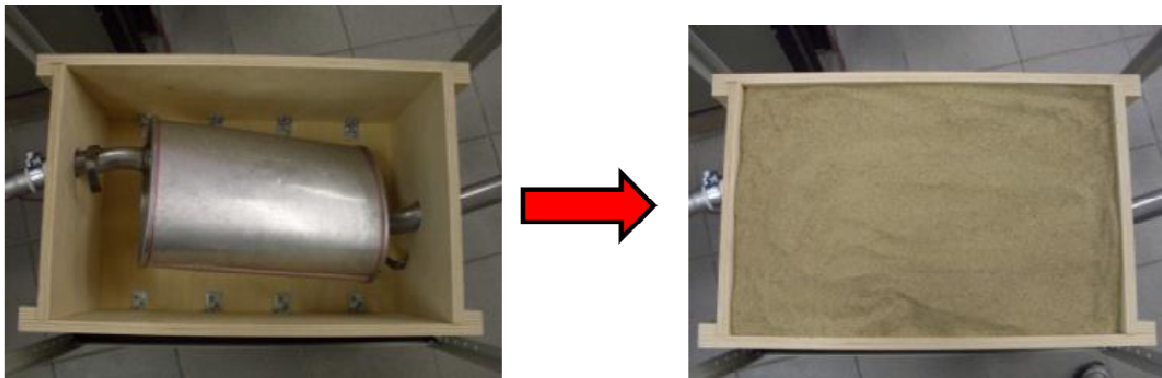


Figure 5.3.5 – A sandbox used to eliminate the shell noise and shell vibrations.

Table 5.3.I summarizes the experimentally tested operating conditions and 1D or 3D analyses carried out to predict the measured TL.

NO WOOL TESTS		
Temperature, K	Flow velocity, m/s	Model
293	no mean flow	1D and 3D
298	20	1D
318	40	1D
WITH WOOL TESTS		
Temperature, K	Flow velocity, m/s	Model
293	no mean flow	1D and 3D
300	20	1D
326	40	1D

Table I – Experimental operating conditions and performed numerical analyses

5.3.3 RESULTS AND DISCUSSION

NO WOOL RESULTS

In this section, 1D and 3D BEM results, under the common hypothesis of absence of inner insulating material and infinitely rigid muffler surfaces, are compared to the ones experimentally obtained under the same conditions. For sake of truth, the sand box utilized during the test to avoid surface vibrations cannot actually prevent baffles vibrations since these latter, as previously mentioned, are not welded on the external shell.

In Figures 5.3.6 and 5.3.7, experimental results are compared to the ones obtained with 1D and BEM approaches. The actual constitutive peculiarities, including leakages between chambers and cross area variations at inlet and outlet tubes, have been taken into account in “Refined schematization” results. Furthermore, results coming from the analyses explained in paragraph 5.2 [15] are shown, too. They refer to the ideal muffler geometry and are indicated as “Initial schematization results”.

The “Refined” 1D and 3D schematizations include eight holes with 3mm diameter added to each baffle, in order to obtain a global area which is reasonably similar to the observed leakage areas (see Figure 5.3.8). Moreover, they take into account small cross section variations measured on the actual muffler. The 3D “Refined” mesh also incorporates a more detailed schematization of the ending tube section.

The frequency range investigated extends up to 1600Hz in case of experiments and 3D simulations, while for 1D simulations it is stopped at 1200Hz, due to the well-known limitations of the 1D approach. A very good agreement between experimental data and “Refined” 1D results is evident at low frequencies. This is the frequency range where the wave propagation can be considered planar and therefore the pressure distribution across each muffler cross-section can be considered constant. The two curves fit well up to around 850

Hz, while at higher frequencies, the higher order modes start to appear in the muffler chambers, and the 1D model loses its accuracy.

“Refined” 3D analysis gives results quite comparable to previous ones at low frequency but, as expected, it is able to reproduce, with remarkable success, the multi-dimensional shape of acoustic waves at high frequencies, too. However, it must be underlined that the latter approach is substantially more time consuming compared to the 1D (more than 1 day versus less than 1 hour).

The comparison between “Initial” and “Refined schematization” results in Figures 5.3.6 and 5.3.7 also demonstrates that the included refinements largely affect the accuracy of TL prediction. In particular, the leakages between the chambers determine an increased TL at very low frequency: in fact they constitute an acoustic connection between the three cavities, which tends to virtually increase the chamber volumes. However, they also introduce a substantial decrease of the two attenuation peaks at 700 Hz and 1200 Hz.

Basing on the above considerations, it comes evident that the manufacturing process should be critically assessed by the muffler makers, since it seems to play a remarkable effect on the acoustic behaviour. The latter is very different from the one conceived during the design phase on the ‘ideal’ geometry. Contemporary, an accurate acoustic simulation of a ‘commercial’ muffler requires a detailed description of all the apparently minor geometrical elements of the device. Current literature is, in fact, full of well-matched numerical and experimental data even if, usually, they do not refer to a commercial low-cost device, whose simulation, as demonstrated, is much more complicated.

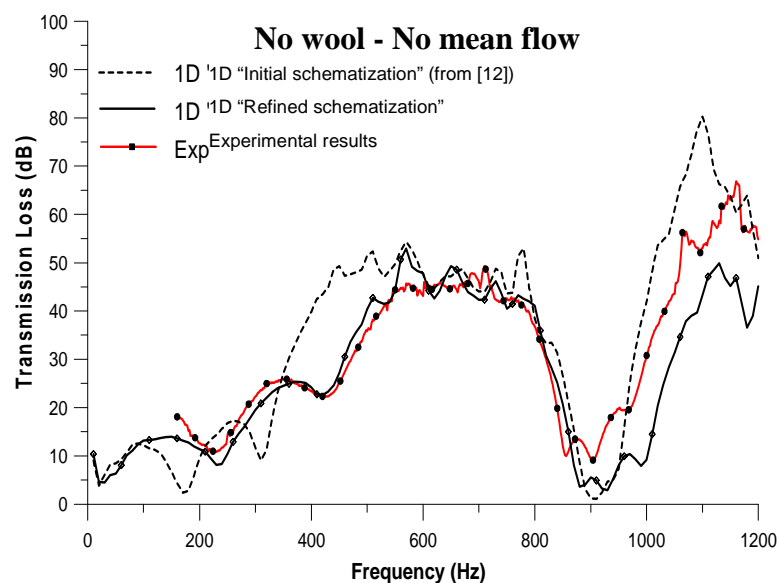


Figure 5.3.6 – 1D and experimental TL data. No wool and no mean flow.

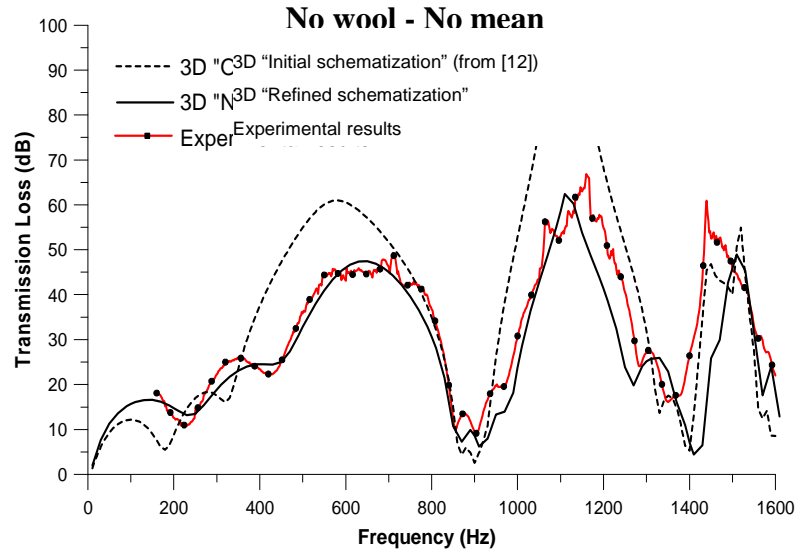


Figure 5.3.7 – 3D-BEM and experimental TL data. No wool and no mean flow.

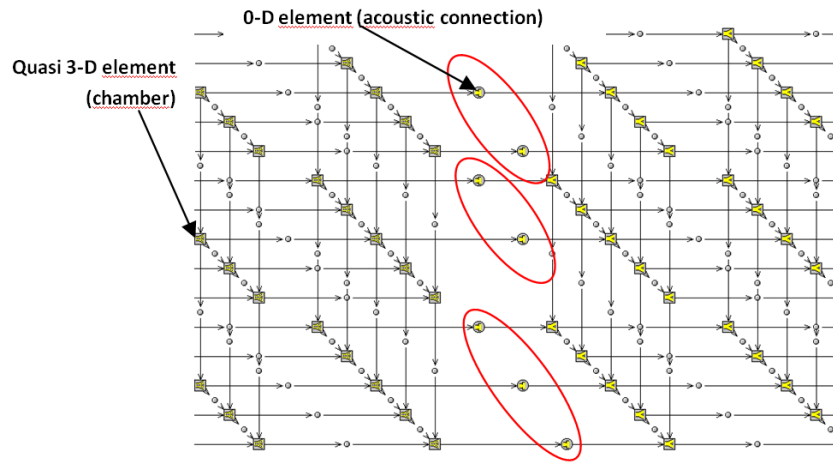


Figure 5.3.8 – Quasi 3-D and 0-D elements utilized for refined 1D schematization.

Of course, the detailed knowledge of the pressure wave distribution within the muffler is of fundamental importance for improving its acoustical behaviour at the design phase. As an example, the 3D pressure distribution, due to the contribution of the higher order modes in the cavities, is clearly noticeable in Figure 5.3.9, at a frequency of 1390 Hz.

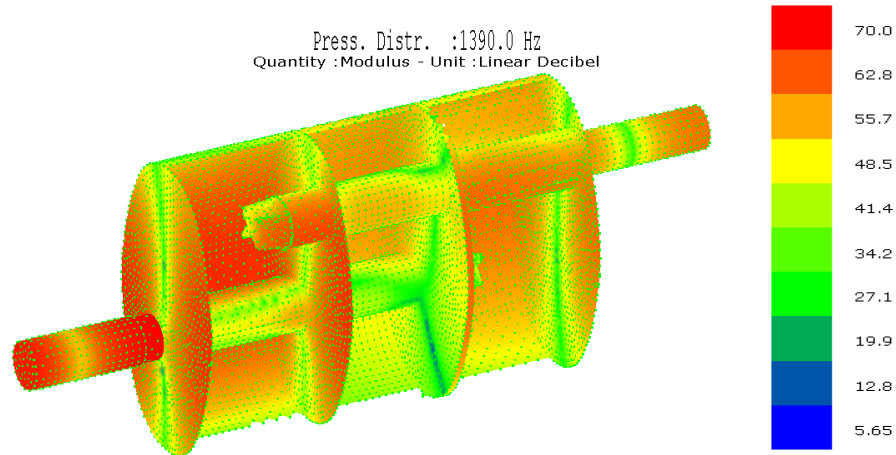


Figure 5.3.9 – 3D analysis. Pressure amplitude distribution at 1390 Hz.

Another important parameter affecting the muffler behaviour is the presence of a mean flow crossing the device. In fact, it determines a partial levelling of the TL peaks and troughs, which can be particularly useful at low frequency, where main engine orders occur [19]. The above effect is clearly depicted in Figures 5.3.10 and 5.3.11, showing the results of imposed mean flows of 20 and 40m/s. Due to limitations of the employed 3D code, only 1D results are discussed in the following. At 20 m/s, a good matching between experimental and numerical results is noticeable up to 850Hz (see Figure 5.3.10). Once again, the “Refined” results better reproduce the overall trend and particularly the attenuation peak around 700 Hz. In presence of a higher mean flow (40 m/s, Figure 5.3.11) a slightly lower accuracy is found, even if the TL trend is still fairly well reproduced in the whole investigated frequency range. Obviously, 1D approach cannot take into account the presence of secondary effects related to the presence of internal sound-generating vortices (flow noise), which extends on the broad band, definitely producing a source of discrepancies with experimental results.

Actually, mean flow should yield a higher TL, by making it pass through perforated pipes, whereby a large aero-acoustic resistance is induced [19]. Looking at numerical results (which are less scattered and extended at lower frequencies than the experimental ones), the above trend is confirmed only up to 450 Hz. Beyond this frequency range, the presence of a mean flow has been found to exert a negative effect on TL: as an example, the TL around 800 Hz worsens of about 12-15 dB when increasing the mean flow from 20 to 40 m/s.

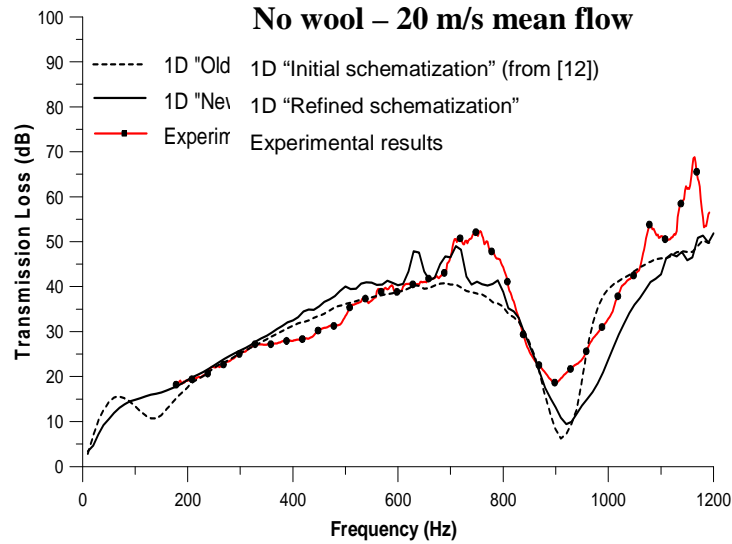


Figure 5.3.10 – 1D and experimental TL curve. No wool and 20m/s mean flow.

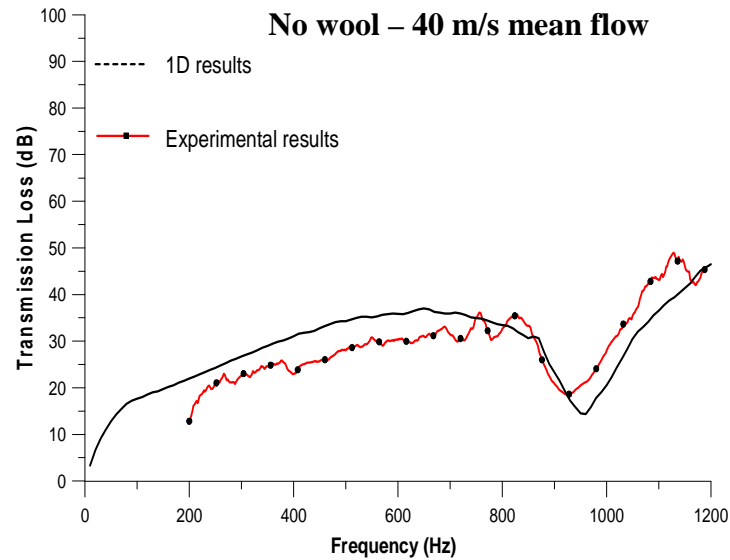


Figure 5.3.11 – 1D and experimental TL curve. No wool and 40 m/s mean flow.

Calculations with imposed mean flow also allow to estimate the fluid-dynamical behaviour of the muffler, in terms of realized pressure losses. Table 5.3.II summarizes the measured and predicted pressure drop (Δp) through the muffler at different mean flow velocities. The good agreement found implies that correct global values of discharge and loss coefficients have been imposed on the holes, the tubes and the orifices utilized to simulate the leakages between the chambers. This also means that 1D analyses can be successfully employed to contemporary characterize both acoustical and fluid-dynamical aspects, allowing to perform an overall optimization of the device.

Mean flow velocity, m/s	Measured Δp , mbar	Simulated Δp , mbar
20	22	22
40	82	84

Table 5.3.II – Measured and Predicted Pressure Losses – No wool.

WOOL EFFECTS

In the present study, numerical calculations have been carried out also considering the presence of inner insulating material. Main wool characteristics are: fibre material density of 2700 kg/m^3 , fibre diameter of about $30\mu\text{m}$ and packing density⁴ approximately equal to 79 kg/m^3 . This information has been deduced by using an electronic microscope of accurate scale (Kern). Figure 5.3.12 shows the structure of the glass wool fibres magnified at the microscope.

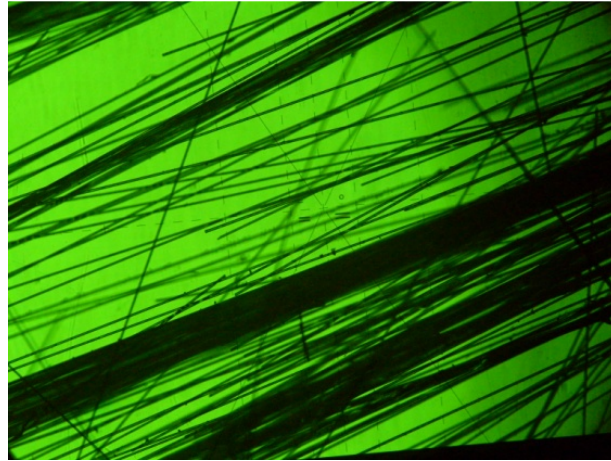


Figure 5.3.12 – A magnified photo of the glass wool fibers used in the muffler.

A slice of absorbing material of thickness s , exposed to a ‘small’ steady mean flow velocity U , realizes a pressure drop, Δp , which is usually quantified by its ‘flow resistivity’, σ (rayl/m), defined as [17]:

$$\sigma = \frac{\Delta p}{Us} \quad (5.3.1)$$

The latter parameter can be estimated basing on several formulations available in current literature [17]. Most of them are empirical or semi-empirical relationships, dealing with different fibre materials and diameters. For randomly oriented glass fibres, with a relatively large ‘constant’ diameter d (greater than $15\mu\text{m}$), the following equation can be used:

⁴ Packing density (or bulk density) is obtained by dividing the weight of a wool bag per bag volume (assessed to be around the 79% of the chamber volume).

$$\sigma = \frac{4 \cdot \mu}{(d/2)^2} \left[\frac{0.55(1-\varepsilon)^{4/3}}{\varepsilon} + \frac{\sqrt{2}(1-\varepsilon)^2}{\varepsilon^3} \right] ; \quad \varepsilon = \frac{\rho_m}{\rho_f} \quad (5.3.2)$$

where μ is the dynamic viscosity of the air (1.84×10^{-5} Pa s), ρ_f the material density and ρ_m the packing density⁵.

For randomly oriented fibres, characterized by a diameter distribution around a mean value (d_{av}), the following formula is indeed more appropriate:

$$\sigma = \frac{3.2 \cdot \mu \cdot (1-\varepsilon)^{1.42}}{(d_{av}/2)^2} \quad (5.3.3)$$

As far as 3D analyses are concerned, properties of wool-included domains have been automatically generated, as a function of material type (fibre glass) and flow resistivity. Equations (5.3.2) and (5.3.3), with reference to the above mentioned wool data, respectively provide $\sigma = 2199$ rayl/m and $\sigma = 1810$ rayl/m. An intermediate value (2000 rayl/m) has been hence used in 3D simulations.

Concerning 1D analyses, indeed, a “flow resistance coefficient”, C_D , must be specified [2]:

$$C_D = 0.6 \sigma \left(\frac{d_{av}^2}{\mu} \right) \varepsilon^{1.5} \quad (5.3.4)$$

With reference to the previously estimated values of wool parameters and flow resistivity, eq. (5.3.4) furnishes a flow resistance coefficient equal to 0.1. In this way, both 1D and 3D calculations employ exactly the same characterization of the insulating material.

Results obtained in absence of mean flow are depicted in Figure 5.3.13. Comparing it with no wool results (Figure 5.3.6 and 5.3.7), an expected improvement of acoustical performance can be noticed. The TL enhancement is extended on the broad band frequencies: the maximum peak is increased of about 12dB, but the most useful performance enhancement is related to the levelling of the troughs at low (250 and 450 Hz) and medium frequencies (900-1000Hz). An increase of about 20dB has been found in the latter frequency range. Both 1D and 3D results correctly reproduce the experimental trend, with a slightly better accuracy

⁵ It is easy to show that $(1-\varepsilon)$ is the material porosity [16].

of 1D analysis at low frequency and a better 3D forecast at medium-high frequency (600-1600Hz).

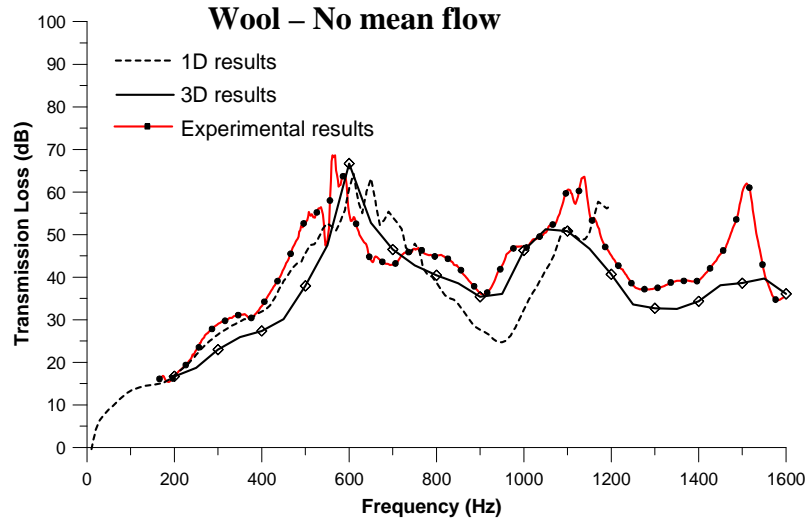


Figure 5.3.13 – 1D, 3D and experimental data. Presence of wool, and no mean flow.

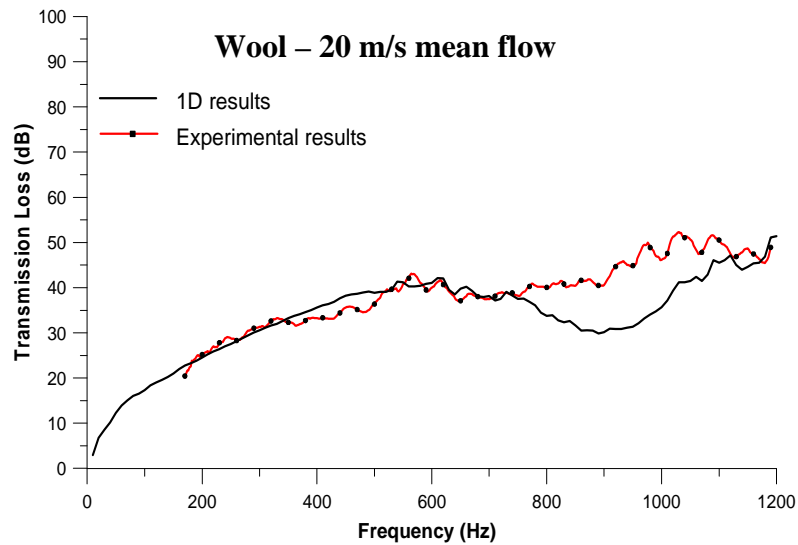


Figure 5.3.14 – 1D and experimental TL curve. Presence of wool and 20m/s mean flow.

Finally, 1D calculations have been carried out to estimate the effects of contemporary presence of insulating material and mean flow (Figures 5.3.14 and 5.3.15). Once again, a satisfactory agreement between numerical and experimental data is shown. If compared to the analogue results without wool (Figures 5.3.10 and 5.3.11), it comes evident that the contemporary presence of wool and mean flow determines the almost complete disappearing of the trough at about 900 Hz. Also in this case, 1D analyses provide the estimated pressure

losses, compared to experimental findings in Table 5.3.III. As expected, higher values are obtained, due to additional losses exerted by wool presence. Moreover, the shown agreement is a confirmation that a good estimate of flow resistivity and wool parameter have been realized.

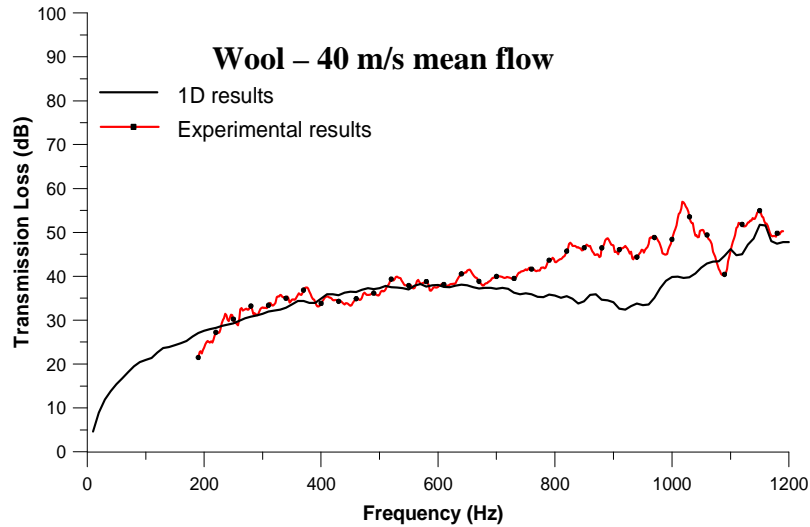


Figure 5.3.15 – 1D and experimental TL curve. Presence of wool and 40m/s mean flow.

Mean flow velocity, m/s	Measured Δp , mbar	Simulated Δp , mbar
20	35	33
40	129	118

Table 5.3.III – Measured and Predicted Pressure Losses – with wool.

5.3.4 FURTHER EXPERIMENTAL STUDIES

As explained in the paragraph 5.3.2, the experimental tests performed to validate the 1D and 3D analyses have been made in a way to reduce the shell vibrations.

Anyway, in this section, a comparison of the measured TL for the real silencer in case of free outer surfaces and in damped conditions, is presented. In Figure 5.3.16, the results have been obtained after eliminating the inner wool. In Figure 5.3.17 the wool is accounted.

As can be seen in Figure 5.3.16, the TL curve of the dampened structure, loses most of the high frequency peaks believably related to the eigenmodes of the vibrating shells.

The difference between TL results of the silencer without the wool and extra damping added is more distinct. The difference of the TL curves is more dominant in the absence of

wool due to the more resonant behaviour of the silencer, lacking the absorptive effect of the wool.

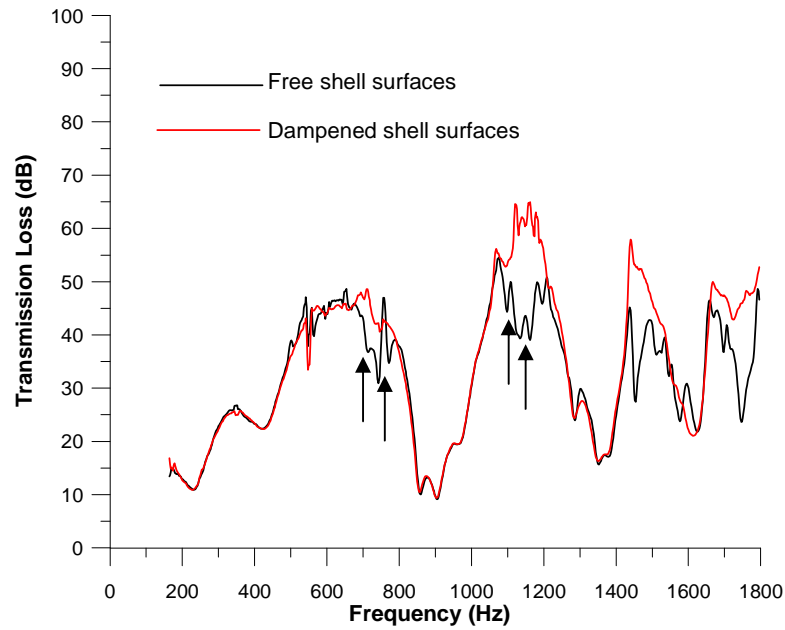


Figure 5.3.16 – Comparison between the measured TL of the muffler without wool, with free and with dampened outer shells.

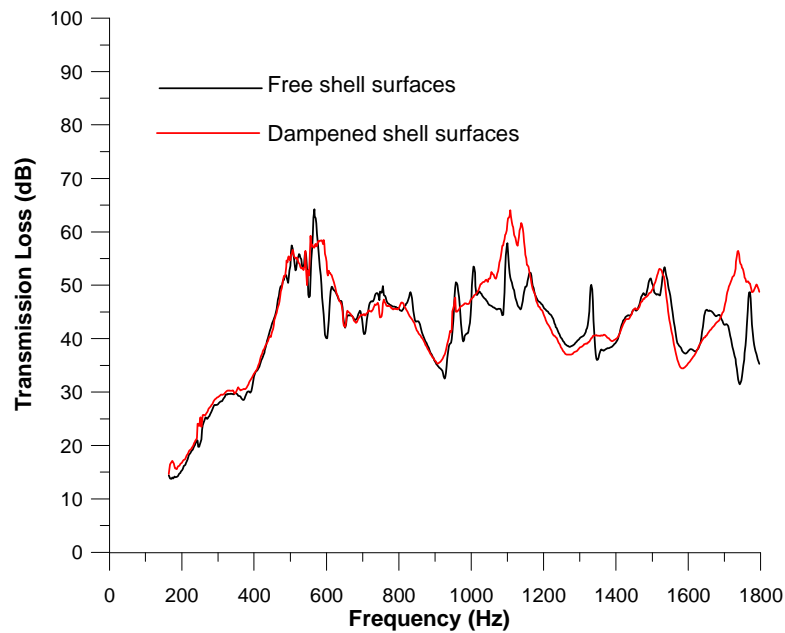


Figure 5.3.16 – Comparison between the measured TL of the muffler with wool, with free and with dampened outer shells.

In the paragraph 5.2 a study of the fluid-structure interaction, referred to the so called “Initial configuration”, has been done by using a combined FEM-BEM approach. In order to numerically evaluate the effects of the surface vibrations of the real muffler, another FEM-

BEM analysis is required for the “Refined configuration”, and it is still in progress. Anyway, in the Table 5.3.III, a list of resonance modes and eigenvalues of the initial muffler configuration is extracted from the Table 5.2.I (Initial configuration, without wool). It is noticeable how several resonance frequencies, indicated in the table with a star, can also be detected in the Figure 5.3.15, where they are indicated with an arrow.

For sake of truth, in the experimental tests, the use of the box filled with sand, does not dampen the vibrations of the inner surfaces, which are almost free to vibrate. Consequently the effects of the vibrations of these surfaces cannot be highlighted. Contrariwise, the numerical fluid-structure analysis presented in the paragraph 5.2, takes into account the vibrations of all the muffler surfaces. For this reason, probably, the number of the resonance frequency founded is higher than the one highlighted in Figure 5.3.16. Consequently, also the modal analysis on the initial muffler schematization results to be quite promising.

mode	Eigenvalue (Hz)
<u>16</u>	<u>582</u>
<u>19</u>	<u>608</u>
<u>20</u>	<u>698*</u>
<u>21</u>	<u>762*</u>
<u>28</u>	<u>1050</u>
<u>30</u>	<u>1073</u>
<u>31</u>	<u>1100*</u>
<u>33</u>	<u>1150*</u>
<u>34</u>	<u>1266</u>
...	...

Table 5.3.III – Fluid-structure resonances of the “initial muffler configuration”.

5.3.5 CONCLUSIONS

1D and 3D BEM models, utilized in a previous work for simulating the acoustical behaviour of a commercial silencer, have been improved and extended. The analyses, in terms of transmission loss and pressure drop, have been carried out at different mean flow velocities and with or without the presence of absorbing material within the device. Both TL and pressure losses have been experimentally verified in each of the above operating conditions. Main results of the paper are listed below:

- Accurate acoustic simulations of a commercial low-cost device require a detailed description of all the apparently minor geometrical elements of the device, mainly determined by the manufacturing process.

- In particular, its quality (i.e. welding and strength surfaces coupling), may determine the presence of leakages between the chambers, which has been found to remarkably affect the acoustical behavior. Leakages, in fact, constitute an acoustic connection between the muffler cavities, tending to virtually increase the chamber volumes, thus increasing the TL at low frequencies and worsening it at medium frequencies.
- For this reason, muffler makers are advised to deal with the above consideration. The quality of the manufacturing process should also be taken into account by the simulations, at design phase.
- 1D results for the considered silencer are proved to be accurate up to 850 Hz, since this approach, as known, is only suitable in the frequency range where a plane wave behaviour establishes. BEM technique has been used only in absence of mean flow: it is much more time consuming, but it is able to provide good results in the whole investigated frequency range (0-1600 Hz).
- 1D calculations carried out with the presence of an imposed mean flow allow to contemporary estimate acoustical and fluid-dynamic behaviour of the muffler, giving the possibility to provide information for the overall muffler optimization.
- As expected, the presence of an insulating material is found to produce a smoother TL profile across a broad band frequency range, while, however, determining a non-negligible increase of pressure losses.

Overall results demonstrate that the combined employment of 1D and 3D models, coupled to an accurate geometrical description and schematization of the device, is able to characterize the effects of most influencing parameters controlling the acoustic and fluid-dynamic behaviour of a commercial automotive silencer.

In addition, experimental analysis the vibro-acoustic effects of the silencer outer shells have been studied and it was found that the lack of stiffness in the muffler structures can significantly reduce the silencing effect, in particular in the absence of absorptive materials and at the higher frequencies. The presented results are in agreement with the modal analysis of the “not refined” muffler schematization presented in the paragraph 5.3.

Further studies are oriented to the development of fluid-structure analysis of the “refined schematization” presented in this paragraph.

5.4 ACOUSTIC AND FLUID-DYNAMIC OPTIMIZATION OF AN AUTOMOTIVE COMMERCIAL CROSS FLOW MUFFLER

The content of this paragraph widely refers to the papers:

F. Auriemma, “Acoustic and Fluid-dynamic Optimization of an Automotive Muffler”, in submission.

In this section, acoustic and fluid-dynamic optimizations of the previously studied commercial muffler have been carried out. To this aim, an external optimizer, based on a genetic algorithm, has been coupled with the 1D solver in two different optimizations: the first one has been addressed on the improving of the muffler TL, in absence of mean flow, and in 100-800Hz frequency range. The second one has been focussed on the best trade off between acoustic and fluid-dynamic muffler performances, in terms of TL and Δp in 100-400Hz frequency range.

The 3D BEM approach has not been used in the optimization process since it is much more time consuming, it is suitable and it has been validated only in absence of mean flow. Moreover, the investigated frequency range, which correspond to the range where most critical frequencies occur in typical operating conditions, is widely covered by the 1D approach.

The optimization study of a muffler has recently been object of study of several scientific works, usually based on a numerical decoupling technique to evaluate the muffler performances, and on a genetic algorithm (GA) as optimizer. Even though a variety of interesting results have been carried out with this approach, three remarkable aspects are frequently neglected:

- The effect of the wool, often included in these devices.
- The requirement of minimizing the back pressure exerted when the exhausted gases flow thorough the muffler.
- The presence of leakages between the three chambers (due to the manufacturing process or to baffle holes).

In this work, all these aspect are taken into account.

5.4.1 1D TL AND PRESSURE DROP DATA

Since the 1D muffler analyses, performed on the “refined schematization” and shown in the paragraph 5.3, have been experimentally validated, all the muffler schematizations utilized in the two optimization processes are obtained by conveniently modifying the geometrical data of this refined model. At each simulation the TL is calculated and averaged in a certain frequency range. The first optimization is focused only on the acoustical muffler performances, and the TL is calculated and averaged in the 100-800 Hz frequency range, i.e. the plane wave region for the considered geometry. In this way, the objective function is defined as:

$$TL_{AV} = \frac{1}{f_f - f_i} \int_{\omega_i}^{\omega_f} TL(f) df \quad (5.4.1)$$

where f_f , f_i and $TL(\omega)$ are respectively the frequencies of 100Hz, 800Hz, and the function transmission loss.

In the second optimization, also fluid-dynamic behavior is accounted: the TL_{AV} , when $f_f=400$ Hz and $f_i=100$ Hz, and the pressure drop across the muffler when a 29 m/s mean flow is imposed at inlet.

5.4.2 MUFFLER OPERATING CONDITIONS

The above mentioned values of the imposed mean flow velocity and of the investigated frequency range in the second optimization process, can be easily explained considering the coupling of the muffler with an ICE. The muffler under investigation, in fact, is designed to equip small car engines, and one of the two optimization procedures shown in the next paragraph has been carried out considering the following engine characteristics and operating conditions:

STROKES	4
NUMBER OF CYLINDER	4
DISPLACEMENT (V)	1 LITRE
LOAD	WIDE OPEN THROTTLE
REGIME	3500 RPM
VOLUMETRIC EFFICIENCY (λ)	0.75
MEAN GAS TEMPERATURE IN THE MUFFLER	473 K

Table 5.4.1 – Engine characteristics and operating conditions

The fundamental frequency of an n_{cyl} cylinders engine is F_0 :

$$F_0 = n_{cyl} \frac{rpm}{60\epsilon} \quad (5.4.2)$$

where rpm are the engine revolutions per minute, and ϵ equal to 1 or 2 for a 2 stroke or a 4 stroke engine respectively. For a four stroke 4 cylinder engine, it corresponds to the second engine order frequency, where the -k engine order frequency is defined as

$$F_0 = k \frac{rpm}{60} \quad (5.4.3)$$

This frequency and its entire multiplies detect the most critical acoustic conditions due to the discharging process. For the engine in Table 5.4.I, $F_0=117\text{Hz}$. Moreover, the mass flow rate discharged by a 4 stroke 4 cylinder engine is:

$$\dot{m} = \frac{V \cdot rpm \cdot \lambda}{60} \quad (5.4.4)$$

For the investigated case, $\dot{m} = 0.002188 \text{ m}^3/\text{s}$. Considering a 31mm diameter inlet muffler cross section, a 29m/s mean flow velocity is obtained.

For these reasons, in order to optimize the acoustic and fluid-dynamic behaviour of the muffler when coupled with the above engine, a 29m/s mean flow velocity at 473K temperature is imposed at inlet. In these conditions, the pressure drop is calculated, and the TL is carried out in 100-400Hz frequency range. This latter has been selected in order to take into account the 2nd, 4th, and 6th engine order frequencies at 3500rpm (117, 233 and 350 Hz respectively), which are usually the most critical ones for these kind of problems.

5.4.3 OPTIMIZATION PROCEDURE

In this work, the two mentioned optimization procedures have been implemented through the use of an external optimizer (ModeFRONTIERTM) coupled with the 1D solver GTPowerTM and two MatlabTM routines.

The BEM 3D approach can be also utilized to optimize the muffler geometry, when an automatic mesh generator is coupled to the solver in the optimization process. Anyway, the 3D calculations are much more time consuming than the 1D ones. Moreover the BE solver utilized in the previous works, does not take into account the presence of flow and it is not suitable to evaluate the pressure drop. For this reason, in optimization procedure presented in this work, the 1D approach has been preferred.

In both procedures, the optimized parameters are the same, and listed in table 5.4.II together with their initial value and their range of variability. Briefly, ten independent degrees of freedom have been considered, including the lengths of the three inner chambers, the tube diameters and the tube ending section diameters, the number and the diameter of the holes on perforate tubes, and the extension of the perforated area on tubes. In Figure 5.4.1 a sketch of the initial configuration including small orifices on baffles, tube perforations and final end tube constriction, are depicted in order to clarify the meaning of the above mentioned parameters. a, b, and c parameters obviously constitute two degrees of freedom, since their sum must be equal to the total muffler length. Orifice diameters on the baffles, wool quantity and characteristics are not “parameterized” since they respectively depend on the manufacturing process and on initial design choices.

Parameter name	Meaning	Initial value	Range of variability
a	Length of the 1 st chamber	110mm	60mm;110mm;155mm
b	Length of the 2 nd chamber	90mm	50mm;95mm;140mm;190mm
c	Length of the 3 rd chamber	103mm	Depending on a, b and total muffler length
D _{tube}	Tubes diameter	37mm	[29mm:45mm] step 2mm
D _{end}	Tubes ending section diameter	15mm	[10mm:20mm] step 2mm
D _{por}	Holes diameter of perforates	3mm	[2.4mm:3.6mm] step 0.15mm
DS _{holes}	Number of holes per 10mm perforated tube	10.28	[2.8:19.7] step 0.92
L1	Non-perforated lengths on tube	10mm	[0mm:75mm] step 5mm
L2		20	[0mm:95] step 5mm
L3		40	[0mm:70mm] step 5mm
L4		10	[0mm:75mm] step 5mm

Table 5.4.II – List of the parameters to optimize, including their initial values and the variability range.

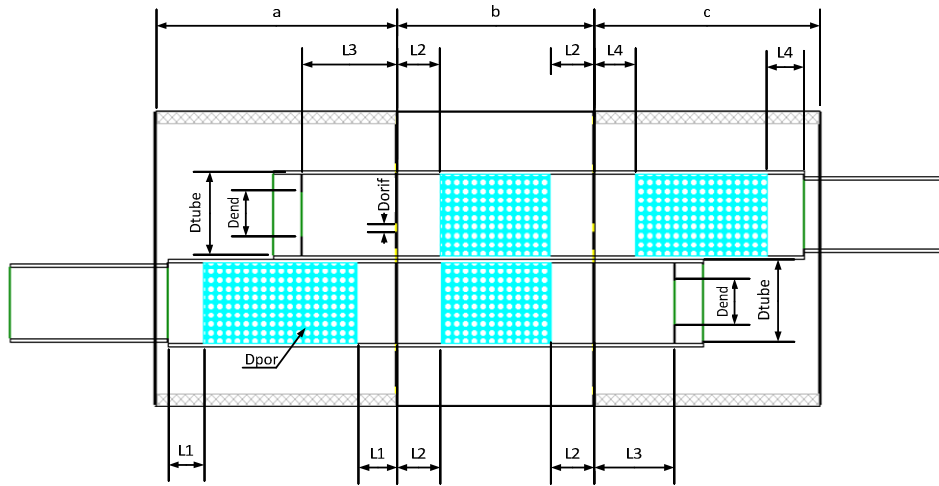


Figure 5.4.1 – Sketch of the initial configuration including parameters to optimize.

The logical development of the two above mentioned optimization problems within the ModeFRONTIER™ environment are explained in Figure 5.4.2a and 2b respectively.

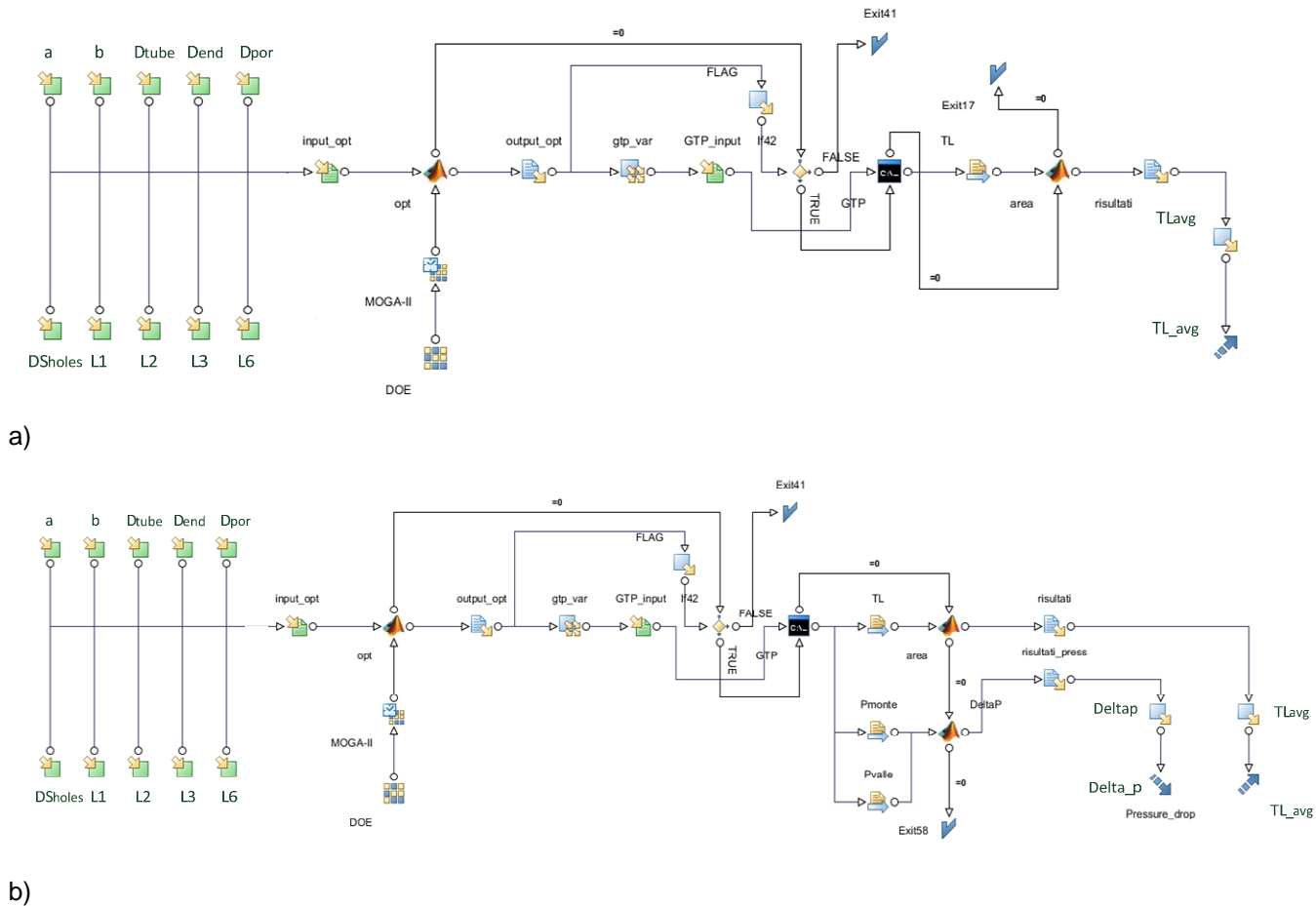


Figure 5.4.2 – Workflows of the optimization problems developed in ModeFRONTIER environment. a) single objective, b) double objective problem.

In order to couple the 1D software with the external optimizer, two MatlabTM routines have been implemented: once a set of values of the considered parameters has been chosen by the optimizer, the first routine checks the congruence of a , b , c , $L3$ and $L4$ in order to avoid unrealistic conditions. These latter might occur when the total chamber length ($a+b+c$) or total tube lengths (due to $L3$ and $L4$ dimensions) are higher than the muffler length (303mm). In this case, a proper flag kills the simulation and a succeeding set of dimensions is provided by the optimizer.

The first routine has also been programmed to automatically vary the 1D muffler discretization according to the data sets provided by the optimizer. In fact, GTPower is able to parameterize the hole diameters and the physical attributes of 1D and 0D elements, whereas the number, the geometrical position and the type of the elements are fixed for a given schematization. Hence, once a selected set of values satisfies the congruence check, the optimizer can directly act on the D_{tube} , D_{end} , D_{holes} , D_{por} , DS_{holes} , but it cannot act on the baffles position nor on the extension of the perforated areas. In order to overcome this issue a discretization of a generic muffler with entirely perforated tubes and with baffles at each discrete value of a , b and c , is utilized. This discretization is represented in Figure 8. Since the perforates are discretized by a certain number of 0D/1D elements (representing the portions of tube) connected to a certain number of 0D elements (constituting the holes), the MatlabTM routine simply deactivates, if needed, a certain number of holes. This number, obviously, depends on dimensions of $L1$, $L2$, $L5$, $L6$. Contrariwise, the D_{por} value is imposed to the hole diameters wherever the perforations are simulated.

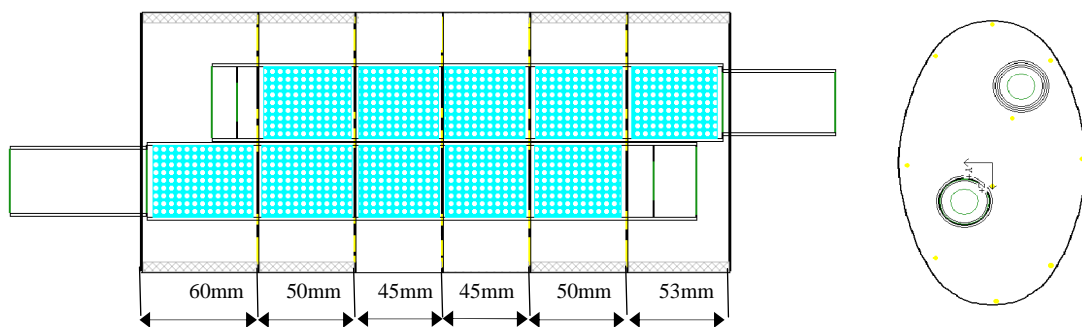


Figure 5.4.3 – Sketch of the generic muffler configuration including baffles at each position and entirely perforated tubes.

Similarly, according to the imposed values of a , b and c , the routine deactivate not required baffles by simply imposing a continuity condition across themselves.

After the 1D analysis has been performed on the obtained model, a second MatlabTM routine is utilized to evaluate the TL_{AV} and the Δp starting for the data provided by GTPowerTM.

To solve the above problem, the MOGA-II algorithm is utilized in both optimizations, belonging to the category of genetic algorithms [20]. In a genetic algorithm, a population of strings (called chromosomes or the genotype of the genome), which encode candidate solutions (called individuals, creatures, or phenotypes) to an optimization problem, evolves toward better solutions. Traditionally, solutions are represented in binary as strings of 0s and 1s, but other encodings are also possible.

The main property that makes these genetic representations convenient is that their parts are easily aligned due to their fixed size, which facilitates simple crossover operations.

The evolution usually starts from a population of randomly generated individuals and happens in generations. In each generation, the fitness of every individual in the population is evaluated, multiple individuals are stochastically selected from the current population (based on their fitness), and modified (recombined and possibly randomly mutated) to form a new population. The new population is then used in the next iteration of the algorithm. Commonly, the algorithm terminates when either a maximum number of generations has been produced, or a satisfactory fitness level has been reached for the population.

5.4.4 RESULTS

In Figure 5.4.4, an history chart of the first optimization process is plotted. The initial configuration has been chosen as first individual of the first considered generation. The calculated TL_{AV} of the initial configuration is about 35dB.

The optimization process converges towards TL_{AV} values of about 40 dB after about 700 generated designs. In Table 5.4.III the geometrical data and the TL_{AV} of the initial and optimal muffler configurations are summarized.

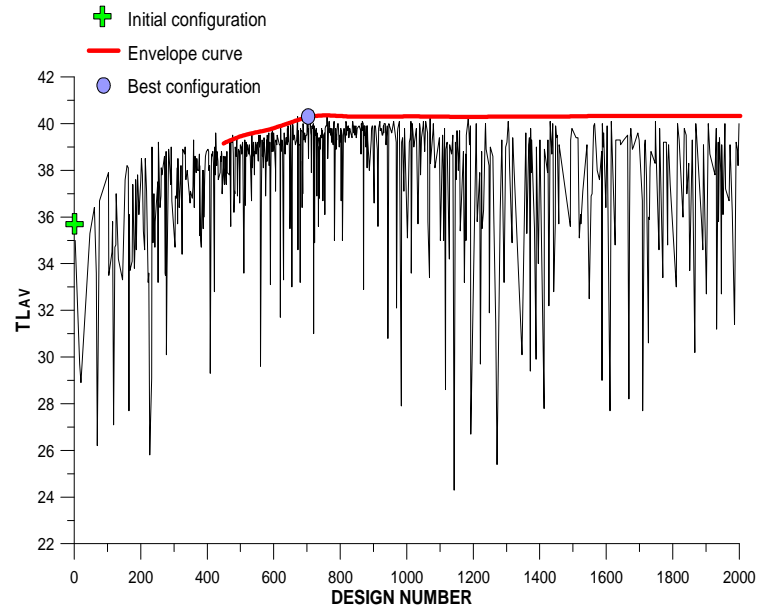


Figure 5.4.4 – History chart of the optimization process.

In Figure 5.4.5a the best muffler configuration is plotted and in Figure 5.4.5b the TL of the initial and the best configurations are displayed and overlapped. It is clearly noticeable that up to 400 Hz there is no improvement in terms of TL. This is mainly due to the total volume of the muffler, which has been imposed to be constant, and to the absence of mean flow, which can positively affect the TL at low frequencies. Indeed from 400 up to 800 Hz the silencer behavior improves even more than 10 dB. As above mentioned, since at frequencies higher than 800Hz the utilized approach for the considered geometry is not reliable, the analysis has been limited up to 800Hz and the worsening of the TL curve above this frequency has no physical meanings.

Configuration	a (mm)	b (mm)	c (mm)	D _{tube} (mm)	D _{end} (mm)	D _{por} (mm)	DS _{holes} (mm)	L1 (mm)	L2 (mm)	L3 (mm)	L4 (mm)	TL _{AV} (dB)
Initial No mean flow	110	110	103	37	20	3	10.28	10	20	40	10	35
Optimal No mean flow	60	140	103	29	12	2.4	6.06	5	40	55	15	40

Table 5.4.III – List of the muffler parameters and TL_{AV} for the initial and optimal configurations.

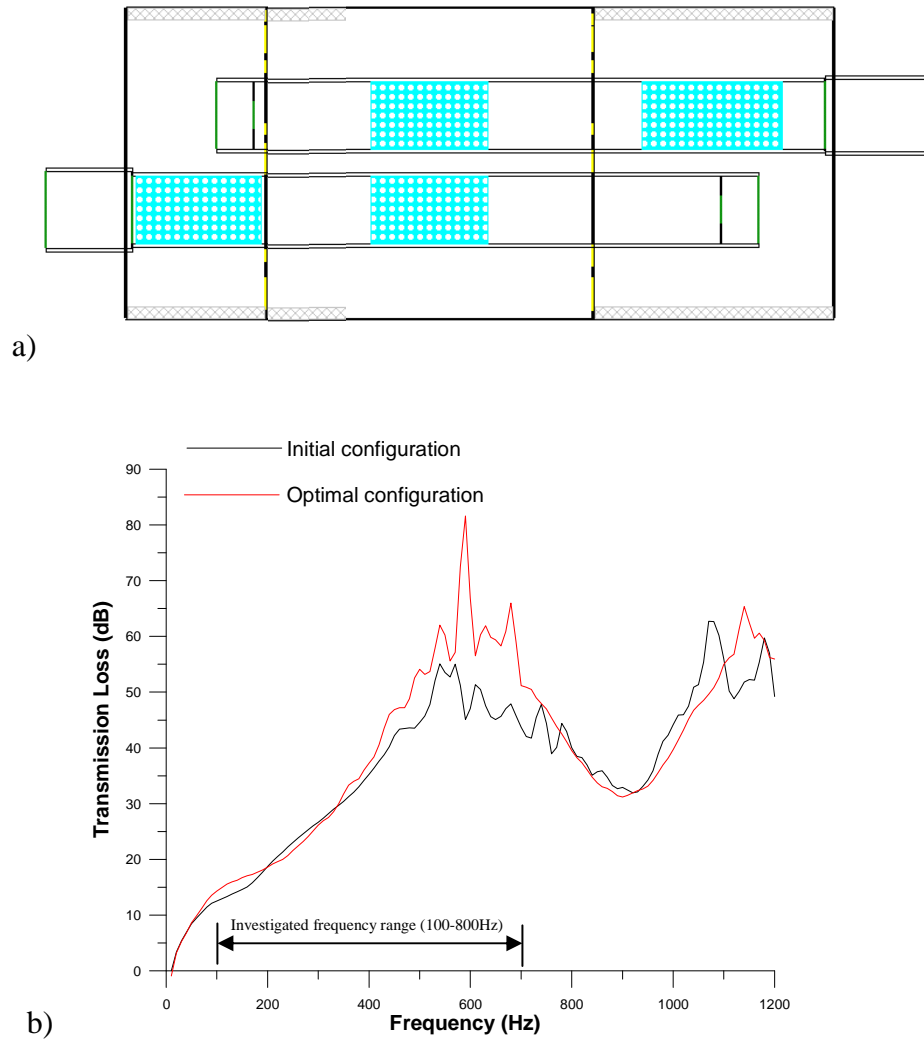


Figure 5.4.5 – a) Optimized shape configuration. – b) TL curve of initial and optimized geometry.

A parallel coordinates diagram including the objective function (TL_{AV}) and the possible values of the considered design parameters, is reported in Figure 10. Since the TL_{AV} range has been limited to a short range of best values (40.0-40.4 dB), a set of best parameter combinations is selected. It is clearly noticeable that all the best solutions are characterized by $a=60\text{mm}$ and $b=140\text{mm}$, by the smallest possible tube diameter (29mm), by small values of hole diameters on perforates (2.4-2.9mm), of $L1$ and $L4$, and a fixed value of $L2$ (40mm). Values 1,2,3 of a parameter in the diagrams respectively mean 60, 110, 155mm. Values 1,2,3 and 4 of b parameter state respectively 50, 95, 140, 190mm when $a=60\text{mm}$, and 45, 90, 140mm when $a=110\text{mm}$ or $a=155\text{mm}$ (see Figure 8).

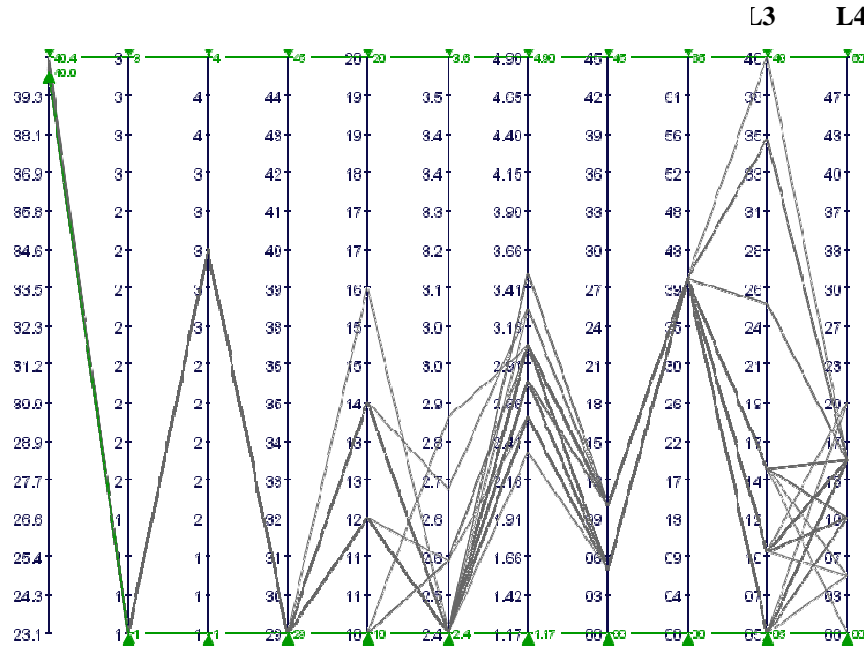


Figure 5.4.6 – Parallel coordinates diagram with TL_{AV} values limited at 40.0-40.4 dB range.

As previously said, also a multi-objective optimization procedure has been implemented aiming to maximize the muffler TL and minimizing the exerted pressure loss. For this type of problems, a multiplicity of solutions is expected, belonging to the so-called Pareto frontier [21].

TL_{AV} and Δp of the performed simulations are depicted in the scatter diagram of Figure 5.4.7, where also the Pareto frontier is highlighted. For a selected value of Δp , the muffler configuration detected by the design point located on this curve and with abscissa Δp , is characterized by having the highest TL_{AV} possible. Conversely, for a chosen TL_{AV} , the muffler configuration which provides the lowest Δp possible, can be easily detected on the Pareto curve.

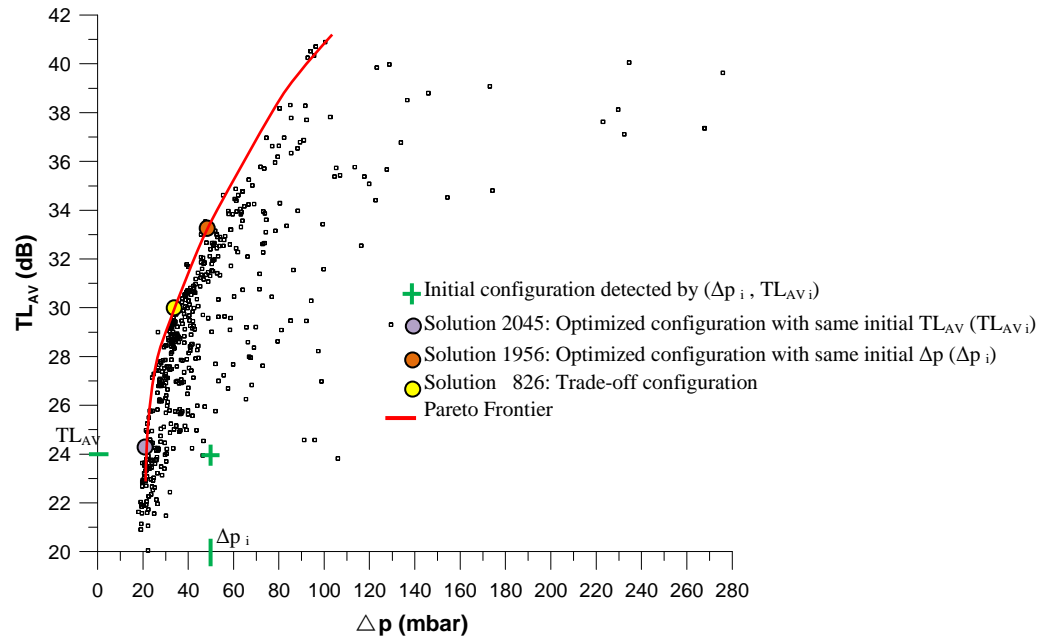


Figure 5.4.7 – Scatter diagram of the optimization process.

Together with the initial configuration results, which provides $TL_{AV}=24$ dB and $\Delta p=50$ mbar, other designs (solutions) are highlighted in the same figure.

Solution 2045 has the same TL_{AV} of the initial configuration, but the lowest Δp possible (21 mbar), whereas Solution 1956 has the same Δp of the initial muffler but the highest TL_{AV} possible (32 dB), whereas. Solution 826 represents a trade-off between a high TL and a low pressure drop: $TL_{AV}=32$ dB and $\Delta p=34$ mbar. The TL curves due to the initial configuration and the above solutions is plotted in Figure 5.4.8. The main geometrical data and acoustic/fluid-dynamic performances are listed in Table 5.4.IV.

It is clearly noticeable that all the selected solutions are characterized by having the central inner muffler chamber smaller and the third chamber bigger than the ones. The increasing of this volume produces definitely a TL improvement at low frequencies (where the optimization is focused on). Moreover, in all the selected solutions, the perforated areas have the almost always the maximum extension (which means small $L1$, $L2$, $L3$) and medium diameters (around 3mm). This implies an increasing of the transfer area between the tubes and the chambers (and the other way round). Anyway, the hole diameters are chosen large enough to do not affect too much the discharge coefficient of the crossing flow. Both things contribute to decrease the pressure drop. Consequently these kinds of configurations have definitely to be preferred since they positively affect the muffler behavior in both terms of acoustic and fluid-dynamic performances.

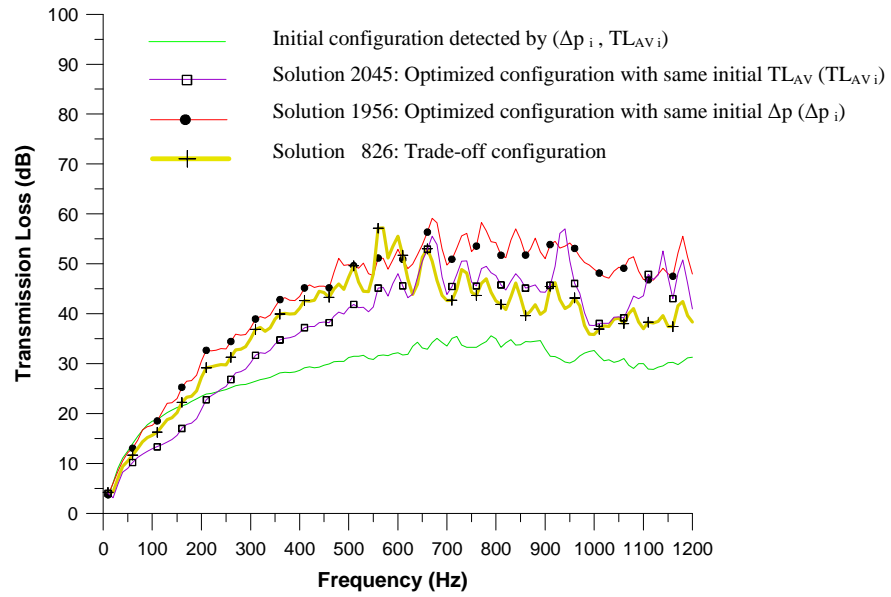


Figure 5.4.8 – TL diagram of the initial configuration, of solutions 2045, 1956 and 826.

Configuration	a (mm)	b (mm)	c (mm)	D _{tube} (mm)	D _{end} (mm)	D _{por} (mm)	DS _{holes} (mm)	L1 (mm)	L2 (mm)	L3 (mm)	L4 (mm)	TL _{AV} (dB)	Δp (mbar)
Initial 29m/s mean flow	110	110	103	37	20	3	10.28	10	20	40	10	24	50
Solution 2045 29m/s mean flow	110	45	148	33	10	3.15	8.86	0	0	95	0	24	21
Solution 1956 29m/s mean flow	110	45	148	31	14	2.8	9.8	0	15	105	10	33	50
Solution 826 29m/s mean flow	110	45	148	33	16	3.15	8.86	0	15	95	0	30	34

Table 5.4.IV – List of the muffler geometrical data and performances for initial configuration and examined solutions.

5.4.5 CONCLUSIONS

In this paragraph two optimization procedures are presented. They are based on a genetic algorithm, aimed to improve acoustic and fluid-dynamic performances of a two tube-three chamber perforated commercial muffler.

The first procedure is single-objective, and focused on the maximization of the TL, averaged in 100-800 Hz frequency range. The second one is double-objective, aiming to maximize the TL and minimize the back pressure exerted when the exhausted gases flow thorough the muffler. In the latter case, the imposed mean flow is equal to 29m/s, and the TL is averaged in 100-400 Hz and. The velocity has been calculated by considering the operating

condition of the engine the muffler is coupled to, and the selected frequency range has been chosen to take into account the frequencies of the 2nd, 3rd, 4th engine orders in the same operating conditions.

The presence of the insulating inner wool has been considered too, together with a certain number of perforations on the baffles, which acoustically connect the volumes of the inner chambers.

TL and pressure drop analyses of the investigated muffler have been performed by using a 1D solver, and experimentally validated in certain conditions (zero, 20 and a 40m/s mean flow, at 293, 383 and 378K respectively).

Even though, in this optimization procedure, only the validated 1D approach has been utilized, TL analyses of the investigated muffler have been performed, in absence of mean flow, also by using a 3D BEM solver. This latter, in fact, can be also utilized to optimize the muffler geometry, when an automatic mesh generator is coupled to the solver in the optimization process. Anyway, the 3D calculations are much more time consuming than the 1D ones. Moreover the utilized BE solver does not take into account the presence of flow and it is not suitable to evaluate the pressure drop. For this reason, in this work the 1D approach has been preferred.

The obtained results demonstrate that, in order to maximize the TL in absence of mean flow, the best solutions are obtained by choosing the length of the central chamber bigger than the original one, the smallest possible tube diameter, small values of hole diameters on perforates, of L1 and L4, and a fixed value of L2. In the best solution there is no improvement, in terms of TL, up to 400 Hz. Indeed from 400 up to 800 Hz the silencer behavior improves even more than 10 dB.

Three different solutions have been selected on the Pareto curve carried out by the double objective optimization. The first one has the same TL average of the initial configuration, but the lowest Δp possible. The second one has the same Δp of the initial muffler but the highest TL_{AV} possible. Eventually the third one represents a trade-off between a high TL and a low pressure drop.. All of these three cases solutions are characterized by having the central inner muffler chamber smaller and the third chamber bigger than the ones of the initial design. The increasing of a volume produces definitely a TL improvement at low frequencies (where the optimization is focused on). Moreover, in all the selected solutions, the perforated areas have the almost always the maximum extension (which means small L1, L2, L3) and medium diameters (around 3mm). Both things contribute to decrease the pressure drop by increasing

the transfer area between the tubes and the chambers, and by imposing perforation diameters large enough to do not worsen the discharge coefficient of the crossing flow.

REFERENCES

1. F. Bozza, A. Gimelli, R. Piazzesi, F. Fortunato, V. Pianese, D. Siano, The Prediction of the Performance and Gasdynamic Noise Emitted by a Medium-Size Spark-Ignition, SAE Paper 2007-01-0380, ISBN: 978-0-7680-1869-1.
2. Gamma Technologies, GT-ISE User's Manual Version 6.1, the GT-SUITE Interactive Simulation Environment, 2004.
3. A.F. Seybert and D.F. Ross, Experimental determination of acoustic properties using a two-microphone random-excitation technique, Journal of the Acoustical Society of America, 61, 1362-1370, 1977.
4. STS, Scientific and technical Software, VNoise Theoretical Manual, An Introduction to Boundary Elements Methods of Acoustics, 2003.
5. Z. Tao, A.F. Seybert, A review of current techniques for measuring muffler transmission loss, Society of Automotive Engineers, 03NVC-38.
6. J.W. Sullivan, M.J. Crocker, Analysis of concentric-tube resonators having un-partitioned cavities, Journal of Acoustical Society of America. 64, 207-215 (1978).
7. D.E. Winterborne, R.J. Pearson, Design Techniques for Engine Manifolds, SAE Int. Publisher, 1999.
8. D. Casilino, S. Moreau, M. Roger, One, no one and one thousand methods for low speed fan noise prediction, International Journal of Aeroacoustics, Vol. 9, No. 3, pp 307-327, 2010.
9. Z. Li, S. Su, C. Liu, Acoustic Attenuation Performance Analysis of Three-pass Perforated Tube Muffler with End-Resonator, SAE 2008 International, 2008.
10. D. Siano, F. Auriemma, F. Bozza, A correlation study of computational techniques of a three pass perforated tube muffler including FEM and 1D methods, SEEP 2009.
11. Y. R. Cheng, A. F. Seybert, T. W. Wu, "A Multidomain Boundary Element Solution for Silencer and Muffler Performance Prediction", Journal of Sound and Vibration - 19 November 1990.
12. Hongguang Liu, Senlin Lu & Falin Zeng, A Study on the Effects of Higher Order Mode Wave on Mufflers Performance, Modern Applied Science, Vol.3, n.1, Jen 2009.
13. A. F. Seybert, T. W. Wu, W. L. Li A Coupled FEM/BEM for Fluid- Structure Interaction Using Ritz Vectors and Eigenvectors, Lexington, KY 40506-0046.
14. C.A. Felippa, K.C. Park, C. Farhat, Partitioned analysis of coupled mechanical systems, Computer methods in applied mechanics and engineering, 190 (2001) 3247-3270.
15. D. Siano, F. Auriemma, F. Bozza, Pros and Cons of Using Different Numerical Techniques for Transmission Loss Evaluation of a Small Engine Muffler, SAE Paper 2010-32-0028, Linz, 2010.
16. D. Siano, F. Auriemma, F. Bozza, Svantaggi e Vantaggi Legati all'Utilizzo di Diversi Metodi Numerici per la Caratterizzazione Acustica di un Silenziatore per Applicazioni Automobilistiche, ATI Cagliari, 2010.
17. T. J. Cox and P. D'Antonio, "Acoustic Absorber and Diffusers –Theory, Design and Application", Taylor and Francis editor, Chapter five.

18. R. Kabral, H. Rämmal, J. Lavrentjev, F. Auriemma, Acoustic Studies on Small Engine Silencer Elements, SAE 2011-32-0514, 2012.
19. M.L. Munjal “Acoustics of Ducts and Mufflers”, New York : Wiley-Interscience, 1987.
20. D. Sasaki, “ARMOGA, An efficient Multi-Objective Genetic Algorithm”, Technical Report, January 2005.
21. I. Ordaz, A probabilistic and multi-objective conceptual design methodology for the evaluation of thermal management systems on air-breathing hypersonic vehicles, UMI Microform, 2000.

Conclusions and future research

Numerical simulations of acoustic and fluid-dynamic performances of automotive silencers have been carried out and included in this thesis. The results, obtained by using different methodologies, have been experimentally validated and an optimization procedure has been proposed to improve the silencer design. The main contributions of the thesis have been published in 5 papers, and summarized below:

Paper 1: The noise attenuation characteristics of a merely reactive three pass perforated muffler with final end resonator have been investigated, in terms of transmission loss, using a non-linear one-dimensional (1D) time domain approach and a linear three dimensional (3D) boundary element method (BEM). As expected, the obtained results agree in plane wave region, i.e. at low frequency, whereas at higher frequency the multi dimensional approach better reproduce the TL trend. Increasing the flow temperature, the TL curve stretches towards the high frequency and the reliability of 1D results is extended. Moreover, the 1D approach has also given reliable results when a mean flow is imposed.

Paper 2 and 3: Pros and cons of using the above methods have been analyzed, in terms of accuracy, computing time and problem formulation by simulating the behavior of a merely reactive two tubes cross-flow muffler. In particular the 1D approach has been proved to efficiently reproduce the presence of a mean flow, through very fast simulations. On the contrary, the BEM simulations are much more time consuming and are limited to the no mean flow case. On the other hand, with a combined 3D FEM/BEM approach it is possible to account the effects of the structure flexibility. In this way, several resonance frequencies have been highlighted, where fluid-structure iterations give important contributions to the attenuation curve. Moreover, the BEM is able to decompose the noise radiated by the outlet muffler into the wave contributions directly coming from the outlet, coming from external reflections, and coming from the surface vibrations.

Paper 4: 1D and 3D BEM models, utilized in the previous work for simulating the acoustical behaviour of a commercial silencer, have been improved validated, and extended by including wool effects. The analyses, in terms of transmission loss and pressure drop, have been carried out at different mean flow velocities, with and without the presence of inner

absorbing material. It has been noticed that, accurate acoustic simulations of a commercial low-cost device, require a detailed description of all the apparently minor geometrical elements. In fact, weldings and strength surfaces coupling, mainly due to the manufacturing process, may determine the presence of leakages between the chambers. They have been found to remarkably affect the acoustical behaviour, constituting an acoustic connection between the muffler cavities. 1D calculations, carried out with the presence of an imposed mean flow, have allowed to obtain very accurate information about the back pressure exerted by the muffler when a mean flow is imposed. The presence of an insulating material has been found to produce a smoother TL profile across a broad band frequency range, while, however, determining a non-negligible increase of pressure losses.

Paper 5: A new optimization procedure, based on a genetic algorithm coupled to a 1D solver by means of a number of matching routines, has been developed and discussed. Two optimized designs have been carried out: the first one gives a muffler configuration with maximized TL. The second one constitutes the best tradeoff between high TL and low back pressure when the presence of exhausted gas flow is accounted. In the former case the maximum TL increasing is more than 20 dB around 550 Hz. In the latter case, the average TL improves of 25% and the pressure losses decrease of 32%.

In the last three decades, acoustics of internal combustion engine mufflers has been object of a number of interesting studies. In fact, despite their apparent simplicity, the physics involved in the functioning of these devices is extremely complex. The description of their acoustic behavior has always been a challenging task for acousticians, and nowadays mufflers constitute a demanding test bench for many numerical simulation methodologies. *Quasi 3D* methods are giving promising results in this field, since they are more efficient, in expansion chamber simulations, than merely 1D approaches, preserving the advantage of being faster than the 3D methods. Anyway, the geometrical constraints due to the available space on car compartment for setting up the mufflers, implies very complex external shapes. In this case, the approach cannot be 1D nor quasi 3D, and further improvements of 3D simulations are desirable. In fact, 3D BEM acoustic solvers are often unable to take into account the presence of a mean flow, and the semi-empirical models utilized to simulate perforate tubes can be definitely improved. FEM simulations are able to account the presence of a mean flow but the problem is still largely unresolved with perforates.

Nowadays, despite of the difficulties in describing or simulating complex mufflers, the achieved levels of attenuations are remarkable. In author's opinion modern targets are the design optimizations, aimed not only to achieve good attenuation characteristics , but also to preserve very low back pressure levels, in order to reduce the engine consumption and to increase the output power. Moreover, especially in motorbike applications, the target is often an *enjoyable* exhaust noise. In order to accomplish these requirements, more efficient optimization procedures must be developed. In fact, the overall analysis would require efficient interaction among an external optimizer, an engine simulator (e.g. based on a 1D approach), a complete acoustic model, and an automatic shape modeler. Especially for industrial application, this is probably the most interesting and attractive goal.